UNIVERSITY OF SOUTHAMPTON

FACULTY OF MEDICINE

Cancer Sciences

Volume 1 of 1

THE ROLE OF EXOSOMES IN TUMOUR-STROMA INTERACTION IN COLORECTAL CANCER

by

Rahul Bhome

Thesis for the degree of Doctor of Philosophy

December 2018

UNIVERSITY OF SOUTHAMPTON

ABSTRACT

FACULTY OF MEDICINE

Cancer Sciences

Thesis for the degree of Doctor of Philosophy

THE ROLE OF EXOSOMES IN TUMOUR-STROMA INTERACTION IN COLORECTAL CANCER

by Rahul Bhome

Colorectal cancer is a global problem with rising incidence. Death is usually due to metastatic dissemination, and therefore, biological factors which influence disease progression are an important focus of study.

The tumour microenvironment is a functional ecosystem of cancer and stromal cells. The stroma plays a critical role in tumour proliferation, invasion and chemoresistance. Cancer-associated fibroblasts, the most abundant stromal cells, are associated with multiple pleiotropic processes, including tumorigenesis, proliferation, angiogenesis, epithelial-mesenchymal transition and resistance to treatment. The bidirectional transfer of information between tumour and stromal compartments is therefore important to elucidate.

One mechanism of paracrine signalling between cancer cells and stromal fibroblasts is by exosomes. These sub-100 nm nanoparticles have a lipid bilayer structure, contain lipid, protein and nucleic acid cargos, and are secreted by all cells. Importantly, these cargos are functional, such that one cell can alter the phenotype of another by exosome transfer. The most stable cargo is microRNA, small non-coding RNA which post-transcriptionally regulates over one-third of all human genes.

This thesis investigates the reciprocal transfer of exosomal microRNAs between cancer cells and stromal fibroblasts, and the effect of this on colorectal cancer progression. The first part demonstrates techniques to isolate, characterise, label and transfer exosomes from cancer cells and fibroblasts. Exosome transfer resulted in miRNA alterations in recipient cells, activation of ERK/ Akt pathways, and functional consequences for proliferation and apoptosis. *In vivo* exosome transfer was demonstrated by generating CRC cells expressing the CD63-GFP fusion protein, which transmitted GFP-positive exosomes to fibroblasts in murine tumour xenografts.

The second part investigates stroma to tumour exosome transfer. Here, exosomal microRNAs were profiled from paired patient-derived normal and cancer-associated fibroblasts. A colorectal cancer stromal exosome panel consisting of microRNAs 329, 181a, 199b, 382, 215 and 21 was identified. Of these, miR-21 had highest abundance and was enriched in exosomes compared to parent cells. Transfer of stromal exosomes to colorectal cancer cells increased miR-21 levels in recipient cells. Orthotopic xenografts, established with miR-21-overexpressing fibroblasts and colorectal cancer cells, led to increased liver metastases, compared to those established with control fibroblasts, highlighting the role of stromal miR-21 in colorectal cancer progression.

The third part investigates tumour to stroma exosome transfer, specifically the influence of epithelial-mesenchymal transition on fibroblast phenotype. Here, exosomes from a panel of epithelial and mesenchymal colorectal cancer cells were used to condition fibroblasts. Epithelial exosomes, rich in miR-200, increased this microRNA in recipient fibroblasts, repressing fibroblast Zinc finger E-box-binding homeobox 1, and reducing transforming growth factor-β-induced myofibroblast transdifferentiation. The converse was true of mesenchymal exosomes, which allowed unattenuated myofibroblast differentiation. Fitting with this, mesenchymal colorectal cancer xenografts contained fibroblasts with less miR-200, expressing more α-SMA and fibronectin, compared to fibroblasts from epithelial xenografts. This provides a mechanism for the accumulation of activated fibroblasts in mensenchymal (metastatic) tumours.

Table of Contents

Table of Tables

Table of Figures

List of Accompanying Materials

There are no accompanying materials.

Academic Thesis: Declaration of Authorship

I, ...**Rahul Bhome**

declare that this thesis and the work presented in it are my own and has been generated by me as the result of my own original research.

The role of exosomes in tumour-stroma interaction in colorectal cancer .....

.....

I confirm that:

1. This work was done wholly or mainly while in candidature for a research degree at this University;
2. Where any part of this thesis has previously been submitted for a degree or any other qualification at this University or any other institution, this has been clearly stated;
3. Where I have consulted the published work of others, this is always clearly attributed;
4. Where I have quoted from the work of others, the source is always given. With the exception of such quotations, this thesis is entirely my own work;
5. I have acknowledged all main sources of help;
6. Where the thesis is based on work done by myself jointly with others, I have made clear exactly what was done by others and what I have contributed myself;
7. Parts of this work have been published as:

   Bhome, R, et al., *The colorectal cancer microenvironment: strategies for studying the role of cancer associated fibroblasts*. Methods Mol Biol, 2018; **1765**: p. 87-98.

   Bhome, R., et al., *Exosomal microRNAs (exomiRs): Small molecules with a big role in cancer.* Cancer Lett, 2018. **420**: p. 228-235.

   Bhome, R, et al., *Exosomal microRNAs derived from colorectal cancer-associated fibroblasts: role in driving cancer progression*. Aging (Albany NY), 2017. **9(12)**: p. 2666-2694.

   Bhome, R., et al., *Profiling the MicroRNA Payload of Exosomes Derived from Ex Vivo Primary Colorectal Fibroblasts.* Methods Mol Biol, 2017. **1509**: p. 115-122.

   Bhome, R., et al., *Translational aspects in targeting the stromal tumour microenvironment: from bench to bedside.* New Horiz Transl Med, 2016. **3**(1): p. 9-21.

Bhome, R., et al., *A top-down view of the tumor microenvironment: structure, cells and signaling.* Front Cell Dev Biol, 2015. **3**: p. 33.

Signed: .....

Date: .....

Acknowledgements

I would like to thank Cancer Research UK and the Medical Research Council for funding this work. I am grateful to the University of Southampton Cancer Sciences Unit for hosting my doctoral project. I have had excellent supervision from Dr Emre Sayan, who has spent countless hours training me in several of the molecular biology techniques used here. Equally, Professor Alex Mirnezami had the vision to embark on this project and has given me direction and unwavering support to investigate my research questions. Finally, a special thank you to my wife, Prachi, my sons, Aaryan and Anshuman, my parents, Leena and Girish and my brother, Rohan, for understanding the demands of a husband, father, son and brother, who is embarking on a clinical academic career.

Definitions and Abbreviations

CRC – colorectal cancer

FAP – familial adenomatous polyposis

HNPCC – hereditary non-polyposis colorectal cancer

PJS – Peutz Jeghers Syndrome

JPS – Juvenile Polyposis Syndrome

CMS – consensus molecular subtyping

EGFR – epithelial growth factor receptor

MDT – multidisciplinary team

TNM – tumour, node, metastasis

CT – computed tomography

MRI – magnetic resonance imaging

5FU – 5-fluorouracil

CEA – carcinoembryonic antigen

TME – tumour microenvironment

CAF – cancer-associated fibroblast

APC – antigen presenting cell

ECM – extracellular matrix

Th – helper T cell

Treg – regulatory T cell

NK – natural killer

SNP – single nucleotide polymorphism

SMA – smooth muscle actin

EMT – epithelial-mesenchymal transition

EndMT – endothelial-mesenchymal transition

FSP – fibroblast specific protein

SDF – stromal cell-derived factor

LOX – lysyl oxidase

LOX-L – lysyl oxidase like protein

BAPN – beta-aminopropionitrile

FGF – fibroblast growth factor

SASP – senescence-associated secretory phenotype

PanIN – pancreatic carcinoma *in situ*

PDAC – pancreatic ductal adenocarcinoma

MMP – matrix metalloprotease

TIMP – tissue inhibitor of metalloprotease

NOF – normal fibroblast

TF – transcription factor

TAM – tumour-associated macrophage

CSFR – colony stimulating factor receptor

DC – dendritic cell

MHC – major histocompatibility complex

PBMC – peripheral blood mononuclear cell

APC – antigen presenting cell

TIL – tumour infiltrating lymphocyte

CTLA-4 - cytotoxic T lymphocyte-associated protein-4

PD-1 - programmed cell death protein-1

G-CSF – granulocyte colony stimulating factor

GM-CSF – granuloycyte macrophage colony stimulating factor

EC – endothelaial cell

MET – mesenchymal-epithelial transition

PDGF – platelet-derived growth factor

VEGF – vascular endothelial growth factor

VDA – vascular damaging agent

HIF – hypoxia-inducible factor

ECM – extracellular matrix

TGF – tumour growth factor

IL – interleukin

TNF – tumour necrosis factor

EV – extracellular vesicle

MVB – multivesicular body

ESCRT – endosomal sorting complex responsible for transport

ISEV – International Society for Extracellular Vesicles

dUC – differential ultracentrifugation

SEC – size exclusion chromatography

TEM – transmission electron microscopy

NTA - nanoparticle tracking analysis

HnRNP - Heterogeneous nuclear ribonucleoprotein

BMDM – bone marrow-derived macrophage

Zeb – zinc finfer E-box-binding homeobox

MET – mesenchymal to epithelial transition

BM-MSC – bone marrow-derived mesenchymal stem cell

NBL – neuroblastoma

ROC – receiver operating characteristic

AUC – area under curve

ExomiR – exosomal miRNA

Zeb - Zinc finger E-box-binding homeobox

NcRNA – non-coding RNA

LncRNA – long non-coding RNA

SncRNA – small non-coding RNA

MiRNA – microRNA

PiRNA – piwi-interacting RNA

SiRNA - small interfering RNAs

SnoRNA - small nucleolar RNA

ScnRNA - scan RNA

PASR - promoter-associated small RNA

TASR - termini-associated small RNA

TiRNA - transcription initiation RNAs

DiRNA - defective interfering RNA

LincRNA – long intergenic non-coding RNA

UTR – untranslated region

Ago – argonaute

AUB – aubergine

NSCLC – non-small cell lung cancer

DCIS – ductal carcinoma *in situ*

EGF – epidermal growth factor

HNSCC – head and neck squamous cell carcinoma

IGF – insulin-like growth factor

ExomiR – exosomal miRNA

BSA – bovine serum albumin

FBS – foetal bovine serum

MEF – mouse embryonic fibroblast

ATCC – American Type Culture Collection

ECACC - European Collection of Authenticated Cell Cultures

ZKD – Zeb1 knock down

PKA – protein kinase A

PKC – protein kinase C

AMPK – AMP-activated protein kinase

ELISA – enzyme-linked immunosorbent assay

TRPS – turnable resistive pulse sensing

SPR – surface plasmon resonance

5EU – 5-ethynyl uridine

ATM – ataxia telangiectasia mutated

HCC – hepatocellular carcinoma

TS – thymidine synthase

DTL - denticless protein homolog

ATII – alveolar type II epithelial cells

tPA – tissue plasminogen activator

Chapter 1 Introduction

1.1 Colorectal cancer

1.1.1 Sporadic and hereditary colorectal cancer

Colorectal cancer (CRC) poses a substantial public health problem, with global incidence set to eclipse two million by 2030 [1]. Although incidence has plateaued in countries with the highest human development index, the trajectory in transitioning countries is still rising [1]. In Europe, CRC represents the second highest cause of cancer-related death, healthcare expenditure, and loss of productivity [2]. The principal cause of mortality from CRC is metastasis. Despite advances in surgical and chemotherapeutic treatment options for metastatic CRC, the majority of patients remain incurable, with a median survival of less than two years [3].

Incidence of CRC is positively associated with age, family history of CRC (primary relative), inflammatory bowel disease, obesity and smoking. Use of the non-steroidal anti-inflammatory drug aspirin is protective [4, 5].

The mutational sequence of CRC was described in 1990 by Fearon and Vogelstein as a series of affected genes, starting with *APC* mutation, followed by *KRAS* mutation, then loss of *DCC*, and finally loss of *TP53* [6]. This directly corresponds with the adenoma-carcinoma sequence of CRC, in which the acquisition of mutations leads to the transformation of normal bowel, to adenomatous polyps, to invasive cancer, over several years [7].

Broadly, CRC is divided into sporadic (70%) and inherited (30%) types. Inherited CRC is typically familial (non-syndromic) or syndromic (2-5% of all CRC), the latter comprising familial adenomatous polyposis (FAP), Lynch syndrome, *MYH*-associated polyposis (MAP) and hamartomatous polyposis conditions (e.g. Peutz-Jeghers syndrome (PJS) and juvenile polyposis syndrome (JPS)). FAP arises from a mutation in the *APC* gene, is inherited in an autosomal dominant manner, and has almost 100% penetrance. This disease is characterised by more than 100 (usually thousands) of polyps in the colon and/or rectum. Almost all FAP patients will develop CRC by the age of 40 if untreated, and recommended management is prophylactic colectomy by age 20 [8]. Attenuated FAP, a less penetrant form, is characterised by 100 or less polyps, usually sparing the rectum, with a delay in onset of polyposis [9, 10]. Lynch syndrome (previously, hereditary non-polyposis colorectal cancer (HNPCC)) is a result of mutations in mismatch repair

genes (*MLH1, MSH2, MSH6, PMS2)*, which are also inherited in an autosomal dominant manner, giving rise to microsatellite instability. Lynch syndrome typically presents with right sided colonic tumours as well as extracolonic tumours (e.g. endometrial, gastric), with a lifetime risk of CRC of 68% for men and 52% for women [11]. Diagnosis is based on Amsterdam II criteria, which state that the individual must have three or more relatives (one should be a first degree relative of the other two) with an associated cancer (e.g. CRC, endometrial, gastric), two or more generations affected, one or more relatives diagnosed before age 50, and FAP excluded [12]. Patients have intensive colorectal surveillance (1-2 yearly), throughout their lives, starting at age 20-25 [13]. MAP results from biallelic mutations of the base-excision-repair gene *MYH*. This is transmitted in an autosomal recessive manner, and presents as a polyposis syndrome resembling attenuated FAP [14, 15]. PJS and JPS are characterised by benign hamartomatous polyps. Both transmitted in an autosomal dominant manner, the former arising from mutation in *STK11* and the latter due to *SMAD4* and *BMPR1A* mutations. PJS typically presents with small bowel, gastric and colonic polyps, together with mucocutaneous pigmentation and affected individuals have a 70% lifetime risk of gastrointestinal cancer [16]. In JPS, histologically "juvenile" polyps are found throughout the gastrointestinal tract but predominantly in the colon. Lifetime risk of CRC is 39% [17].

Familial CRC is broadly divided into high-risk and common categories. High-risk familial CRC refers to those individuals who meet Amsterdam criteria for Lynch syndrome but do not have MMR deficiency, suggesting that there is a significantly penetrant susceptibility gene which is yet to be found. In contrast, common familial CRC refers to those individuals with a primary relative who has CRC and arises from a number of different low penetrance susceptibility genes [16].

Knudson's two hit hypothesis states that two mutational events have to accrue to result in cancer [18]. In sporadic CRC the likelihood of two events occurring in a given time is smaller than in hereditary CRC, where one event already exists at birth. Hence, sporadic CRC is typically a disease of older age than hereditary CRC.

1.1.2 Molecular subtypes of CRC

Gene expression profiling is useful in stratifying tumours according to behaviour, recurrence and response to treatment, but for several years there was no consensus on how to subtype CRC [19, 20]. In 2015, the Consensus Molecular Subtyping (CMS) classification was published, dividing CRC into four main subtypes [21]. This project combined 18 datasets, comprised of over 4000 patients, incorporating prospective and retrospective studies, which utilised various gene expression platforms (e.g. gene expression microarray, RNA sequencing) and proteomic studies. CMS subtypes are described in **Table 1-1**.

Table 1-1. The CMS classification of CRC.

Subtype	Molecular Classification	Frequency[1] (%)
CMS1	**MSI Immune** – hypermutated, microsatellite unstable, strong immune activation	14
CMS2	**Canonical** – epithelial, chromosomally unstable, WNT/ MYC signalling	37
CMS3	**Metabolic** – epithelial, metabolic dysregulation	13
CMS4	**Mesenchymal** – transforming growth factor β activation, stromal invasion, angiogenesis	23

It has since been suggested that the CMS classification is heavily skewed by stromal components of CRC. To overcome this, Isella and colleagues generated patient-derived xenografts (PDXs) from 244 paired normal and tumour specimens from CRC patients, using the principle that murine stroma replaces tumour stroma. PDXs were then subjected to RNA sequencing [22]. From this work, five CRC intrinsic subtypes (CRIS) were proposed: (i) CRIS-A: mucinous, glycolytic, enriched for microsatellite instability or *KRAS* mutations; (ii) CRIS-B: transforming growth factor (TGF)-β pathway activity, epithelial–mesenchymal transition, poor prognosis; (iii) CRIS-C: elevated epithelial growth factor receptor (EGFR) signalling, sensitivity to EGFR inhibitors; (iv) CRIS-D: *WNT* activation, *IGF2* gene overexpression and amplification; and (v) CRIS-E: Paneth cell-like phenotype, TP53 mutations.

1.1.3 Detection and staging of CRC

CRC can present with local symptoms (e.g. rectal bleeding, change in bowel habit), with or without systemic upset (e.g. fatigue, malaise), clinical signs (e.g. palpable mass) and/or iron-deficiency anaemia. With the introduction of bowel cancer screening in the UK, a greater number of asymptomatic CRC is being detected [23]. Since 2006, 60-74-year-old men and women are asked to provide stool samples for the detection of faecal occult blood (FOB), every two years. In this capacity, the faecal immunochemical test (an antibody to haemoglobin) is set to replace the existing guaiac faecal occult blood test due to its superior sensitivity and patient acceptability [24]. Since 2013, as an alternative to FOB testing, some UK centres are calling 55 year old men and women for bowel scope screening (one off flexible sigmoidoscopy), which has been shown to

[1] Frequencies do not total 100% because some tumours display a mixed phenotype.

reduce CRC diagnoses by 33% and mortality by 43% (by the timely detection and removal of pre-cancerous polyps) [25].

In the UK, as in most countries with an established healthcare system, there are guidelines for the investigation of suspected CRC, and its subsequent management [26]. Gold standard investigation is by optical colonoscopy or computed tomography (CT) colonoscopy (virtual colonoscopy). Visualisation of the entire large bowel is recommended because synchronous tumours exist in 3.5% of cases [27]. Colonic and rectal cancers are staged and managed differently. Both rectal and colonic cancers are staged by CT chest, abdomen and pelvis. In addition, rectal cancers are locally staged by magnetic resonance imaging (MRI), to assess the likelihood of local recurrence, which is dependent on circumferential resection margin, nodal status, height of the tumour and levator muscle involvement. In patients with rectal cancer who cannot have MRI, or in cases where trans-anal resection is considered, an endorectal ultrasound may be offered for further assessment. In the UK and the majority of the world, the Tumour, Node, Metastasis (TNM) classification is used to stage CRC [28]. Based on an individual stage for tumour (T), node (N) and metastasis (M), the overall stage (0-4) is determined. Stage 0 is carcinoma in situ. Stage 1 is small volume (T1-2) node negative cancer. Stage 2 is larger volume (T3-4) node negative cancer. Stage 3 is any node positive cancer without distant metastases, and stage 4 is any distant metastatic disease. The American Joint Committee on Cancer seventh edition TNM staging for CRC is provided in Appendix **A**.

Dukes' staging of CRC requires pathological assessment of the resected bowel following surgery, and is still used to determine candidates for adjuvant chemotherapy. Dukes' observations, made on 215 rectal resections, proposed three stages of rectal cancer: limited to the rectal wall (A), penetrating the rectal wall without lymph node disease (B) and presence of any lymph node metastasis (C) [29]. This staging system has acquired several modifications and is now applied to both colonic and rectal tumours.

1.1.4 Management of CRC

Management of CRC is decided by a multidisciplinary team (MDT) of surgeons, oncologists, radiologists and pathologists. Operable colonic carcinoma is not currently considered for neoadjuvant treatment, although the FOXTROT trial has recruited patients with locally advanced (T3/4) colonic tumours to investigate whether neoadjuvant fluoropyrimidine, followed by surgery, followed by standard adjuvant treatment, will improve 2-year recurrence compared to surgery and adjuvant treatment alone [30]. Following colonic resection, patients are re-discussed at the MDT with a view to adjuvant chemotherapy depending on histological assessment of the resected specimen and the patient's ability to withstand treatment. Patients with a Duke's C tumour

(lymph node involvement) are recommended to have treatment. This is typically with regimens containing a fluoropyrimidine such as FOLFOX (folinic acid, 5-fluorouracil (5FU) and oxaliplatin), FOLFIRI (folininic acid, 5FU and irinotecan) and XELOX (capecitabine and oxaliplatin), lasting 6-7 months.

Operable rectal cancer is managed differently. The risk of local recurrence is determined by MRI, with high-risk rectal tumours deemed less than 1 mm from the resection margin, low in height and involving the levator muscle. Moderate risk tumours are cT3b or greater without any threat to the resection margin or, where there is lymphadenopathy away from the resection margin, or, where there is extramural vascular invasion. Low-risk tumours lack any of the features above. Patients with high-risk tumours are recommended long-course neoadjuvant chemo-radiotherapy (45 Gy in 25 fractions with systemic 5FU or capecitabine), followed by a 6-10-week delay to surgical resection. Patients with moderate risk tumours are recommended short course pre-operative radiotherapy (25 Gy in five fractions) followed by surgery within 11 days of the first fraction. Patients with low risk tumours should not be routinely offered neoadjuvant treatment. The use of adjuvant chemotherapy after rectal resection is similar to that after colonic resection, with Duke's C tumours warranting treatment. Finally, stage IV CRC is potentially curable depending on the anatomical location, number and volume of the metastases.

Follow-up for operable colonic and rectal cancer patients is similar. All patients should have 6-monthly serum carcinoembryonic antigen (CEA) measurements for three years, CT of the chest, abdomen and pelvis twice in the first three years post-treatment and colonoscopy at 1-year and 5-years. Local or distant disease recurrence mandates another MDT discussion and a decision about whether cure or palliation is now achievable. Radical surgery such as pelvic exenteration is possible for locally recurrent rectal cancer for example [26].

1.2 Tumour Microenvironment

1.2.1 Organisation of the tumour microenvironment

The TME is a functional ecosystem of tumour and stromal cells that interact through paracrine and juxtacrine signalling. The stroma is a histological unit consisting of peri-tumoral cells within an extracellular scaffold. Stromal cells can be broadly categorised by their pro- or anti-tumour effects and these are shown in **Figure 1-1**. This section describes important stromal constituents, subdivided into mesenchymal cells, immune cells, vascular cells and extracellular matrix (ECM).

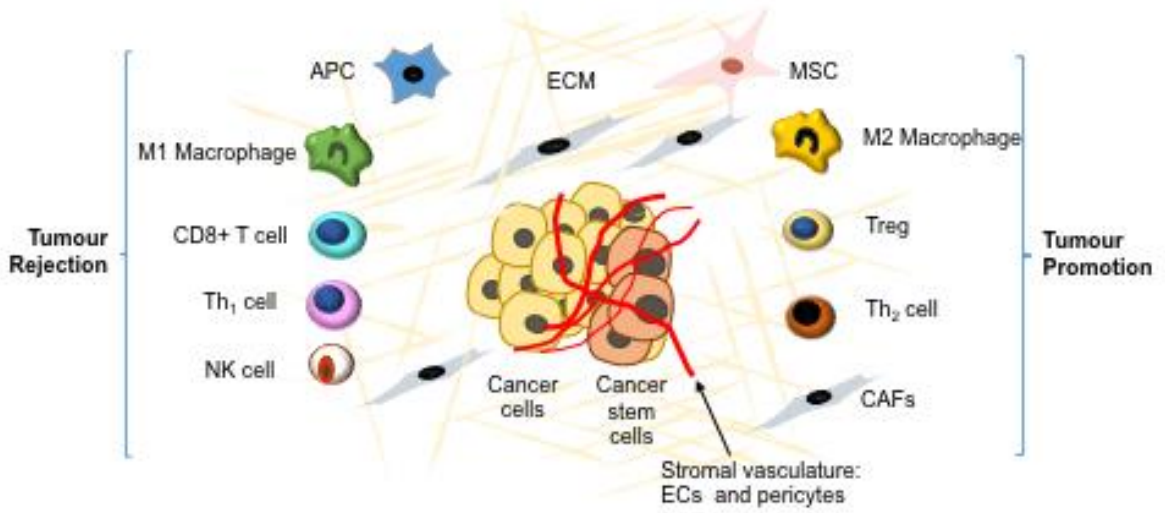

Figure 1-1. Cellular composition of the tumour microenvironment. APC – antigen presenting cell; ECM – extracellular matrix; MSC – mesenchymal stem cell; Treg – regulatory T cell; Th – helper T cell; CAF – cancer-associated fibroblast; EC – endothelial cell; NK – natural killer cell. From *Bhome et al. (2015)* [31].

A symbiotic relationship exists between tumour and stroma. Stromal cells are corrupted by cancer cells, creating a permissive microenvironment which facilitates tumour progression [32]. Unlike cancer cells, which arise through a series of mutations, stromal cells are untransformed, or, genetically stable [33, 34]. For example, using a genome-wide 500K single nucleotide polymorphism (SNP) array, it was shown that loss of heterozygosity and copy number alterations are extremely rare in cancer-associated fibroblasts (CAFs), from breast and ovarian tumours [35]. Therefore, drugs targeting the stromal component of the TME should be less susceptible to resistance. This has led to an exponential rise in research into the stroma in the past 20 years [36]. However, the first references to the stromal TME are over a century old and important developments were made throughout the twentieth century. **Table 1-2** summarises the important studies.

Table 1-2. Landmarks in our understanding of the TME.

Time frame	Finding	Reference(s)
Late 1800s	"Seed and soil" hypothesis: a specific microenvironment is required for tumours to establish at a secondary site.	Paget (1889) [37]
Early 1970s	Tumour angiogenesis factor isolated: birth of angiogenesis.	Folkman et al. (1971) [38]
Mid 1970s	Macrophages first identified in TME of solid tumours: characterisation of immune TME.	Hersh et al. (1976) [39] Russel et al. (1976) [40]
Early 1980s	Tumour cells shown to digest extracellular matrix components: the importance of ECM in tumour invasion.	Jones and De Clerck (1980) [41]
Early 1980s	Soluble factors from tumour cells stimulate colony formation of normal cells: the role of transforming growth factors in the TME.	Moses et al. (1981) [42] Nickell et al. (1983) [43]
Mid 1980s	Fibroblasts shown to exchange nucleotides with HeLa cells: stroma-tumour interaction.	Delinassios and Kottaridis (1984) [44]
Mid 1990s	ECM induces β-casein expression in mammary cells: potential for TME elements to alter gene expression in pre-malignant cells.	Roskelley et al. (1994) [45]
Late 2000s	MicroRNAs are shuttled between cells in secreted vesicles: novel cell-cell communication in the TME.	Valadi et al. (2007) [46]

From *Bhome et al. (2015)* [47]

1.2.2 Mesenchymal cells

1.2.2.1 CAFs

1.2.2.1.1 What are CAFs?

Several definitions for CAFs exist, but the widely accepted definition is that CAFs are a heterogeneous population of cells derived from the mesoderm, which are juxtaposed to cancer cells. Furthermore, the consensus view is that CAFs are activated or recruited by the insult of a

growing tumour. In contrast, normal, or, tissue-resident fibroblasts, are a more discrete population of quiescent cells, which are capable of activation in response to certain paracrine cues [48, 49].

Dvorak described cancer as a wound that does not heal [50]. In situations where tissue is damaged, fibroblasts are recruited and undergo myofibroblastic transdifferentiation in order to close the wound. When the repair is complete, the myofibroblast population subsides. In the analogous situation, as a tumour grows, surrounding tissue is damaged and myofibroblasts are activated. However, because the insult persists, fibroblasts remain activated [51]. It is important to note that not all CAFs are myofibroblasts. Nonetheless, α-smooth muscle actin (SMA) positivity is most commonly used to denote the activated CAF phenotype, and TGF-β is widely accepted as the main cancer cell-secreted factor which activates CAFs [52-55].

CAFs are the predominant cell type in the stroma, responsible for production of growth factors, cytokines, chemokines, enzymes and extracellular matrix (ECM) [49, 56]. The increased seceretory activity of CAFs compared to quiescent fibroblasts, meant that for a long time, the default presumption was that CAFs were primarily pro-tumorigenic. However, there is a growing body of evidence to support the anti-tumour effects of CAFs, which is outlined below [49, 57].

1.2.2.1.2 The origin of CAFs

CAFs are a heterogeneous population of cells, suggesting that they are derived from different lineages. The majority of CAFs have been shown to arise from resident quiescent fibroblasts, recruited bone-marrow-derived mesenchymal cells and adipocytes [58]. Activation of quiescent fibroblasts to CAFs is likely to be a complex and multifaceted process, given the degree of heterogeneity in the CAF population. This process is often abbreviated to TGF-β-mediated myofibroblast transdifferentiation, a phenomenon first described by Desmouliere and colleagues over 25 years ago [54]. However, this is one of several different mechanisms. Orimo's group showed using an orthotopic breast cancer model, that tissue-resident fibroblasts are activated to CAFs by two positive feedback loops, driven by TGF-β and stromal cell-derived factor (SDF)-1 [59]. More recently, Mitra et al. showed downregulation of miR-31 and -214, and upregulation of miR-155 in primary CAFs from ovarian cancer metastases. Gain and loss of function studies showed that these miRNAs can also regulate the CAF phenotype [60]. Bone marrow cells are also important in determining CAF activation. Systemic endocrine signals such as osteopontin from tumours have been shown to recruit $Sca1^{+}cKit^{-}$ bone marrow cells into the circulation. The activated bone marrow cells secrete granulins, creating a myofibroblastic, desmoplastic stroma around indolent responding tumour cells [61].

In terms of CAF recruitment, Quante et al. showed in an inflammation-induced mouse model of gastric cancer, that 20% of CAFs were derived from bone marrow [62]. Here, IL-1β mice were irradiated, and given bone marrow transplants containing GFP-positive cells. Twelve months after transplant, 20% of α-SMA positive cells in regions of gastric dysplasia were GFP-positive. Transdifferentiation of adipocytes to CAFs is less often reported, but there are *in vitro* data showing that conditioned medium from metastatic breast cancer cells stimulates expression of α-SMA and fibronectin in adipose-derived stem cells [63].

CAFs may also differentiate from epithelial cells (epithelial-mesenchymal transition; EMT), endothelial cells (endothelial-mesenchymal transition; EndMT) and pericytes. Iwano et al. demonstrated using bone marrow chimeras and transgenic mice, that fibroblasts in a renal fibrosis model arise from tubular epithelium, raising the possibility that some CAFs might transdifferentiate from normal parenchyma [64]. Kalluri's group was the first to describe TGF-β-mediated endothelial-mesenchymal transition, in the context of cardiac fibrosis and cancer [65, 66]. In B16F10 mouse melanomas, they showed double positive staining of cells with endothelial (CD31) and fibroblast (α-SMA/ fibroblast specific protein (FSP)-1) markers, which they believed to be in transit between endothelial and mesenchymal states. To definitively show that stromal fibroblasts had differentiated from endothelial cells, they traced *Tie2-cre*–positive endothelial cells from perivascular CD31-positive cells to peritumoral FSP-1 and α-SMA-positive cells, showing that 30-40% of CAFs originated as endothelial cells. Similarly, Hosaka and colleagues described pericyte-fibroblast transition stimulated by platelet-derived growth factor (PDGF)-BB. Lineage tracing of pericytes in *CreERT2* mice showed that these cells also had the ability to gain fibroblast and myofibroblast markers [67].

1.2.2.1.3 CAF markers

Despite the ability to perform complex lineage tracing studies, identifying the origin of different CAF populations is still hampered by the lack of definitive CAF markers. A plethora of candidate markers have been suggested, and can be broadly classified into: ECM components (e.g. collagens, fibronectin, tenascin-C, periostin, lysyl oxidase (LOX), matrix metalloproteases (MMPs) and tissue inhibitors of metalloproteases (TIMPs)); growth factors/ cytokines (e.g. TGF-β, vascular endothelial growth factors (VEGFs), PDGFs, fibroblast growth factors (FGFs)); receptors (e.g. TGF-βR, PDGFR, FGFR) and; cytoskeletal proteins (e.g α-SMA, FSP-1) [68]. There is overlap between these markers but this depends on tissue type. For example, CAFs from Rip1 Tag2 pancreatic tumours and 4T1 breast tumours were compared for expression markers [69]. In pancreatic tumours, over 40% of CAFs were positive for both FSP-1 and α-SMA, but in breast tumours only 10% of CAFs were double positive. Another problem with commonly used CAF markers such as

vimentin and FSP-1, is their overlap with mesenchymal (metastatic) carcinoma cells. In fact FSP-1 has actually been used as a marker of metastatic cancer cells in lineage tracing studies [70].

1.2.2.1.4 Role of CAFs in tumour progression

It is not clear how CAFs contribute to tumorigenesis, but studies have demonstrated neoplastic transformation in their presence [71]. Olumi et al. showed that when human prostate CAFs were co-cultured with normal prostate epithelial cells, they stimulated rapid epithelial growth and altered histology [72]. Moreover, simulation of CAF signalling by Wnt-1-transfected fibroblasts caused morphological transformation in mammary epithelial cells [73]. Furthermore, overexpression of TGF-β and hepatocyte growth factor (HGF) in primary stromal fibroblasts, was shown to induce hyperplastic and neoplastic transformation in mammary epithelial cells, when injected orthotopically into mammary fat pads [74].

In early cancer, the host tissue is remodelled to accommodate the developing tumour. Microscopically this is characterized by compositional changes and stiffening of the ECM [75]. CAFs express the enzyme LOX and LOX-like proteins (LOX-L) 1-4, which allow crosslinking of ECM substrates such as collagen with elastin. This stiffens the ECM and stimulates integrin-dependent mechanotransduction pathways which promote invasion [76]. LOX/LOX-L expression correlates with worse prognosis in head and neck, lung, ovarian and breast cancers [77]. LOX inhibitors such as beta-aminopropionitrile (BAPN) have been shown to reduce breast cancer cell motility *in vitro* [78]. In cervical cancer models, BAPN was shown to reduce hypoxia-induced EMT, invasion and migration [79]. Bondareva et al. showed that BAPN reduced metastasis of MDA-231 breast cancer cells only if given at the same time or prior to systemic injection of tumour cells [80]. This suggests that LOX may be important in very early metastatic processes.

CAFs play an important role in angiogenesis by secreting FGF-2 and VEGF [81, 82]. Hanahan's group used the multi-kinase inhibitor, imatinib, to treat HPV-16 transgenic mice, which develop cervical carcinoma [81]. Invasive and pre-invasive tumours treated with imatinib, were poorly angiogenic, and intratumoral fibroblasts showed reduced FGF-2 expression. These effects were recapitulated with PDGFR monoclonal antibody treatment, suggesting that FGF-2 is dependent on PDGFR activation. Furthermore, brivanib (a dual VEGF/ FGF tyrosine kinase inhibitor) was shown to effectively block angiogenesis in a pancreatic neuroendocrine tumour model [83]. Huynh and colleagues showed that brivanib reduced tumour size in human xenografts of hepatocellular carcinoma by increasing apoptosis, and reducing proliferation and microvessel formation [84]. This is of particular interest because selective inhibition of VEGFR alone, with bevacizumab, leads to drug resistance, as discussed below [85]. Importantly, the angiogenic effects of CAFs are not limited to their local environment. For example, fibroblast expression of stromal cell-derived

factor-1 (SDF-1/ CXCL12) acts as a systemic chemotactic signal for circulating immature endothelial cells (ECs), leading to breast cancer vascularization and metastasis [86].

There is growing evidence to suggest that CAFs induce invasiveness and metastatic capability of cancer cells. Epithelial-mesenchymal transition (EMT) is a cellular programme that induces cancer cell metastasis, through loss of epithelial cell polarity, and acquisition of a migratory phenotype [87]. CAFs have been shown to promote this transition in multiple cancers [88, 89]. Moreover, there is evidence to suggest that CAFs guide metastatic cells to prime the secondary site for colonization [90]. More recently, CAFs have been shown to facilitate invasion of epithelial cancer cells in an EMT independent manner [91]. Here, it was shown that juxtacrine signalling between N-cadherin on CAFs and E-cadherin on cancer cells, was necessary for CAFs to lead cancer cells to invasion.

It was previously thought that senesecent fibroblasts were metabolically inactive bystanders in the TME. However, we now know that senescent fibroblasts express and secrete a wide variety of molecules, collectively known as the senescence-associated secretory phenotype (SASP) [92]. Coppe et al. classified the SASP as consisting of cytokines (e.g. IL-6, IL-1), chemokines (e.g. IL-8, CXCL-1, -2), insulin-like growth factor binding proteins, other soluble factors (e.g. granulocyte colony stimulating factor (G-CSF), granulocyte macrophage colony stimulating factor (GM-CSF)), extracellular proteases (MMPs), extracellular insoluble molecules (e.g. fibronectin) and non-protein molecules (nitric oxide and reactive oxygen species). Campisi's group showed that co-culture of senescent fibroblasts with pre-malignant (*P53* mutant but non-tumorigenic) and malignant cells led to increased proliferation *in vitro*. This finding was consistent, regardless of the means by which senecence was initiated (*Ras* oncogene induced, hydrogen peroxide). Strikingly, pre-malignant ScP2 mouse mammary cells, which are non-tumorigenic, produced tumours when co-injected with senescent fibroblasts. Interestingly, Mellone and colleagues showed that a large proportion of senescent fibroblasts were α-SMA positive, and shared ultrastructural and contractile features with TGF-β transdifferentiated myofibroblasts, highlighting a close relationship between the two [93]. However, the transcriptomic profiles of senescent fibroblasts and classical myofibroblasts were different, particularly with regard to ECM genes, supporting the idea of heterogeneity, even within the α-SMA-positive CAF population.

1.2.2.1.5 Anti-tumour effects of CAFs

Recent evidence suggests that CAFs may have some anti-tumour effects. Ozdemir et al. crossed PKT mice, which faithfully progress from pancreatic carcinoma *in situ* (PanIN) to pancreatic ductal adenocarcinoma (PDAC), with *α-SMA-tk* mice, to produce a mouse which could be depleted of α-SMA positive fibroblasts, upon ganciclovir treatment [94]. α-SMA positive myofibroblasts were

depleted at both PanIN and PDAC stages, and in both cases, this led to an increase in invasive, undifferentiated, necrotic tumours. Furthermore, the overall lymphocytic infiltrate (including CD8+ cells) in the tumours was increased when myofibroblasts were depleted, but the frequency of permissive regulatory T cells, and expression of the immune checkpoint inhibitor, CTLA-4, was also increased. In keeping with this, Carstens and colleagues used tyramide signal amplification microarray on human PDAC tissue sections, to show that increased α-SMA positive fibroblast number does not correlate with low cytotoxic T cell number, suggesting that desmoplasia is not a physical barrier for T cells, as was previously thought [95]. Moreover, the CAF secretome includes several pro-inflammatory signals such as IFNγ and IL-6, which recruit anti-tumoral CD8+ T cells and NK cells [96]. The immune stroma is discussed below in more detail.

1.2.2.2 Mesenchymal stem cells

Mesenchymal stem cells (MSCs) are pluripotent stem cells, defined by their adherence properties, ability to differentiate into different cell types and surface markers (CD73, CD90, and CD105) [97]. As mentioned above, at least 20% of CAFs originate from MSCs, and recruitment is dependent on soluble factors, such as TGF-β and SDF-1, which CAFs typically express [62]. Cancer cells can also induce differentiation of MSCs to CAFs. For example, the exposure of human MSCs to conditioned media from MDA231 breast cancer cells stimulated expression of myofibroblast markers such as α-SMA [98].

Weinberg and colleagues marked the importance of MSCs in breast cancer metastasis [99]. In this study, MSCs were co-injected with weakly metastatic breast cancer cells, which significantly increased the metastatic potential of tumour xenografts. In this context, breast cancer cells are thought to provoke CCL5 secretion by MSCs, which then serves to increase their own motility, invasion and metastatic potential. Similarly, HS-5 human bone marrow stromal cells increased proliferation, migration, and invasion of Huh7 hepatocellular cancer cells *in vitro* [100]. These effects were attenuated by knocking down *CCL5*. Furthermore, there is evidence to suggest that MSC-derived CCL5 promotes EMT several other tumour types, including colorectal and gastric [101, 102]. In terms of clinical translation, the CCR5 receptor antagonist maraviroc was shown to reduce the total body burden of primary and secondary prostate tumours in mice [103]. This drug is now in human trials for advanced colorectal cancer (NCT01736813).

1.2.3 Immune cells

Immune cells in the TME can have pro- or anti-tumour effects. Tumour progression can be stunted or inhibited by immune surveillance, but established tumours and metastases have the ability to modify the TME in order to escape immunity [104]. The immune response produced by

M1 macrophages, T helper-1 cells, cytotoxic T cells, antigen presenting cells (APCs) and natural killer (NK) cells supports tumour rejection; whereas, M2 macrophages, regulatory T cells, and T helper-2 cells support tumour progression [105] (**Figure 1-2**).

1.2.3.1 T-lymphocytes

1.2.3.1.1 Cytotoxic T cells

CD8+ T cells bind to 'non-self' antigens presented by host major histocompatibility complex (MHC) class 1 molecules through the T cell receptor, triggering apoptosis in host cells, including cancer cells [106]. High levels of CD8+ tumour-infiltrating lymphocytes (TILs) have been shown to predict better outcomes in various cancers such as melanoma, ovarian, colorectal, breast and head and neck [107-111].

The initial approach in harnessing the anti-tumour effects of TILs was adoptive T cell therapy, which was trialled for several years in advanced melanoma. Here, patients were lymphodepleted by cytotoxic chemotherapy, then given autologous TILs, which had been isolated from the tumour and expanded *in vitro*. In the study by Rosenberg et al, 9 of 15 patients showed regression of their melanoma burden, lasting in some cases for over a year [112]. In a similar study nearly 20 years later, 18 of 35 patients showed objective clinical or radiological responses, with a mean duration of one year. Persistence of CD8+ cells after transfusion determined the degree of efficacy in this study [113]. Nonetheless, this clearly shows that efficacy of standard adoptive T cell transfer did not improve in this time frame.

Genetic modification of T cells to express a specific T cell receptor or chimeric antigen receptor (CAR), has been the focus of T cell therapy in the past decade, and offers a potentially curative treatment for patients with advanced cancers [114, 115]. In fact, the US Food and Drug Administration (FDA) has recently approved CAR T cell therapy for refractory or relapsing B cell acute lymphoblastic leukaemia and diffuse large B cell lymphoma. It was Gross and colleagues, nearly 30 years ago, who were the first to demonstrate the feasibility of engineering T cells to express T-cell receptor constant domain (typically the zeta chain of CD3) fused to a specific antibody variable region. This endows "antibody-like" specificity to T cells, which are still able to produce a functional effector response through the T cell receptor. However, first generation CAR T cell therapy was largely unsuccessful because the activated T cells became anergic, or underwent activation-induced cell death in the absence of a second, co-stimulatory, signal [116]. Second generation CARs were designed with CD28 or 4-1BB co-stimulatory domains to overcome this, and allow clonal expansion of effector T cell when confronted with antigen [117, 118]. CD19 CAR T cells, targeting B cells, have shown the greatest success in large clinical trials for B cell

malignancies but smaller reports have shown efficacy of CAR T cells in solid tumours such as glioblastoma and pancreatic cancer [119-122].

1.2.3.1.2 Immune checkpoints

Immune checkpoints are important regulators of CD8+ and Treg cell activity. In the cancer setting, a vast number of new antigens are generated. To prevent autoimmunity, immune checkpoints are activated to dampen pro-inflammatory T cell responses, at the cost of allowing immune escape of cancer cells [123]. The most well-known immune checkpoints are cytotoxic T lymphocyte-associated protein-4 (CTLA-4) and programmed cell death protein-1 (PD-1). CTLA-4 mainly prevents co-stimulation of the CD28 receptor and represses early activation of CD8+ T cells, predominantly in lymphoid tissues [124]. PD-1 attenuates the later CD8+ response, mainly in peripheral tissues [125]. In their seminal work, Allison's group transfected CRC cells with B7-1 (CD80), a co-stimulatory molecule for CD28, and injected them into Balb/c mice. Treatment of mice with anti-CTLA-4 antibodies induced tumour rejection, more than that observed with anti-CD28 antibodies, which was sustained on repeat exposure to tumour cells [126].

The introduction of immune checkpoint inhibitors in the treatment of metastatic melanoma has been greeted with a great deal of enthusiasm. An important phase 3 trial of advanced melanoma patients showed that the CTLA-4 inhibitor, ipilimumab, significantly improved overall survival with or without co-administration of the melanoma antigen gp100 [127]. In a more recent randomised controlled trial, the PD-1 inhibitor nivolumab, as monotherapy or in combination with ipilimumab, effectively improved progression-free survival compared to ipilimumab monotherapy. As expected, in patients with PD-1 ligand (PD-L1) negative tumours, combination therapy was more effective than monotherapy [128]. Similarly, targeting PD-L1 with the monoclonal antibody atezolizumab has proved efficacious with tolerable side effects, in a phase 1 trial of metastatic melanoma, NSCLC and renal cell cancer, in patients with tumours expressing high total and high CD8+ T cell levels of PD-L1 [129]. Similar results were seen in a phase 1 trial of metastatic urothelial bladder cancer [130]. This drug is now in phase 2 studies for metastatic NSCLC (POPLAR trial) [131].

In CRC, mismatch repair deficiency is associated with a high somatic mutational burden. This generates greater numbers of neoantigens, necessitating enhanced checkpoint inhibition. Le et al. conducted a phase 2 trial of the PD-1 inhibitor pembrolizumab (FDA-approved for melanoma and NSCLC; [132, 133]) in patients with mismatch repair deficient and proficient metastatic cancers. Patients with mismatch repair deficient tumours responded better to PD-1 inhibition, providing proof of principle for this concept [134].

1.2.3.1.3 Regulatory T cells

Tregs are CD4+/ CD25+ T cells, specifically expressing FoxP3, which are capable of suppressing the effects of other immune cells [135, 136]. Several studies have shown that high numbers of intratumoral Tregs are associated with advanced stage or recurrence, in various malignancies including ovarian, breast, oesophagogastric and liver [137-140]. Specific targeting of Tregs has shown promise in animal and early human studies. For example, mice bearing a renal cell carcinoma were given anti-CD25 monoclonal antibody against Tregs and inoculated with pre-primed CD8+ T cells. At day 50, tumours were undetectable in all the mice. In contrast, untreated mice, or mice treated with either CD8+ T cells or anti-CD25 did not survive [141]. Rech et al. repurposed the anti-CD25 monoclonal antibody daclizumab (FDA-approved for prophylaxis of organ rejection) to the same effect [142]. As well as downregulating Tregs, daclizumab was shown to reprogram them to express the pro-inflammatory cytokine interferon-gamma (IFN-γ) *in vitro*. Translating these findings to a small phase 1 study of metastatic breast cancer patients, daclizumab reduced Treg numbers within one week, a phenomenon which lasted for at least seven weeks. Samples from all evaluable patients showed greater CD8+ T cell response to at least one tumour antigen (hTERT peptide) after daclizumab treatment and vaccination. However, when comparing cohorts who received daclizumab plus vaccination, or vaccination alone, although immune response rate and overall survival was greater in the combination cohort, this was not statistically significant [142].

The PI3K-Akt pathway is an important regulator of Treg activity. Selective inhibition of the PI3Kδ isoform has been shown to repress AKT activation and proliferation of Tregs *in vitro* and *in vivo*, whilst conserving a conventional population of CD4+ T cells [143]. Similarly, Ali and colleagues knocked down PI3Kδ in mice and showed reduction in primary tumour growth in melanoma, lung, thymoma and breast xenografts, and reduction of metastasis when 4T-1 breast cancer cells were injected systemically. Knockdown mice had reduced numbers of Tregs in draining lymph nodes when injected with 4T-1 cells, and allogenic Treg transfer from one knockdown animal to another upregulated intratumoral CD8+ T cells in the thymoma model. Furthermore, pharmacological inhibition of PI3Kδ with PI-3065 had similar effects to knockdown in the breast cancer model and improved survival in a pancreatic cancer model [144].

1.2.3.1.4 Helper T cells

There are several classes of CD4+ Th cells but Th1 and Th2 are functionally prominent in cancer progression [145]. Th1 cells are necessary for the activation and persistence of CD8+ cells. Indeed, intravenous injection of antigen-specific Th1 cells induced CD8+ cell-mediated tumour regression in a fibrosarcoma model [146]. In murine B cell lymphoma and myeloma models of successful

immunosurveillance, Th1-associated cytokines (IL-2, IL-12 and IFNγ) were consistently identified in implanted tumour-Matrigel plugs [147]. The role of Th2 cells is less clear but in patients with renal carcinoma and melanoma, circulating CD4+ cells display Th2-polarized (IL-5) responses to MAGE-6 epitopes in active disease, and Th1-polarised (IFNγ) responses in remission [148]. Similarly, CD4+ cells from patients with stage I renal carcinoma showed predominantly Th1-polarised responses to EphA2, whereas CD4+ cells from later stages showed progressively more Th2-polarised responses [149]. Overall, the presence of Th2 cells marks poor prognosis compared to Th1 cells.

1.2.3.2 Antigen-presenting cells

APCs process foreign antigens and present them alongside MHC I or II molecules to naïve CD8+ and Th cells, respectively. Professional APCs such as dendritic cells, macrophages and B cells are so named because they process and present antigens most effectively. Fibroblasts are an example of non-professional APCs, which do not constitutively express MHC II, but can stimulate T-cells by expressing IFN-γ [150].

APCs from the TME of rat colonic carcinoma did not stimulate CD8+ cells as well as non-tumour APCs [151]. This was attributed to a lack of co-stimulatory factor B7, suggesting that cancer cells make APCs functionally deficient. Human renal and pancreatic cancer cell lines express IL-6 and macrophage colony stimulating factor, which alter the differentiation of APCs from CD34+ to CD14+ progenitors. CD14+ cells express little MHC II and cannot evoke a significant immune response, thereby lacking APC function and allowing tumour escape [152, 153]. Furthermore, in the presence of malignant cells, APC progenitors differentiate into immature myeloid-derived suppressors [154] and M2 macrophages (see below) [155], both of which are immunosuppressive.

In terms of cancer therapy, APCs have been used to improve the efficacy of adoptive T cell transfer. The ideal adoptive treatment will use T cells which proliferate, persist, target and destroy tumour cells [156]. Autologous and artificial APCs have been used to this effect, however the use of autologous APCs is cumbersome and time consuming [157]. Artificial APCs have been generated using Drosophila cells, murine fibroblasts and K562 human leukaemic cells [158-160]. The overarching principle is to produce a cell which expresses restricted HLA antigens in combination with transfected co-stimulatory molecules such as ICAM-1 (CD54) and B7.1 (CD80). Alternatively, magnetic beads embedded with HLA antigens and HLA expressing extracellular vesicles have been employed instead of feeder cells in the experimental setting [161, 162]. More recently, Butler and colleagues transfected K562 cells with HLA-A2, CD80 and CD83, to produce aAPC-A2 cells, which were used to expand autologous MART-1 specific CD8+ T cells from PBMCs *ex vivo*. MART-1 T cells were then given to patients with advanced melanoma. This therapy has

the benefit of not requiring lymphodepletion or IL-2 treatment, and consequently, there were no severe adverse effects [163].

1.2.3.3 Macrophages

Macrophages are phagocytic cells that play a critical role in innate and adaptive immunity. Classical M1 polarisation (IL-12^{high}/ IL-10^{low}) is associated with tumour rejection, whereas alternative M2 polarisation (IL-12^{low}/ IL-10^{high}) is associated with tumour progression [164, 165]. Tumour-associated macrophages (TAMs) are a mixed population of M1 and M2 cells, although some suggest that they generally possess the M2 phenotype, because they are incapable of activating sufficient nitric oxide and pro-inflammatory cytokine responses to tumour cells [166, 167]. Furthermore, TAMs are associated with Treg activation, PD-L1-mediated checkpoint activation, angiogenesis and invasion [137, 168-170]. In terms of their cytokine-independent effects, TAMs have been shown to promote endothelial recruitment and angiogenesis via the release of adrenomedullin in melanoma [171]. In another study, TAMs directly enhanced the invasiveness of SKBR3 breast cancer cells by exporting miR-223 in extracellular vesicles [172].

Many studies have shown that stromal TAMs predict poor prognosis in cancers such as lung, endometrial, thyroid and breast [110, 173-175]. Indeed, a recent meta-analysis of stromal TAMs in cancer prognosis showed worse overall survival in gastric, urogenital and head and neck cancers but surprisingly, a better overall survival in colorectal cancer [176].

In order to selectively target TAMs, Luo et al. produced a DNA vaccine against legumain, a stress protein which TAMs overexpress [177]. In the prophylactic group, pulmonary metastases from intravenously injected breast, colon and NSCLC cells were significantly reduced following vaccination. In the therapeutic group, overall survival was significantly better if animals were vaccinated after orthotopic injection of breast cancer cells. Moreover, the survival of TAMs is dependent on colony stimulating factor receptor-1 (CSFR-1). Ries and colleagues blocked CSFR-1 dimerization with a novel monoclonal antibody, RG7155 (emactuzumab). *In vitro*, this resulted in cell death of TAMs. *In vivo*, this led to reduction of TAMs with an associated increase in CD8+ T cells, and was associated with less tumour growth in animal models of colorectal cancer and fibrosarcoma [178]. In a small phase 1 study, administration of this agent led to at least a partial metabolic response in all seven patients with diffuse-type giant cell tumour [178]. More recently, Cassier et al. reported an objective response in 24 of 28 patients with similar tumours [179].

1.2.3.4 Natural killer cells

NK cells are innate immune cells, which are able to directly kill tumour cells in several different *in vitro* and *in vivo* cancer models, by detecting cell surface changes such as reduced MHC I [180,

181]. NK cells express the death ligands FasL and TRAIL which bind to Fas and DR5 receptors on target cells to trigger apoptosis [182]. Alternatively, NK cells express CD16 which mediates antibody dependent cell-mediated cytotoxicity [183, 184]. Additionally, NK cells select out APCs which do not express MHC I sufficiently, thereby maintaining a pool of APCs which are best equipped to present foreign antigens [185].

However, MHC class 1 molecules on tumour cells are able to bind killer inhibitory receptors on NK cells to dampen their cytotoxic effects [186]. Furthermore, NK-mediated immunity is reduced by tumour-secreted cytokines such as TGF-β [187]. For example, NK cells isolated from triple negative breast cancers exhibited less antibody-mediated cytotoxicity, a phenomenon that was reversed by addition of the pro-inflammatory IL-2/IL-15 complex [188]. In contrast to this, microarray analysis of intratumoral NK cells from NSCLC patients showed upregulation of pro-cytotoxic genes (NKp44, granzyme-A and -B), compared to extratumoral NK cells [189]. To explain this, the authors propose that NK cells are activated but functionally exhausted in the tumour setting. Thus, the activity, rather more than the presence of NK cells, may determine better prognosis in cancer.

NK cell immunotherapy has been popular in several recent human studies, the majority of which concern haematological malignancies, and are summarised by Eguizabal et al. [190]. Different methods of enhancing NK activity include in vivo cytokine stimulation and adoptive transfer of *ex vivo*-stimulated autologous or allogenic NK cells. Early phase 2 studies used IL-2 to stimulate resident NK cells, and proved to be effective in metastatic melanoma and metastatic renal cell carcinoma [191, 192]. However, this was associated with severe side effects including sepsis-related mortality. In terms of adoptive therapy, Ishikawa et al. conducted a small phase 1 study with malignant gliomas [193]. Peripheral blood mononuclear cells (PBMCs) were isolated from each patient and NK cells were expanded *ex vivo* using IL-2. Autologous NK cells were then injected into the tumour cavity and/ or intravenously in a total of 16 courses. MRI showed partial responses after three of the 16 courses. Importantly, there were no significant neurological side effects. Another phase 1 study in patients with NSCLC used allogenic NK cells from donor relatives, expanded *ex vivo* with IL-15 and hydrocortisone. There was partial response in 2 of 16 patients and disease stabilization in 6 patients. Again, there were no local or systemic side effects [194]. Infusion of the cell line NK-92 has also proved to be well tolerated in patients with a range of advanced malignancies with a persistence of at least 48 hours [195]. The requirement to generate large numbers of NK cells for immunotherapy has now driven research into NK cell production from embryonic stem cells [196].

1.2.3.5 Neutrophils

Neutrophils are myeloid cells of the innate immune system, which are critical first responders against infection. In the healthy state, they are the most numerous immune cell, but for a long time, neutrophils were thought to be passive by-standers in cancer, mainly because of their short half-life (seven hours in humans) [197]. However, more recent studies suggest that paracrine signalling from cancer cells prolongs neutrophil survival in the TME, and it was shown *in vivo* that neutrophils persist longer in tumours than in the spleen [198, 199]. The literature provides as many studies supporting the role of neutrophils in tumour progression as it does in tumour rejection. However, there is a consensus in the field that neutrophil to lymphocyte ratio (NLR) is increased in cancer patients [200]. Use of this as a prognostic marker is limited because baseline neutrophil counts vary so much between individuals, in response to therapy (steroids, cytotoxic drugs), and due to other co-morbidities. Nonetheless, there has certainly been more attention paid to neutrophils in the TME, in recent years.

Malanchi's group used the MMTV-PyMT spontaneous breast cancer model to show that $CD11b^{+}Ly6G^{+}$ neutrophils were recruited to the lungs prior to metastasis, and that their numbers increased upon metastatic colonisation [201]. In *Gcsf* knock out mice (neutropenic), there was significantly less metastasis, without altering size of the primary tumours. Of note, there was no depletion of macrophages in the metastatic lungs by this approach. Similar results were obtained with MMTV-PyMT mice crossed with neutrophil elastase-Cre and ROSA-Flox-STOP-Flox diphtheria toxin, which were specifically deficient in neutrophils.

De Visser's group proposed that neutrophils dampen CD8+ T cell response to tumours. In their model, they orthotopically injected spontaneous mammary tumours from KEP mice into wild type mice, which faithfully resulted in lung metastasis [202]. Treatment with Ly6G antibodies did not affect primary tumour growth but markedly reduced lymph node and lung metastases, demonstrating the importance of neutrophils in the metastatic process. Furthermore, they discovered that γδ T cells produced IL-17, which led to marked G-CSF-dependent recruitment of neutrophils. Strategies to neutralise IL-17 or deplete γδ T cells, significantly reduced lung metastasis.

Currently, there are phase 1 and 2 trials in metastatic breast cancer using the agent reparixin, a noncompetitive allosteric inhibitor of CXCR1 and CXCR2 chemokines, which is thought to prevent migration of neutrophils to tumours [203]. Other strategies include IL-17 and G-CSF neutralisation, but the neutropenia induced by such strategies may lead to profound and intolerable infections.

1.2.4 Vascular cells

The stromal vasculature is made up of a capillary network of ECs surrounded by pericytes that provide structural and physiological support. It is well established that hypoxia limits tumour progression, resulting in VEGF-mediated angiogenesis [38].

1.2.4.1 Pericytes and endothelial cells

In healthy tissue, pericytes intimately cover ECs, and through the expression of VEGF and angiopoetin-1 they lead to increased EC survival and structural stabilisation [204]. Reciprocally, ECs express PDGF-B, and recruit pericytes from the stroma [205]. In a tumour, tissue hypoxia and subsequent upregulation of pro-angiogenic factors such as VEGF and angiopoetins, has the effect of loosening connections between pericytes and ECs [206]. Ultimately, pericytes detach completely and this allows a disordered budding of new capillaries which underlies angiogenesis [207]. PDGFR antagonists, targeting pericytes, have been shown to stunt growth of end stage pancreatic islet cell tumours in mice [208]. However, the beneficial effect on the primary lesion seems to be at a cost. Kalluri and colleagues have shown that inhibiting pericytes in an invasive breast cancer model has two detrimental effects. Firstly, it reduces pericyte coverage of ECs which correlates directly with metastasis, and secondly, it aggravates tissue hypoxia, which drives the EMT/ mesenchymal-epithelial transition (MET) cascade [209]. Given this evidence, it seems prudent not to target pericytes but to focus on their downstream angiogenic signals.

It is well established that hypoxia develops as a tumour expands and that its size is limited without neovascularisation or angiogenesis. Folkman et al. first reported that a soluble factor, now known as VEGF, was responsible for angiogenesis [38]. VEGF is released by pericytes and binds to VEGFRs on ECs, which become the tip of a sprouting chain. The tip migrates towards the highest VEGF concentration which is present in the most hypoxic regions of the tumour. ECs which lie behind the tip bind to each other through surface ligand-receptor interactions and form a new capillary [210].

Several monoclonal antibodies have been developed to target VEGF-driven angiogenesis. Bevacizumab, targeting VEGF-A, is the most well-known amongst these. It received US FDA approval in 2004 for use in metastatic colorectal cancer, in combination with standard chemotherapy [211]. Since then it has been used in advanced NSCLC, renal, ovarian and cervical cancers, supported by evidence from large phase 3 studies [212-215]. However, there are a certain group of patients who do not respond to treatment, or develop resistance [216]. Fan et al. showed that long term exposure (three months) of CRC cell lines to bevacizumab, led to increased expression of VEGF-A, B and C, increased phosphorylation of VEGFR-1 and -2, increased invasion

and migration, and increased metastasis when injected *in vivo* [217]. Moreover, VEGF inhibition has mostly had clinical success in combination with traditional chemotherapy, possibly because it normalises stromal vessels and allows better drug delivery [218]. Nonetheless, anti-VEGF agents are still being developed. For example, the VEGFR-2 monoclonal antibody ramucirumab is licensed for use in advanced gastric cancer after phase 3 trials showed survival benefit as a single agent (REGARD trial; [219]) and in combination with paclitaxel (RAINBOW trial; [220]).

Another class of anti-angiogenic drugs are the VEGF/ PDGF-receptor tyrosine kinase inhibitors which have shown significant response in several phase 3 trials. These drugs inhibit tyrosine kinase receptors from activating intracellular serine/ threonine kinases such as Raf. As a result, there is reduced proliferation and angiogenesis [221]. Sorafenib is an oral multi-kinase inhibitor which is approved for use as monotherapy in advanced renal cell, hepatocellular and thyroid carcinomas. The first large phase 3 study of sorafenib monotherapy in 2007, showed increased progression free survival compared to placebo in advanced renal cell carcinoma [222]. Another randomised controlled trial showed an increase in overall survival and time to radiological progression in advanced hepatocellular carcinoma [223]. Most recently, an increase in progression free survival has been shown in radioactive iodine-refractory differentiated thyroid cancer [224].

Whereas anti-angiogenic anti-cancer drugs target new vessel formation, vascular damaging agents (VDAs) target existing vessels, causing ischaemia and haemorrhagic necrosis of the tumour [225]. There are two classes of VDAs: small molecule microtubule targeting drugs and ligand based drugs. Small molecule agents exploit differences between tumour and normal vessels such as greater proliferation and reliance on a cytoskeleton. Ligand based drugs target proteins such as VEGF-receptors which are overexpressed in tumour vessels [226]. Fosbretabulin (CA4P) is an example of a small molecule VDA, which binds to tubulin, causing microtubule depolymerisation [227]. CA4P has reached phase 2 trials for advanced anaplastic thyroid carcinoma and relapsed ovarian carcinoma [228, 229].

An interesting ligand-based approach is to fuse toxins to stromal vascular ligands. Rosenblum's group constructed the fusion molecule VEGF(121)/rGel which combines a VEGF ligand with the plant toxin gelonin [230]. This has shown promise in reducing tumour growth in animal models of bladder, metastatic breast and metastatic prostate cancer [230-232].

Reduced oxygen tension in the TME leads to upregulation of hypoxia inducible factors (HIFs) by ECs [233]. HIF-1 regulates EC proliferation and HIF-2 causes EC senescence [234, 235]. Branco-Price and colleagues showed that there was slower migration of tumour cells through HIF-1α deficient EC layers, and reduced metastasis in HIF-1α deficient mice. HIF-2α deletion has the

opposite effects [236]. Consequently, digoxin has been found to inhibit HIF-1α [237]. It is currently in a phase 2 study which aims to assess tissue HIF1α levels in resected breast cancers after 2 weeks of digoxin pre-treatment (NCT01763931).

1.2.5 Extracellular matrix

The ECM constitutes the cellular scaffold of the TME, providing structural support to tumour and stromal cells. It is produced by mesenchymal cell types including fibroblasts, chondrocytes and osteoblasts, and comprises proteoglycans (e.g. hyaluronan, versican) and fibrous proteins (e.g. collagen, elastin, fibronectin, laminin, periostin, tenascin-C) [238, 239]. The ECM is biologically active and plays a role in cellular adhesion, migration, proliferation and survival [240].

In the cancer setting, fibroblasts express vast amounts of ECM proteins, leading to tissue stiffening [241]. Paszek and colleagues suggested that matrix stiffness is an exogenous force whilst Rho-dependent cytoskeletal tension is an endogenous force on cancer cells. The summation of these forces results in clustering of integrins and activation of ERK and Rho-associated kinase signalling which leads to increased proliferation and contractility, respectively [242]. Furthermore, the inflammatory reaction in the TME triggers desmoplasia, characterised by dense deposition of ECM components, such as collagen [243]. Desmoplasia was first linked with poor cancer outcomes over 20 years ago, and is most commonly associated with pancreatic cancer [244, 245]. Additionally, MMPs expressed by stromal and epithelial cells remodel the ECM, particularly the basement membrane [246]. The combined ECM effects of stiffness, reciprocal contractility, desmoplasia and barrier function, are important in tumorigenesis and cancer progression. Below are outlined some key ECM constituents.

Type IV collagen is a major component of the basement membrane, and possibly the most important protein in the ECM, separating cancer from stroma [247]. Type IV collagen binds to integrin receptors on cancer cells, particularly in desmoplastic tumours such as pancreatic carcinoma, promoting their survival [248]. Galectin-1 is a carbohydrate binding protein with several important effects on cancer cells, namely, adhesion to the ECM, increased migration, and stromal immune suppression [249]. Proteoglycans such as heparan sulfate maintain the physical connections between different ECM components [250]. Indeed, salivary gland tumours expressing more heparanase are associated with poorer survival [251]. Glycoproteins such as fibronectin and laminin-1 are ligands for β-integrins, cellular proteins which mediate cell-ECM signalling [252]. ECM expression of fibronectin and laminin-1 correlates with poor prognostic features in breast cancer [253]. In fact, in a three-dimensional breast cancer model, inhibition of fibronectin-$\alpha_v\beta_1$ binding prompted apoptosis and greater radiosensitivity [254].

Hyaluronan is associated with a permissive TME [255]. The dense hyaluronan matrix surrounding cancer cells makes it difficult for chemotherapeutic drugs to penetrate. This is a particular problem for monoclonal antibody therapy, because it prevents antibody directed cell-mediated cytotoxicity by NK cells. Singha et al. showed that co-administration of recombinant hyaluronidase with the monoclonal antibody traztuzumab and NK cells, significantly reduced tumour growth in ovarian cancer xenografts [256]. Recombinant hyaluronidase (PEGPH20) has been successfully profiled for safety in phase 1 trials in advanced pancreatic cancer [257]. There is currently an ongoing phase 2 trial of PEGPH20 in untreated stage 4 pancreatic carcinoma in combination with paclitaxel and gemcitabine (NCT01839487).

The matricellular protein periostin is a ligand for $\alpha_v\beta_3$ and $\alpha_v\beta_5$ integrins on epithelial cells, promoting cell motility [258]. Underwood et al. showed that periostin is associated with poor overall survival and disease-free survival in oesophageal adenocarcinoma [259]. Additionally, periostin was shown to be secreted by CAFs, and had the effect of activating the Akt survival pathway in oesophageal cancer cells. Periostin is upregulated in colorectal primary and secondary tumours [260]. *In vitro*, periostin was shown to directly increase proliferation of several colorectal cancer cell lines. This effect was attenuated by addition of a periostin-specific antibody, which triggered cancer cell apoptosis, and worked synergistically with 5FU. Animal studies have shown that MZ-1, a monoclonal antibody to periostin, can reduce growth and metastatic potential of A2780 ovarian cancer xenografts [261].

Decorin was shown to be differentially expressed in the tumour mass of malignant angiosarcomas compared to benign haemangiomas [262]. Grant et al. transfected sarcoma and carcinoma cell lines with decorin. These cells produced significantly less VEGF than their wild type counterparts. Conditioned media from the transfected cells reduced EC attachment, migration and differentiation. *In vivo*, decorin transfected xenografts were smaller and showed less neovascularisation [263]. Furthermore, Xu et al. created an oncolytic adenovirus carrying the decorin gene (Ad.dcn) which significantly reduced bony metastases in a murine prostate cancer model [264].

Tenascin-C is preferentially expressed by various tumours [265]. Monoclonal antibody therapy with 81C6 has reached phase 2 trials in patients with malignant gliomas, showing favourable efficacy when compared to brachytherapy or radiosurgery [266]. In this study, 33 patients had injection of radioiodine-labelled 81C6 to cerebral resection cavities followed by standard chemoradiotherapy. Median survival was better in this cohort than in historical controls receiving standard treatment. An alternative to antibody therapy is the use of RNA interference (RNAi) to downregulate tenascin-C. In one human study, double stranded RNA targeting tenascin-C (ATN-

RNA) was injected into the resection cavities of nearly 50 patients with malignant brain neoplasms, and showed survival benefit in astrocytomas and glioblastomas [267].

The key enzymes regulating ECM turnover are MMPs and tissue inhibitors of metalloproteinases (TIMPs). MMPs are zinc-dependent endopeptidases, capable of degrading almost all ECM proteins. Increased MMP expression is associated with most tumours [268]. Traditionally, it was thought that cancer cells secreted MMPs in order to digest the ECM and permit invasion [269]. We now know that MMPs are secreted by both tumour and stromal cells, and are important in other aspects of cancer progression such as angiogenesis and metastasis [270, 271]. TIMPs negatively regulate MMP activity. TIMP-3 is most specific to the ECM [272]. When breast cancer and ocular melanoma cell lines were transfected with TIMP-3 and injected into nude mice, tumour growth was significantly reduced [273]. Methylation of the *TIMP-3* gene promoter is the mechanism by which TIMP-3 is inactivated in cancer [274]. TIMPs are not simply MMP inhibitors. TIMP-3 for example, prevents VEGF from binding to VEGFR-2, thereby inhibiting angiogenesis [275].

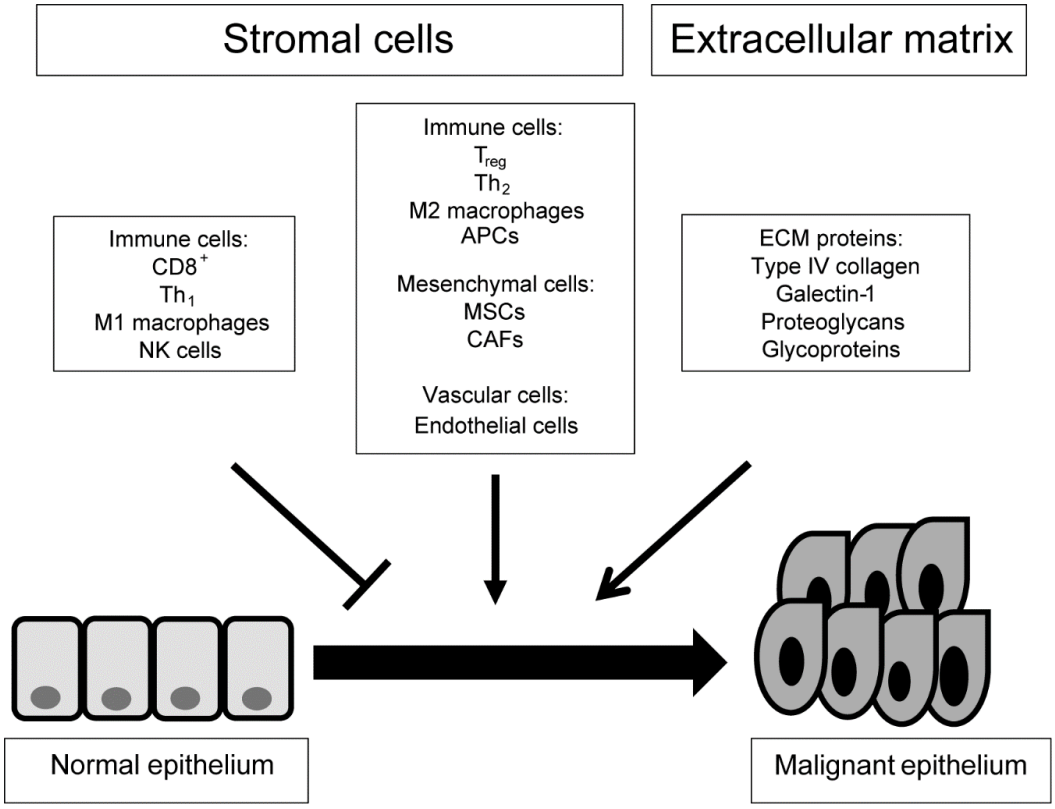

Figure 1-2. Stromal players in cancer progression. Cellular and acellular components of the stroma and their contribution to tumour development and progression. ECM, extracellular matrix; APC, antigen presenting cell; NK, natural killer; T_{reg}, regulatory T cell; T_h, helper T cell; CAF, cancer-associated fibroblast; MSC, mesenchymal stem cell. From *Bhome et al.(2015)* [47].

1.2.6 Summary

For a long time, Paget's theories about the “soil” remained in the shade and ignored [37]. In recent years however, there has been a focus of research efforts in this field, simultaneously bringing to light a variety of stromal-directed therapeutic strategies. The appeal of the stromal TME is its genetic stability and reduced likelihood of Darwinian emergence of resistance, as seen in cancer cells. Moreover, stromal-directed therapy offers two key benefits. Firstly, it creates an arid “soil”, making it more difficult for a tumour to establish at both primary and secondary sites. Consequently, it may reduce the required doses of traditional cytotoxic chemotherapeutic drugs. **Table 1-3** summarises stromal-directed therapeutics in solid cancers.

Table 1-3. Stromal directed therapies in solid cancers: a summary of clinical trials.

Target	Therapy	Mechanism	Phase	Cancer type	FDA Approval	Reference(s)
CAF	Beta-amino-propionitrile	LOX inhibitor	Pre-clinical	Breast		Levental et al., 2009 [76]; Bondareva et al., 2009 [80]
	Brivanib	FGF/ VEGF receptor antagonist	Phase 3	Hepatocellular		Kudo et al., 2014 [276]
	Pirfenidone	Antifibrotic	Pre-clinical	Pancreatic		Kozono et al., 2013 [277]
MSC	Maraviroc	CCR5 antagonist	Phase 1	Colorectal		NCT01736813
CD8+ T cell	Autologous T cells	Adoptive T cell	Phase 2	Melanoma		Dudley et al., 2005 [113]
	TCR T cells	Adoptive T cell	Phase 1/2	Melanoma		Morgan et al., 2006 [114]
	CAR T cells	Adoptive T cell	Pre-clinical	Melanoma		Yvon et al., 2009 [115]
	Nivolumab	PD-1 inhibitor	Phase 3	Melanoma	Yes	Larkin et al., 2015 [128]
	Pembrolizumab	PD-1 inhibitor	Phase 2/3	Mismatch repair deficient tumours; Melanoma; NSCLC	Yes (melanoma; NSCLC)	Le et al., 2015 [134]; Robert et al., 2015 [132]; Garon et al.,2015 [133]
	Ipilimumab	CTLA-4 inhibitor	Phase 3	Melanoma	Yes	Hodi et al., 2010 [127]
	Atezolizumab	PD-L1 inhibitor	Phase 2	NSCLC		Fehrenbacher et al., 2016 [131]
Treg	Daclizumab	CD25 mAb	Phase 1	Breast		Rech et al., 2012 [142]
	PI-3065	PI3K delta inhibitor	Pre-clinical	Breast; Pancreatic		Ali et al., 2014 [144]
TAM	Emactuzumab	CSFR1 antagonist	Phase 1	Diffuse type giant cell tumour		Cassier et al., 2015 [179]
NK Cell	IL-2	Resident NK stimulation	Phase 2	Melanoma; renal		Atkins et al., 1999 [191]; Fisher et al., 2000 [192]
	Autologous NK cells	Adoptive NK	Phase 1	Glioma		Ishikawa et al., 2004 [193]
	Allogenic NK-92 cells	Adoptive NK	Phase 1	Various		Tonn et al., 2013 [195]
APC	Artificial aAPC-A2 cells	MART-1 T cell generation	Phase 1	Melanoma		Butler et al., 2011 [163]
EC/ Pericyte	Bevacizumab	VEGF receptor antagonist	Phase 3	Colorectal, NSCLC, renal, ovarian, cervical	Yes (all)	Hurwitz et al., 2004 [211]; Sandler et al., 2006 [212]; Escudier et al., 2007 [213]; Perren et al., 2011

Target	Therapy	Mechanism	Phase	Cancer type	FDA Approval	Reference(s)
						[214]; Tewari et al., 2014 [215]
	Ramucirumab	VEGF receptor antagonist	Phase 3	Gastric	Yes	Fuchs et al., 2014 [219]; Wilke et al., 2014 [220]
	Sorafenib	VEGF/ PDGF receptor inhibitor	Phase 3	Renal; hepatocellular; thyroid	Yes (all)	Escudier et al., 2007 [222]; Llovet et al., 2008 [223]; Brose et al., 2014 [224]
	Fosbretabulin	Small molecule VDA	Phase 2	Thyroid; Ovarian		Mooney et al., 2009; Zweifel et al., 2011
	VEGF(121)/rGel	Ligand-based VDA	Pre-clinical	Bladder; Breast; Prostate		Mohamedali et al., 2005 [231]; Ran et al., 2005 [232]; Mohamedali et al., 2006 [230]
	Digoxin	HIF-1 alpha inhibitor	Phase 2	Breast		NCT01763931 (clinicaltrials.gov)
Pericyte	SU6668	PDGF receptor	Animal	Pancreatic		Bergers et al., 2003 [208]
Hyaluronan	PEGPH20	Recombinant hyaluronidase	Phase 1b/ 2	Pancreatic		Hingorani et al., 2016 [257]; NCT01839487
Periostin	MZ-1	mAb	Pre-clinical	Ovarian		Zhu et al., 2011 [261]
Decorin	Ad.dcn	Oncolytic virus	Pre-clinical	Prostate		Xu et al., 2015 [264]
Tenascin-C	81C6	mAb	Phase 2	Glioma		Reardon et al., 2002 [266]
	ATN-RNA	RNA interference	Phase 1	Glioma		Wyszko et al., 2008 [267]

From *Bhome et al. (2016)* [31]

1.3 Exosomes

1.3.1 Background

There has been an exponential rise in exosome-related studies in the field of cancer biology (Fig. 1-3). This excitement was initially driven by exosomes as potential diagnostic and prognostic biomarkers [278-280] and has matured into an appreciation of the functional roles that exosomes play in processes such as pre-metastatic niche formation [281, 282], metastatic organotropism [283] and therapy resistance [284]. MicroRNAs (miRNAs) are small non-coding RNAs, referred to as master regulators of the genome [285-287], which are often dysregulated in cancer [288-292]. Their presence and intercellular transfer in exosomes has prompted deeper exploration of exosomal miRNAs (exomiRs), both as markers and signalling vehicles [46, 293-295]. We use the term “exomiRs” to describe miRNAs which are packaged, secreted and transferred between cells in exosomes. This is an emerging field and far less is known in comparison to exosomes in general (**Figure 1-3**). This section includes an introduction to exosome biology, postulated mechanisms for miRNA loading into exosomes, mechanistic roles of exomiRs in cancer progression and biomarker potential of exomiRs in several common cancers.

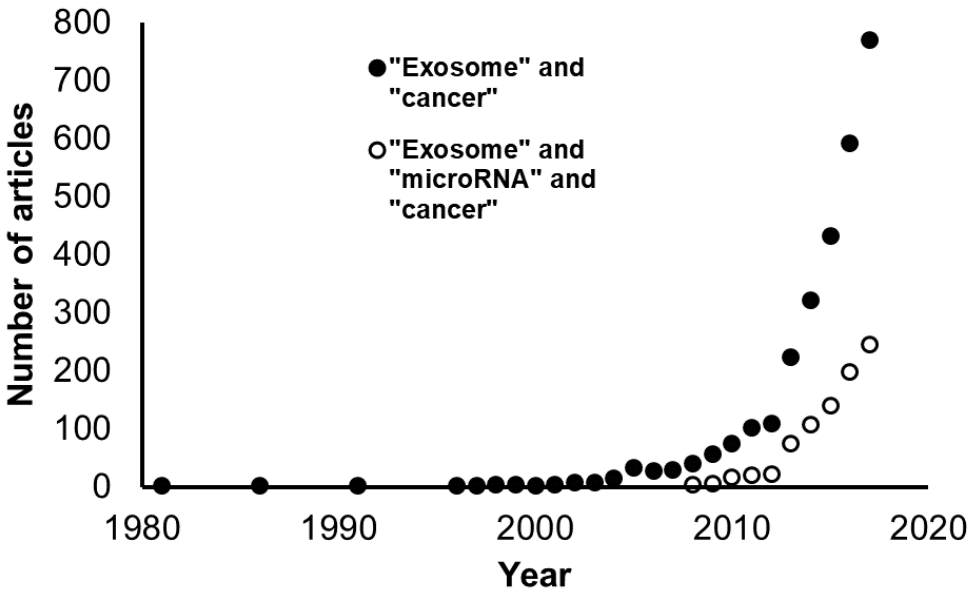

Figure 1-3. The rise in exosome research. Articles indexed by Pubmed over time containing search terms “exosome and cancer” and “exosome and microRNA and cancer”. From *Bhome et al. (2018)* [296].

1.3.2 Nomenclature

Exosomes are naturally occurring extracellular vesicles (EVs), ranging in size between 40-100 nm, with an endosomal origin [297]. However, the original definition by Trams and colleagues is much broader, encompassing all secreted vesicles with a biological function [298]. A technical definition is that exosomes are vesicles that sediment at 100,000 *g* [299]. The Lyden group recently subclassified smaller EVs, into large exosomes (90-120 nm) and small exosmes (60-80 nm), using asymmetric flow field-flow fractionation [300]. Interestingly, using this approach, they discovered even smaller non-membranous particles (~35 nm), termed exomeres. Larger vesicles (greater than 100 nm) have been labelled microvesicles [301] or microparticles [302], as vesicles which sediment at 10 000 *g*. Ectosomes, or shedding vesicles, are distinguished by their origin at, and outward budding from, the cell membrane [303]. These classes are not mutually exclusive, for example, microvesicles are ectosomes because they originate at the cell membrane [304]. Another level of complexity is added by naming vesicles according to their cargo, for example, "oncosomes", which contain oncogenic proteins [305]. Although the use of these different terms exists in the literature, the International Society for Extracellular Vesicles (ISEV) recommends use of the collective term "extracellular vesicles" (EVs) and strongly encourages researchers in the field to characterize their vesicles of interest by size, morphology and protein expression [306].

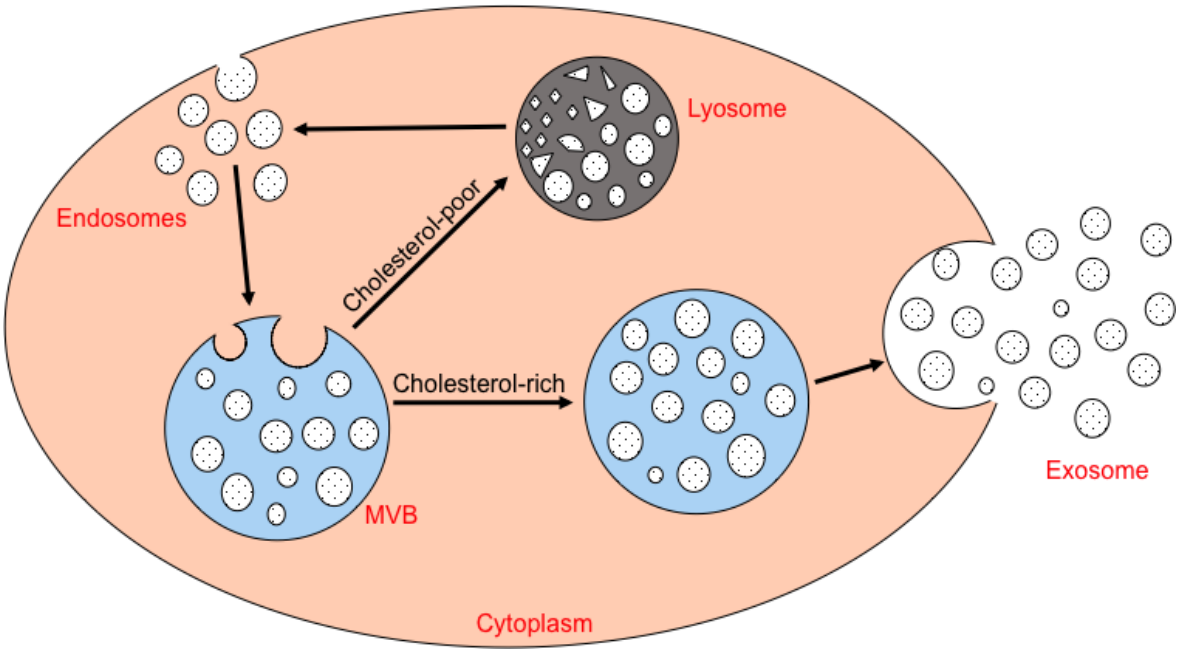

Figure 1-4. Exosomes: extracellular vesicles with an endosomal origin. Endosomes are packaged into MVBs, which are trafficked either to the cell membrane for secretion (cholesterol-rich) or to lysosomes (cholesterol-poor) for degradation. MVBs fuse with the cell membrane to release exosomes. From *Bhome et al. (2018)* [296].

1.3.3 Biosynthesis and trafficking

Exosomes were first described in 1981 as a by-product of reticulocyte maturation [298]. In the ensuing decades, exosomes were shown to be secreted by a large variety of different cell types, and we now believe that all cells produce exosomes [162, 307].

Exosomes are continuously released and recycled by cells. Through the process of endocytosis, exosomes re-enter cells, where they are called endosomes. Endosomes are packaged in multivesicular bodies (MVBs). MVBs rich in cholesterol are trafficked to the cell membrane where they fuse, and are released as exosomes, whilst those which are cholesterol deficient are recycled through lysosomes [308] (**Figure 1-4**).

Intracellular transport systems involved in MVB packaging are thought to be highly conserved, resembling vacuole transport in yeast. Endosomal sorting complex responsible for transport (ESCRT) proteins, such as ALIX and TSG101 are associated with this process [309]. ESCRT -0, I and II complexes recognize and sequester ubiquitinated membrane proteins at the endosomal membrane, and ESCRT –III is responsible for cutting and inward budding [310]. However, combined knock down of ESCRT -0, -I, -II and –III, still resulted in exosome production, suggesting that ESCRT-independent MVB packaging pathways exist [311].

Exosome release is thought to be dependent on intracellular calcium, Rab GTPases and SNARE proteins, although the precise coordination of events is unclear [312-314]. Rab11, Rab35 and Rab27a/b have been highlighted as key mediators of exosome release but it is still debatable whether they are redundant or whether any cell specificity exists [313, 315, 316]. Moreover, data suggest that SNAREs are important in the final interaction between MVB and cell membrane, based on our knowledge of lysosomal trafficking [314]. However, the specific complexes involved in this process are not thoroughly described.

Recipient cells take up exosomes by several mechanisms including endocytosis, micropinocytosis and phagocytosis. Endocytosis can be clathrin-mediated [317] or caveolin-dependent [318], and cholesterol-rich micro-domains in the cell membrane (lipid rafts) may facilitate this [319]. Micropinocytosis involves membrane invaginations which pinch off to draw extracellular content (e.g. fluid and exosomes) into the cytosol [320]. Phagocytosis of exosomes, which is more efficiently carried out by professional phagocytic cells, such as macrophages, is mostly PI3K-dependent [321]. Additionally, exosomes can directly bind to the recipient cell membrane and empty their contents [322].

Systemic injection of fluorescently labelled exosomes suggests that exosomes might be taken up non-specifically [323], but recent evidence suggests otherwise, for example, organotropic exosomes homing to specific sites by integrin-substrate interactions [283].

1.3.4 Isolation and characterisation

Exosomes are most commonly isolated from cell culture supernatant, blood or urine by differential ultracentrifugation (dUC), which involves sequential pelleting of contaminating cells (500*g*), cellular debris (2000 *g*), apoptotic bodies and microparticles (10 000*g*) and exosomes (100 000*g*) [299]. Alternatively, a combination of filtration and ultracentrifugation can be used [324]. More recently, techniques such as size exclusion chromatography (SEC) and Optiprep™ density gradient centrifugation techniques have emerged in an attempt to reduce contamination of exosome preparations with protein aggregates and smaller soluble proteins [325, 326].

The International Society for EVs (ISEV) has published recommendations for EV characterisation [306]. General characterisation is typically by detecting protein expression, where at least three EV markers (e.g. ALIX, TSG101, CD63, CD81) should be enriched. Characterisation of single vesicles by size is used to demonstrate the degree of heterogeneity in the sample. It is recommended that two techniques (e.g. electron microscopy, nanoparticle tracking analysis (NTA)) are employed to show the uniformity of size distribution [327, 328]. **Figure 1-5** shows exosome characterisation by electron microscopy and immunogold staining.

However, the exosome field is in flux, and regular updates to the recommendations are expected [329]. To help standardise techniques, Van Deun and colleagues have recently developed the EV-TRACK knowledgebase [330]. This enables authors to deposit methodological parameters (e.g. source of EVs, rotor type, centrifugal force, protein markers) into a central repository, in exchange for an EV metric, which quantifies the robustness of their protocol.

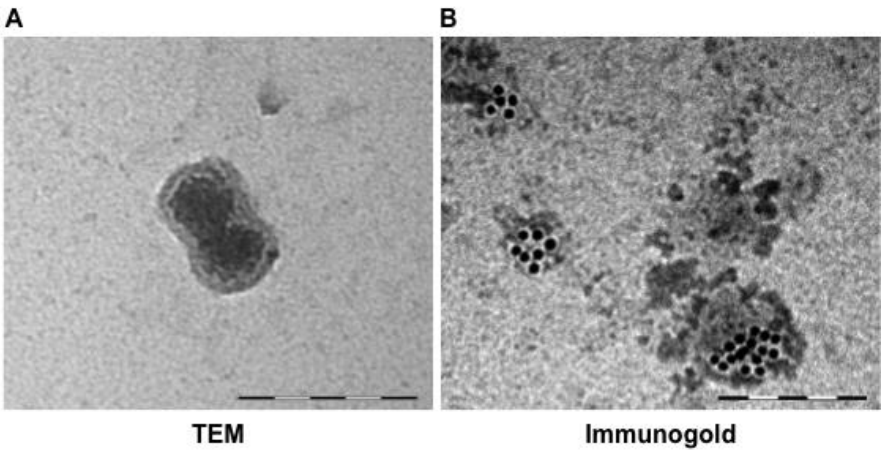

Figure 1-5. Size, morphology and expression profile characterise exosomes. (A) Transmission electron microscopy (TEM) of MRC5 fibroblast exosome (120 000x) demonstrating bi-layered structure. **(B)** Immunogold staining of primary mesenchymal stem cell exosomes with CD63. Scale bars in both panels represent 200 nm. From *Bhome et al. (2018)* [296].

1.3.5 Exosome-mediated RNA transfer

A major breakthrough in the field came in 2007, when it was shown for the first time that exosomes could transfer functional RNAs [46]. Valadi and colleagues isolated exosomes from MC/9 murine mast cells, and co-cultured them with HMC-1 human mast cells. Mouse-specific mRNAs and proteins were detectable in the human cells, suggesting that exosomes deliver mRNA, which can be translated by the recipient cell's machinery [46]. Interestingly, exosomes were found to contain large amounts of small RNAs, which were proven to be miRNAs. In the following years, transfer of miRNAs in exosomes has been demonstrated across multiple cell types [331-333].

1.3.6 Sorting of miRNAs into exosomes

1.3.6.1 Evidence for selectivity

Goldie and colleagues showed that despite exosomes containing proportionally less small RNA than whole cells, the small RNA fraction was enriched in miRNAs [334]. This was shown by Guduric-Fuchs and colleagues to be specific to a subset of miRNAs, suggesting a selective loading mechanism [335]. Other studies have shown that exomiR profiles differ between cancer patients and healthy controls, suggesting that pathophysiological changes can modulate this mechanism [336]. In keeping with this, *KRAS* status of cancer cells can determine their exomiR profile [337]. Proposed mechanisms for exomiR sorting are outlined below.

1.3.6.2 RNA-induced silencing complex (RISC)

In 2009, two back-to-back articles highlighted the physical and functional association between miRNA-associated RISC proteins and MVBs [338, 339]. Gibbings and colleagues separated conditioned medium from monocytes using Optiprep™ density gradient and showed that early fractions co-expressed MVB-associated markers and RISC proteins, specifically GW bodies (GW182, Ago2). This was confirmed using several combinations of immunofluorescent RISC-MVB markers [338]. Lee et al. knocked out Hsp4 in *Drosophila* with the effect of reducing MVB turnover [339]. MiRNA levels were significantly higher in Ago1 co-immunoprecipitates in these cells compared to wild type controls. These studies were the first to demonstrate the relationship between RISC and MVBs, raising the possibility that these proteins may be relevant in exomiR sorting.

1.3.6.3 Ceramide

Kosaka and colleagues were the first to show that exosomal miRNA content is regulated by ceramide [340]. In this study, the neutral sphingomyelinase-2 (nMase-2) inhibitor GW4869 was used to reduce ceramide biosynthesis in HEK293 cells. This resulted in a marked reduction in endogenous miR-16 and exogenous miR-146a in isolated exosomes. Although the nMase-2 inhibitor also reduced the quantity of cell-secreted exosomes, miRNA levels were still significantly lower after normalization. This was confirmed by knocking down and overexpressing nMase-2, which resulted in decreased and increased exomiR concentrations, respectively. Importantly, genetic modulation had no effect on cellular miRNA levels. NMase-2 inhibition has since been used in several studies as a tool for reducing exomiR concentration [333, 337]. It is worth mentioning that modulation of cell membrane constituents to alter exosome content should be viewed with caution. Exosomes are lipid-based vesicles, therefore, any step in their biogenesis, loading or uptake could be altered as a result of changes in cellular lipid homeostasis.

1.3.6.4 Sequence motifs and guide proteins

Using Jurkat cells, Villarroya-Beltri and colleagues discovered that 75% of exomiRs had a GGAG motif (extra seed sequence) at their 3' end [341]. By applying site-directed mutagenesis to this motif in the predominantly exosomal miR-601, and transfecting this into Jurkat cells, they reduced its concentration in exosomes. Conversely, mutagenesis of the predominantly cellular miR-17, to include GAGG, led to an increased exosomal concentration. Exosome preparations from primary T-cells were then pulled down using streptavidin beads biotinylated with either an exomiR (miR-198) or a cellular miRNA (miR-17) and subjected to mass spectrometry to identify exomiR-linked proteins. Heterogeneous nuclear ribonucleoprotein (hnRNP) A2B1 was precipitated by the exomiR

but not the cellular miRNA. Using electro-mobility shift assays, hnRNPA2B1 was shown to directly bind miR-198 but not mutant miR-198, or miR-17. Interestingly, the molecular weight of hnRNPA2B1 was found to be 10-12 kDa higher in exosomes compared to cells, and it was subsequently shown that this protein is sumoylated in exosomes.

Using a similar experimental approach on murine 3A hepatocytes, Santangelo et al. showed that miRNAs with a GGCU motif in their extra seed sequence bind to hnRNP-Q (also known as SYNCRIP) which guides them into exosomes [342]. Importantly, it was shown in this study that hnRNPA2B1 and hnRNP-Q bind selectively to miRNAs bearing respective GGAG or GGCU motifs, suggesting that there is sequence specific miRNA sorting into exosomes.

1.3.6.5 3’ end non-template terminal nucleotide additions

3’ end non-template terminal nucleotide additions were previously found to be important in miRNA-RISC interactions [343]. Koppers-Lalic and co-workers investigated their role in exomiR sorting in B cells [344]. By RNA sequencing, they found that exomiRs were significantly more likely to be uridinylated at their 3’ end, whereas cellular miRNAs were more likely to be adenylated. The same findings were replicated in urinary exosomes of healthy individuals, suggesting that this phenomenon is not limited to B cells. Furthermore, this sorting mechanism was also shown to apply to small cytoplasmic Y RNAs, and may be generalisable to other small RNAs.

1.3.6.6 Cellular levels of miRNAs and miRNA targets

De Palma’s group transduced *Dicer*$^{fl/fl}$ murine bone marrow-derived macrophages (BMDMs) with a Cre-expressing lentivirus to silence *Dicer* [345]. This disproportionately reduced exomiR levels compared to cellular miRNA levels. Conversely, overexpression of miR-511-3p, in immortalised BMDMs, led to a disproportionate increase in its exosomal levels. However, when artificial and naturally occurring (*Rock2*) target sequences complimentary to miR-511-3p were overexpressed in these cells, exosomal levels fell, suggesting that both cellular miRNA levels and miRNA targets determine exomiR sorting. To validate this, BMDMs were derived from *Lyz2.*Cre mice, which are deficient in lysozyme-2, a predicted target of the miRNA, miR-218-5p. As expected, their exosomes were shown to be more abundant in miR-218-5p, compared to wild type BMDMs. Therefore, cellular availability of miRNAs has to be considered as a factor which determines the abundance of exomiRs.

1.3.7 Functional roles of exomiRs in cancer progression

1.3.7.1 Receptor-mediated exomiR signalling

On the understanding that viral small RNAs bind toll-like receptors (TLRs) in immune cells [346], Fabbri and colleagues discovered that exomiRs bind to TLRs in cancer cells, to exert their effects [347]. Firstly, they co-cultured HEK293 cells overexpressing CD9-GFP with murine macrophages, in which TLR-containing endosomes were labelled. CD9+ exosomes were internalised, and found to co-localise with TLRs. Next, TLR8-GFP was overexpressed in HEK293 cells, and liposomal formulations of cy5-labeled miRNAs were applied, to show co-localisation of extracellular miRNAs to TLRs. Peritoneal macrophages from wild type and *TLR7*-/- mice were then exposed to liposomal miRNAs, showing that miRNAs stimulated cytokine production in wild type but not *TLR7* deficient cells, thereby demonstrating a functional consequence of exomiR-TLR binding. Extrapolating this finding, it is plausible that exomiRs could also bind surface TLRs before being be internalized. This is one mechanism of exomiR signalling and others are likely to exist in parallel.

1.3.7.2 ExomiRs transfer phenotypic traits between cancer cells

Work from O'Driscoll's group previously showed that phenotypic traits such as invasiveness could be transmitted to recipient cells through exosome transfer [348]. Following on from this, Le and colleagues showed that exomiR transfer, specifically miR-200 family members, could influence metastatic capability in breast cancer cells [349]. Using miR-200-rich exosomes from epithelial 4T1 cells to treat mesenchymal 4T07 cells, they were able to transfer miR-200 and downregulate the EMT transcription factor, Zinc finger E-box-binding homeobox (Zeb)-2, reverting the 4T07 cells to an E-cadherin-expressing epithelial phenotype. When 4T07 cells were injected systemically with 4T1 exosomes, there was far greater lung colonisation (metastases), suggesting that exosomal miR-200 transfer can drive mesenchymal to epithelial transition (MET) *in vivo*, allowing circulating tumour cells to seed at the secondary site.

1.3.7.3 Stroma-derived exomiRs influence cancer cells

Donnarumma and colleagues profiled exomiRs of patient-derived breast cancer-associated fibroblasts (CAFs) and normal fibroblasts (NOFs), and identified miR-21, miR-143 and miR-378 to be more abundant in CAF exosomes [350]. Using cy3-labelling they showed that these exomiRs could be transferred from CAFs to breast cancer cells, resulting in enhanced mammosphere formation and expression of epithelial-mesenchymal transition (EMT) transcription factors. Exosomes from NOFs transfected with these exomiRs had the same effects on stemness and EMT. Supporting these data, Boelens and co-workers showed that fibroblast exosomes, containing non-

coding RNAs, could induce RIG-I-STAT1 signalling in breast cancer cells, shifting the population to $CD44^{high}/CD24^{low}$ [284]. These cells had cancer stem cell attributes and were chemo- and radioresistant.

Beyond fibroblasts, Ono et al. attributed latency of metastatic breast cancer cells to exomiR transfer from bone marrow-derived mesenchymal stem cells (BM-MSCs) [351]. In this study, bone-tropic MDA231 cells were co-cultured with primary BM-MSC exosomes, leading to a decreased proportion of $CD44^{high}$ cells. Having sorted the $CD44^{high}$ cells, they showed that BM-MSC exosomes reduced proliferation and increased resistance to docetaxel. MiR-23b was found to be abundant in BM-MSC exosomes, and its transfection into MDA231 cells recapitulated the observed effects on proliferation and stemness. These functional consequences were attributed to miR-23b repression of the cell cycle regulator MARCKS.

Challagundla and colleagues identified reciprocal exomiR transfer between neuroblastoma (NBL) cells and monocytes [333]. In this study, NBL cells were shown to deliver miR-21 to monocytes, stimulating M2 polarization, and through TLR8/ NFκB activation, increasing monocyte secretion of exosomal miR-155. Monocyte exosomes were reciprocally taken up by NBL cells with resultant transfer of miR-155, and repression of the telomerase inhibitor, TERF1. As expected, xenografted subcutaneous tumours in cisplatin treated mice were significantly larger in the presence of injected liposomal miR-155.

1.3.8 ExomiRs as novel cancer biomarkers

1.3.8.1 The appeal of exomiR markers

For several years, miRNAs have been put forward as suitable diagnostic, prognostic and predictive biomarkers [352-356]. This is largely based on their ability to distinguish normal and malignant phenotypes, as well as different tumour types [288, 357, 358]. Equally, their stability in comparison to proteins and other nucleic acids, both in the circulation and in fixed tissues makes them particularly well-suited to sampling and analysis [359, 360].

Circulating exomiRs may have added advantages as biomarkers over and above ‘free’ miRNAs. Firstly, exosome secretion from malignant tissue is greater than corresponding normal tissue, as evidenced by higher concentrations in biofluids such as plasma, urine and ascites [293, 352, 361, 362]. Secondly, circulating exomiRs were shown to be representative of the parental tumour, in terms of miRNA profile [278, 293, 336]. Thirdly, exosome-encapsulated miRNAs are highly protected from degradation, even in suboptimal storage conditions and in the presence of RNase [363, 364]. These factors may increase sensitivity of exomiR-based biomarkers. This is important

because circulating tumour DNA (ctDNA) tests such as CancerSEEK, although demonstrating extremely high specificity, have been criticised for limited sensitivity (median 70%) [365]. A combination of ctDNA, protein and exomiR signatures may provide a solution to this problem in the future.

However, these potential advantages should be taken in context. The majority of circulating miRNAs are not exosomal, but in fact bound to argonaute proteins [366]. Furthermore, stoichiometric analysis has revealed that in exosome preparations from plasma, there are over 100 exosomes for every abundant miRNA copy [367]. Despite this, the significantly increased load of circulating exosomes in the malignant state, coupled with the stability of miRNAs, has allowed the generation several putative exomiR markers. Moreover, although exomiRs are not currently used in clinical practice, the benefits to patients conferred by liquid biopsy strategies, has cast a spotlight on exomiRs for this purpose. A selection of biomarker studies pertaining to common cancers, are summarised below.

1.3.8.2 Lung cancer

Rabinowits and co-workers highlighted the potential of exomiRs in their initial cohort of 27 stage I-IV lung adenocarcinoma patients, and nine healthy controls [293]. Using a panel of 12 miRNAs, previously associated with lung adenocarcinoma (miR-17-3p, miR-21, miR-106a, miR-146, miR-155, miR-191, miR-192, miR-203, miR-205, miR-210, miR-212 and miR-214), they showed that plasma exomiR profiles correlated with tumour-derived exomiR profiles, and all 12 exomiRs were more abundant in patients compared to controls.

More recently, Jin et al. tested the accuracy of plasma exomiRs in the diagnosis of stage I NSCLC [294]. Using a combined exomiR panel (let-7b, let-7e, miR-24 and miR-486), and individual panels for adenocarcinoma (miR-181b and miR-361b) and squamous cell carcinoma (miR-10b and miR-320b), they sampled the plasma of 60 symptomatic patients undergoing initial investigation. Receiver operating characteristic (ROC) curves produced area under the curve (AUC) values of 0.90 or greater for all panels.

1.3.8.3 Ovarian and breast cancer

Taylor's group was one of the first to demonstrate the utility of circulating exomiRs as diagnostic tools in ovarian cancer patients [352]. Using a previously validated signature of eight miRNAs (miR-21, miR-141, miR-200a, miR-200b, miR-200c, miR-203, miR-205 and miR-214), they showed that tumour miRNAs correlated with EpCAM-positive serum exomiRs, and that these could clearly distinguish ovarian papillary adenocarcinoma from benign ovarian disease in age-matched patients.

In breast cancer, Hannafon and colleagues profiled exomiRs from a normal mammary epithelial cell line (MCF10A) and multiple breast carcinoma lines (e.g. MCF7 and MDA231), and showed that miR-1246 was enriched in tumour-derived exosomes [368]. Using orthotopic patient-derived xenografts, they demonstrated that miR-1246 was more abundant in the plasma of implanted mice than controls, suggesting that tumour-derived exosomes contribute to the pool of circulating exosomes, which could be easily sampled. This was validated using plasma from patients with various subtypes of breast cancer, compared to healthy controls. In terms of distinguishing breast cancer subtypes, Eichelser and co-workers showed that exosomal miR-373 in the serum was significantly increased in triple negative patients, compared to those with luminal tumours or healthy controls [369]. Furthermore, transfection of miR-373 into MCF7 cells, led to reduced oestrogen receptor expression, suggesting that this is a functional exomiR marker.

1.3.8.4 Prostate cancer

It was previously shown that miR-141 was elevated in serum of advanced prostate cancer patients [359]. Li et al. showed that miR-141 was enriched in serum exosomes compared to whole serum, and that levels were four fold higher in prostate cancer patients compared to those with benign prostatic hypertrophy, or, healthy controls [370]. Furthermore, in a prognostic capacity, this exomiR could distinguish localised from metastatic disease with greater than 80% sensitivity and specificity.

Huang et al. identified plasma exosomal miR-1290 and miR-375 to be associated with overall survival in castration-resistant prostate cancer, allowing them to develop a multivariate model, combining these exomiRs with prostate-specific antigen, and time to failure of hormonal therapy [371]. Similarly, Bryant and colleagues identified that plasma exomiRs could predict recurrence after radical prostatectomy [372]. In this cohort of 47 recurrent and 72 non-recurrent patients, miR-375 and -141 were increased in both plasma exosomes and microvesicles.

1.3.8.5 Colorectal cancer

Ogata-Kawata and colleagues identified 16 exomiRs which were more abundant in serum exosomes from CRC patients compared to healthy controls, and more abundant in conditioned medium from CRC cell lines compared to a normal colon line [278]. Using 29 paired pre- and post-resection samples, they selected and validated seven exomiRs (let-7a, miR-1229, miR-1246, miR-150, miR-21, miR-223, miR-23a), which were reduced following surgery. Each of these generated AUC values of 0.61 or more.

Using a similar approach, Matsumura et al. found that serum exomiRs which were more abundant in a recurrent case of CRC than a non-recurrent case, and miRNAs overexpressed in CRC tissue

compared to normal colonic mucosa, converged on the miR-17-92 cluster (miR-17, -18a, -19a, -20a, -19b-1, and -92a) [295]. In a validation cohort of 90 CRC patients and 12 healthy controls, miR-19a was more abundant in serum exosomes from CRC patients at all stages. In a separate cohort of over 200 CRC patients followed up for five years, circulating exosomal miR-19a was able to determine overall and disease-free survival.

1.3.9 Summary

The development of malignant cells, able to spread and populate distant microenvironments, is a complex and multi-step process, resulting from aberrant gene expression and cellular miscommunications, consequent to the accumulation of genetic and epigenetic abnormalities. The discovery of exosomes and their emerging and varied functions in biology and pathology undoubtedly represents one of the most exciting findings in the medical sciences in recent years. Unravelling their functions has exposed yet more complexity in the regulation of gene expression and cellular behaviour, and how normal mechanisms can become imbalanced in cancer. An ever-increasing body of literature now attests to a link between these small packets of information, their non-coding RNA content and malignant disease, with their impact stretching across all described hallmarks of cancer.

Challenges in the field such as differing techniques for exosome isolation, tools to accurately quantify and characterize exosomal RNA, and demonstration of *in vivo* exomiR transfer, still remain [373]. Nonetheless, exomiRs are providing important clues and huge opportunities for diagnosis and prognostication. Early studies indicate that exomiR expression patterns can impact the biological behaviour of all cancers studied, and suggest that the clinical behaviour of many more tumours may be affected by the local, regional and systemic exosome and exomiR milieu. In the future, a greater dissection of the cellular and molecular pathways controlled by exosomes and their non-coding RNA cargo, will undoubtedly provide exciting new insights into neoplastic processes, and highlight promising areas for the development of novel therapeutic strategies.

1.4 Non-coding RNAs

1.4.1 Background

Non-coding RNAs (ncRNAs) are master regulators of the genome, controlling the most fundamental cellular processes. Several hundred studies have demonstrated their dysregulation across a range of cancer types, and translational follow-on studies have led to the development of putative ncRNA biomarkers for identification and staging of cancer. Additionally, mechanistic studies have identified key functions for ncRNAs in cancer progression, and highlighted actionable pathways to be targeted by ncRNA-directed therapies. Consequently, ncRNA therapeutics are now entering later stage clinical trials. This section describes the classification of ncRNAs, their biology and their potential clinical applications.

1.4.1.1 The role of ncRNAs in gene expression

NcRNAs are master regulators of gene expression, controlling over one third of the entire genome [31, 374]. NcRNA molecules are not translated into proteins, instead, they regulate the process of DNA fashioning RNA, which formulates protein, either by translational repression, mRNA degradation, transcriptional silencing or epigenetic transformation.

NcRNAs comprise long non-coding RNAs (lncRNAs), which exceed 200 base pairs and small ncRNA (sncRNA), which are sub-200 base pairs. SncRNAs can be subdivided further into microRNAs (miRNAs), piwi-interacting RNAs (piRNAs), small interfering RNAs (siRNAs), small nucleolar RNA (snoRNAs), scan RNAs (scnRNAs), promoter-associated small RNAs (PASRs), termini-associated small RNAs (TASRs), transcription initiation RNAs (tiRNAs) and defective interfering RNAs (diRNAs) [375-377]. **Figure 1-6** illustrates the hierarchical classification of ncRNAs.

MiRNAs are the most widely studied ncRNAs and are are differentially expressed according to tissue type, and between cancer and normal cells [288]. They have been shown to play a critical role in the regulation of fundamental cellular processes and pathways, including, differentiation, proliferation and apoptosis, and can become destabilized in cancer [291]. Moreover, the majority of miRNA loci are found in cancer-associated genomic regions [378].

Due to their involvement in key cellular processes, the role of ncRNAs in diagnosis, prognosis and treatment of primary, metastatic and recurrent cancers, could be vast [295]. Throughout this section, the value of ncRNAs as diagnostic, prognostic and predictive tumour biomarkers is discussed. Diagnostic biomarkers are utilised in detection and identification of a cancer, prognostic biomarkers indicate the likely disease outcome, and predictive biomarkers predict how a patient will respond to treatment. In terms of therapy, miRNA-based treatments have been in

development for some time, and many are now being tested in early-phase clinical trials. Although further refinement is needed, this is clearly promising. This section will look at the biology of ncRNAs in more detail, focusing on miRNAs, piRNAs and lncRNAs, with a view to highlighting their clinical relevance.

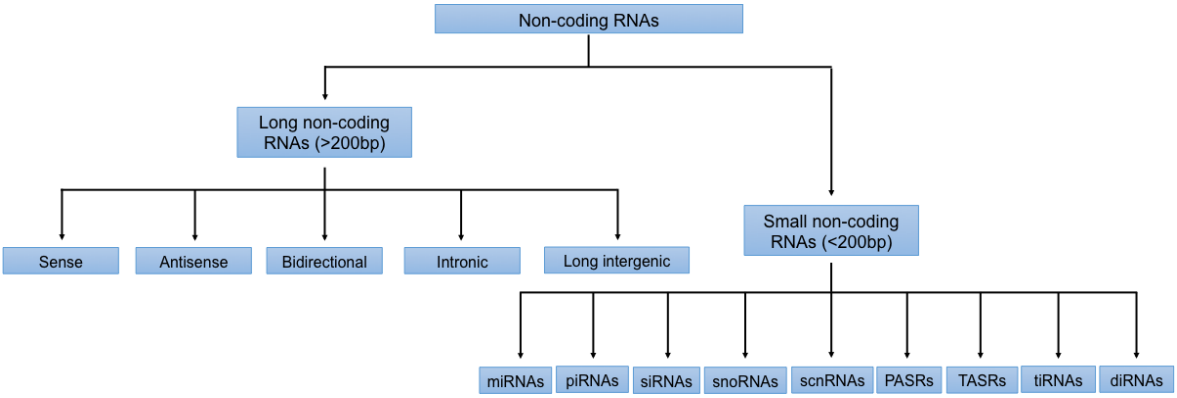

Figure 1-6. A hierarchical classification of ncRNAs. Long and short ncRNAs are distinguished by size, with an arbitrary cut off at 200 bp. There are several small ncRNA subfamilies. LncRNAs are differentiated by their genomic position. miRNA - microRNA; piRNA – piwi-interacting RNA; siRNA – short interfering RNA; snoRNA – small nucleolar RNA; scnRNA – scan RNA; PASR - promoter-associated small RNAs; TASR- termini-associated small RNAs; tiRNA – terminal interfering RNA; diRNA – defective interfering RNA. From *Bhome et al. (2018)* [379].

1.4.1.2 NcRNA nomenclature

NcRNA nomenclature is governed by complex rules, which can lead to confusion, and merits clarification at the outset. MiRNAs have a species specific prefix (e.g. hsa- *Homo sapiens*, or, mmu- *Mus musculus*), followed by miR-, which denotes miRNA, and lastly, a unique number which typically relates to how early on they were identified (e.g. hsa-miR-21 is the human equivalent of the mouse mmu-miR-21, and was the 21st miRNA to have been identified) [380]. The corresponding miRNA genes are identically named, save for italics and capitalisation, depending on the species concerned. A lack of capitalisation of the "r" (e.g. hsa-mir-21) suggests that the miRNA being referred to is the genomic locus of the miRNA, or perhaps a precursor product, such as an extended hairpin. MiRNAs from the same family, which closely resemble each other (e.g. typically differing by only 1-2 nucleotides), are given lettered suffixes such as miR-200a, miR-200b and miR-200c [381]. An additional layer of terminology comes after the "a" or "b" suffix. In general, from each precursor or extended hairpin, two mature products can be derived, one arising from the 5´ arm of the hairpin, and one from the complementary 3´ arm. Previously, the suffix "*" was used to differentiate these different products, with the 3´ product thought to be more minor and generally non-functional, and hence assigned a "*" (e.g. miR-200a*). In more

recent times however, this assumption has been questioned, and a number of studies have successfully demonstrated functional 3´ sequences, and production of miRNA 3´ sequences with as great a function as the 5´ sequence [382, 383]. Consequently, the older "*" designation has been retired in preference for a -3p or -5p suffix.

PiRNAs are similarly named, according to species first, followed by "piR", and finally a unique number (e.g. hsa-piR-00035) [384]. LncRNAs have a different naming system, whereby the name is a combination of Latin characters (capitalised for human lncRNAs) and Arabic numerals (e.g. MALAT1*)*. There is no species-specific prefix and the name should have some relevance to its function (e.g. BANCR – BRAF-activated non-coding RNA). For the thousands of lncRNAs yet to be assigned a function, the name should reflect its relationship with the proximal protein coding gene, in terms of whether it is antisense (-AS), intronic (IT) or overlapping (OT). LncRNAs which span genes are called long intergenic ncRNAs (lincRNAs) [385].

1.4.1.3 A brief history of ncRNAs

NcRNAs are not a new phenomenon, first described over 20 years ago. In 1993, consecutive articles published in the journal *Cell* by Victor Ambros' and Gary Ruvkun's groups described the function of the 22 nucleotide RNA produced by the *C. elegans lin-4* gene in repressing mRNA of the *lin-14* gene, by binding to its 3´ untranslated region (UTR) [285, 386]. However, it was not until several years later in 2000, when another miRNA, let-7, was described, that ncRNAs began to become popular in modern scientific culture, and we were allowed a glimpse of what is now recognised as a vast array of ncRNAs in cells and extracellular environments [387, 388].

Similarly, the first lncRNAs (H19 and Xist) were discovered as long ago as the early 1990s, as a product of genes which encoded a non-classical RNA molecule, involved in epigenetic regulation [389-391]. However, there were many opponents who considered this "junk", or, transcriptional "noise" [392]. By 2005, with the use of genome tiling array and deep sequencing, the mammalian transcriptome was further probed to irrefutably establish lncRNAs as we know them: long transcripts which do not code for protein, located in various positions with respect to protein coding genes [393, 394].

PiRNAs were formally described in 2006 as small RNAs which bind to an Argonaute subfamily called PIWI proteins [395-397]. However, it was later shown that piRNAs included a previously discovered group of small RNAs called repeat-associated RNAs [398], which had already been discovered some years earlier [399]. In the past decade, much of the work into piRNAs has focused on the germline because PIWIs and piRNAs are highly enriched in these tissues [400].

1.4.1.4 NcRNA biology and mechanism of action

MiRNA genes are spread widely throughout the genome, comprising up to five percent, and often centred around the introns of protein coding genes [401, 402].These genes are initially transcribed by RNA polymerase II into long transcripts called pri-mirs which often contain multiple stem loops. Pri-mirs are cleaved by the nuclear enzyme Drosha to form pre-mirs which are approximately 70 nucleotides long. Pre-mirs are exported to the cytoplasm and further modified by the enzyme Dicer to produce mature double stranded miRNAs, which are 20-25 nucleotides long. One strand of the miRNA is combined with the RNA induced silencing complex (RISC) and the other interacts with the target mRNA by binding to its 3´UTR region [403]. This leads to translational repression, or, less often, mRNA degradation, depending on the degree of sequence complimentarity [291].

PiRNAs are 25-33 nucleotides in length depending on the PIWI clade to which they bind. PiRNAs are derived from transposons, mRNAs and lncRNAs. Transposon-derived piRNAs are most frequently referred to in the literature. It must be noted that piRNA biogenesis is still poorly understood, but two distinct pathways have been described, producing primary and secondary piRNAs. Primary piRNAs are transcribed from piRNA gene clusters, initially forming long single stranded precursors, which undergo two or more nucleolytic reactions (one of these catalysed by Zucchini) before exiting the nucleus [404]. Secondary piRNAs arise from the adaptive ping-pong cycle. Here, piRNA transcripts bind with cytoplasmic PIWIs, such as Argonaute-3 (Ago-3) and Aubergine (AUB) in *Drosphila*. In this example, PiRNA-Ago3 sequences are complimentary to piRNA-AUB sequences such that piRNA-Ago3 can cut piRNA precursors to produce a sequence which will bind AUB and vice versa. This leads to ping-pong amplification [405, 406]. Matured piRNAs can act via multiple mechanisms, for example, piRNA-PIWI constructs can re-enter the nucleus to silence genes directly [407]. Another putative mechanism is that piRNAs form piRISC complexes, similar to miRISC complexes [408]. **Figure 1-7** is a schematic representation of miRNA and piRNA origin and function.

LncRNAs are difficult to easily define because their biogenesis, structure and functions are so variable [409]. Unlike other ncRNAs, lncRNA genes are poorly conserved between species [410], suggesting that identical sequences are not a prerequisite for a particular function. LncRNAs are generally classified by their position with respect to protein coding genes, into one of five groups. Sense lncRNAs overlap with the sense strand of a protein coding gene. Antisense lncRNAs overlap with the antisense strand. Bi-directional refers to lncRNAs within 1000 base pairs of a protein coding gene but on the opposite strand. Intronic lncRNAs are located entirely within introns and intergenic lncRNAs are distant from protein coding genes [411].

Most lncRNAs are transcribed by RNA polymerase II, spliced, and polyadenylated. However, there are exceptions, such as intronic lncRNAs, which are typically synthesised by RNA polymerase III (see **.**

) [412]. It is unclear to what extent post-transcriptional modification occurs, and in what proportion of lncRNAs. However, certain lncRNAs may be precursors to miRNAs, for example H19 is a precursor to miR-675 [413].

LncRNAs are thought to act via several different mechanisms. Epigenetic silencing occurs by lncRNA targeting of chromatin modification complexes, either at the same locus (*cis*) or at a different locus (*trans*). For example, Xist silences the entire additional X chromosome in females, to make it equivalent to the single X chromosome in males, by binding to *polycomb receissive complex-2* (*PRC2*) and allowing co-localisation of its histone mark to the inactive X [414]. Furthermore, the process of lncRNA transcription can in itself open or close access to a protein coding gene by transcription machinery, with SRG1 inhibiting the *SER3* gene in this way [415]. In addition, lncRNAs can occlude or facilitate the binding of transcription factors by hybridising to their binding sites. For example, Evf2 recruits the transcription factor Dlx-2 in this way [416]. The term “enhancer RNA” came about because the majority of initially discovered ncRNAs had inhibitory functions on protein coding genes, enhancers being the exception. HOTTIP is such an enhancer which binds the protein WDR5 and targets the MLL histone methyltransferase to activate the H3K4me3 mark [417].

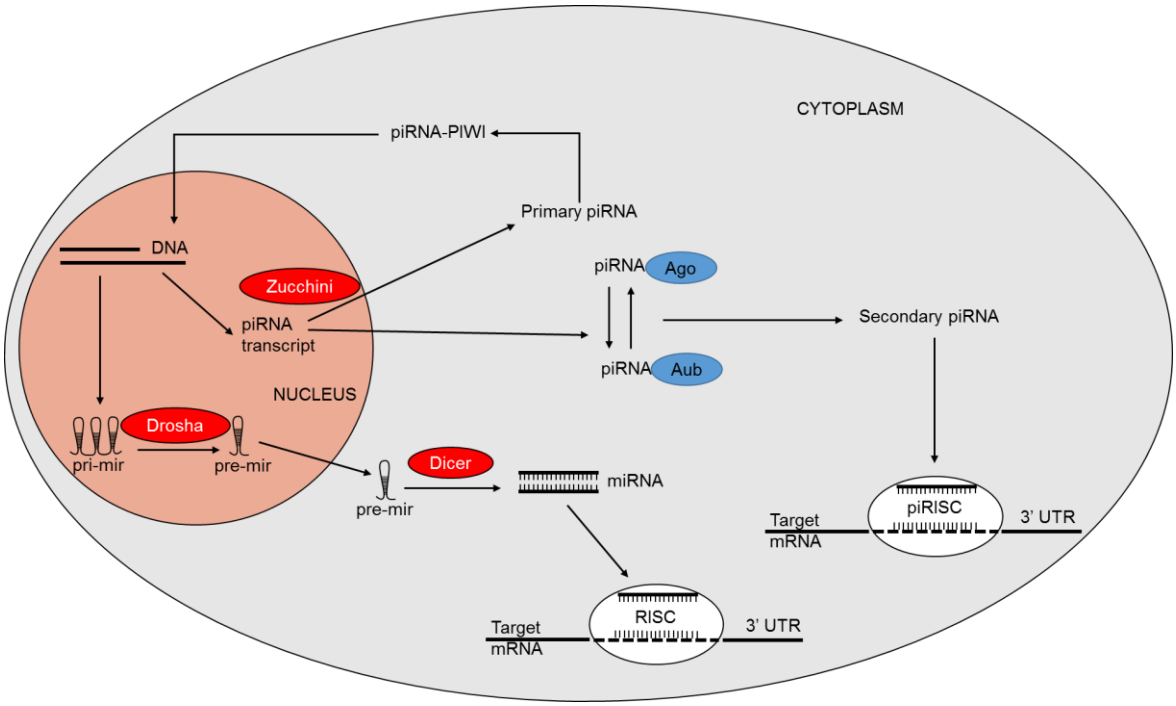

Figure 1-7. The biogenesis and function of small ncRNAs. MiRNA genes are transcribed to form pri-mirs which have a multiple hairpin structure. Drosha cleaves these into pre-mirs, which are

transported out of the nucleus and converted to mature miRNAs by Dicer, in the cytoplasm. Mature miRNA sequences form part of the RISC complex, and by targeting the 3´UTR region of target mRNAs lead to translational repression or degradation. PiRNA genes are transcribed to produce transcripts which mature into primary or secondary piRNAs. Primary piRNAs undergo nucleolysis by enzymes such as Zucchini. Secondary piRNAs arise from the ping-pong cycle where one piRNA-PIWI complex can cut another piRNA-PIWI complex, producing new substrates for each other. Mature piRNAs can form complexes with PIWIs which enter the nucleus to silence genes or alternatively form piRISC complexes to repress or degrade mRNA. From *Bhome et al. (2018)* [379].

Table 1-4. Classification of LncRNAs.

Type of LncRNA	Genomic Location	RNA polymerase	Polarity	Examples
Sense	Exonic	Pol II	Sense	DREH, MVIH
Antisense (Natural Antisense Transcripts)	Exonic	Pol III	Antisense	XIST, HOTAIR
Bidirectional	<1000 bp from protein coding gene (opposite direction)	Pol II	Sense and Antisense	HOTTIP, Sox8OT
Intronic	Intronic	Pol III, Pol IV (plants)	Sense and Antisense	LET, PCA3
Long Intergenic (LincRNA)	Between protein coding genes	Pol II	Sense and Antisense	H19, MALAT-1

From *Bhome et al. (2018)* [379]

1.4.1.5 NcRNAs in cancer diagnosis

Interest in ncRNAs has been driven by the hope that they may function as diagnostic biomarkers in cancer. The National Institutes of Health Biomarkers Definitions Working Group defined biomarkers as “a characteristic that is objectively measured and evaluated as an indicator of normal biological processes, pathogenic processes, or pharmacologic responses to a therapeutic intervention” [418]. Existing biomarkers are often poorly specific, and consequently, there is a need for development in this field. Several groups have profiled cancer patients and their unaffected counterparts, to identify cancer-associated miRNA signatures, from the host tissue [288], the circulation [419], and other biological fluids, such as urine [420]. Some of the early diagnostic biomarkers were proposed for cancers such as B cell chronic lymphocytic leukaemia [421], glioblastoma [422] and non-small cell lung cancer (NSCLC) [423]. Typically, these studies identified clusters of miRNAs rather than individual genes. In terms of piRNAs, the field is younger,

and hence there has been less work done. However, tissue expression of piR-651 was shown to be upregulated in several solid cancers including colon, lung and breast [424]. In another study, circulating levels of piR-823 were significantly lower in a gastric cancer cohort than normal controls [425]. However, one of the most promising ncRNA biomarkers is for the early detection of non-invasive prostate cancer. The combination of lncRNA PCA3 and the *TMPRSS2-ERG* fusion transcript outperforms serum PSA in this regard, and this test has received FDA approval [426]. However, this ncRNA biomarker is one of very few that has reached this stage of development.

There are certain methods which might improve specificity of ncRNA biomarkers. Distinguishing ncRNAs from cancer and stromal compartments is one method, which has been proposed in cancerous and pre-cancerous lesions [427, 428]. As an extension of this, the ratio of tumour to stromal ncRNA may provide further specificity. Another concept is to combine mRNA and ncRNA signatures together. As an example, in pancreatic ductal adenocarcinoma, there are several differentially expressed miRNAs (e.g. miR-802), snoRNAs (e.g. HBII-296B), piRNAs (e.g. piR-017061) and lncRNAs (e.g. LINC00261). Furthermore, miR-802, was found to target *TCF4* mRNA. Overall, this produces a combined sncRNA/lncRNA/mRNA signature which could provide better specificity as a disease biomarker [429].

Many of the potential biomarkers discussed thus far refer to tissue expression of ncRNAs, typically from formalin-fixed paraffin embedded tissues. This is because ncRNAs, particularly miRNAs, are known to be extremely stable in terms of their resistance to degradation [360]. In addition, robust miRNA profiles have been demonstrated in the circulation [359, 430], and in other bodily fluids such as urine and cerebrospinal fluid [431]. The appeal of these biomarkers is that they do not require a tissue biopsy and are therefore less invasive. It must be remembered however, that for a specific tumour type, the tissue and associated fluid profile may not correlate. An approach to overcome this has been to profile ncRNAs from circulating extracellular vesicles: partly because vesicular ncRNA seems to be protected from degradation [363], and partly because it is more representative of the primary tumour [352].

The data clearly indicate that ncRNAs are promising new biomarkers for cancer. Additional work needs to be completed to corroborate exactly how much information these signatures give us, above and beyond the diagnostic utilities we already have. In the context of cancer diagnosis, ncRNAs are likely to be used in addition to histological assessment, either when histological assessment is equivocal, or to subtype a tumour. It is conceivable that they may play a role in cases of unknown primary, or, inaccessible primary tumour, where biopsy is not possible. It is unlikely that formal histological assessment will ever lose its place as the gold standard in cancer diagnosis. However, in the context of screening, circulating or urinary ncRNAs have the promise of

non-invasive, rapid and cheap tests, highlighting at-risk patients and potentially allowing implementation of preventative therapy. At present, the reality is that there are no such tests in mainstream use, and high quality validated clinical biomarker studies will be required to drive this change.

1.4.2 NcRNAs in tumour staging

Staging determines prognosis, and therefore, the intensity and modality of treatment that is chosen. There are several staging systems in place: TNM, described by Denoix over fifty years ago, being the most widely accepted for solid tumours [432]. Other staging systems such as Duke's staging for colorectal cancer have had the same intention: to categorize patients into lower and higher risk groups for cancer-related mortality [29]. Discriminating between patients in this way allows for appropriate intensities of treatment. For example, in the UK a patient with T2N0M0 colonic cancer will typically have a surgical resection and then enter a programme of follow up, whereas a patient with T2N2M0 (nodal) disease will have surgical resection followed by adjuvant chemotherapy to reduce the risk of recurrence.

Some of the key findings with ncRNA signatures, in particular miRNAs, are that they can discriminate between cancer stage [433], as well as subtype [434], and can be used to indicate prognosis [435]. A recent example is the lncRNA TUBA4B, which negatively correlates with nodal disease and overall survival in NSCLC [435]. In terms of subtyping, there has been much attention on ncRNAs which can discriminate between ductal carcinoma in situ (DCIS) and invasive breast cancer, and predict which DCIS patients will go on to develop invasive cancer [436].

Beyond simply detecting the presence of cancer cells, there is evidence to suggest that ncRNAs may be useful in distinguishing metastatic from non-metastatic tissue. Bullock et al. showed that high miR-214 and low miR-192/194 in the stroma could distinguish Dukes A from Dukes C colorectal tumours (56). Similarly, MALAT1 was shown to differentiate "good" from "bad" early-stage NSCLC [437]. These findings are important because they may help identification and stratification of patients with micrometastatic disease. Therefore, ncRNA biomarkers, either from the cancer compartment or the stroma, may highlight patients for whom neo-adjuvant or adjuvant treatment should be offered to counter the threat of micrometastases. The use of such prognostic biomarkers allows treatment intensification for those predicted to have metastatic disease, whilst at the same time sparing those predicted to have only local disease.

Another facet of ncRNA signatures is that they might be useful in predicting response to treatment, as predictive biomarkers. Certain studies have shown that miRNAs can predict radiosensitivity and radioresistanc in breast cancer [438, 439]. Linked miRNA-mRNA profiles of

DNA repair and cell cycle pathways, in patients having breast-conserving surgery followed by radiotherapy, have been shown to predict local recurrence [440]. These are patients whose treatment should be augmented to completion mastectomy and or chemotherapy. Another recent study has shown that miR-133b represses the M2 isoform of pyruvate kinase in NSCLC, reversing the Warburg effect, and making tumour cells more sensitive to radiation [441].

Similarly, miRNAs have been linked with chemoresistance across cancer types, including, colorectal [442], small cell lung [443], and ovarian [444]. One mechanism, is that miRNAs, such as miR-25, control autophagy, which can influence chemosensitivity [445]. In terms of piRNAs, PIWIL2 overexpression was shown to mediate cisplatin resistance by enhancing chromatin condensation and improving DNA repair efficiency [446].

Since the conception of a unified approach to cancer staging over fifty years ago, we have made great strides in prognostication, mainly it must be said, due to advances in imaging modalities. However, we still encounter patients whose outcome defies their given stage. This suggests that there is still room for improvement, which is where ncRNAs show promise, not only in precision staging but in ascertaining response to treatment.

1.4.3 NcRNA-directed therapy in cancer

The basis of ncRNA-directed cancer therapy, is the fact that ncRNAs are dysregulated in the cancer setting, with oncogenic ncRNAs upregulated and tumour suppressing ncRNAs downregulated. For example, let-7 is a well-known tumour suppressing miRNA, which controls timing of the cell cycle, and is downregulated in various cancer types including lung cancer [421, 447]. Overexpression of let-7 in A549 lung cancer cells was shown to halt cell division [447]. More recently, P53-dependent miR-34 was shown to repress translation of the checkpoint inhibitor PD-L1. Peritumoral injection of miR-34a in lipid nanoparticles (MRX34) reduced intratumoral *PD-L1* mRNA and protein levels, and increased CD8+ T cells, promoting an anti-tumour effect in the microenvironment [448]. MiR-34 has remained popular in the search for ncRNA-based treatment. Transfection of human breast cancer cell lines with liposomal miR-34a resulted in decreased proliferation, invasion and increased apoptosis, via the repression of Bcl-2 and Sirtuin-1. Moreover, combination treatment with miR-34a and 5FU was more effective than either alone, in reducing cell viability [449]. Similarly, delivery of miR-125a, another tumour suppressor, to *HER-2*-positive breast cancer cells, results in downregulation of Akt and ERK pathways, reducing proliferation and migration. In the context of radiotherapy, miR-34 expression seems to increase, affording protection to breast cancer cells, suggesting that in this context, an anti-miR-34 therapy is desirable [450]. Several of these experimental approaches have been extended beyond miRNAs.

It was recently observed that the lncRNA DQ786243 is upregulated in colorectal cancer cell lines (SW620 and HT29) and primary tissue. Knocking down this lncRNA with siRNA arrested the cell cycle, and when knock down cells were established as xenografts, tumour growth was shown to be attenuated [451].

Several studies have been presented, which aim to target cancer cells, using a ncRNA-directed approach. However, the stroma is an equally appealing target, considering that its mutational burden and potential to develop treatment resistance is far less than the cancer compartment [47]. In a breast cancer model, PTEN-dependent miR-320 was shown to repress the transcription factor ETS2. *PTEN* ablation resulted in low miR-320 and high ETS2, which produced a pro-invasive and pro-angiogenic secretome in mammary fibroblasts [452].

One approach in miRNA drug design is to create a mimetic such as MRX34, which targets mRNAs [453], as the general consensus is that ncRNA agonists are more effective than antagonists [454]. In this respect, piRNAs have better specificity because unlike miRNAs, each piRNA binds more selectively with its respective PIWI proteins, reducing the likelihood of collateral pathway activation or inactivation. Developing this concept, PIWI proteins could potentially be targeted by antibodies to achieve the same effect, delivering an even more specific therapy. There are several candidates which could be targeted in this manner, such as PIWIL1, which has been shown to suppress microtubule polymerization and increase proliferation and migration in various cancer cell lines [455]. Another advantage over miRNAs is that piRNAs are not all subjected to post-transcriptional enzymatic processing, alleviating the need to synthesise precursors.

In carcinomas, the process of EMT describes the epigenetic and phenotypic changes which allow cancer cells to effectively metastasise [456]. Briefly, the activation of cellular signalling cascades through the receptors of TGFβ, HGF, PDGF, Epidermal Growth Factor (EGF) and integrins, leads to activation of EMT transcription factors (TFs), such as Zeb, Twist and Snail, which causes loss of epithelial cell polarity, and acquisition of an invasive phenotype [457]. NcRNAs are thought to play a key role in regulating the process of EMT. For example, the miR-200 family (miR-200a, miR-200b, miR-200c, miR-141 and miR-429) is critical in regulating Zeb-mediated EMT [458]. Other classes of ncRNA have also been implicated in the control of EMT. LncRNA-ROR knockdown in gallbladder carcinoma cell lines has been shown to reverse EMT [459]. There is clearly some promise in the potential for ncRNA-directed treatments in the prevention of EMT, as anti-metastatic drugs.

Unfortunately, the reality is that very few of these important observations have been translated into useable anti-cancer treatments. To date there have been two phase 1 trials of ncRNAs, both utilising miRNAs. MRX34 is a miR-34a mimic delivered in lipid nanoparticles, which accumulates in

the liver [453]. Initial results were promising for patients with advanced hepatocellular, colon and neuroendocrine cancers [460], however, the trial was terminated early because of severe immunological reactions (NCT01829971). The other trial, for malignant mesothelioma and NSCLC, is assessing a novel treatment known as TargomiRs which consists of three components: a miR-16 mimic, non-living bacterial mini-cells as a delivery vehicle, and an EGFR monoclonal antibody [461]. This trial is currently recruiting (NCT02369198). **Table 1-5** summarises clinical trials of ncRNAs in cancer.

Several experimental studies have demonstrated that ncRNAs can be manipulated to achieve an anti-tumour effect. We must not neglect stromal ncRNAs when considering novel therapeutics because these signals are less likely to be corrupted by mutations. EMT is a critical step in metastasis which is controlled by ncRNAs, and can be completely reversed by their ectopic expression, leading to the possibility of anti-metastasis agents. However, even with such a wide range of possible targets, regulating an array of cancer-relevant pathways, hardly any ncRNA-directed therapeutics have reached late-stage human trials. Nonetheless, the ncRNA field is constantly evolving, and with the characterisation of novel ncRNAs such as piRNAs, there is hope for more specific targeted treatments, with more acceptable side effect profiles.

Table 1-5. A summary of ncRNA-directed cancer therapies in human trials.

Therapy	Disease	Mechanism	Phase	Status	Results	Identifier
TargomiRs	Malignant pleural mesothelioma and NSCLC	miR-16 mimic delivered with EGF receptor antibody in non-living bacterial mini-cells	1	In progress	Recruiting.	NCT02369198
APN401	Recurrent or advanced melanoma, renal, or pancreatic cancer	Autologous PBMCs transfected with siRNA against Cbl-b	1	In progress	Recruitment complete but results pending.	NCT02166255
siRNA-EphA2-DOPC	Advanced recurrent solid cancers	siRNA targeting EphA2	1	In Progress	Recruiting.	NCT01591356
Proteasome siRNA and tumour antigen RNA-transfected dendritic cells	Metastatic melanoma	DCs transfected with siRNA to activate immunoproteasome beta subunits LMP2, LMP7 and MECL1	1	Completed	Efficacy of DC immunotherapy enhanced. Well tolerated [462].	NCT00672542
Atu027	Advanced solid tumours	siRNA targeting protein kinase N3 in the vascular endothelium	1	Completed	Some efficacy demonstrated. Well tolerated [463].	NCT00938574
Atu027 and gemcitabine	Pancreatic ductal carcinoma	siRNA targeting protein kinase N3 in the vascular endothelium	1b/2a	Completed	Efficacy demonstrated. Moderately well tolerated: some grade 3 and grade 4 adverse events.	NCT01808638
TKM-080301	Colorectal, pancreas, gastric, breast, and ovarian cancers with hepatic metastasis or primary liver cancer	siRNA within lipid nanoparticles targeting PLK-1	1	Completed	Efficacy demonstrated. Well tolerated.	NCT01437007
siG12D LODER (Local Drug EluteR)	Pancreatic ductal adenocarcinoma	siRNA targeting KRAS oncogene	1	Completed	Some efficacy demonstrated. Well tolerated [464].	NCT01188785
siG12D LODER in combination with gemcitabine or FOLFIRINOX	Pancreatic ductal adenocarcinoma	siRNA targeting KRAS oncogene	2	In progress	Not yet recruiting.	NCT01676259
DCR-MYC	Solid tumours, multiple myeloma, lymphoma	siRNA targeting Myc oncogene	1	In progress	Not yet recruiting.	NCT02110563
DCR-MYC	Hepatocellular carcinoma	siRNA targeting Myc oncogene	1b/2	In progress	Recruitment complete but results pending.	NCT02314052

Therapy	Disease	Mechanism	Phase	Status	Results	Identifier
Minor histocompatibility antigen (MiHA)-loaded PD-L-silenced DC vaccination	Haematological malignancies	siRNA to increase potency of DC vaccination	1/2	In progress	Recruiting.	NCT02528682
MRX34	Primary liver cancer, SCLC, NSCLC, lymphoma, melanoma, multiple myeloma, renal cell carcinoma	miR-34a mimic delivered in liposomes allowing accumulation in the liver	1	Terminated	Terminated due to severe immune reactions.	NCT01829971

From *Bhome et al. (2018)* [379]

1.4.4 Summary

The field of ncRNAs is relatively young and continues to evolve at a rapid pace. More and more classes of ncRNA are being discovered, each with their unique biology, mechanism of action and functional effects. MiRNAs are the most well-defined ncRNAs, and there is a consensus on their biogenesis and function. However, for piRNAs and lncRNAs, this is less clear and more work is required to fully elucidate their actions and functions. There has been a great deal of excitement about ncRNAs in cancer, largely because their expression profiles can differentiate healthy from diseased tissue, in a variety of malignancies. Furthermore, there have been many elegant studies showing that ncRNAs regulate cell cycle and cancer-relevant pathways. As diagnostic biomarkers, circulating or urinary ncRNAs have the potential to be non-invasive and cheap tests, with a high degree of acceptability by patients and healthcare providers. Although diagnostic ncRNA biomarkers are not routinely used in clinical practice, the US FDA has set a precedent by approving their use in this setting. In terms of prognostication, the hope is that ncRNA signatures, in combination with existing modalities, will be able to more precisely stage and subtype cancers, such that high-risk patients can have treatment intensification and lower risk patients can be spared from potentially toxic treatments. It is very exciting that ncRNAs are already showing potential in cancer therapy. MiRNA-based drugs have rapidly reached human trials, which is a major feat in itself, and with the hope that piRNA-directed agents will provide even more specific targeting of deregulated pathways, the future of such an approach is promising. Looking forward, a more precise dissection of the pleiotropic processes and pathways controlled by ncRNAs will undoubtedly bring novel insights into the mechanisms of carcinogenesis and tumour progression, and pinpoint additional promising areas for the development of novel anti-cancer therapeutics.

1.5 Aims and objectives

1.5.1 Hypothesis

Transfer of exosomal cargo between tumour and stromal compartments influences CRC progression.

1.5.2 Aims

i. To isolate and characterise exosomes from multiple cell types.
ii. To demonstrate exosome transfer between cells *in vitro* and *in vivo*.
iii. To identify and functionally annotate exomiR cargo from CRC stroma.
iv. To investigate the role of CRC exosomes in determining fibroblast phenotype.

1.5.3 Objectives

i. Exosomes will be isolated from cell culture conditioned media from primary and established fibroblasts, and CRC cells, by dUC. Characterisation of exosome preparations by size, morphology and protein markers, will be conducted by transmission electron microscopy (TEM), nanoparticle tracking analysis (NTA) and western blotting.
ii. *In vitro* exosome transfer will be demonstrated by direct labelling of exosomes with fluorescent membrane dyes, followed by delivery to recipient cells, and detection of fluoresecnt signal in recipient cells by microscopy and flow cytometry. *In vivo* exosome transfer will be demonstrated by generation of CRC cells stably expressing fluorescently conjugated exosome markers (e.g. CD63-GFP), which will then be used to establish xenografts with alternatively labelled fibroblasts (e.g. PKH26). Xenografts will be imaged by confocal microscopy to demonstrate transfer.
iii. Paired primary CAFs and nearby normal fibroblasts (NOFs) will be extracted and sub-cultured from CRC biopsies. Exosomes will be isolated from CAFs and NOFs. Exosomal RNA will then be subjected to multiplexed RNA profiling (NanoString) to identify differentially abundant exomiRs, which will be functionally assessed by stromal overexpression in orthotopic CRC xenografts.
iv. Exosomes will be isolated from epithelial and mesenchymal CRC cells, and used to condition fibroblasts. Differential effects on cellular pathways will be investigated by western blotting. As the most stable cargo which is transferred in exosomes, miRNAs will be profiled in epithelial and mesenchymal CRC exosomes, to identify exomiRs

associated with EMT. Recipient fibroblasts will be assayed for miRNAs before and after exosome conditioning to check whether miRNAs of interest increase. Candidate miRNA mimics will then be transfected into fibroblasts to recapitulate the effect of exosomes. Finally, isogenic CRC cells, differing only in EMT TF expression, will be injected with fluorescently labelled fibroblasts into nude mice. Tumours will be dissociated and flow-sorted to select for the labelled fibroblast population. Labelled fibroblasts will be interrogated for miR-200, *ACTA2* and *FN1*. In parallel, tumours will be subjected to immunohistochemistry for EMT and myofibroblastic markers.

Chapter 2 Materials and Methods

2.1 Exosome isolation, characterisation and transfer

2.1.1 Isolation

Exosomes were isolated by dUC. Briefly, fibroblasts were grown to 70% confluence in 12 x 175 cm^2 flasks (10 x 10^7 cells), and cancer cells in 3 x 175 cm^2 flasks (8-9 x 10^7 cells), at which point the growth medium was replaced with equivalent medium containing exosome-free FBS. After 72 h, conditioned medium was harvested and centrifuged at 400*g* for 5 min at 4°C to pellet cellular contaminant, followed by 2000*g* for 10 min at 4°C to pellet debris. The supernatant was then passed through a 0.22 µm filter and ultracentrifuged at 100 000*g* for 75 min at 4°C using the TFT 50.38 rotor (Sorvall). The resulting exosome pellets were pooled, washed with PBS and ultracentrifuged again at 100 000*g*. The final exosome pellet was solubilised in 200 µl PBS and stored at -80°C (**Figure 2-1**). We submitted all relevant data pertaining to exosome isolation and characterisation to the EV-TRACK knowledgebase to assess the quality of this methodology (EV-TRACK ID: JZ2312SI) [330].

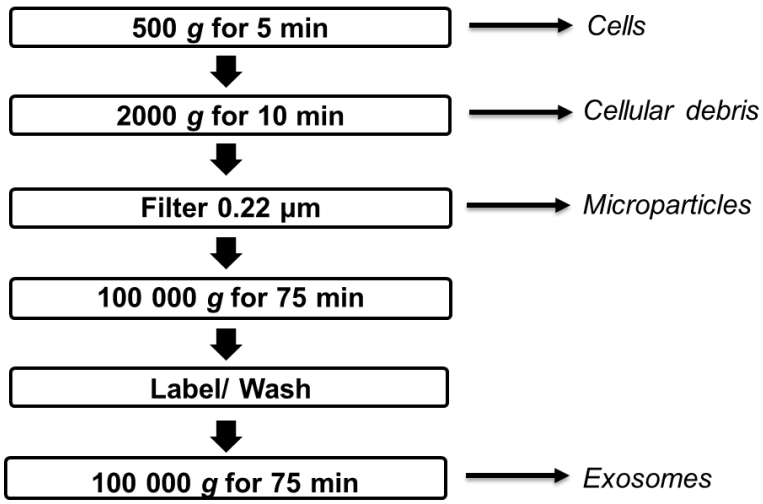

Figure 2-1. Size-based exosome isolation protocol. Exosomes were isolated by dUC with a single filtration step. Labelling was typically with lipophilic dyes. The final exosome pellet was resuspended in PBS, except for TEM, where sterile water was used.

2.1.2 Characterisation

2.1.2.1 Transmission electron microscopy

Following exosome isolation, the washed pellet was resuspended in 100 µl ultrapure water and stored at 4°C for up to seven days prior to processing. Briefly, 10 µl exosome sample was dropped on to Parafilm (cat no. PM998; Bemis). A carbon coated formvar copper grid (cat no. TG50Cu; EM Resolutions) was placed on the droplet to immerse its coated side, and incubated for 30 s at room temperature. Excess sample was blotted away using absorbent paper. The grid was then incubated with 10 µl negative stain (5% ammonium molybdate/ 1% trehalose) for 10 s. Excess negative stain was removed by blotting. The grid was visualized at increasing magnification up to 120 000x using the Tecnai 12 microscope (FEI).

2.1.2.2 NTA

The size distribution of exosomes was measured by NTA (NS300; NanoSight), equipped with an EMCCD camera and a 405 nm diode laser. Silica beads (100 nm diameter; cat no. 140120-10; Microspheres-Nanospheres) were used to calibrate the instrument. Exosome samples were diluted 1:5000 in PBS to optimise the particle number in the field of view. For each sample, five videos, each of 90 s duration, were captured. Analysis was performed using the instrument software (NTA 2.3.0.15). NTA was conducted at Ghent University by myself and Joeri Tulkens.

2.1.2.3 Western blotting

Exosomes were initially sonicated for 10 s at power output 1.0 using the Fisherbrand Model 50 Sonic Dismembrator (ThermoFisher). Protein concentration was determined by BCA assay as per manufacturer instructions (Pierce BCA Protein Assay Kit cat no. 23225; ThermoFisher). Briefly, Reagent A was mixed with Reagent B in a 50:1 ratio, and 150 µl pipetted into individual wells of a 96-well flat-bottomed plate. Standards were set up by adding 1, 5 and 12.5 µl of 2 µg/µl bovine serum albumin (BSA) to individual wells, equating to 2, 10 and 25 µg/µl. 5 µl of sample was added to individual wells and incubated at 37 °C for 30 min. Plates were allowed to cool down and then read at an absorbance of 562 nm on a plate reader (Varioskan LUX Multimode Microplate Reader; ThermoFisher). A standard curve was generated in Microsoft Excel, and from the equation of the best-fit line (y = mx + c), sample concentrations were determined. A one-fourth volume of 5X SDS gel loading buffer (10% SDS; 50% Glycerol; 0.25 mM Tris-HCl (pH 6.8); 0.25% Bromophenol blue; 10% β-mercaptoethanol) was then added, and the sample boiled at 95 °C for 5 min.

Typically, 20-30 µg of protein was separated under reducing conditions in 8, 10, 12 or 15% SDS-PAGE gels (see Appendix **B**), using a constant voltage of 120 mV, until the dye front reached the

bottom of the gel. Proteins were then transferred on to nitrocellulose membranes (Amersham Protan 0.1 NC nitrocellulose membranes (cat no. 10600000; GE Healthcare), using the sandwich transfer method, with a constant voltage of 20 mV, applied for 16 h. Membranes were blocked in 4% milk (in TBS-T) for 1 h, and then incubated in primary antibody for 1 h at room temperature. Primary antibodies were typically diluted in 2.5% BSA (in TBS-T). Following primary antibody incubation, membranes were washed three times in TBS-T (5 min per wash), and then incubated with secondary antibody for 1 h. Horseradish peroxidase-conjugated secondary antibodies (polyclonal swine anti-rabbit (cat no. P021702-2) and polyclonal rabbit anti-mouse (cat no. P016102-2); 1:3000; Dako) were diluted in 4% milk (in TBS-T). Membranes were then washed three times with TBS-T, and specific signal was visualised using the SuperSignal West Dura (cat no. 34075) or West Femto (cat no. 34094) Chemiluminescent detection kit (ThermoFisher). The same secondary antibodies and chemiluminescent detection kits were used for all western blots presented in this thesis. A list of primary and secondary antibodies is provided in Appendix **B**.

For exosome characterisation, proteins were detected with Alix (3A9; 1:500), TSG101 (4A10; 1:500; Abcam, Cambridge, UK), CD63 (Ts63; 1:500), CD81 (1.3.3.22; 1:500; ThermoFisher, Waltham, USA), GM130 (35/GM130; 1:500; BD Biosciences, San Jose, USA), *β*-actin (C4; 1:5000; BD Biosciences, San Jose, USA) and cytochrome C (4272; 1:1000; Cell Signaling Technology) primary antibodies.

2.1.3 Transfer

2.1.3.1 In vitro

2.1.3.1.1 Fluorescent labelling of exosomes

Exosomes were isolated using the above method, up to and including the first 100 000*g* ultracentrifugation. Pooled exosomes were then labelled with the lipophilic dye DiO (absorbance 484 nm, emission 501 nm; cat no. V22886; ThermoFisher) or DiD (absorbance 644 nm, emission 665 nm; cat no. V22887; ThermoFisher), at a working concentration of 1:2500, and incubated at 37^{o}C for 20 min. Labelled exosomes were washed with PBS and centrifuged again at 100 000*g* for 75 min at 4^{o}C to produce a labelled exosome pellet.

2.1.3.1.2 Fluorescence microscopy

DiO-labelled exosomes were used to condition DLD1-mCherry cells for 24 h at a concentration of 15 µg/ml (exosomal protein content; dose based on previous studies [465, 466]), in a 6-well format. Cells were washed with PBS to remove ‘free’ exosomes and viewed with the 10x objective

of the Olympus CKX41 microscope (Olympus), in green and red channels. Acquired images were split into respective colour channels and merged using Adobe Photoshop (ver. CS6).

2.1.3.1.3 Confocal microscopy

DiO-labelled exosomes were co-cultured with DLD1-mCherry cells for 24 h at 15 µg/ml on 22 x 22 mm glass microscope slides (cat no. 631-0122; VWR International). Cells were washed with PBS and fixed with ice-cold 50:50 acetone-methanol for 5 min, after which the fixative was replaced with PBS. Cells were imaged using the Leica TCS SP5 confocal microscope at 60x (Leica Microsystems), by Dr David Johnston, Biomedical Imaging Unit, University of Southampton.

2.1.3.1.4 Flow cytometry

To show exosome transfer by flow cytometry, DiD-labelled exosomes were co-cultured with DLD1 cells for 24 h at a concentration of 15 µg/ml, in a 6-well format. Cells were washed with PBS, trypsinised, pelleted and re-suspended in 400 µl of DMEM. The presence of exosomes in DLD1 cells was assessed by detection of DiD signal in the far red (FL4) channel using a flow cytometer (FACS Calibur, BD Biosciences).

2.1.3.1.5 MiRNA changes in recipient cells

To determine the optimal concentration for exosome treatment, 2 x 10^5 DLD1 or SW480 cells were conditioned with MRC5 and primary colorectal CAF exosomes (see 2.2 for details on CAF isolation) at concentrations of 15 (low) and 100 µg/ml (high), for 24 h, in a 6-well format. To detrmine the optimal duration of exposure, DLD1 cells were conditioned with MRC5 exosomes for 6 and 48 h, at a concentration of 15 µg/ml. Control cells were treated with an equivalent volume of exosome-depleted conditioned medium (supernatant remaining after exosome isolation). At the appropriate interval, cells were washed with PBS to remove extracellular exosomes, trpsinised and pelleted (400*g* for 5 min), and RNA extracted. Cellular levels of miR-16-5p, miR-29b-3p, miR-21-5p and miR-199b-5p, were determined by RT-qPCR. Doses and durations of exosome treatment were based on previous studies [46, 465-470]. RNA extraction, Taqman cDNA synthesis and qPCR protocols, are described in detail below (section **2.1.5**).

2.1.3.2 In vivo

2.1.3.2.1 Generation of stably overexpressing CD63-GFP cells

1 x 10^6 HEK293T cells were seeded into individual wells of a 6-well plate. The following day, when cells were 90% confluent, they were transfected with viral packaging mix and the CD63-GFP plasmid, using Lipofectamine 3000 (cat no. L3000008; ThermoFisher). In tube A, 7 µl

Lipofectamine 3000 was diluted in 250 µl OptiMEM I (cat no. 31985062; ThermoFisher). In tube B, 2.25 µg ViraPower lentiviral packaging mix (cat no. K497500; ThermoFisher), 750 ng pCT-CD63-GFP plasmid (cat no. CYTO120-PA-1; SBI) and 6 µl p3000 reagent, were added to 250 µl OptiMEM. The contents of Tube A and B were mixed (final volume 500 µl), incubated at room temperature for 20 min, and then added to a single 6-well of HEK293T cells containing 1 ml DMEM. Cells were incubated at 37^{o}C for 6 h before the medium was replaced with 2 ml fresh DMEM. Viral supernatant was collected at 24 and 52 h post-transfection, filtered (0.22 µm filter) and stored at -80^{o}C.

Virus particles containing CD63-GFP were applied to HCT116 cells with hexadimethrine bromide (Polybrene; cat no. H9268; Sigma) at a final concentration of 8 µg/ml. Cells were washed after 24 h, trypsinised and seeded on 96-well plates at a density of 80 cells/plate (≤1 cell/well) to obtain single cell clones. Following puromycin selection at a concentration of 2 µg/ml for 3 weeks, positive clones were identified using fluorescence microscopy, and validated by western blotting.

2.1.3.2.2 Western blotting for CD63 and GFP in transduced cells

The western blotting protocol for exosome samples is described above (section **2.1.2.3**) and was similar for cells, save for the preparation of the lysate. Cell pellets were lysed in 2X Laemmli buffer (4% SDS; 20% Glycerol; 0.125 mM Tris-HCl (pH 6.8)), with the volume of buffer dependent on the size of the pellet. Typically, for a pellet from one well of a 6-well plate, 160-200 µl was used. The lysate was then sonicated, using the same conditions described above, and protein concentration determined by BCA assay. A one-fourth volume of complete 5X SDS gel loading buffer was then added, and the sample boiled at 95^{o}C for 5 min. The sequence of loading, running, transfer, blocking, primary and secondary antibody incubation, washing and detection was identical to that described for exosome samples.

For validation of HCT116-CD63-GFP cells, proteins were detected using CD63 (Ts63; ThermoFisher; 1:500) and GFP (D5.1; Cell Signaling; 1:1000) primary antibodies. HSP90 (68/Hsp90; BD; 1:1000) and β-actin (C4; BD Biosciences; 1:5000) were used as equal loading controls.

2.1.3.2.3 PKH26 labelling of fibroblasts

PKH26 labelling was conducted as per manufacturer recommendations using the PKH26 fluorescent cell linker kit (cat no. PKH26GL; Sigma). A suspension containing 2×10^7 single MRC5 fibroblasts was washed once using DMEM without serum. Cells were centrifuged (400*g*) for 5 minutes into a loose pellet and the supernatant discarded. A 2X cell suspension was prepared by adding 1 ml of Diluent C (cat no. CGLDIL) to the cell pellet and resuspended. Immediately prior to staining, a 2X dye solution (4×10^{-6} M) was prepared by adding 4 µL of the PKH26 ethanolic dye

solution (cat no. P9691) to 1 ml of Diluent C. The 1 ml of 2X cell suspension was immediately added to 1 ml of 2X dye solution and mixed by pipetting. Final concentrations after mixing the indicated volumes were 1×10^7 cells/ml and 2×10^{-6} M PKH26. After intermittent mixing for 5 min, 10 ml of complete DMEM was used to stop the reaction. Labelled cells were centrifuged at 400*g* for 10 min at 20-25 °C and the supernatant discarded. Cells were washed with complete DMEM twice more before being resuspended in the appropriate volume for use.

To investigate the duration for which PKH signal could be detected in labelled cells, MRC5 fibroblasts were labelled with PKH26, as described above. Immediately after labelling, 1 x 10^6 cells were seeded into a 10 cm dish. Cells were passaged every time they reached 80% confluency, and followed over a period of 14 days. A proportion of cells were collected on days 0, 7, 14 and 28, for analysis by flow cytometry. PKH signal was detected in the FL2 channel using the FACS Calibur (BD Biosciences) instrument.

2.1.3.2.4 Co-culture of HCT116-CD63-GFP cells and PKH-labelled fibroblasts

To confirm transfer of fluorescent exosomes by HCT116-CD63-GFP cells *in vitro* (prior to *in vivo* studies), co-cultures were set up between HCT116-CD63-GFP cells and MRC5-DiD fibroblasts. There were six conditions: (i) HCT116 control cells; (ii) HCT116-CD63-GFP; (iii) MRC5 control; (iv) MRC5-DiD; (v) HCT116 control + MRC5 control and; (vi) HCT116-CD63-GFP + MRC5-DiD. All conditions were set up in individual wells of a 6-well plate, in duplicate. For co-cultures, 2 x 10^5 fibroblasts were seeded and allowed to adhere for 6 h before 5 x 10^4 CRC cells were seeded on top. For monocultures, fibroblasts and CRC cells were seeded at equivalent time points and densities to co-cultures. For all conditions, cells were washed, trypsinised, and pelleted, 24 h after seeding CRC cells. Cells were resuspended in 400 µl DMEM. For each condition, cells were interrogated for signal in FL1 (GFP) and FL4 (DiD) channels using a flow cytometer (FACS Calibur, BD Biosciences).

2.1.3.2.5 Establishing CRC xenografts in mice

All mice were housed in a specific pathogen-free facility at the University of Southampton and given a commercial basal diet and water *ad libitum*. 5 x 10^5 HCT116-CD63-GFP cells were mixed with 1 x 10^6 PKH26-labelled MRC5 fibroblasts in a total volume of 100 µL DMEM, to which 100 µL Matrigel® (cat no. 354230; Corning) was added. The final volume of 200 µL was injected subcutaneously and bilaterally into the dorsal skin of 6-8-week-old CD1 nude mice (n=3). Injections were carried out by Lisa Dunning (Biomedical Research Facility, University of Southampton). After three weeks (when tumours were palpable) animals were sacrificed and tumours excised.

2.1.3.2.6 Fixing, sectioning and imaging of tumours

Tumours were immediately fixed in 4% paraformaldehyde for 2 h and then cryoprotected in 30% sucrose overnight. Tumours were then mounted in OCT medium (cat no. 62550-01; Electron Microscopy Sciences) and snap frozen in liquid nitrogen. This extended protocol was used to preserve fluorescent signals emanating from the tissue. Sections of 5 μm thickness were cut using a cryostat and thaw-mounted on to gelatin-coated histological slides before being dried at 37°C for 30 min. Sectioning and mounting was done by Sonya James (Microscopy Core Facility, Cancer Sciences, University of Southampton). Mounted sections were imaged at 60x using the Leica TCS SP5 confocal microscope (Leica Microsystems), by David Johnston (Biomedical Imaging Unit, University of Southampton).

2.1.4 Exosome conditioning of miRNA knock out cells

2.1.4.1 MiRNA knock out cells

In an attempt to demonstrate that exosomes definitively transfer miRNAs to recipient cells, miRNA knock out embryonic stem (ES) cells were conditioned with CRC exosomes, and then assayed for the knocked out miRNA, with the expectation that CRC exosomes would deliver the miRNA to the deficient cells. The Sanger MirKO mouse ES cell line Mir141/Mir200c cluster 6N3 (mirko_11A2; cat no. 036330-UCD, Mouse Biology Program UC Davis) was purchased and established in culture. In this cell line, the miRNA gene was replaced via homologous recombination by a LoxP-F3-PGK-EM7-PuroΔtk-bpA-LoxP-FRT targeting vector [471].

Cells were defrosted into individual wells of a 6-well plate on a feeder layer of mouse embryonic fibroblasts (MEFs), provided by Katherine Parry, University of Southampton. ES cell medium was KO DMEM, high glucose (cat no. 10829-018; Gibco) supplemented with 15% FBS, 2mM L-glutatmine, 1mM NE Amino Acids (cat no. 11140-050; Gibco), leukaemic inhibitory factor (LIF) 1000 U/ml (provided by Rosanna Smith, University of Southampton) and β-mercaptoethanol 1μM. ES cells were passaged three times and seeded on the MEF feeder layer, before being seeded independently (**Figure 2-2**).

2.1.4.2 Experimental conditions for miRNA knock out cells

5 x 10^5 miR-200c/141 knock out ES cells were seeded into individual wells of a 6-well plate. The following day, exosomes from DLD1 or SW480 cells were incubated with the ES cells at a concentration of 15 μg/ml. Control ES cells were treated with an equal volume of exosome-depleted medium. After 24 h, cells were washed, trypsinised, pelleted and stored at -80°C until further use. Cell lysates were obtained from MEFs and SCC7 mouse squamous carcinoma cells

(Ruhcha Sutavani, University of Southampton), for use as positive controls. Following RNA extraction, miR-200c and miR-141 levels in the untreated ES cells, exosome-treated ES cells, MEFs, and SCC7 cells, were determined by Taqman RT-qPCR, as described below (section **2.1.5.3**).

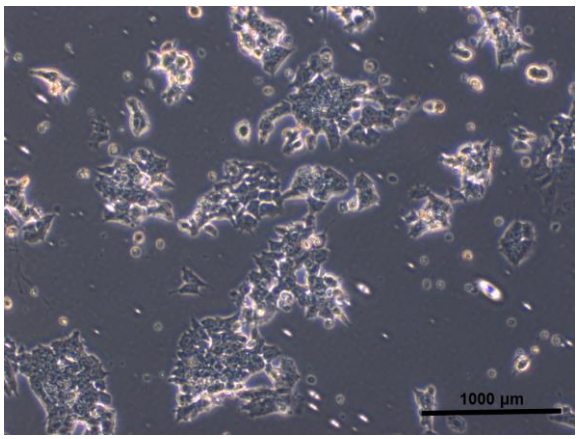

Figure 2-2. Mouse ES cells. MiR-200c/141 knock out ES cells in feeder-free conditions (10x objective).

2.1.5 RNA extraction and RT-qPCR

2.1.5.1 RNA extraction

Total cellular RNA was isolated from cells using the miRNeasy mini kit (cat no. 217004 Qiagen), as per manufacturer instructions. Briefly, 700 µl QIAzol lysis reagent was added to the cells, and the sample was disrupted and homogenized by passage through a 20-guage needle. The homogenate was then incubated at room temperature for 5 min. 140 µl chloroform was added to the homogenate, mixed thoroughly and incubated for a further 2 min at room temperature. The mixture was centrifuged at 12000*g* for 15min at 4^{o}C, after which the aqueous phase was collected. One and a half volumes of 100% ethanol were added to the aqueous phase and centrifuged in 700 µl aliquots through an RNeasy Mini spin column at 10000*g* for 15 s at room temperature. The spin column was then washed twice with RPE buffer. RNA was eluted with 30 µl of nuclease free water. RNA concentration and quality were measured by NanoDrop 8000 spectrophotometer (ThermoFisher).

2.1.5.2 Spectrophotometer (NanoDrop)

Immediately following extraction, 1 µl of RNA was analysed for concentration and purity using the NanoDrop 8000 spectrophotometer. The principle of measurement is based on the Beer-Lambert equation: c = (A x ε)/b, where ‘c’ is the nucleic acid concentration in ng/µL, ‘A’ is the absorbance in AU, ‘ε’ is the wavelength-dependent extinction coefficient in ng-cm/µL and ‘b’ is the path

length in cm. For RNA, 'ε' is assigned the value 40 ng-cm/ µl. Purity was estimated using 260/280 and 260/230 ratios, with "pure" RNA assigned the values 2 and 2-2.2 respectively.

2.1.5.3 TaqMan qPCR

TaqMan miRNA assay reactions were performed to quantitate miRNA expression in cellular RNA samples, after exosome conditioning. Total RNA was converted into cDNA using the Taqman Advanced miRNA cDNA Synthesis Kit (cat no. A28007; ThermoFisher). Input material was 4 ng of total RNA (2 µL of 2 ng/µl). For the poly A tailing reaction, 2 µL RNA was combined with 0.5 µL 10X Poly(A) Buffer, 0.5 µL ATP, 0.3 µL Poly(A) Enzyme and 1.7 µL RNase-free water (total reaction volume 5 µL). The reaction was incubated at 37 °C for 45 min, followed by 65 °C for 10 min. For the adaptor ligation reaction, the product of the poly A tailing reaction was combined with 3 µL 5X DNA Ligase Buffer, 4.5 µL 50% PEG 8000, 0.6 µL 25X Ligation Adaptor, 1.5 µL RNA Ligase and 0.4 µL RNase-free water (total reaction volume 15 µL). The reaction was incubated at 16 °C for 60 min. For the reverse transcription reaction, the product of the adaptor ligation reaction was combined with 6 µL 5X RT Buffer, 1.2 µL dNTP Mix (25 mM each), 1.5 µL 20X Universal RT Primer, 3 µL 10X RT Enzyme Mix and 3.3 µL RNase-free water (total reaction volume 30 µL). The reaction was incubated at 42 °C for 15 min, followed by 85 °C for 5 min. For the miR-Amp reaction, 5 µL of the reverse transcription product was combined with 25 µL 2X miR-Amp Master Mix, 2.5 µL 20X miR-Amp Primer Mix and 17.5 µL RNase-free water. The reaction was incubated at 95 °C for 5 min, followed by 14 cycles of 95 °C for 3 s/ 60 °C for 30 s, and finally, 99 °C for 10 min.

For the PCR reaction, the miR-Amp product was diluted 1:10 with RNase-free water, and 5 µL added to one well of a 96-well plate. This was combined with 10 µL TaqMan® Fast Advanced Master Mix (2X), 1 µL TaqMan® Advanced miRNA Assay (20X) and 4 µL RNase-free water (total reaction volume 20 µL). Reactions were set up in triplicate with the following cycling conditions: 95 °C for 20 s, followed by 40 cycles of 95 °C for 3 s/ 60 °C for 30 s, using the Applied Biosystems 7500 qPCR instrument.

Expression levels were normalised to miR-423-5p (endogenous reference gene) calculated from the triplicate of CT values, using the ΔΔCT method, and expressed relative to one of the samples that was assigned the value 1. Mean relative levels were calculated for each sample. Assay reference numbers were as follows: miR-16-5p (477860_mir), miR-21-5p (477975_mir), miR-29b-3p (478369_mir) and miR-423-5p (478090_mir).

2.1.6 Functional assays with exosomes

2.1.6.1 Cellular signalling pathways

DLD1 cells were treated with MRC5 exosomes at a final concentration of 15 µg/ml for 24h, after which cells were washed with PBS and pelleted. For western blotting, cell lysates were prepared and western blotting performed, as described above (section **2.1.3.2.2**). Proteins were detected with p44/42 MAPK/ ERK1/2 (137F5; 1:2000), phospho-p44/42 MAPK /ERK1/2 (D13.14.4E; 1:1000), Akt (C67E7; 1:1000), phospho-AKT (Ser473; D9E; 1:500), Bad (11E3; 1:1000) and phospho-Bad (Ser136; D25H8; 1:500) (Cell Signaling Technology) primary antibodies. HSP90 (68/Hsp90; 1:1000) (BD Biosciences) was used as an equal loading control.

2.1.6.2 Chemoresistance assay

There were four experimental conditions: (i) DLD1 cells, (ii) DLD1 cells treated with oxaliplatin, (iii) DLD1 cells co-cultured with MRC5 exosomes and (iv) DLD1 cells co-cultured with MRC5 exosomes and treated with oxaliplatin. Where applicable, DLD1 cells were co-cultured for 24 h with MRC5 exosomes at a concentration of 15 µg/ml, after which they were washed with PBS to remove 'free' exosomes. Where exosomes were not used, exosome-depleted conditioned medium of equivalent volume was used as a control. Oxaliplatin (Sigma-Aldrich, Saint Louis, USA) was used at a working concentration of 200 µM for 24 h, and where applicable, was added to the growth media after the 24 h exosome conditioning.

For subG1 DNA analysis, the protocol described by Sayan et al. was used [472]. Briefly, cells were detached, pelleted, fixed with 70% ice-cold ethanol and stored at -20^{o}C overnight. Next morning, cells were centrifuged at 500 g for 5 min and fixation solution discarded. Cells were then re-suspended in 100 µl PBS by gentle vortexing. To stain for DNA, cells were incubated with 0.260 U RNase (in PBS) for 30 min followed by 50 µM propidium iodide (in PBS) for 30 min. SubG1 DNA content was analysed using a flow cytometer (FACS Calibur, BD Biosciences, San Jose, USA) with duplet exclusion.

2.1.6.3 Proliferation assay

DLD1 cells were seeded in quadruplicate at a density of 1000 /well in a 96 well plate. The following day (day 0), MRC5 exosomes were added to achieve a concentration of 15 µg/ml. An equivalent volume of exosome-depleted conditioned medium was added to control cells. Cells were fixed sequentially on days 0, 2, 3, 4 and 5 with ice-cold 50:50 acetone-methanol. On day 5, all cells were stained with 1 µg/ml DAPI, washed with PBS, and the centre of each well viewed

with the 4x objective of a fluorescence microscope with UV filter (CKX41; Olympus). Cell nuclei were counted using ImageJ software (NIH; http://rsb.info.nih.gov/ij/) [473].

2.1.7 Cell lines

DLD1 and SW480 human colorectal adenocarcinoma cells were procured from American Type Culture Collection (ATCC), and MRC5 human foetal lung fibroblasts from The European Collection of Authenticated Cell Cultures (ECACC). All were authenticated by STR profiling by the supplier. DLD1, SW480 and MRC5 were grown in DMEM (cat no. D5796; Sigma) supplemented with 10% FBS (cat no. P40-37500; Pan Biotech), 2 mM L-Glutamine (cat no. G7513; Sigma) and 1% penicillin streptomycin (cat no. P4333; Sigma). Mirko_11A2 mouse ES cells, procured from Mouse Biology Program (UC Davis), were grown in ES cell medium (described above). MEFs were a gift from Katherine Parry (Human Health and Development, University of Southampton), and were grown in DMEM supplemented with 20% FBS, 2 mM L-Glutamine and 1% penicillin streptomycin. SCC7 mouse head and neck squamous cell carcinoma cells were a gift from Rucha Sutavani (Cancer Sciences, University of Southampton), and were grown in DMEM supplemented with 10% FBS, 2 mM L-Glutamine and 1% penicillin streptomycin All cells were maintained at 37 °C in a humidified atmosphere of 5% CO_2. Conditioned medium from CRC organoids was provided by Hayley Francies (Wellcome Sanger Institute, Cambridge). Information regarding cell lines is provided in Appendix **B**.

2.1.8 Statistical analysis

Where individual images (microscopy, western blotting, NTA and flow cytometry) are displayed, these are representative of at least two separate experiments. Graphics represent the mean ± SEM, unless otherwise stated. RT-qPCR was performed in triplicate and differences in mean relative values were tested by 2-tailed, unpaired t-test. Cell counting was performed in quadruplicate, and differences in mean relative counts, for different days, were compared by 2-tailed, paired t-test. Events acquired by flow cytometry were analysed in a 2x2 contingency table by a 2-tailed Fisher's exact test. Statistical analysis of SubG1 flow cytometry data is based on differences in mean percentages (from three separate experiments), tested by 2-tailed, unpaired t-test. The threshold level of significance was set at 0.05 for all statistical tests. The level of statistical significance was denoted by $p<0.05$ (*); $p<0.01$ (**); and $p<0.001$ (***).

2.2 Stromal exomiR profiling in CRC

2.2.1 Derivation of primary colorectal fibroblasts

2.2.1.1 Patient material

All patients were prospectively recruited as part of an ongoing UK National Institute of Health Research Clinical Research Network study (UKCRN ID 6067; NCT03309722), investigating the molecular pathology of CRC, and designed to identify novel biomarkers. Other results and further details from this ongoing study have been previously reported [427, 474-476]. Study oversight activities and monitoring were performed at an independent clinical research organisation. All patients provided written informed consent and the study was approved by the regional research ethics committee. Pathological verification of diagnosis and staging was in accordance with the Association of Coloproctology of Great Britain and Ireland guidelines [477]. Information relating to patient demographics, pre-operative risk, imaging, surgery, pathological features, post-operative management and oncological outcomes were extracted. Exclusion criteria included evidence of a hereditary tumour, presence of multiple tumours, tumours with histologically identified extensive necrosis and tumours with synchronous metastases at presentation.

Samples from patients with biopsy proven CRC were obtained fresh at the time of surgery. Patient characteristics are summarised in **Table 2-1**. Three consecutive patients, none of whom had received neoadjuvant chemotherapy or radiotherapy, were prospectively included. Immediately following excision of the surgical specimen, 1-2 cm diameter biopsies were taken from the tumour site and from normal colonic epithelium, proximal to the tumour, complying with the traditional view of resection margins in colorectal cancer surgery [478-480].

Table 2-1. Demographic and clinical characteristics of study patients.

	CRA-460-14 (#1)	CRA-463-14 (#2)	CRA-602-15 (#3)
Age (yrs)	79	68	79
Sex	F	M	M
Ethnicity	Caucasian	Caucasian	Caucasian
Tumour Site	Rectum	Sigmoid	Sigmoid
pTNM	T3N0M0	T4aN0M0	T4aN2M0
AJCC Stage	II	II	III
Dukes' Stage	B	B	C1
Differentiation	Moderate	Moderate	Well-moderate
EMVI Status	Negative	Negative	Negative
MSI Status	Negative	Negative	Negative
Neoadjuvant Treatment	No	No	No

From *Bhome et al. (2017)* [481]

2.2.1.2 Extraction of primary fibroblasts

Fresh tissue was collected in 10 ml phosphate buffered saline (PBS), supplemented with 2% (double-strength) penicillin–streptomycin (Penicillin (200 U/ml)–streptomycin (200 µg/ml; cat no. P4333; Sigma) and 0.1% (0.25 µg/ml) amphotericin B (Fungizone; cat no. 15290018; ThermoFisher), and washed three times with PBS. Tumour and normal biopsies were divided into 2-3 mm fragments in sterile conditions. Each fragment was attached to one well in a 12-well tissue culture plate containing Dulbecco's Modified Eagle's Medium (DMEM; cat no. D5671; Sigma) supplemented with 20% foetal bovine serum (FBS), 1% L-glutamine (200mM; cat no G7513; Sigma); 2% penicillin–streptomycin and 0.1% amphotericin B, and incubated at 37°C/ 5% CO_2. Growth medium was changed every 72 h. Outgrowth of fibroblasts was typically seen at 4 weeks, at which point cells were expanded in the standard manner (**Figure 2-3**).

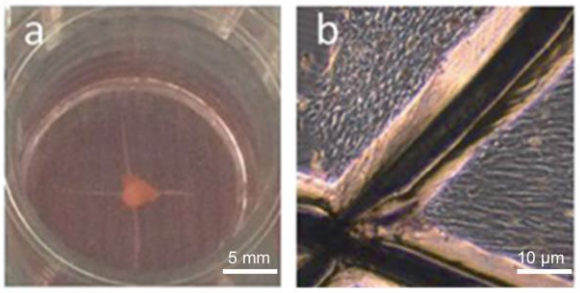

Figure 2-3. **Extraction of primary fibroblasts.** (**A**) The colonic or rectal tumour biopsy is divided into 2-3 mm fragments, fixed to the centre of a cross in a 12-well plate, and covered with 1 ml medium. (**B**) After 4-6 weeks, there is a confluent outgrowth of fibroblasts from the centre of the well (10x objective). The cross appears black. Note that the fragment has been removed by this stage. From *Bhome et al. (2018)* [482].

2.2.1.3 Detection of myofibroblastic markers in primary fibroblasts

Cell lysates were prepared, and western blotting performed, as described above (section **2.1.3.2.2**). Proteins were detected with α-smooth muscle actin (SMA) (1A4; 1:2000; Sigma-Aldrich, Saint Louis, USA), fibronectin-EDA (MAB1940; 1:2000; Merck Millipore, Burlington, USA), palladin (1E6; 1:1000; Novus Biologicals, Littleton, USA) and vimentin (Vim 3B4; 1:1000; Dako, Glostrup, Denmark) primary antibodies. HSC-70 (B-6; 1:2000; Santa Cruz Biotechnology, Dallas, USA) was used as an equal loading control.

2.2.1.4 Immunostaining of actin filaments in primary fibroblasts

Primary NOF and CAF cells (pair #2) were seeded on 22x22 mm glass microscope slides (as above) and grown to 70% confluence. Cells were washed with PBS, then fixed with ice-cold 50/50 acetone-methanol for 5 min. Cells were then incubated for 30 min with 50 µg/ml phalloidin-FITC (cat no. P5282; Sigma), followed by 5 min with 1 µg/ml DAPI (cat no. D9542; Sigma), then washed with PBS. Cells were viewed using the 40x objective of the Olympus CKX41 microscope. Staining intensity and surface area were measured for nine distinct cells in each field of view using ImageJ software (NIH; http://rsb.info.nih.gov/ij/).

2.2.2 RNA extraction and quality control

2.2.2.1 RNA extraction

Total cellular RNA was isolated using the miRNeasy mini kit (section **2.1.5.1**) and total exosomal RNA using the miRNeasy micro kit (cat no. 217084; Qiagen), as per the manufacturer instructions. Briefly, 700 µl QIAzol lysis reagent was added to the cells or exosomes and the sample disrupted

and homogenized by passage through a 20G needle (cells) or vortexing for 1 min (exosomes). The homogenate was then incubated at room temperature for 5 min. 140 µl chloroform was added to the homogenate, mixed thoroughly and incubated for a further 2 min at room temperature. The mixture was centrifuged at 12000 *g* for 15min at 4°C, after which the aqueous phase was collected. One and a half volumes of 100% ethanol were added to the aqueous phase and centrifuged in 700 µl aliquots through an RNeasy Mini (cells) or RNeasy MinElute (exosomes) spin column at 10000 *g* for 15 s at room temperature. The spin column was then washed twice with RPE buffer (cells), or with RWT followed by RPE followed by 80% ethanol (exosomes). RNA was eluted with 30 µl (cells) or 14 µl (exosomes) nuclease free water. RNA concentration and quality were measured by NanoDrop 8000 spectrophotometer (ThermoFisher) and 2100 Bioanalyzer (Agilent).

2.2.2.2 Bioanalyzer

An Agilent RNA 6000 chip was used together with the Agilent 2100 Bioanalyzer. 9 µl gel-dye mix was dispersed into all wells using a pressurized plunger system. A further 9 µl gel-dye mix was pipetted into two other wells. 5 µl marker was pipetted into each of the 12 sample and one ladder wells. 1 µl sample or ladder was pipetted into each corresponding well. The chip was vortexed at 2400 rpm for 60 s using the IKA vortex mixer. The chip was then inserted into the Bioanalyzer and read to produce an electropherogram for all samples.

2.2.3 NanoString miRNA profiling

2.2.3.1 NanoString miRNA assay

The multiplexed NanoString nCounter miRNA expression assay (NanoString Technologies) was used to profile 801 human miRNAs. The assay was performed according to the manufacturer's protocol. Briefly, 100 ng of total RNA (33 ng/µl) was used as input material. A specific DNA tag was ligated to the 3' end of each mature miRNA, providing exclusive identification for each miRNA species in the sample. The tagging was performed in a multiplexed ligation reaction utilising reverse complementary bridge oligonucleotides to achieve ligation of each miRNA to its designated tag. All hybridization reactions were incubated at 64°C for 18 h. Excess tags were then removed and the resulting material was hybridized with a panel of fluorescently labelled, bar-coded, reporter probes specific to the miRNA of interest. Abundances of miRNAs were quantified on the nCounter Prep Station by counting individual fluorescent barcodes and quantifying target miRNA molecules present in each sample.

2.2.3.2 NanoString data analysis

Raw NanoString miRNA data were quantile-normalized using the voom function as implemented in the limma R package (version 3.30.9). MiRNAs were tested for differential abundance using an empirical Bayes moderated t-test in limma, and p-values were corrected for multiple testing by the positive false discovery rate. Results were then graphically displayed in a heat map showing the 20 largest changes in miRNA expression.

Several other miRNAs (miR-21, miR-17-92 cluster, miR-95, miR-135a/b, miR-155 and miR-499) were selected based on their experimentally proven relevance in colorectal cancer and their roles as oncomirs [483]. Raw NanoString counts were normalized to miR-451, miR-16, miR-30a-5p and miR-30e-5p (a combination of best predicted and experimentally utilized stable endogenous exosomal miRNA controls [278, 295, 484]).

To identify miRNAs that were enriched in exosomes compared to cells, a global mean normalization method was used because there is no validated panel of miRNAs, which are stably expressed in both exosomal and cellular compartments [485]. For each miRNA of interest, exosomal levels were expressed relative to cellular miRNA levels.

MiRNAs of interest were validated in a distinct biological replicate of the corresponding NanoString sample by RT-qPCR. Relevant data were deposited in the ExoCarta database [486].

2.2.3.3 Taqman RT-qPCR validation

TaqMan Advanced (ThermoFisher, Waltham, USA) miRNA assay reactions were performed to quantitate miRNA expression in cellular and exosomal RNA samples according to manufacturer instructions. Expression levels were normalised to miR-423-5p (endogenous reference gene), calculated from the triplicate of CT values, using the ΔΔCT method, and expressed relative to NOF exosomes, which were assigned the value 1. Mean relative levels were calculated for each sample. The assay reference numbers were as follows: miR-21-5p (477975_mir), miR-181a-3p (479405_mir), miR-199b-5p (478486_mir), miR-215-5p (478516_mir), miR-329-3p (478029_mir), miR-382-5p (478078_mir) and miR-423-5p (478090_mir). The Taqman Advanced cDNA synthesis and qPCR protocols are described above (section **2.1.5.3)**.

2.2.3.4 MiRNA pathway analysis

Statistical relevance of potential biological pathways that could be affected by the changes observed in miRNA expression was calculated by the miRPath web-based platform [59]. Putative miRNA target genes were determined using the homology search algorithm microT-CDS with the use of TarBase (database of >600 000 experimentally validated interactions between miRNAs and

genes) [86]. For microT-CDS, a recommended microT prediction threshold of greater than 0.8 was set. The pathway enrichment analysis of multiple miRNA target genes was performed by comparing the input list to miRNA targets contained in all KEGG pathways. All significantly altered miRNAs were used simultaneously for the pathway enrichment analysis. The significance levels between miRNAs and every pathway were calculated by the Fisher-exact meta-analysis method, with the use of unbiased empirical distribution [487]. The resulting *p*-values signify the probability of a pathway being targeted by at least one miRNA out of the selected group. *P*-values were adjusted using false discovery rate (FDR) and the significance level set to 0.05 [488].

MiRNAs of interest were also submitted to the Ingenuity Pathway Analysis microRNA Target Filter (QIAGEN, https://www.qiagenbioinformatics.com/products/features/microrna-target-filter). In this analysis, mRNA targets and corresponding canonical pathways were predicted from a combination of TargetScan, TarBase, miRecords and the Ingenuity Knowledge Base. Ingenuity Pathway Aanalysis was undertaken by Quan Gu (University of Glasgow).

Relationships between miRNAs and small molecules were recovered using miRNet [489], which aggregates interaction data from multiple databases including TarBase, miR2Disease, HMDD, PhenomiR, SM2miR and PharmacomiR. This was undertaken by Kirill Veselkov (Imperial College London).

2.2.4 Orthotopic CRC model

All mice were housed in a specific pathogen-free facility at the University of Southampton and given a commercial basal diet and water *ad libitum*. Prior to undertaking orthotopic injections, to demonstrate persistence of injected fibroblasts *in vivo*, three 6-8-week-old female CD-1 nude mice (Charles River, Margate, UK) were co-injected with $5x10^5$ HCT116 CRC cells and $5x10^5$ PKH26-labelled MRC5 fibroblasts into dorsal subcutaneous tissue bilaterally. At three weeks, animals were sacrificed and tumours excised. Tumours were fixed, sectioned and imaged by confocal microscopy as described above (section **2.1.3.2.6**).

An orthotopic colorectal cancer model was used as previously described [475]. Briefly, six 6-8 week old female CD-1 nude mice (Charles River) were anaesthetised using isoflurane, followed by laparotomy and exteriorisation of the caecum. For each animal, $1x10^6$ SW620 human CRC cells and $5x10^6$ human MRC5 fibroblasts (stably overexpressing miR-21, or, scrambled sequence control miRNA; n=3 in each group) were combined with Matrigel® (cat no. 354230; Corning) to a total volume of 100 µl. The cell/ matrix combination was orthotopically injected into the submucosal layer of the cecum under magnified vision. The cecum was then returned to the peritoneal cavity and the abdominal wall closed in layers with absorbable suture material.

Tumours were allowed to grow for 8-10 weeks until the first mice showed signs of weight loss, at which time all mice were humanely euthanized. Colon, liver and spleen were harvested. Excised tissue was paraffin embedded, stained with haematoxylin and eosin and mounted on to slides, before assessment by a specialist histopathologist who was blinded to the outcome of the experiment. Orthotopic injections, visceral extraction and tissue processing was conducted by Professor Alex Mirnezami (**Figure 2-4**). Percentage liver replacement (surface area of tumour relative to total surface area) for multiple sections of each control and "miR-21" liver was measured using ImageJ software (NIH; http://rsb.info.nih.gov/ij/). Values from each tissue section were combined to give an overall mean for each group.

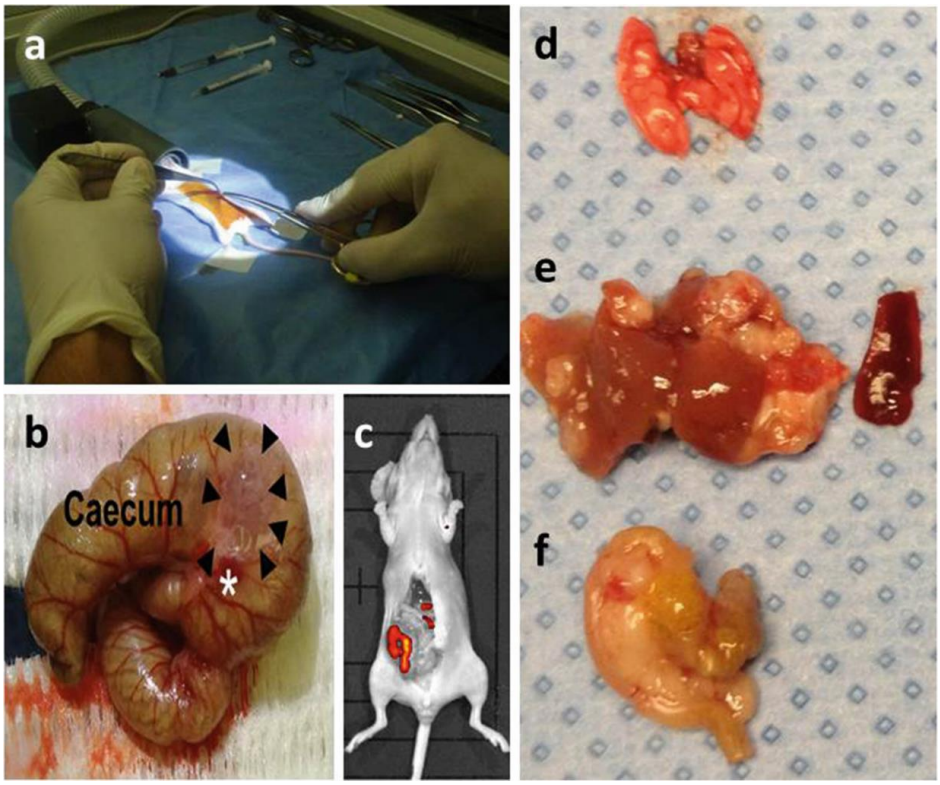

Figure 2-4. Orthotopic CRC mouse model. (A) Mouse is positioned supine in a sterile field and maintenance inhaled anaesthesia provided by nose cone. The skin is prepared with Betadine solution and a midline laparotomy performed. (B) 8-10 weeks after caecal injection of CRC cells +/- fibroblasts, the large bowel is excised to reveal a primary tumour (arrows). (C) If injected cells are fluorescently labelled, the tumour is apparent by *in vivo* imaging techniques. (D) Lungs, (e) liver (with metastases) and spleen and (f) large bowel are removed for macroscopic and histological analysis. From *Bhome et al. (2018)* [482].

2.2.5 Cell lines and transfection

2.2.5.1 Cell lines

DLD1 and SW480 human colorectal adenocarcinoma cells were procured from ATCC, and MRC5 human foetal lung fibroblasts from ECACC. Cells were authenticated by STR profiling, by the supplier. DLD1, SW480 and MRC5 were grown in DMEM supplemented with 10% FBS, 2 mM L-Glutamine and 1% penicillin streptomycin. Primary human colorectal fibroblasts were isolated and subcultured as per the protocol described above (section **2.2.1.2**). Primary cells were established in DMEM, supplemented with 20% FBS, 2 mM L-Glutamine, 2% penicillin-streptomycin and 0.1% amphoteracin B, and switched to DMEM/ 10% FBS (without amphoteracin B) after four passages. All cells were maintained at 37 °C in a humidified atmosphere of 5% CO_2. Information regarding cell lines is provided in Appendix **B**.

2.2.5.2 Transfections

MiR-21 and scrambled control (miR-SCC) miRNA were stably expressed in MRC5 fibroblasts by transfecting precursor miRNA expression plasmids containing IRES-driven GFP reporters and subsequently selecting with puromycin. Transfections were performed using the Xfect transfection reagent (cat no. 631318; Clontech). These cells were generated by Marc Bullock (Cancer Sciences, University of Southampton).

Stable mCherry expression in DLD1 cells was achieved by transfecting mCherry (N2) plasmid and selecting single cell clones with neomycin. Positive clones were identified using fluorescence microscopy. Transfection was performed using the Lipofectamine 3000 transfection reagent (cat no. L3000008; ThermoFisher). These cells were generated by Hajir Al-Saihati, University of Southampton.

2.2.6 Statistical analysis

Where individual images (microscopy, western blotting and flow cytometry) are displayed, these are representative of at least two separate experiments. Graphics represent the mean ± SEM, unless otherwise stated. RT-qPCR was performed in triplicate and differences in mean relative values were tested by 2-tailed, paired (for paired NOF-CAF samples) or unpaired (Student's) t-test, as appropriate. Cell counting was performed in quadruplicate and differences in mean relative counts, for different days, were compared by 2-tailed, paired t-test. Events acquired by flow cytometry were analysed in a 2x2 contingency table by a 2-tailed Fisher's exact test. Statistical analysis relating to NanoString data and pathway analysis is described in detail above. Percentage

liver replacement was compared by two-tailed Student's t-test. The threshold level of significance was set at 0.05 for all statistical tests. The level of statistical significance was denoted by $p<0.05$ (*); $p<0.01$ (**); and $p<0.001$ (***).

2.3 The role of exosomes in EMT-driven fibroblast phenotype

2.3.1 Cell lines

DLD1, HCT116, SW620 and SW480 human colorectal adenocarcinoma cells were procured from ATCC. The mutational status of CRC cells is shown in **Table 2-2**. MRC5 and IMR90 human foetal lung fibroblasts were procured from ECACC. All commercially acquired cell lines were characterised by STR profiling, by the supplier. HFFF2 human foetal foreskin fibroblasts were a gift from Professor Gareth Thomas (University of Southampton). Primary human normal colonic fibroblasts (NOF) were isolated by myself, as described above (section **2.2.1.2**). Immortalised primary human colonic cancer-associated fibroblasts (colon CAF) were a gift from Professor Olivier DeWever (Ghent University). All cells were grown in DMEM, supplemented with 10% FBS, 2 mM L-Glutamine and 1% penicillin-streptomycin, and maintained at 37 °C in a humidified atmosphere of 5% CO_2. Information regarding cell lines is provided in Appendix **B**.

Table 2-2. Origin, microsatellite and mutational status of CRC cell lines.

Cell line	**Origin**	**MSI/ MSS**	***KRAS***	***BRAF***	***PIK3CA***	***PTEN***	***TP53***
DLD1	Male; colon; Dukes' C	MSI	G13D	wt	E545K;D549N	wt	S241F
HCT116	48 year-old male; ascending colon; Dukes' D	MSI	G13D	wt	H1047R	wt	wt
SW620	51 year-old male; lymph node; Dukes' C	MSS	G12V	wt	wt	wt	R273H;P309S
SW480	50 year-old male; colon; Dukes' B	MSS	G12V	wt	wt	wt	R273H;P309S

2.3.2 Generation of SW480 ZKD cells

2.3.2.1 Transfection of HEK293T cells

1 x 10^6 HEK293T cells were seeded into individual wells of a 6-well plate. The following day, when cells were 90% confluent, they were transfected with viral packaging mix and ZEB1 shRNA plasmid, using Lipofectamine 3000 (ThermoFisher). In tube A, 7 µl Lipofectamine 3000 was diluted

in 250 µl OptiMEM I (cat no. 31985062; ThermoFisher). In tube B, 2.25 µg ViraPower packaging mix (cat no. K497500; ThermoFisher), 750 ng ZEB1 pLenti shRNA (cat no. SHCLND-NM_030751; Sigma) and 6 µl p3000 reagent, were added to 250 µl OptiMEM. The contents of Tube A and B were mixed (final volume 500 µl), incubated at room temperature for 20 min, and then added to a single 6-well of HEK293T cells containing 1 ml DMEM. Cells were incubated at 37^{o}C for 6 h before the medium was replaced with 2 ml fresh DMEM. Viral supernatant was collected at 24 and 52 h post-transfection, filtered (0.22 µm filter) and stored at -80^{o}C. Details of the ZEB1 pLenti shRNA are as follows: ZEB1 MISSION shRNA Plasmid DNA; clone NM_030751.4-1268s21c1; sequence – CCGGTGTCTCCCATAAGTATCAATTCTCGAGAATTGATACTTATGGGAGACATTTTTG.

2.3.2.2 Infection and selection of SW480 clones

3 x 10^5 SW480 cells were seeded into individual wells of a 6-well plate. The following day, medium was replaced with 1 ml viral supernatant, containing hexadimethrine bromide (Polybrene; cat no. H9268; Sigma) at a final concentration of 8 µg/ml. Cells were washed after 24 h, trypsinised and seeded on 96 well plates at a density of 80 cells/plate (≤1 cell/well) to obtain single cell clones. Following puromycin selection at a concentration of 2 µg/ml for 3-4 weeks, positive clones were identified by microscopy and validated by western blotting.

2.3.3 EMT status of CRC cells

Cell lysates were prepared, and western blotting performed, as described above (section **2.1.3.2.2**). Proteins were detected with Zeb1 (Santa Cruz Biotechnology; 1:500), E-cadherin (clone 36; BD Biosciences; 1:1000), pan cytokeratin (C11; Cell Signaling Technology; 1:10000) and vimentin (3B4; Dako; 1:1000) primary antibodies. HSP90 (68/Hsp90; BD Biosciences; 1:1000) was used as an equal loading control.

2.3.4 Akt/ ERK activity of CRC cells

Cell lysates were prepared, and western blotting performed, as described above (section **2.1.3.2.2**). Proteins were detected with p44/42 MAPK/ ERK1/2 (137F5; 1:2000), phospho-p44/42 MAPK /ERK1/2 (D13.14.4E; 1:1000), Akt (C67E7; 1:1000) and phospho-AKT (Ser473; D9E; 1:500) (Cell Signaling Technology) primary antibodies. β-actin (C4; BD Biosciences; 1:5000) was used as an equal loading control.

2.3.5 Conditioning of fibroblasts with CRC exosomes

Exosomes were isolated from cell culture conditioned media, from CRC cells, using the same protocol described above (dUC; section **2.1.1**). $4x10^5$ MRC5 fibroblasts were seeded into individual wells of a 6-well plate. The following day, fibroblasts were conditioned with exosomes from DLD1, HCT116, SW620 and SW480 cells for 24 h, at three different concentrations: 5, 15 and 45 µg/ml, in exosome-free medium. At 24h, fibroblasts were washed with PBS, trypsinised, pelleted,and stored at -20^{o}C until further use.

2.3.5.1 Western blotting for cellular pathways

Cell lysates were prepared, and western blotting performed, using the protocol described above (section **2.1.3.2.2**). Proteins were detected with phospho-(Ser/Thr) PKA substrate (9621), phospho-Akt Substrate (RXRXXS*/T*) (23C8D2; 1:1000), phospho-(Ser) PKC substrate (2261; 1:1000), phospho-MAPK/CDK substrates (PXS*P or S*PXR/K) (34B2; 1:1000), phospho-AMPKα (Thr172) (40H9; 1:1000), phospho-(Ser/Thr) ATM/ATR substrate (4F7; 1:1000), p44/42 MAPK/ ERK1/2 (137F5; 1:2000), phospho-p44/42 MAPK /ERK1/2 (D13.14.4E; 1:1000), Akt (C67E7; 1:1000) and phospho-AKT (Ser473; D9E; 1:500) (Cell Signaling Technology) primary antibodies. β-actin (C4; BD; 1:5000) was used as an equal loading control.

2.3.5.2 Assessment of cell cycle profile

4 x 10^5 MRC5 fibroblasts were conditioned with exosomes from either SW620 (epithelial) or SW480 (mesenchymal) cells at a concentration of 5 µg/ml (effective dose for pERK attenuation), or an equivalent volume of exosome-depleted medium (control), for 24 h, in exosome-free medium, in 6-well plates. Cells were assessed at either 24 or 96 h. Cells assessed at the later time point were grown in exosome-free conditions after the initial 24 h exosome conditioning.

For flow cytometry, the cell pellet was resuspended in 400 µl ice-cold PBS and added dropwise to a FACS tube containing an equal volume of ice-cold 70% ethanol (fixative), which was being vortexed simultaneously. Cells were then stored overnight at -20 ^{o}C. Next morning, cells were centrifuged at 500*g* for 5 min and resuspended in 100 µl ice-cold PBS. To stain for DNA, cells were incubated with 0.260U RNase (in PBS) for 30 min followed by 50 µM propidium iodide (in PBS) for 30 min. DNA content was analysed using a flow cytometer (FACS Calibur, BD Biosciences) with duplet exclusion.

2.3.5.3 Fibroblast proliferation assay

1 x 10^4 MRC5 fibroblasts were seeded into 48-well plates, in exosome-free medium. The following day, exosomes from SW620 (epithelial) or SW480 (mesenchymal) were added at a concentration of 5 µg/ml (day 0). After 24 h of exosome conditioning, exosomes were washed off and medium changed (day 1). Cells were fixed with ice-cold 50:50 acetone-methanol for 2 min, in quadruplicate, on days 1-4. On day 4, cells were stained with 1 µg/ml DAPI for 5 min, washed with PBS, and the centre of each well viewed with the 4x objective of a fluorescence microscope with UV filter (CKX41; Olympus). Cell nuclei were counted using ImageJ software (NIH; http://rsb.info.nih.gov/ij/) [473].

2.3.6 RNA extraction and quality control

Total RNA (including small RNA) was extracted from cells and exosomes using the mirNeasy mini and micro kits respectively, as described above (sections 2.1.5.1, 2.2.2.1). RNA quality and concentration was determined using the NanoDrop 8000 spectrophotometer (ThermoFisher), as described in section **2.1.5.2**. RNA was stored at -80 °C until further use.

2.3.7 MiRNA array

The Cancer MicroRNA qPCR Array with QuantiMir™ (cat no. RA610A-1; SBI System Biosciences, Palo Alto, USA) was used to profile CRC cells and exosomes for 95 cancer-related miRNAs. The protocol was conducted as per manufacturer instructions and consisted of cDNA synthesis followed by RT-qPCR.

For cDNA synthesis, input material was 100 ng cellular or exosomal RNA. The first step was poly A tailing and required the combination of 5 µl RNA (~100ng), 2 µl 5X PolyA Buffer, 1 µl 25mM MnCl2, 1.5 µl 5mM ATP and 0.5 µl PolyA Polymerase (total recation volume 10 µl). The reaction was incubated at 37 °C for 30 min. The next step was to anneal the Anchor dT Adaptor by adding 0.5 µl Oligo dT Adaptor and incubating at 60 °C for 5 min, followed by 20 °C for 2 min. The final step was to synthesise cDNA by adding 4 µl 5X RT Buffer, 2 µl dNTP mix, 1.5 µl 0.1M DTT, 1.5 µl RNase-free water and 1 µl Reverse Transcriptase (total reaction volume 20.5 µl). This reaction was incubated at 42 °C for 60 min, followed by 95 °C for 10 min. The resulting cDNA was stored at -20°C until further use.

For each sample being profiled, a qPCR master mix was made, consisting of 1750 µl 2X SYBR Green qPCR Mastermix buffer, 60 µl Universal Reverse Primer (10 µM), 20 µl cDNA and 1670 µl RNase-free water. The Primer plate contained 95 desiccated miRNA primers (as well as the small

nuclear RNA U6 as an internal control). These were each resuspended with 11 µl of RNase-free water and the plate kept on ice. 29 µl of master mix and 1 µl of primer were then pipetted into each well of a new 96-well plate, being careful to maintain the miRNA configuration of the Primer plate (e.g. let-7 in well A1, miR-7 in well A2, etc). The qPCR cycling conditions were as follows: (1) 50°C for 2 min, (2) 95°C for 10 min, (3) 95°C for 15 s, (4) 60°C for 1 min (40 cycles of steps 3 and 4) and data read at 60°C for 15 s. Samples were processed in triplicate, with each replicate requiring one 96-well plate.

A global mean normalization method was used, as previously described [485]. Here, the mean CT value from 95 miRNAs was subtracted from the CT value of the miRNA of interest (ΔΔCT). The mean ΔΔCT value of the three replicates was then calculated. The logarithmic mean ΔΔCT value was converted into a linear value using the formula "$2^{(-\Delta\Delta CT)}$". Linear values were used to compare miRNA abundance between samples. Unbiased hierarchical clustering analysis was performed using the limma R package (version 3.30.9).

2.3.8 RT-qPCR for miR-200 in CRC cells and exosomes

TaqMan Advanced (ThermoFisher) assays were performed to quantitate miR-200 family expression in cellular and exosomal RNA samples from DLD1, HCT116, SW620, SW480 and SW480 ZKD. Input material was 4 ng of total cellular or exosomal RNA. Expression levels were normalised to miR-423-5p (endogenous reference gene) calculated from the triplicate of CT values using the ΔΔCT method, and expressed relative to SW480 cells or exosomes, which were assigned the value 1. Mean relative levels were calculated for each sample. The assay reference numbers were as follows: miR-200a-3p (478490_mir), miR-200b-3p (477963_mir), miR-200c-3p (478351_mir), miR-141-3p (478501_mir), miR-429 (477849_mir). Taqman cDNA synthesis and PCR protocols are described above (section **2.1.5.3**).

2.3.9 Luciferase reporter assays

2.3.9.1 Purification of plasmids

ZEB1 3'UTR (pCI-neo-RL-ZEB1; cat no. 35535), *ZEB1* 3'UTR mutated at the miR-200b binding site (pCI-neo-RL-ZEB1 200bmutx5; cat no. 35537) and control (fragments of HNF4A 3'UTR; pRL Con850-1207; cat no. 31447) plasmids were acquired from Addgene as bacterial stabs. Partial sequences are shown in Appendix **B**.

For each plasmid, a pipette tip coated with bacteria was transferred into a universal tube containing 6 ml LB medium. Puromycin was added to achieve a final concentration of 1 µg/ml.

The universal tube was agitated at 37 °C overnight and then stored at 4 °C until further use. The QIAprep® Spin Miniprep Kit (cat no. 27104; Qiagen) was used to purify palsmids, as per manufacturer instructions. Briefly, bacteria were centrifuged at 5000*g* for 15 min at room temperature, resuspended in 250 µl Buffer P1 and transferred to a microcentrifuge tube. 250 µl Buffer P2 was then added and mixed by inverting the tube 5 times until the solution became clear. 350 µl Buffer N3 was added and mixed immediately by inverting the tube 5 times. The tube was then centrifuged at 17900*g* for 10 min and the supernatant applied to a QIAprep spin column. The column was centrifuged at full speed for 30 s and the flow-through discarded. The column was then washed by adding 0.75 ml Buffer PE and centrifuged again at full speed for 30 s, and the flow-through discarded. DNA was then eluted in 50 µl DNase/ RNase-free water and concentration determined using the NanoDrop 8000 spectrophotometer.

2.3.9.2 Transfections

1 x 10^4 HEK293 cells, or, 2 x 10^4 MRC5 fibroblasts, were seeded into each well of a 96-well plate. The following day, each 96-well was transfected with 15 ng Firefly, 15 ng mCherry, 200 ng luciferase reporter construct (ZEB1 3'UTR, 200b mutant 3'UTR or control 3'UTR) and 2 pmol miRNA mimic or scrambled sequence control, using 0.5 µl Lipofectamine 2000 (cat no. 11668027; ThermoFisher) in 100 µl OptiMEM (cat no. 31985070; ThermoFisher). After 4h (HEK293) or 6 h (MRC5), transfection efficiency was assessed by detection of mCherry signal by fluorescence microscopy. The medium was then changed to regular DMEM. Cells were then left for a further 24 h before detection of luciferase activity.

2.3.9.3 Luciferase measurement

Firefly and Renilla luciferase activity was measured using the Dual-Glo® Luciferase Assay System (cat no. E2940; Promega). Cells were first equilibrated room temperature. 100 µl Luciferase Assay Reagent was added to each well and incubated for 10 min on a rocker at room temperature. Firefly luciferase activity was then measured using a luminometric plate reader (Varioskan LUX Multimode Microplate Reader; ThermoFisher). 100 µl Stop & Glo Reagent was then added to each well and incubated for 10 min on a rocker at room temperature. Renilla luciferase activity was then measured on the same plate reader. For each well, Renilla activity was normalised by Firefly activity.

2.3.10 Extended conditioning of fibroblasts with CRC exosomes and myofibroblast transdifferentiation

2.3.10.1 Selection of appropriate fibroblast cell line

To identify the most appropriate fibroblast cell line to use for TGF-β-mediated myofibroblast transdifferentiation, IMR90, MRC5, primary colon NOF, HFFF2 and primary colon CAF, were seeded into 6-well plates at a density of 4 x 10^5 cells/ well. The following day, 2 ng/ml TGF-β (cat no. 240-B; R&D Systems), or an equivalent volume of PBS (control) was added to the culture medium. After 48 h, cells were washed, trypsinised, pelleted and stored at -20^{o}C until further use. Cell lysates were prepared, and western blotting performed, as described above (section **2.1.3.2.2**). Proteins were detected with Zeb1 (sc25388; 1:500; Santa Cruz Biotechnology), fibronectin-EDA (MAB1940; 1:2000; Merck Millipore) and α-SMA (1A4; 1:2000; Sigma) primary antibodies. β-actin (C4; BD Biosciences; 1:5000) was used as an equal loading control. Fibroblasts used in this part of the project are detailed in **Table 2-3**.

Table 2-3 Fibroblasts tested for *in vitro* transdifferentiation.

Fibroblast	Origin	Primary/ established	Modification	Source
IMR90	Lung	Established	Nil	ATCC
MRC5	Lung	Established	Nil	ATCC
NOF	Colon	Primary	Nil	Self-generated
HFFF2	Foetal foreskin	Established	Nil	Professor Gareth Thomas, Southampton
CAF	Colon	Primary	hTERT immortalisation	Professor Olivier DeWever, Ghent

2.3.10.2 Duration of TGF-β treatment

To determine the optimal duration of TGF-β exposure, MRC5 fibroblasts were seeded into 6-well plates at a density of 4 x 10^5 cells/ well. The following day, untreated (control) cells were collected, and remaining cells were treated with 2 ng/ml TGF-β. Cells were collected at 24, 36, 48, 60 and 72 h after addition of TGF-β, and stored at -20^{o}C until further use. Cell lysates were prepared, and western blotting performed, as described above (section **2.1.3.2.2**). Proteins were detected with Zeb1 (sc25388; 1:500; Santa Cruz Biotechnology), fibronectin-EDA (MAB1940; 1:2000; Merck Millipore) and α-SMA (1A4; 1:2000; Sigma) primary antibodies. β-actin (C4; BD Biosciences; 1:5000) was used as an equal loading control.

2.3.10.3 Experimental set up for exosome-conditioning of fibroblasts

To replicate the *in vivo* situation, fibroblasts were conditioned with CRC exosomes every day for five days. 4 x 10^5 MRC5 fibroblasts were seeded into 6-well plates, in exosome-free medium. The next day (day 0), the medium was changed and SW480 control (mesenchymal) or ZKD (epithelial) exosomes were added to achieve a final concentration of 15 µg/ml. Medium was changed and fresh exosomes added in a similar fashion on days 2-5. Cells were passaged on day 3 and day 5, and approximately one-third collected for RNA analysis. On day 6, the medium was changed to a low serum (0.1% FBS) exosome-free medium, and on day 7, TGF-β was added to achieve a concentration of 2 ng/ml [490, 491]. An equal number of wells were untreated, as controls. Cells were collected on day 9 for western blotting.

2.3.10.4 RT-qPCR for miR-200 in exosome-conditioned fibroblasts

TaqMan Advanced (ThermoFisher) assays were performed to quantitate miR-200 family expression in MRC5 fibroblats conditioned with either SW480 control (mesenchymal) or ZKD (epithelial) exosomes on day 3 and day 5. Input material was 4 ng of total cellular or exosomal RNA. Expression levels were normalised to miR-423-5p (endogenous reference gene) calculated from the triplicate of CT values using the ΔΔCT method, and expressed relative to MRC5 fibroblasts conditioned with mesenchymal exosomes (day 3), which were assigned the value 1. Mean relative levels were calculated for each sample. The assay reference numbers were as follows: miR-200a-3p (478490_mir), miR-200b-3p (477963_mir), miR-200c-3p (478351_mir), miR-141-3p (478501_mir), miR-429 (477849_mir). Taqman cDNA synthesis and PCR protocols are described above (section **2.1.5.3**).

2.3.10.5 Protein expression in exosome-conditioned fibroblasts

Cell lysates were made from exosome-conditioned MRC5 fibroblasts, and western blotting performed, as described above (section **2.1.3.2.2**). Proteins were detected with Zeb1 (sc25388; 1:500; Santa Cruz Biotechnology), fibronectin-EDA (MAB1940; 1:2000; Merck Millipore) and α-SMA (1A4; 1:2000; Sigma) primary antibodies. β-actin (C4; BD Biosciences; 1:5000) was used as an equal loading control.

2.3.11 MiRNA and siRNA transfection of fibroblasts

2.3.11.1 Experimental set up for transfections

4 x 10^5 MRC5 fibroblasts were seeded into 6-well plates (day 0). The following day (day 1), cells were transfected with miR-200 mimics, ZEB1 siRNA or scrambled sequence control RNA. Six hours

after transfection, cells were split 1:2. On day 3, medium was switched to low serum medium (0.1% FBS), and on day 4, TGF-β (2 ng/ml) was added to half the wells (the remainder were controls). On day 6, cells were collected for western blotting.

2.3.11.2 Transfections

60%-confluent MRC5 fibroblasts were transfected with miR-200 mimics (miR-200b/ -200c) or ZEB1 siRNA. To start with, cells were in 6-well plates, with each well containing 2 ml DMEM. For each miRNA mimic or siRNA being transfected, 100 pmol was added to 250 µl OptiMEM (cat no. 31985070; ThermoFisher) in an Eppendorf tube. In a separate tube, 5 µl Lipofectamine 2000 transfection reagent (cat no. 11668027; ThermoFisher) was added to 250 µl OptiMEM. After exactly 5 min, the lipofectamine/ OptiMEM mixture was combined with the oligonucleotide/ OptiMEM mixture and left for 20 min. This combination total volume 500 µl) was then added to one 6-well of fibroblasts and left for six hours before splitting the cells, as outlined above. MISSION miR-200b-3p (cat no. HMI0352; Sigma) and miR-200c-3p (cat no. HMI0354; Sigma) mimics, Hs_ZEB1_6 FlexiTube siRNA (cat no. SI04951072; Qiagen) and MISSION siRNA universal negative control #1 (cat no. SIC001; Sigma) were used. Transfection efficiency was determined 48 h after transfection by RT-qPCR for miR-200b and -200c, or western blotting for Zeb1. qPCR and western blotting protocols are described above (sections 2.1.3.2.2 and 2.1.5.3, respectively). Specific details regarding PCR assays and primary antibodies are given in Appendix **B**.

2.3.11.3 Protein expression in transfected fibroblasts

Cell lysates were made from transfected MRC5 fibroblasts, and western blotting performed, as described above (section **2.1.3.2.2**). Proteins were detected with Zeb1 (sc25388; 1:500; Santa Cruz Biotechnology), fibronectin-EDA (MAB1940; 1:2000; Merck Millipore) and α-SMA (1A4; 1:2000; Sigma) primary antibodies. β-actin (C4; BD Biosciences; 1:5000) was used as an equal loading control.

2.3.12 Effect of EMT on fibroblast phenotype *in vivo*

2.3.12.1 Animal model

All mice were housed in a specific pathogen-free facility at the University of Southampton and given a commercial basal diet and water *ad libitum*. 6-8 week old CD-1 nude mice were injected subcutaneously with 7.5 x 10^5 SW480 control cells and 2 x 10^6 MRC5 PKH-labelled fibroblasts (mesenchymal tumours; n=6 injections), or, 7.5 x 10^5 SW480 ZKD cells and 2 x 10^6 MRC5 PKH-labelled fibroblasts (epithelial tumours; n=6). Prior to injection, cells were mixed, pelleted and

resuspended in 100 µl medium, to which an equal volume of Matrigel® (cat no. 356237; Corning) was added.

2.3.12.2 Staining of mouse tumours

At two weeks, animals were sacrificed and tumours excised. Two tumours from each of the groups (mesenchymal and epithelial), were fixed overnight at room temperature in 10% neutral buffered formalin, then sectioned and stained with: (i) haematoxylin and eosin; (ii) Zeb1 (sc25388; Santa Cruz Biotechnology; 1:500); (iii) α-SMA (1A4; Dako; 1:200). Sectioning and mounting of tumours was performed by Jane Norman in the Histochemical Imaging Unit, University of Southampton. Staining was performed by Monette Lopez in Cellular Pathology, University Hospitals Southampton NHS Trust.

2.3.12.3 Dissociation of tumours into single cells

The remaining tumours (four from each group) were pooled together and dissociated into single cells for flow-sorting. The following solutions were required:

(i) Collagenase stock solution (25 mg/ml): 500 mg of lyophilized Collagenase A (cat no. 10103586001; Roche) in 20 ml of HBSS (cat no. 14024092; ThermoFisher), filter sterilised (0.22 µm).

(ii) Hyaluronidase stock solution: 13.75 mg of lyophilized Hyaluronidase (cat no. H3506; Sigma) in 10 ml of HBSS, filter sterilised. Always freshly prepared.

(iii) Digestion solution: 500 µl of 25 mg/ml Collagenase A (see above); 1.25 ml of 1 mg/ml Hyaluronidase (see above); 50 µl of 200mM L-glutamine (cat no. G7513; Sigma); 500 µl FBS; 10 ml DMEM/F12 (cat no. 11320033; ThermoFisher).

(iv) Dispase: 1 g Dispase II (cat no. 4942078001; Roche) in 200 ml modified HBSS, filter sterilised. (Modified HBSS contained 1% 1M HEPES.)

Tumours were collected in ice-cold DMEM/F12 medium (cat no. 21331020; Gibco/ ThermoFisher) and then sterilised by immersion in 70% ethanol for 5 s, followed by washing in two changes of regular DMEM. Tumours were then cut into fragments of 1 mm^3 and incubated at 37 ^oC for 2h with the digestion solution (0.125% collagenase; 0.0125% hyaluronidase; 1mM L-glutamine; 5% FBS; in 10 ml DMEM/F12). The tissue was agitated every 30 min by vortexing for 1 s. After 2 h, the tissue was vortexed for 5 s and then centrifuged at 350*g* for 5 min. The pellet was resuspended in 30 ml of HBSS (containing 2% FBS) and centrifuged at 350*g* for 5 min. This was repeated with HBSS without serum. The pellet was then resuspended in 5 ml prewarmed 0.25% Trypsin-EDTA (cat no. T4049; Sigma) and continuously mixed for 2 min by pipetting, to mechanically dissociate the organoid-like structures. 30 ml of HBSS (+ 2% FBS) was added and the cell suspension

centrifuged at 350*g* for 5 min. 2 ml of 5 mg/ml prewarmed Dispase, containing 20 µl of 10 mg/ml DNase I (cat no. 10104159001; Roche) were then added to the cell pellet. The cells were then pipetted up and down for 2 min to dissociate the remaining clumps. 30 ml of cold HBSS (+ 2% FBS) was then added and the cells centrifuged at 350*g* for 5 min. The pellet was resuspended in HBSS (+ 2% FBS) and filtered through a 40 µM cell strainer into a new tube. This was then centrifuged again at 350*g* for 5 min and the supernatant discarded. The final cell pellet was resuspended in regular DMEM and taken for flow-sorting.

2.3.12.4 Flow-sorting of PKH26-positive and –negative cells

Cells were sorted on FACS Aria (BD Biosciences). Instrument parameters were set up using unlabelled MRC5 fibroblasts, after which samples of interest were sorted. First, debris and apoptotic cells were gated out. Next, additional gates were drawn in the PKH26 and forward scatter channels to select viable PKH-positive cells. Cells registered above the control gate were considered PKH-positive. Specific parameters were as follows: 488 nm (blue) laser; Neutral Density Filter 1.0; Longpass Mirror 556LP; Bandpass Filter 576/26. Cells were collected in 15 ml Falcon tubes containing DMEM/ 10% FBS, which had been previously coated with FBS at 4^{o}C for 1 h. Immediately after sorting, cells were centrifuged at 500*g* for 5 min and the pellet stored at -80^{o}C until further use. Cell sorting was conducted by Dr Carolann McGuire (Flow Cytometry Unit, University of Southampton).

2.3.12.5 RT-qPCR of PKH-positive and -negative cells

In this instance, RNA was extracted from cells using the miRneasy micro kit (cat no. 74004; Qiagen) due to the small number of cells (section **2.2.2.1**). Quality control was performed using the NanoDrop 8000 spectrophotometer (section **2.1.5.2**).

TaqMan Advanced (ThermoFisher) assays were performed to quantitate miR-200 family expression in PKH-positive cells (MRC5 fibroblasts) and PKH-negative (CRC) cells. Input material was 4 ng of total cellular or exosomal RNA. Expression levels were normalised to miR-423-5p (endogenous reference gene), calculated from the triplicate of CT values using the ΔΔCT method, and expressed relative to mesenchymal (SW480 control) tumours, which were assigned the value 1. Mean relative levels were calculated for each sample. The assay reference numbers were as follows: miR-200a-3p (478490_mir), miR-200b-3p (477963_mir), miR-200c-3p (478351_mir), miR-141-3p (478501_mir), miR-429 (477849_mir). Taqman cDNA synthesis and PCR protocols are described above (section **2.1.5.3**).

The miScript II RT kit (cat no. 218160; Qiagen) was used to generate cDNA for mRNA quantitation, as per manufacturer instructions. Input material was 100 ng of RNA (5 µl of 20 ng/µl), extracted

using the miRneasy micro kit (see above). For each sample, 5 µl RNA was combined with 4 µl 5x miScript HiFlex Buffer, 2 µl 10x miScript Nucleics Mix, 2 µl miScript Reverse Transcriptase and 7 µl RNase-free water (total reaction volume 20 µl). The reaction was incubated at 37 °C for 60 min, followed by 95 °C for 5 min. cDNA was stored at -20 °C until further use.

SYBR Green RT-qPCR assays were performed to quantitate *ACTA2* and *FN1* expression in PKH-positive cells. Reactions were set up in 96-well plates. Each well contained 12.5 µl of 2x QuantiTect SYBR Green PCR Master Mix (cat no. 204141: Qiagen), 2.5 µl 10x miScript Primer Assay, 7.5 µl of RNase-free water and 2 µl of cDNA template (total reaction volume 25 µl . Reactions were set up in triplicate with the following cycling conditions: 95 °C for 15 min, followed by 40 cycles of 94 °C for 15 s/ 55 °C for 30 s/ 70 °C for 34 s, using the Applied Biosystems 7500 qPCR instrument. Expression levels were normalised to *GAPDH* (endogenous reference gene) calculated from the triplicate of CT values using the ΔΔCT method, and expressed relative to mesenchymal (SW480 control) tumours, which were assigned the value 1. Mean relative levels were calculated for each sample. The miScript Primer Assays were: Hs_ACTA2_1_SG QuantiTect Primer Assay (product no. QT00088102; Qiagen) and Hs_FN1_1_SG QuantiTect Primer Assay (product no. QT00038024; Qiagen); and Hs_GAPDH_1_SG QuantiTect Primer (product no. QT00079247; Qiagen).

2.3.13 MLEC assay

2.3.13.1 Experimental set up for MLEC assay

MLEC cells, stably transfected with truncated PAI-1 promoter fused to firefly luciferase, were obtained from Max Mellone, University of Southampton. 5 x 10^5 cells were seeded into each well of a 24-well plate. The following day, cells were treated with 0, 250, 500, 1000 or 2000 pg/ml TGF-β (cat no. 240-B; R&D Systems) to generate a dose-response curve. In parallel, cells were treated with conditioned medium (diluted 1:1 with fresh medium) from SW480 control or SW480 ZKD cells. All standards and experimental conditions were conducted in triplicate. After 24 h, firefly luciferase activity was detected, as a surrogate for TGF-β activity.

2.3.13.2 Quantifying TGF-β activity

At 24 h, medium was aspirated and replaced with 100 µl Passive Lysis Buffer (cat no. E1941; Promega). Cells were then incubated at room temperature for 20 min on a rocker. 20 µl of each lysate was then transferred to each well of a 96-well plate, and 100 µl Luciferase Assay Reagent (cat no. E1500; Promega) was added to each well. Firefly luciferase activity was then measured using a luminometric plate reader (Varioskan LUX Multimode Microplate Reader; ThermoFisher).

In parallel, 5 µl of cell lysate was used to measure protein concentration by BCA assay (section **2.1.2.3**). Firefly luciferase activity was normalised by protein concentration for each well.

2.3.14 Statistical analysis

Where individual images (microscopy, western blotting and flow cytometry) are displayed, these are representative of at least two separate experiments. Graphics represent the mean ± SEM, unless otherwise stated. RT-qPCR was performed in triplicate and differences in mean relative values were tested by 2-tailed, unpaired (Student's) t-test. Cell counting was performed in quadruplicate, and differences in mean relative counts, for different days, were compared by 2-tailed, paired t-test. Events acquired by flow cytometry were analysed in a 2x2 contingency table by a 2-tailed Fisher's exact test. Luciferase assays were performed in triplicate and differences in mean relative values were tested by 2-tailed unpaired t-test. The threshold level of significance was set at 0.05 for all statistical tests. The level of statistical significance was denoted by $p<0.05$ (*); $p<0.01$ (**); and $p<0.001$ (***).

Chapter 3 Results

3.1 Exosome isolation, characterisation and transfer

3.1.1 Introduction

The study of exosome biology is relatively young but is unfolding at an exponential rate, as shown above (**Figure 1-3**). Although guidelines relating to minimal requirements in exosome methodology exist, the rapid increase in exosome-related studies in recent years, has meant that such guidelines are frequently neglected [306, 330]. Furthermore, cells are capable of producing a variety of heterogeneous vesicles (e.g. exosomes, microparticles, oncosomes), and it is sometimes unclear which population is being referred to. In addition, there exist multiple methods for exosome isolation, ranging from commercially available kits to dUC, SEC and Optiprep™ density gradient centrifugation. For these reasons, it is essential to clearly define the method for exosome isolation, and to characterise the preparation according to approved guidelines. Similarly, many groups have shown that exosomes have functional effects *in vitro* and *in vivo*, based on the fact that exosomes can be transferred from cell to cell [46, 284, 348]. It is critically important, at the outset of such studies, to demonstrate exosome transfer in the tissue of interest, using labelling and tracking strategies [492, 493]. In this section, we present the characteristics of exosomes from cancer cells and fibroblasts, isolated by dUC. We show their effects on miRNA levels and ERK/ Akt signalling in recipient cells. Furthermore, we describe *in vitro* and *in* vivo exosome labelling strategies, using lipophilic tracers and CD63-GFP-expressing cells, to show exosome shuttling between tumour and stromal cells.

3.1.2 Characterisation of exosomes

In order to isolate exosomes from MRC5 fibroblasts, dUC was performed, producing an exosome pellet which was enriched in vesicle-associated tetraspanins (CD63 and CD81), endosomal proteins (TSG101 and Alix), and devoid of organelle-specific markers such as GM130 (Golgi) and cytochrome C (mitochondria; **Figure 3-1**A). Unfixed MRC5 exosomes visualized by transmission electron microscopy (TEM) demonstrated a uniformly circular morphology with size distribution 40-120 nm (80 000x), and at higher magnification (120 000x) the lipid bilayer structure was clearly seen (**Figure 3-1**B), in keeping with previous descriptions [494]. Nanoparticle tracking analysis (NTA) confirmed a modal size of 113+/-1.3 nm and exosome concentration of 1.57+/-0.16 $x10^{12}$/ ml, which corresponded with a protein concentration of 0.50+/-0.04 µg/µl (**Figure 3-1**C). The same protocol was used to isolate exosomes from various other cell types including breast cancer

cells (MDA231; **Figure 3-2**) and colorectal cancer organoids (COL085; **Figure 3-3**) to demonstrate reproducibility.

The composition of exosomal RNA seems to vary from cellular RNA, as evidenced by Bioanalyzer traces (**Figure 3-4**). For example, the proportion of small RNAs is much higher in exosomes compared to cells, and the reverse is true for ribosomal RNAs. The lack or absence of ribosomal RNA peaks means that RIN numbers cannot be calculated for exosomal RNA (RIN 1, totally degraded RNA; RIN 10, totally intact RNA), which is corroborated by other studies [495]. This meant that spectrophotometer data was used to assess exosomal RNA quality. For exosomes, A260/230 values were often found to be 1.6-2.0, whereas A260/280 values were consistently 1.8-2. This is likely to be due to the phenol-based RNA extraction method (miRNeasy micro kit), where QiaZol contamination is detectable at an absorbance of 230 nm. This was far less apparent for cells, because RNA yields were typically much higher (>100 ng/µl), likely reducing the impact of contaminants on absorbance values.

Cancer cells produced more exosomes per cell than fibroblasts, a difference in the order of 100-fold (**Table 3-1**). Hence, starting material when isolating exosomes from fibroblasts was greater. Epithelail (DLD1) and mesenchymal (SW480) CRC cells produced comparable numbers of exosomes. Exosome protein concentration correlated with particle concentration, demonstrating its utility as an index of exosome number.

This methodology meets criteria set by the International Society for Extracellular Vesicles for characterizing extracellular vesicles [306]. Furthermore, this isolation and characterisation protocol was assigned an Extracellular Vesicle (EV) Metric of 77% which is in the 99th percentile for all experiments on the same sample type [330]. It is worth mentioning that the exosome preparations described here could contain other extracellular vesicle populations, but given the enrichment of endosomal markers and the particular size distribution, the predominant vesicle type is likely to be exosomes.

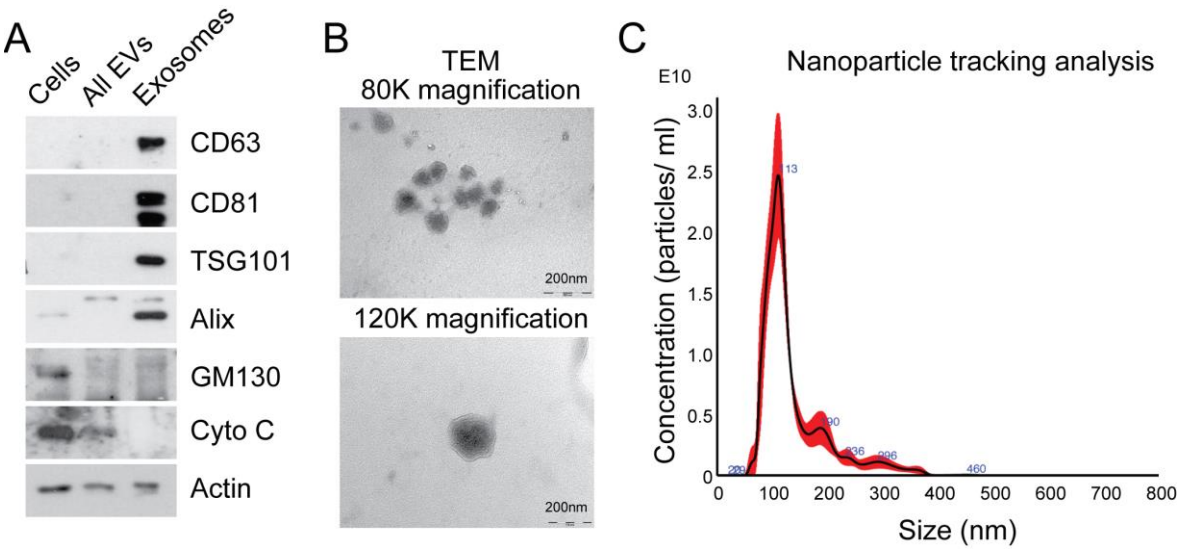

Figure 3-1. Characterisation of fibroblast exosomes isolated by dUC. (**A**) Western blot analysis to assess expression of exosomal markers in MRC5 exosomes. "Cells" refers to total cellular protein, "all EVs" refers to the total vesicular fraction isolated by a single ultracentrifugation of conditioned medium at 100 000 *g*, and "exosomes" refers to small extracellular vesicles isolated by filtration and serial centrifugation. Representative of two separate experiments. (**B**) TEM of MRC5 fibroblast exosomes at 80 000x and 120 000x demonstrating homogenous, cup-shaped vesicles with size in the order of 100 nm. Scale bar represents 200 nm in both panels. Representative of two separate preparations. (**C**) NTA of MRC5 fibroblast exosomes represented as size vs. concentration. Representative of two separate experiments, each with five tracking videos.

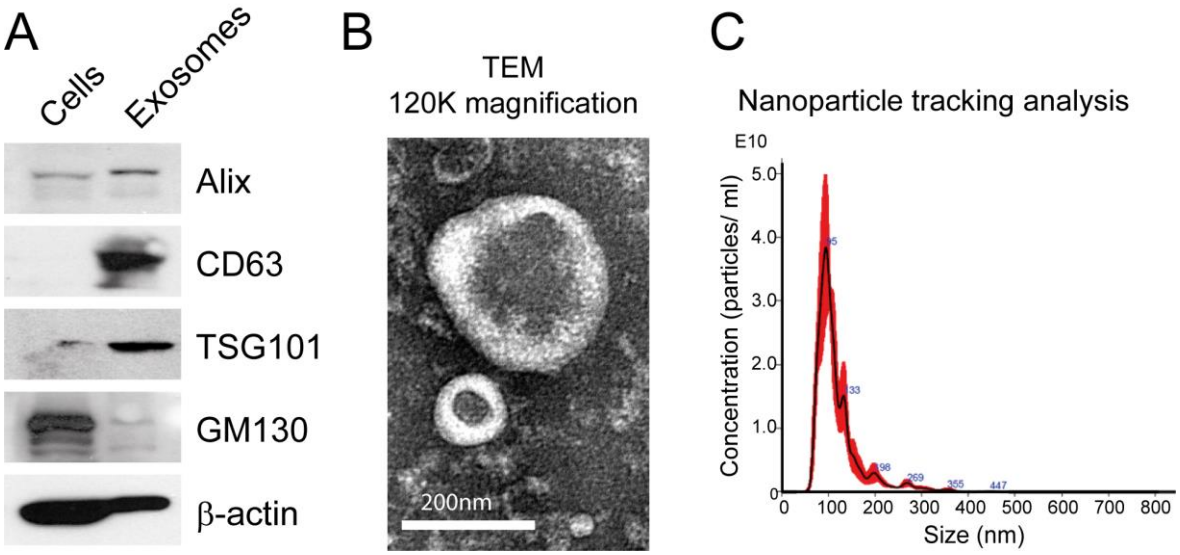

Figure 3-2. Characterisation of breast cancer exosomes. Exosomes isolated from MDA231 metastatic breast cancer cells. (**A**) Western blotting for exosomal markers. Representative of two separate experiments. (**B**) TEM at 120 000x; scale bar indicates 200 nm. Representative of two

separate preparations. (**C**) NTA; modal diameter 95 nm. Representative of two separate experiments, each with five tracking videos.

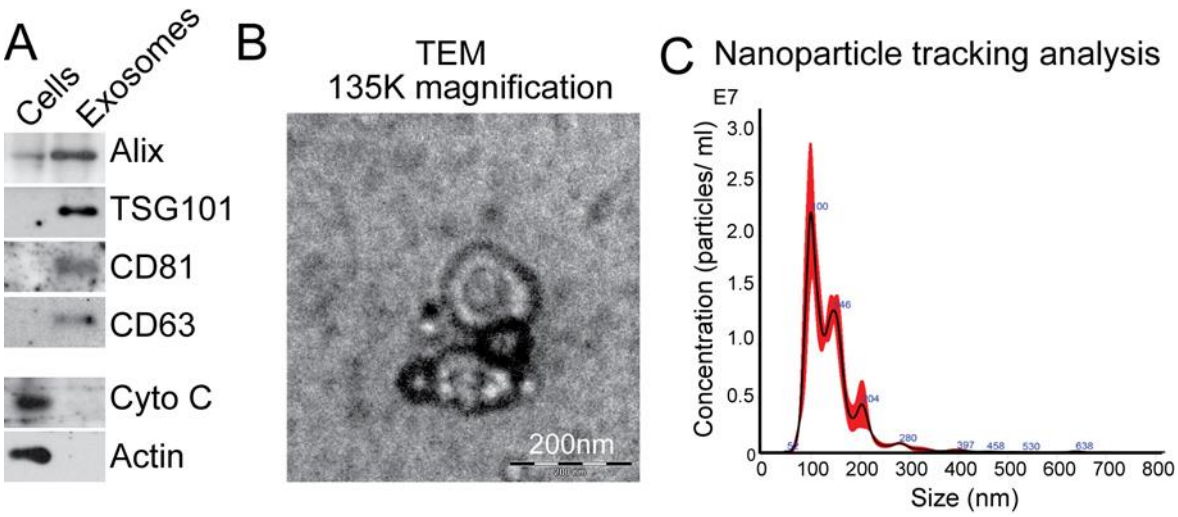

Figure 3-3. Characterisation of CRC exosomes. Exosomes isolated from colorectal cancer organoids. (**A**) Western blotting for exosomal markers. Representative of two separate experiments. (**B**) TEM at 135 000x; scale bar indicates 200 nm. Representative of two separate preparations. (**C**) NTA; modal diameter 100 nm. Representative of two separate experiments, each with five tracking videos.

Table 3-1. Exosome production by different cell types.

Cell type	Number of cells	Mean particle concentration (per ml)	Protein concentration (µg/ µl)	Particles/ cell
MRC5	1.1×10^8	1.57×10^{12}	0.50	2.85×10^3
Primary fibroblast	1.0×10^8	4.39×10^{11}	0.21	0.88×10^3
MDA231	6.1×10^7	2.09×10^{12}	0.78	6.85×10^4
DLD1	6.7×10^7	1.99×10^{12}	1.02	5.94×10^4
SW480	5.2×10^7	1.64×10^{12}	0.88	6.31×10^4
CRC organoid	5.4×10^5	1.49×10^9	0.13	0.55×10^3

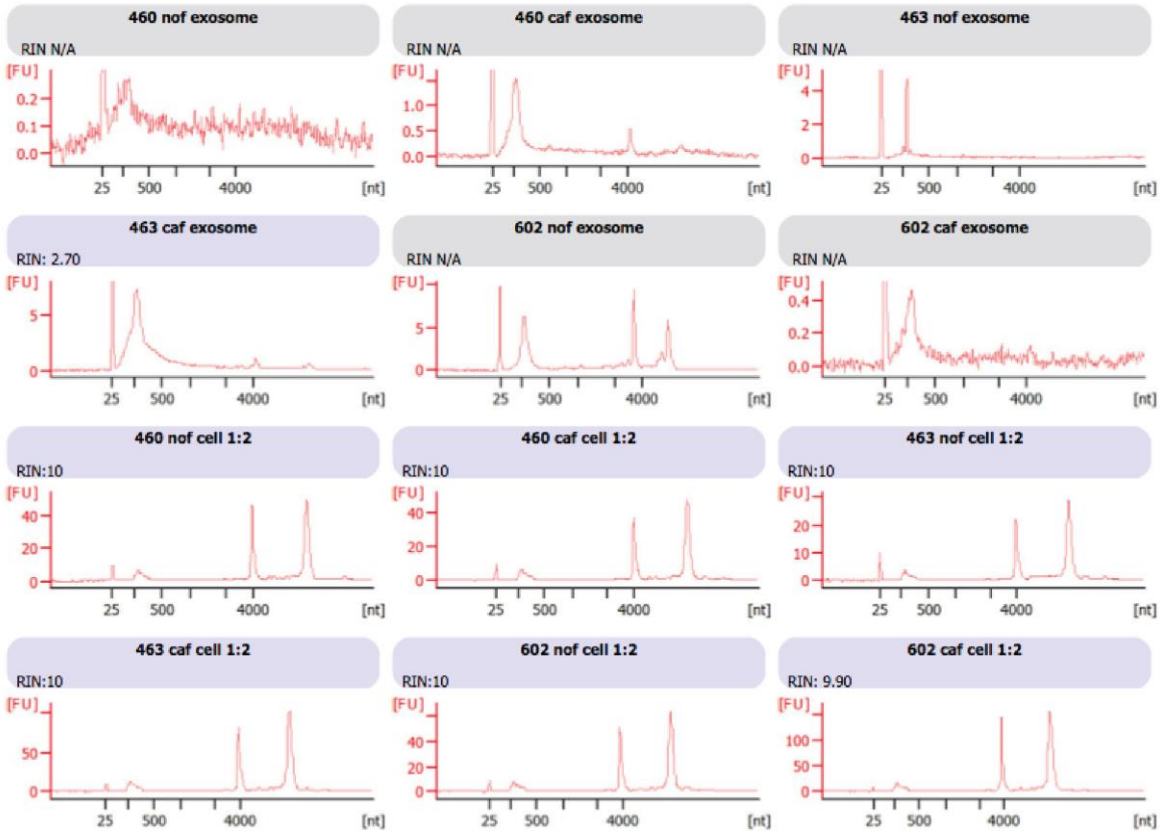

Figure 3-4. Assessment of RNA by Bioanalyzer reveals distinct cellular and exosomal profile. Exosomal RNA generally lacks both the 18s and 28s ribosomal RNA peaks which are seen clearly in cellular RNA. Therefore, RIN (RNA Integrity Number) is not applicable to exosomal RNA. RIN of all cellular RNA samples was greater or equal to 9.90. Cellular RNA samples were diluted 1:2. The peak at 25 nt represents the marker, the next (sub-500) nt peak represents small RNAs, and the final two peaks represent 18s and 28s ribosomal RNAs respectively. Individual sample names are shown above each electropherogram. Representative of two separate experiments.

3.1.3 Visualising transfer of exosomes

To demonstrate exosome transfer, DiO-labelled MRC5 exosomes (green) were used to treat DLD1 cells stably expressing mCherry (red). Fluorescence microscopy showed co-localisation of exosomes with cells (**Figure 3-5**A) and confocal imaging confirmed their intracellular location (**Figure 3-5B**). In the representative confocal image (**Figure 3-5**B), there are approximately 10 cells, two of which have strongly taken up exosomes, with the others having taken up far fewer exosomes. Flow cytometry was used to better quantify the extent of MRC5 exosome (**Figure 3-6**A) and primary CAF exosome (**Figure 3-6**B) uptake by DLD1 cells. The shift in FL4 suggests that nearly all cells (>95%) took up exosomes. However, the FL4 intensity in exosome-treated cells, ranges

from 10^2 to 10^4 units, suggesting that some cells took up 100 times more exosomes than others, in keeping with confocal images.

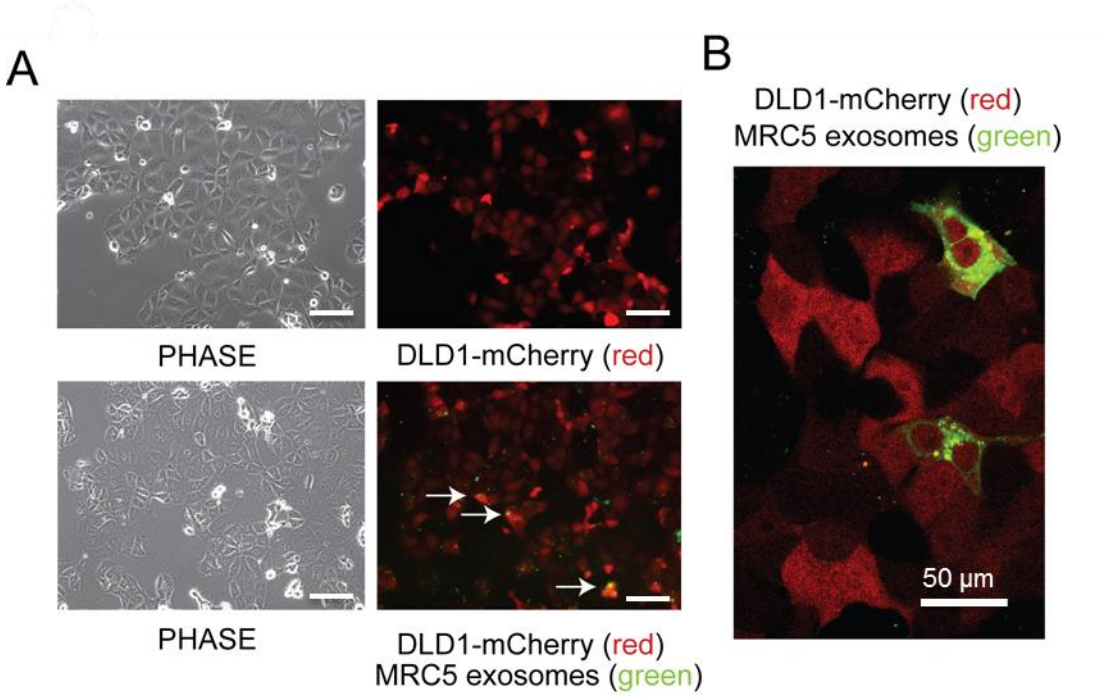

Figure 3-5. Transfer of labelled exosomes *in vitro*: microscopy. (**A**) Culture of mCherry-tagged DLD1 cells (red) in the absence (*top*) or presence (*bottom*) of DiO-labelled MRC5 exosomes (green), visualised by fluorescence microscopy (10x objective). Co-localisation of exosomes with cells is demonstrated by arrows. Scale bars represent 200 µm. Representative of two separate experiments. (**B**) Culture of mCherry-DLD1 cells with DiO-labelled MRC5 exosomes visualized by confocal microscopy (60x objective), demonstrating the presence of exosomes within cells. Representative of two separate experiments.

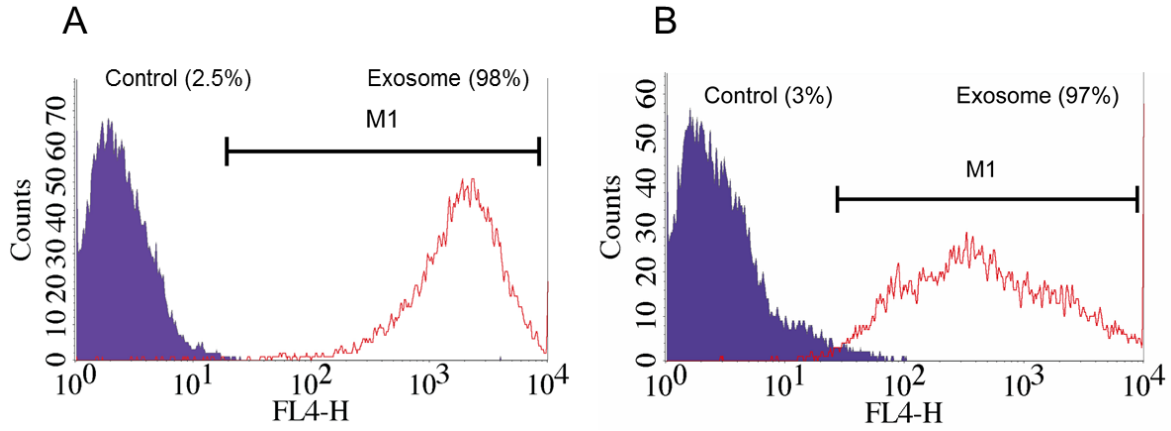

Figure 3-6. Transfer of labelled exosomes *in vitro*: flow cytometry. (**A**) Flow cytometry of DLD1 cells untreated (control) and treated with MRC5 exosomes (exosome) and; (**B**) DLD1 cells (control)

treated with primary CAF exosomes (exosome). The proportion of cells under the M1 region is given as a percentage. Representative of two separate experiments.

3.1.4 Exosome transfer results in miRNA changes in recipient cells

To investigate whether stromal exosomes alter miRNA levels in recipient CRC cells, DLD1 and SW480 cells were conditioned with MRC5 and primary CAF exosomes. To determine the effect of exosome concentration on miRNA levels, low (15 μg/ml) and high (100 μg/ml) amounts of MRC5 exosome were used. For both DLD1 and SW480, the low concentration resulted in significant increases in miR-16 and miR-29b (arbitrarily chosen). However, the high concentration actually reduced levels of both these miRNAs in both CRC cells (**Figure 3-7**A). This finding was validated by using a different source of exosomes (primary CAFs), and assaying for different miRNAs (miR-21 and miR-199b), in DLD1 cells (**Figure 3-7**B**).** It seems that exosomes increase miRNA levels in recipent cells but only up to a certain concentration, beyond which the effect is reversed. Delivering such a high concentration of exosomes may have the effect of diluting cellular miRNAs, if we consider that 100 μg of fibroblast exosomes (3×10^{11} particles) delivered to 2×10^5 CRC cells, corresponds to $>1 \times 10^6$ exosomes per cell (the volume of 1×10^6 exosomes (each 0.1 x 0.1 x 0.1 μm^3) is in the same order of magnitude as one CRC cell (10 x 10 x 10 μm^3)). Alternatively, such a high load of exosomes may stimulate the cell to increase outward flux of miRNA-containing exosomes, as a protective mechanism.

Thus far, exosome conditioning was conducted over 24 h, as with previous studies, and there were clearly changes in miRNA levels in this time frame [46, 470]. To investigate whether exposure time influenced miRNA changes, DLD1 cells were conditioned with a fixed concentration of MRC5 exosomes (15 μg/ml) for 6 and 48 h. There was no effect on miR-16 or -29b levels after 6 h, but a significant increase in both miRNAs was detected at 48 h (**Figure 3-8**), in the same order of magnitude as was seen previously with 24 h exposure. These kinetics expriments informed our decision to use a starting concentration of 15 μg/ml for 24 h, in future exosome-conditioning experiments.

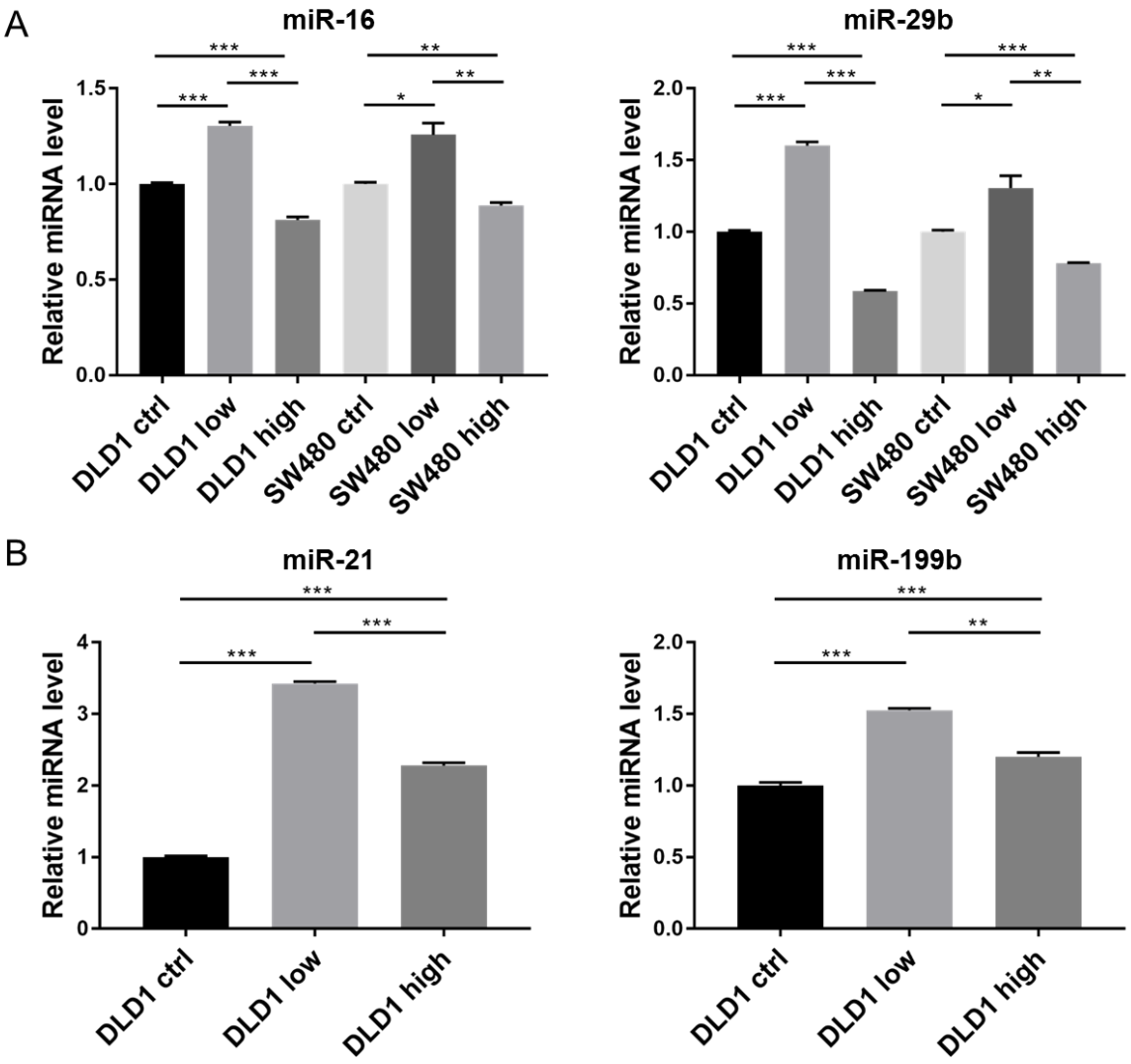

Figure 3-7. Exosome concentration determines miRNA changes in recipient cells. Treatment of DLD1 and/or SW480 cells with (**A**) MRC5 and (**B**) primary CAF exosomes, with resultant changes in cellular miRNA levels. "Low" corresponds to an exosome concentration of 15 µg/ml, and "high" to 100 µg/ml. Control (ctrl) cells were treated with an equivalent volume of exosome-depleted medium. MiRNA levels shown are relative to DLD1 or SW480 control cells, which were assigned the value "1". Representative of two separate experiments, each with three technical replicates.

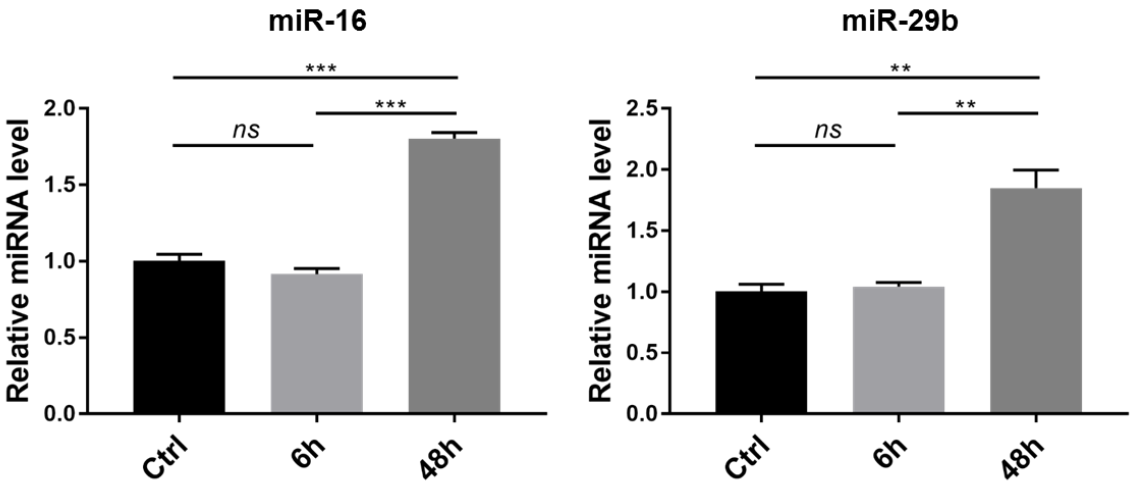

Figure 3-8. Duration of exosome exposure affects miRNA changes in recipient cells. DLD1 cells conditioned with MRC5 exosomes for 6 and 48 h, with resulting changes in miR-16 and miR-29b. Control cells were collected at T_0, prior to addition of exosomes. MiRNA levels shown are relative to control cells, which were assigned the value "1". Representative of two separate experiments, each with three technical replicates.

3.1.5 Exosome conditioning of miRNA knock out cells

We have shown that delivery of exosomes causes an increase in miRNA levels in recipient cells. However, it is unclear whether exosomes were directly transferring miRNAs, or whether recipient cells upregulate endogenous miRNAs in response to exosomes. The aim of this experiment was to show that exosomes deliver miRNAs to recipient cells. To this end, miR-200c/141 knock out ES cells were conditioned with miR-200c-rich CRC exosomes. Detection of miR-200c in the knock out cells would unequivocally demonstrate exosomal miRNA transfer.

Fluorescence microscopy was used to demonstrate exosome uptake by ES cells, suggesting that they behave in a similar manner to other cells (**Figure 3-9**A). We next wanted to demonstrate that the ES cells were truly deficient in miR-200c/141. SCC7 (murine epithelial carcinoma) cells and MEFs were used as positive controls, with the knowledge that epithelial cells express more miR-200 than mesenchymal cells (which should express very little, if any) [458]. The aim was to show that fibroblasts expressed less miR-200c/141 than carcinoma cells, and that knock out cells expressed even less miR-200c/141 than fibroblasts. However, when knock out cells were profiled for miR-200c by qPCR, miRNA levels were demonstrably higher than in MEFs, and in the case of miR-141, higher than in MEFs and carcinoma cells (**Figure 3-9**B). The data suggest that either the ES cells were not genuinely miR-200c/141 knock out, or, that the PCR assay was non-specifically detecting closely-related miRNAs.

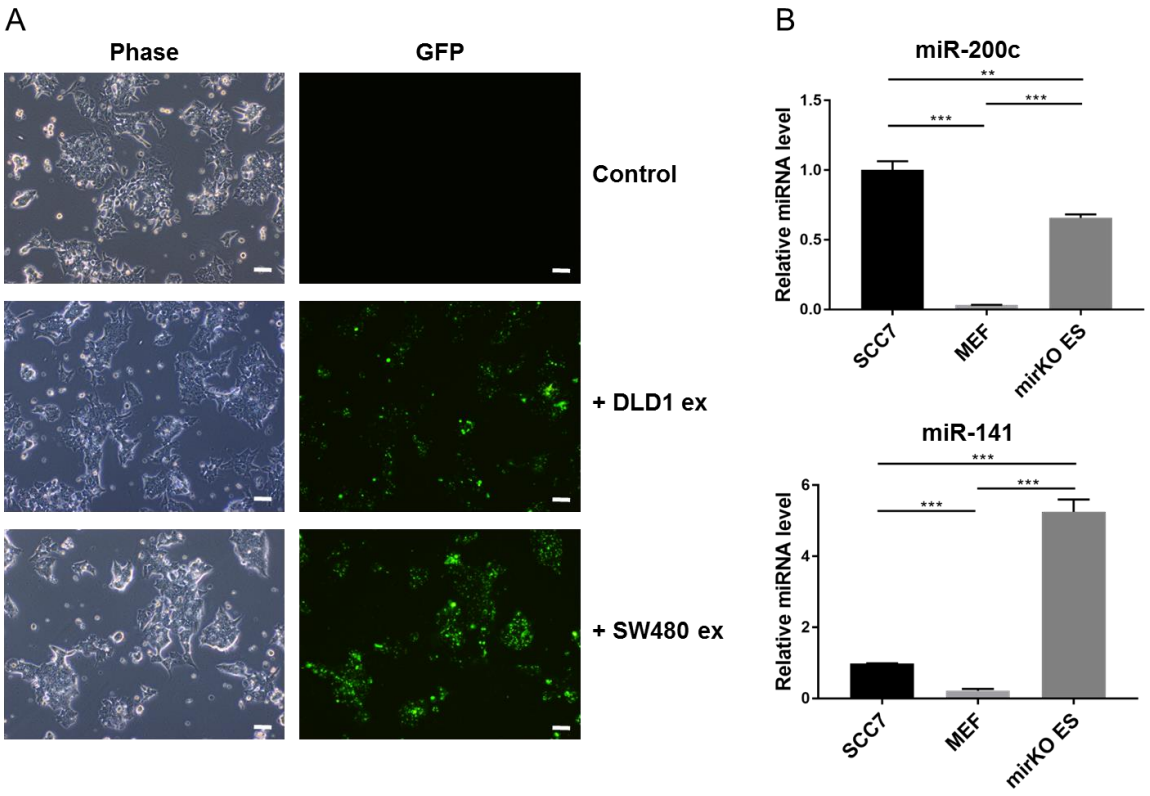

Figure 3-9. MiRNA knock out ES cells. (**A**) DiO-labelled exosomes from DLD1 and SW480 cells transferred to ES cells: phase and GFP channel (10x objective). Control represents untreated ES cells. Scale bars represent 100 µm. Representative of two separate experiments. (**B**) MiR-200c/141 levels in knock out ES cells compared to SCC7 (murine head and neck carcinoma) and MEF. MiRNA levels shown are relative to SCC7 cells, which were assigned the value "1". Representative of two separate experiments, each with three technical replicates.

3.1.6 *In vivo* exosome transfer

To demonstrate *in vivo* exosome transfer, HCT116 cells expressing the Cytotracer pCT-CD63-GFP were generated. The CD63-GFP fusion protein was detected by western blotting. With anti-CD63 antibody, bands were detectable at 63 Kd for both control and CD63-GFP clones (constitutive CD63) but only CD63-GFP clones demonstrated an additional band at 90 Kda representing the fusion protein (**Figure 3-10**A). With the anti-GFP antibody, a band was detected for HCT-CD63-GFP cells at 90 Kda, which corresponds with the combined molecular weight of GFP and CD63 (27 + 63 = 90 Kd; **Figure 3-10**A). There was no detectable GFP band for control cells.

Control and CD63-GFP cells were counterstained with DAPI (nucleus) and phalloidin (F-actin/ cytoskeleton). CD63-GFP cells were shown to contain GFP-positive vesicles localising to the cytoplasm, consistent with endosomes (**Figure 3-10**B). Furthermore, HCT116 control and CD63-GFP cells were co-cultured with MRC5 control and MRC5-DiD-positive cells, respectively (**Figure**

3-11). As expected, there was a shift in FL1 for CD63-GFP cells compared to control, and a shift in FL4 for DiD-labelled cells compared to control. When these cells were co-cultured, 18% of cells registered as double positive (GFP and DiD; bottom right panel), suggesting transfer of fluoresent material between cells. It is likely that GFP-positive vesicles from HCT116 cells were transferred to fibroblasts but equally, DiD-positive vesicles from fibroblasts may have been transferred to CRC cells. DiD was used to label fibroblasts in this experiment, rather than PKH, because GFP and PKH spectra overlap significantly, making them difficult to resolve by flow cytometry, with the lasers available in this unit.

Before conducting *in vivo* work with labelled fibroblasts, the duration of PKH26 detectability was determined *in vitro*. MRC5 fibroblsts were labelled with PKH and passaged for 28 days. As expected, the population of PKH-positive cells declined at each interval, but signal was still detectable in 24% of cells at 28 days (**Figure 3-12**).

To demonstrate *in vivo* exosome transfer, HCT116-CD63-GFP cells were co-injected with MRC5-PKH fibroblasts, subcutaneously, into nude mice. As long as four weeks after injection, confocal microscopy demonstrated GFP-positive vesicles within PKH-positive cells, suggesting *in vivo* transfer of exosomes from CRC cells to fibroblasts (**Figure 3-13**). The snapshot in **Figure 3-13** (left panel) shows a typical area where the demarcation between cancer and stromal compartments is highlighted. There is dense PKH staining in the stromal compartment, consistent with fibroblasts, and more GFP-positive vesicles in the cancer compartment, consistent with CRC cells. However, there are clearly PKH-positive cells (fibroblasts) in the stromal compartment which have taken up GFP-positive vesicles (exosomes). The associated z-stack images (right panels) demonstrate regions containing overlapping DAPI (nucleus), PKH (fibroblast) and GFP (exosome) signal, confirming HCT116 exosomes within MRC5 fibroblasts.

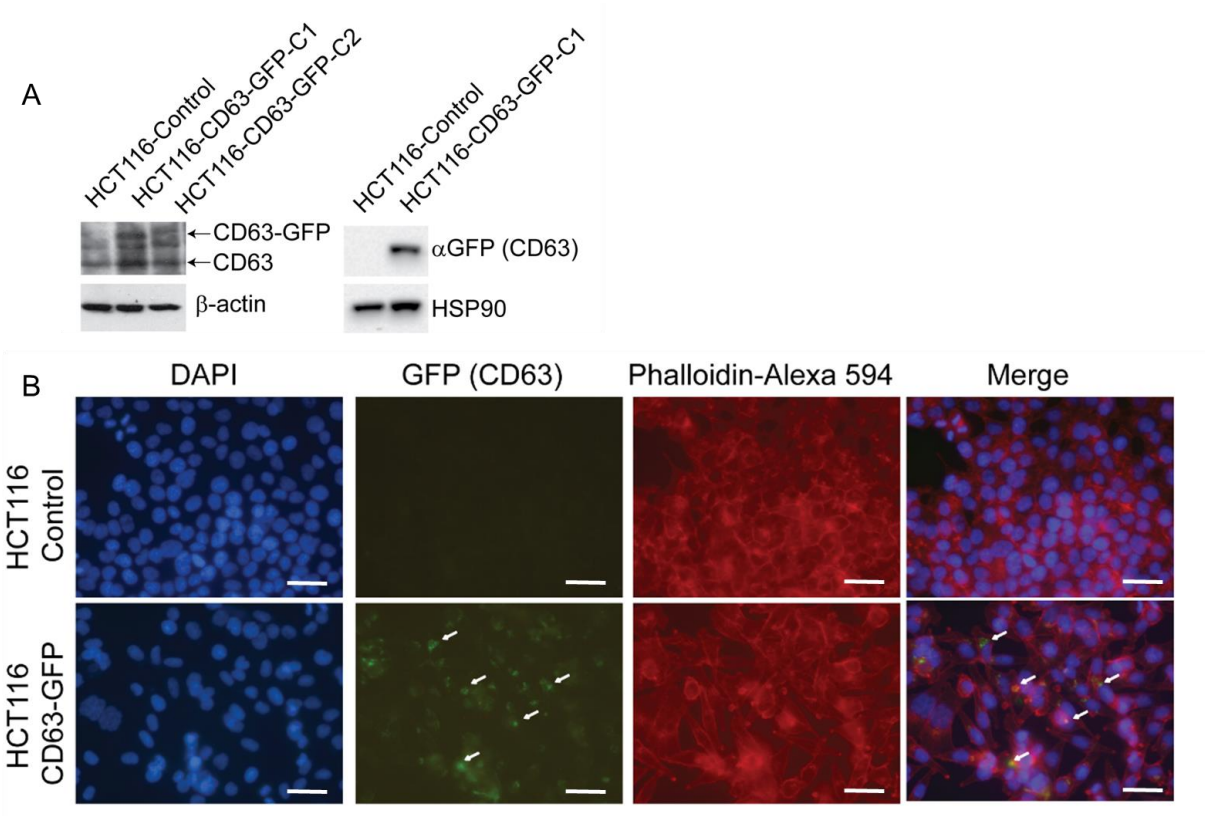

Figure 3-10. CD63-GFP cells. (**A**) HCT116-CD63-GFP clones probed with CD63 and GFP antibodies; C1 – clone 1, C2 – clone 2. Notice that the CD63-GFP fusion protein is detected at 90 Kd. Representative of two separate experiments. (**B**) Fluorescence microscopy of HCT116 control and CD63-GFP cells, counterstained with DAPI and Phalloidin (40x objective). Arrows mark GFP signal. Scale bars represent 35 µm. Representative of two separate experiments.

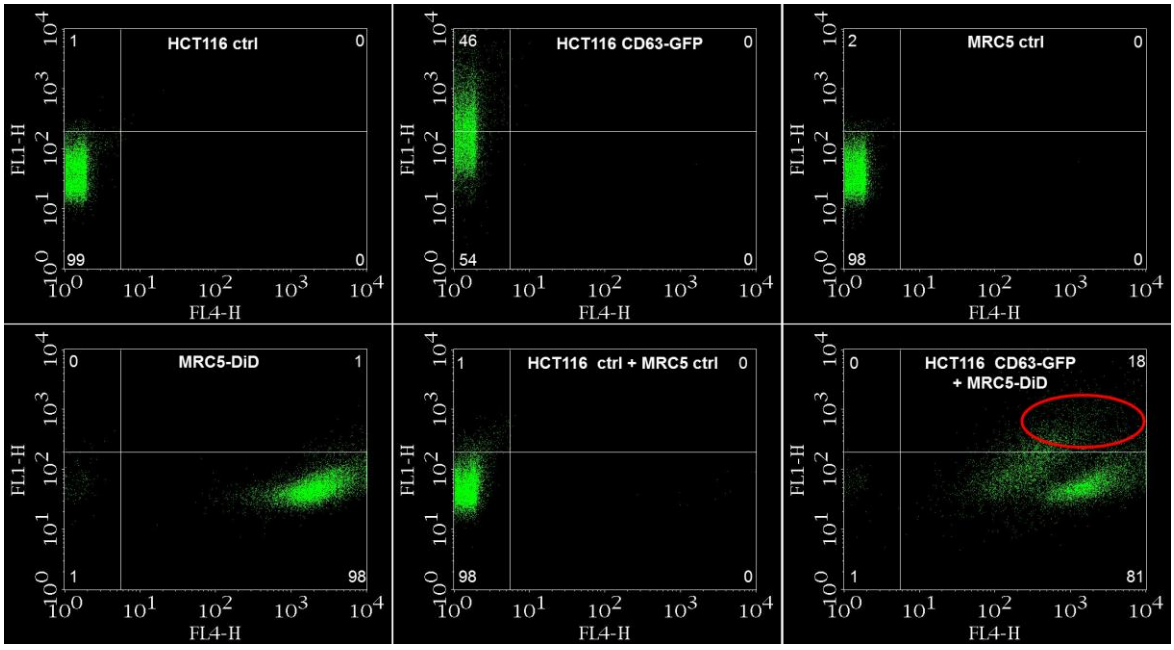

Figure 3-11. Co-culture of HCT116-CD63-GFP and MRC5-DiD cells. Different monoculture and co-culture conditions of labelled and unlabelled HCT116 and MRC5 cells subjected to flow cytometry.

FL1 channel corresponds with GFP signal and FL4 with DiD. The red circle indicates a population of double positive cells. Arbitrary logarithmic scale. Quadrant statistics are given as percentages. Representative of two separate experiments.

A

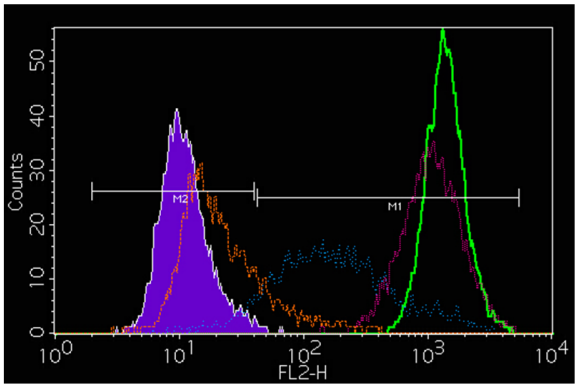

B

Time (days)	PKH26	M1 (%)	M2 (%)	Colour
0	-	1	99	Purple (fill)
0	+	99	1	Green
7	+	92	8	Violet
14	+	83	17	Blue
28	+	24	76	Orange

Figure 3-12. Detectability of PKH26 signal. (**A**) MRC5 fibroblasts labelled with PKH26, were passaged for 28 days, and PKH signal was measured by flow cytometry on days 0, 7, 14 and 28. Arbitrary gates were drawn to resolve the labelled (M1; *right*) and unlabelled (M2; *left*) population. (**B**) Gate statistics for cells sampled at different time points. Control cells were unlabelled (PKH26-). Representative of two separate experiments.

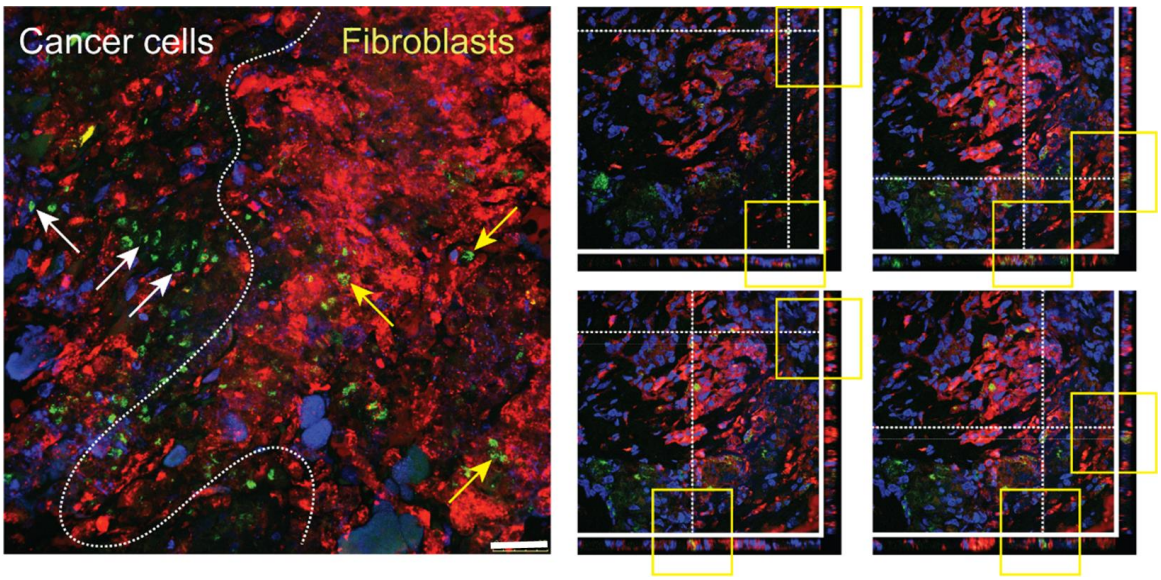

Figure 3-13. *In vivo* exosome transfer. (*Left*) Representative tissue section from a tumour xenograft established with HCT116-CD63-GFP and MRC5-PKH cells (60x objective). Arrows mark GFP-positive exosomes. Dashed line represents boundary between cancer and stromal compartments. Scale bar represents 25 µm. (*Right*) Z-stacks through different levels of a single tissue section to highlight the presence of GFP-positive exosomes within PKH-positive fibroblasts. Representative of nine tissue sections (three from each tumour xenograft).

3.1.7 Functional effects of exosome transfer

Having shown that fibroblast exosomes can be delivered to cells, we investigated effects on cellular signalling pathways, and the functional consequences of these. MRC5 exosomes increased ERK phosphorylation in DLD1 cells (**Figure 3-14**A, *left*). Similarly, AKT phosphorylation increased, resulting in phosphorylation of a direct AKT target, Bad, at amino acid 99 (**Figure 3-14**A *middle, right*) [496].

This was associated with a protective effect on CRC cells in the presence of oxaliplatin, a first line agent in neoadjuvant and adjuvant treatment of CRC (**Figure 3-14**B) [497]. The proportion of subG1 CRC cells at baseline was 6%, rising to 41% in the presence of 200 μM oxaliplatin. In the presence of exosomes, oxaliplatin was less effective, with a rise in subG1 cells from 8% to 33%. Detailed sub-G1 flow cytometry analysis is shown in **Figure 3-15**. A concentration of 200 μM oxaliplatin was chosen after preliminary work on a number of CRC, breast and hepatoma cell lines, as this dose reliably induces 40-60% apoptosis (by subG1 analysis). Plasma concentrations in patients have been reported in the order of 4 μg/ml (after five cycles), which equates to 10 μM, but actual tissue concentrations are not known [498].

Contrary to expectation, there was a sustained proliferation defect in DLD1 cells conditioned with fibroblast exosomes (**Figure 3-14**C), despite ERK activity increasing. This is unusual because ERK is is known to activate cyclin dependent kinases in G1, allowing entry into the cell cycle [499]. Increased phosphorylation of ERK would therefore be expected to increase cell proliferation. One possible explanation is that exosome treatment causes a rapid and excessive increase in pERK, inducing arrest at the G2/M transition, which others have shown previously [500].

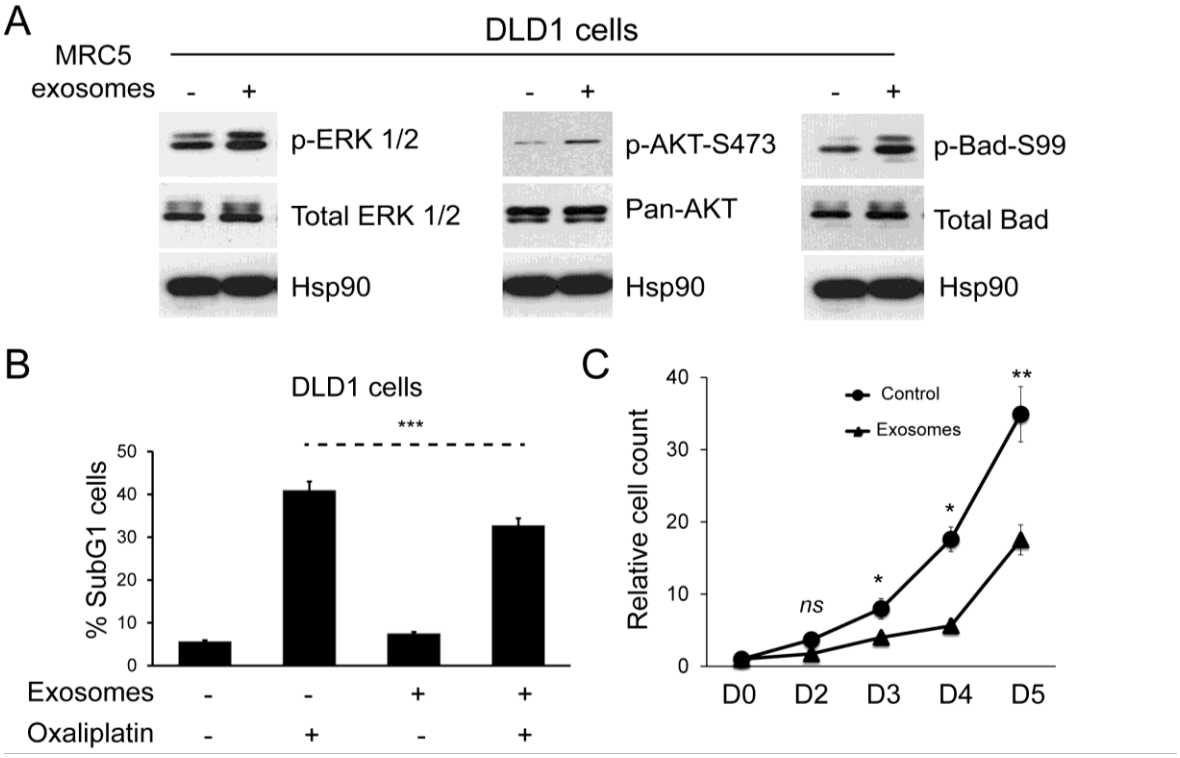

Figure 3-14. Fibroblast exosomes influence cellular signalling in CRC cells resulting in resistance to chemotherapy and altered proliferation. (**A**) Western blot demonstrating ERK (*left*), AKT (*middle*) and Bad activity (*right*) in DLD1 cells in the absence and presence of MRC5 exosomes. MRC5 exosomes induced ERK, AKT and Bad (serine 99) phosphorylation but total ERK, AKT and Bad expression was unchanged. HSP90 was used as an equal loading control. Representative of two separate experiments. (**B**) Apoptosis of DLD1 cells induced by oxaliplatin in the absence and presence of MRC5 fibroblast exosomes. Representative of two separate experiments, each with three technical replicates. (**C**) Proliferation of DLD1 cells in the absence and presence of MRC5 fibroblast exosomes. A significant proliferation defect occurs from day 3 onwards in exosome-exposed CRC cells. Cell counts are relative to day 0, which was given the value 1. Representative of two separate experiments, each with four technical replicates.

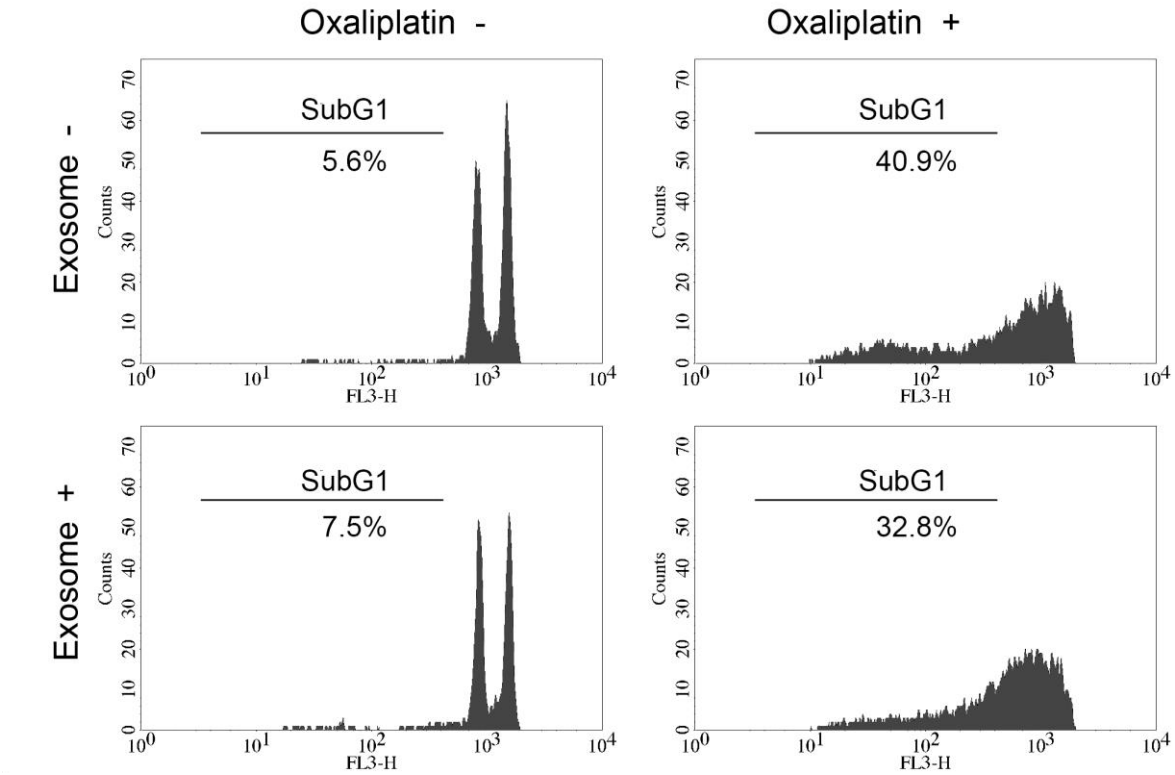

Figure 3-15. SubG1 analysis by flow cytometry demonstrates protective effect of fibroblast exosomes in the presence of oxaliplatin. (*Top left*) Control DLD1 cells; (*top right*) DLD1 cells treated with 200 µM oxaliplatin for 24 h; (*bottom left*) DLD1 cells co-cultured with 15 µg/ml MRC5 fibroblast exosomes for 24 h; (*bottom right*) DLD1 cells co-cultured with 15 µg/ml MRC5 exosomes for 24 h, then treated with 200 µM oxaliplatin for 24 h. Cells registered prior to the G1 peak (subG1) are considered apoptotic. Representative of two separate experiments.

3.1.8 Discussion

Exosomes were isolated from fibroblasts, CRC cells and organoids by dUC, yielding vesicles with diameter in the order of 40-120 nm, with a lipid bilayer structure, and enrichment of endosomal (Alix, TSG101) and membranous (CD63, CD81) markers. Different cell types were shown to produce different numbers of exosomes by NTA, with stromal cells and organoids producing ~10^3 particles/ml and cancer cells ~10^4-10^5 particles/ml. Uptake of exosomes was shown by conditioning cells of interest with fluorescently-labelled exosomes, and detection of fluorescent signal in recipient cells. This was associated with changes in miRNA levels in recipient cells, which was dose and time dependent. The optimal conditions for detecting miRNA changes upon exosome transfer were found to be 15 µg/ml of exosomes for 24 h. Next, *in vivo* exosome transfer was shown using CD63-GFP CRC cells (producing GFP exosomes), which were co-injected to mice with PKH-labelled fibroblasts. Confocal imaging of tumour xenografts demonstrated the presence of GFP-positive vesicles within PKH-positive cells, demonstrating that transfer had

occurred. Finally, the importance of exosomes in stromal-tumour crosstalk was demonstrated by fibroblast exosomes altering ERK and Akt activity in CRC cells, with functional effects on apoptosis and proliferation.

3.2 Stromal exomiR profiling in CRC

3.2.1 Introduction

The consensus view of a tumor resembling an organ has highlighted the critical role of the tumor microenvironment in recent years [501]. The shift in focus has revealed that stromal cells such as cancer-associated fibroblasts (CAFs) are key players in modulating tumor progression [31, 47, 502]. Moreover, a dynamic and reciprocal interaction between cancer and stromal cells has been demonstrated, highlighting the profound impact that stromal cells have on proliferation, angiogenesis, invasion, metastasis and chemoresistance, thereby promoting cancer progression through multiple pleiotropic mechanisms [31, 47, 502]. It is therefore understandable, that a significant number of genes which stratify better and worse prognoses, are defined by the stromal compartment [503].

Recent work by our group has revealed that deregulated miRNA expression in CRC stroma is of clinical significance [427, 504]. One miRNA taken forward was miR-21, an oncogenic miRNA overexpressed in several solid tumors, which regulates the tumor suppressor PDCD4 in CRC [505, 506]. Whilst previous studies identified miR-21 upregulation in CRC, these considered whole-tissue only [507, 508]. In contrast, we and others, have shown that miR-21 is overexpressed in CRC stroma by CAFs, stratifying patients with early-stage CRC for recurrence, disease free survival and overall survival [427]. Mechanistically, it was shown that overexpression of miR-21 in CAFs promotes increased invasiveness, proliferation and chemotherapy resistance in surrounding tumor cells by paracrine signaling [504]. Clearly then, it is important to elucidate mechanisms by which stromal gene expression is relayed to cancer cells. Exosomes provide one such mechanism [284].

With a focus on CAFs as stromal drivers of tumor progression, we aimed to investigate the exosome-mediated crosstalk between CAFs and cancer cells. To achieve this, paired CAFs and NOFs were derived from human donors, from which exosomes were isolated, and their miRNA content profiled using a high sensitivity direct detection array (NanoString). Here, for the first time, we identified a novel stromal exosome signature in CRC, as part of a prospective biomarker study. Furthermore, we reiterated the importance of stromal miR-21 in CRC progression using an orthotopic murine model, and demonstrate that one of the mechanisms of miR-21 transfer between stromal and cancer compartments is mediated by exosomes.

3.2.2 CAFs display a myofibroblastic phenotype

Having established that exosomes from normal fibroblasts have functional effects on CRC cells (**Figure 3-14**), we sought to characterise the cargo of tissue-specific colorectal NOF and CAF exosomes. To achieve this, we established a collection of paired patient-derived primary colorectal NOFs and CAFs from which exosomes could be derived.

In order to demonstrate phenotypic differences between NOFs and CAFs, matched pairs of *ex vivo*-derived colorectal NOFs and CAFs were isolated and characterised using a panel of established markers (**Figure 3-16**A) [509-512]. CAFs occupied a greater surface area than NOFs in two dimensions (**Figure 3-16**B-D), in keeping with previous studies [243]. Intensity of phalloidin staining for F-actin filaments was also significantly higher in CAFs compared to NOFs (**Figure 3-16**C, E), indicating a higher stress fibre density [513].

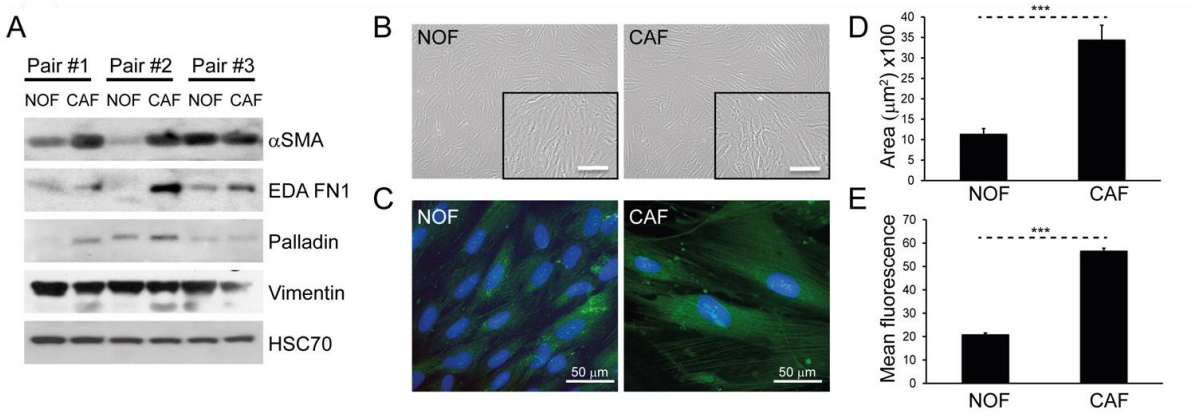

Figure 3-16. CAFs and NOFs are biochemically and morphologically different. (**A**) Western blot of paired primary NOFs and CAFs for myofibroblastic markers. HSC-70 was used as an equal loading control. EDA FN1 – fibronectin. Representative of two separate experiments. (**B**) Light microscopy of colorectal NOF and CAF cells (10x objective). Scale bars represent 100 µm. (**C**) Fluorescence microscopy demonstrating phalloidin staining of F-actin filaments (green), counterstained with DAPI (blue; 40x objective). Representative of three NOF-CAF pairs. (**D**) Mean surface area and intensity of phalloidin staining in nine individual NOF and CAF cells from one NOF-CAF pair, representative of three pairs. From *Bhome et al. (2017)* [481].

3.2.3 CAF and NOF exosomes are distinguishable by a specific miRNA signature

To identify differentially abundant miRNAs, exosomes were isolated from *ex vivo* cultures of primary NOF-CAF pairs and RNA subjected to NanoString assay. Hierarchical cluster analysis of NanoString data separated NOF and CAF exosomes according to miRNA expression, with nine of the 20 most-changing miRNAs less abundant in CAF exosomes, and 11 more abundant (**Figure**

3-17A, B). Abundance of several other miRNAs was significantly different in CAF and NOF exosomes but only the top 20 most-differing miRNAs are shown. To extend the panel of miRNAs beyond these 20, we established stringent criteria such that candidate miRNAs had to be: (i) oncogenic, (ii) stromal in origin, (iii) abundant in exosomes and (iv) enriched in exosomes. Ten experimentally validated oncomirs, with relevance in CRC, were selected for further assessment: miR-21, miR-135b, miR-20a/20b, miR-19b, miR-19a, miR-155, miR-181a, miR-130b, miR-95 and miR-499a [483]. Normalized NanoString counts are shown for three NOF-CAF exosome pairs with respect to these oncomirs (**Figure 3-18**).

With a focus on miRNAs which were deliverable in CAF exosomes, and using the criteria mentioned above, a total of six miRNAs (miR-329-3p, miR-181a-3p, miR-199b-5p, miR-382-5p, miR-215-5p and miR-21-5p), which were more abundant in CAF compared to NOF exosomes, were successfully validated by qPCR (**Figure 3-19**). Furthermore, there was significant correlation between NanoString and RT-qPCR fold changes for abundance of miRNAs in NOF and CAF exosomes (R^2=0.81; p=0.04), confirming validity of the NanoString platform (**Figure 3-20**).

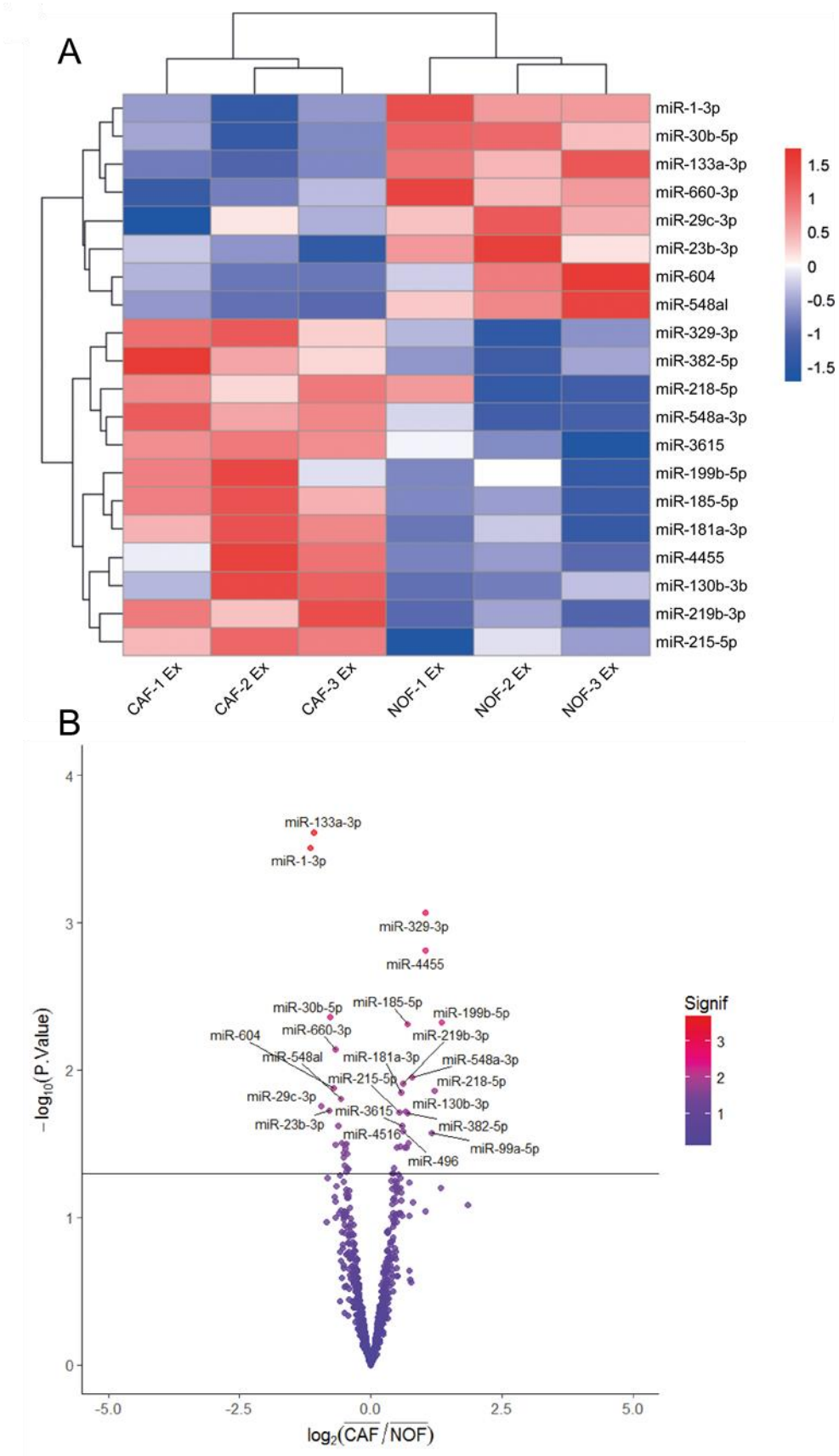

Figure 3-17. Differential expression of miRNAs in NOF and CAF exosomes. (**A**) Hierarchical cluster analysis of miRNAs in NOF and CAF exosomes. The 20 most changing miRNAs are shown. NOF Ex - NOF exosome; CAF Ex – CAF exosome. (**B**) Volcano plot displaying miRNAs which are more or less

abundant in CAF compared to NOF exosomes (x-axis) against statistical significance (y-axis). This is an alternative representation of data displayed in the. Threshold of statistical significance set at 0.05. Representative of two separate experiments. From *Bhome et al. (2017)* [481].

miRNA	460 NOF Ex	460 CAF Ex	463 NOF Ex	463 CAF Ex	602 NOF Ex	602 CAF Ex
miR-21-5p	12132	16327	8216	16316	5404	6330
miR-135b-5p	46	72	31	78	71	1635
miR-20a/b-5p	146	306	89	284	158	210
miR-19b-3p	135	311	115	218	135	232
miR-19a-3p	81	196	85	184	146	141
miR-155-5p	109	110	55	138	92	110
miR-181a-3p	53	107	53	171	71	81
miR-130b-3p	40	61	32	145	67	75
miR-95-3p	43	45	27	62	31	32
miR-499a-5p	26	44	38	53	50	17

Figure 3-18. MiR-21 is abundant and differentially expressed in exosomes from primary colorectal fibroblasts. Heat map of normalized NanoString counts for NOF and CAF exosome samples for ten experimentally validated CRC oncomirs. Global normalisation method used for raw NanoString counts. Arbitrary blue-red scale, with red indicating relatively higher abundance, and blue, relatively lower abundance. Representative of two separate experiments. From *Bhome et al. (2017)* [481].

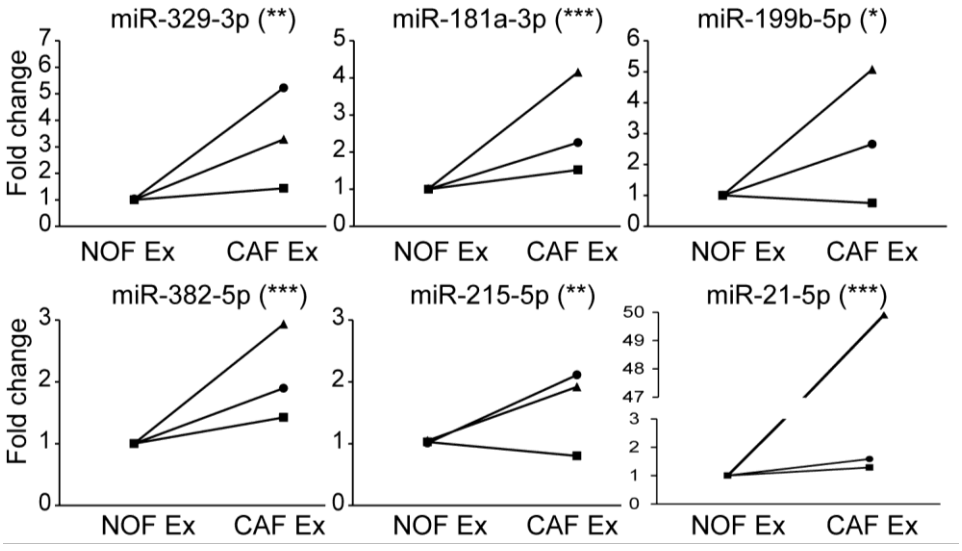

Figure 3-19. qPCR validation confirms panel of six miRNAs more abundant in CAF than NOF exosomes. qPCR results presented as relative fold changes between NOF and CAF exosomal miRNA for each NOF-CAF exosome pair. NOF exosome was assigned the value 1 for each NOF-CAF exosome pair (n=3). Mean values have been plotted. Asterisks indicate level of statistical

significance. Representative of two separate experiments, each with three technical replicates. From *Bhome et al. (2017)* [481].

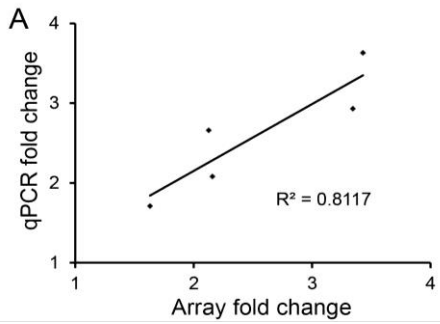

B

miRNA	Array fold change	qPCR fold change
329-3p	3.43	3.63
181a-3p	2.13	2.66
199b-5p	3.35	2.93
382-5p	2.16	2.08
215-5p	1.63	1.71

Figure 3-20. NanoString miRNA fold changes correlate with qPCR fold changes. (**A**) Scatter plot of miRNA fold changes between NOF and CAF exosomes determined by NanoString (x-axis) and validated by qPCR (y-axis). Pearson product moment correlation coefficient, $R^2 = 0.81$; p=0.02. (**B**) Numerical values of miRNA fold changes between NOF and CAF exosomes by NanoString and qPCR. Representative of two separate experiments. From *Bhome et al. (2017)* [481].

3.2.4 Exosomal miRNA signature targets multiple cancer-relevant pathways

More than 99% of the total 236 Kyoto Encyclopedia of Genes and Genomes (KEGG) pathways have miRNA sources and targets in man, emphasising the vast impact of miRNA-mediated regulation within biological pathways. KEGG pathways regulated by miRNAs have tens of thousands miRNA-gene interactions. The number of miRNA-gene interactions related to biological pathways in KEGG for our putatively annotated miRNAs were, respectively, 174: hsa-miR-181a-3p, 299: hsa-miR-199b-5p, 128: hsa-miR-382-5p and 1438: hsa-miR-21-5p. Of these, miR-21 may have the highest regulatory activity of biological pathways by targeting over 1400 genes. Thirty-six KEGG pathways targeted by the combined miRNA panel were identified, including “miRNAs in cancer”, “proteoglycans in cancer”, “colorectal cancer” and “pathways in cancer” (**Supplementary Table 1**, **Figure 3-21**). This was reiterated by Ingenuity Pathway Analysis (**Table 3-2**, **Table 3-3**). A novel approach to identify miRNA-small molecule interactions revealed that this miRNA panel interacts with several drugs utilized in cancer therapy. Of note, a recurrent association between miR-21 and 5FU, a first line agent in neoadjuvant, adjuvant and palliative CRC, was identified (**Supplementary Table 2**) [76, 497].

Figure 3-21. CAF-derived exosomal miRNAs converge on multiple cancer-relevant pathways. Statistical significance of 36 KEGG pathways co-regulated by miR-329-3p, miR-181a-3p, miR-199b-5p, miR-382-5p, miR-215-5p and miR-21-5p. Data represented as –log 10 (*p* value). Fisher-exact meta-analysis method with FDR-adjusted *p*-values. From *Bhome et al. (2017)* [481].

Table 3-2. Ingenuity Pathway Analysis of "Diseases and Disorders" associated with miR-329-3p, miR-181a-3p, miR-199b-5p, miR-382-5p, miR-215-5p and miR-21-5p.

Name	*p*-value	Molecules
Cancer	4.87E-02 – 3.31E-09	6
Organismal Injury and Abnormalities	4.87E-02 – 3.31E-09	6
Reproductive System Disease	4.82E-02 – 3.31E-09	5
Connective Tissue Disorders	4.06E-02 – 1.23E-04	2
Inflammatory Response	4.06E-02 – 5.08E-04	4

From *Bhome et al. (2017)* [481]

Table 3-3. Ingenuity Pathway Analysis of "Molecular and Cellular Functions" associated with miR-329-3p, miR-181a-3p, miR-199b-5p, miR-382-5p, miR-215-5p and miR-21-5p.

Name	*p*-value	Molecules
Cellular Development	2.03E-02 – 3.67E-05	4
Cellular Growth and Proliferation	2.03E-02 – 3.67E-05	4
Cell Morphology	4.17E-02 – 5.62E-04	2
Cell-To-Cell Signalling and Interaction	7.84E-03 – 5.62E-04	2
Cellular Movement	3.62E-02 – 8.42E-04	2

From *Bhome et al. (2017)* [481]

3.2.5 MiR-21 is upregulated in colorectal cancer fibroblasts and enriched in their exosomes

Our group previously showed that miR-21 is a stromal signal in CRC, originating from fibroblasts, and able to influence cancer cells by paracrine mechanisms [427, 504]. Cellular and exosomal profiles of NOFs and CAFs in this project reinforced this, with significantly higher miR-21 levels in CAFs compared to NOFs (**Figure 3-22**A, B). Importantly, we already showed that CAF exosomes contain miR-21 (**Figure 3-18**), and that delivery of CAF exosomes to CRC cells results in increased miR-21 (**Figure 3-7**B). Furthermore, miR-21 was the only miRNA enriched in exosomes compared to parent cells (Figure 3-22C). Hence, miR-21 meets all the criteria set above, in that it is oncogenic, stromal in origin, abundant in exosomes and enriched in exosomes, and was therefore the subject of our *in vivo* study.

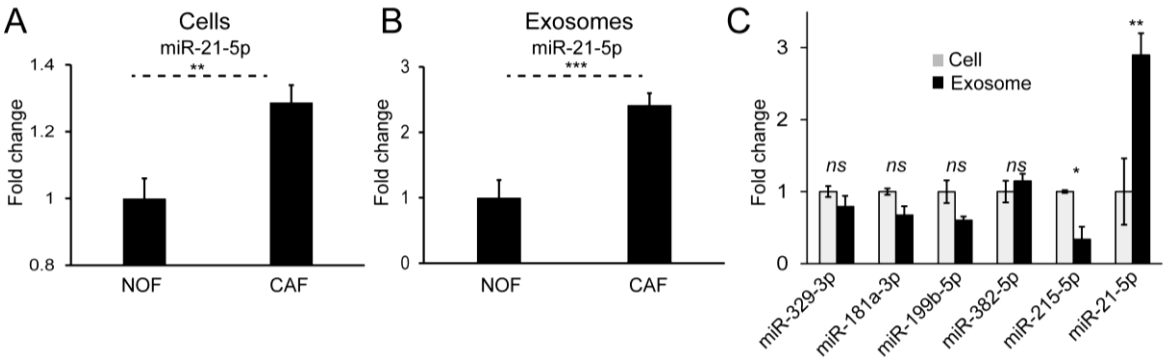

Figure 3-22. MiR-21 is more abundant in CAF cells and exosomes and enriched in the exosomal compartment. (**A**) On a whole-cell level, CAFs express significantly more miR-21 than NOFs. (**B**) CAF exosomes contain significantly more miR-21 than NOF exosomes. Results obtained by Taqman qPCR and presented as mean relative fold changes for each NOF-CAF pair (n=3). Representative of two separate experiments, each with three technical replicates. (**C**) NanoString counts normalized by global mean expression for CAF cells and exosomes. Exosomal counts are expressed relative to cellular counts which were assigned the value 1. Representative of two separate experiments, each comparing three cell and exosome samples. From *Bhome et al. (2017)* [481].

3.2.6 Ectopic stromal miR-21 overexpression enhances CRC metastasis in an orthotopic murine model

Firstly, in order to demonstrate that human fibroblasts persist in murine xenografts, PKH26-labelled MRC5 cells (red) were co-injected with CRC cells to form subcutaneous tumours in nude mice. The PKH26 signal was detectable five weeks after injection (**Figure 3-23**A), suggesting that injected fibroblasts persist in the microenvironment of these tumours, and that they were not out-competed by murine fibroblasts.

To date, no direct role for stromal miRNAs in promoting metastasis has been shown in an *in vivo* CRC model. In part, this reflects the limitations posed by conventional non-metastatic heterotopic xenografts. Consequently, we next sought to evaluate the *in vivo* activity of miR-21 using an orthotopic CRC model, modified from our group's previous description [475]. MiR-21 or control non-targeting sequence (control) was stably overexpressed in MRC5 fibroblasts, as previously described [504]. Direct caecal co-implantation of SW620 CRC cells with MRC5 fibroblasts stably overexpressing miR-21 (SW620/MRC5-miR-21) resulted in a greater number and size of metastatic tumour deposits in the liver when compared to control (SW620/MRC5-control), equating to eight times more liver replacement by secondary CRC deposits (**Figure 3-23**B-D). No

metastases were noted in the spleens of either group. Histological analysis confirmed the presence of colorectal adenocarcinoma in the liver metastases.

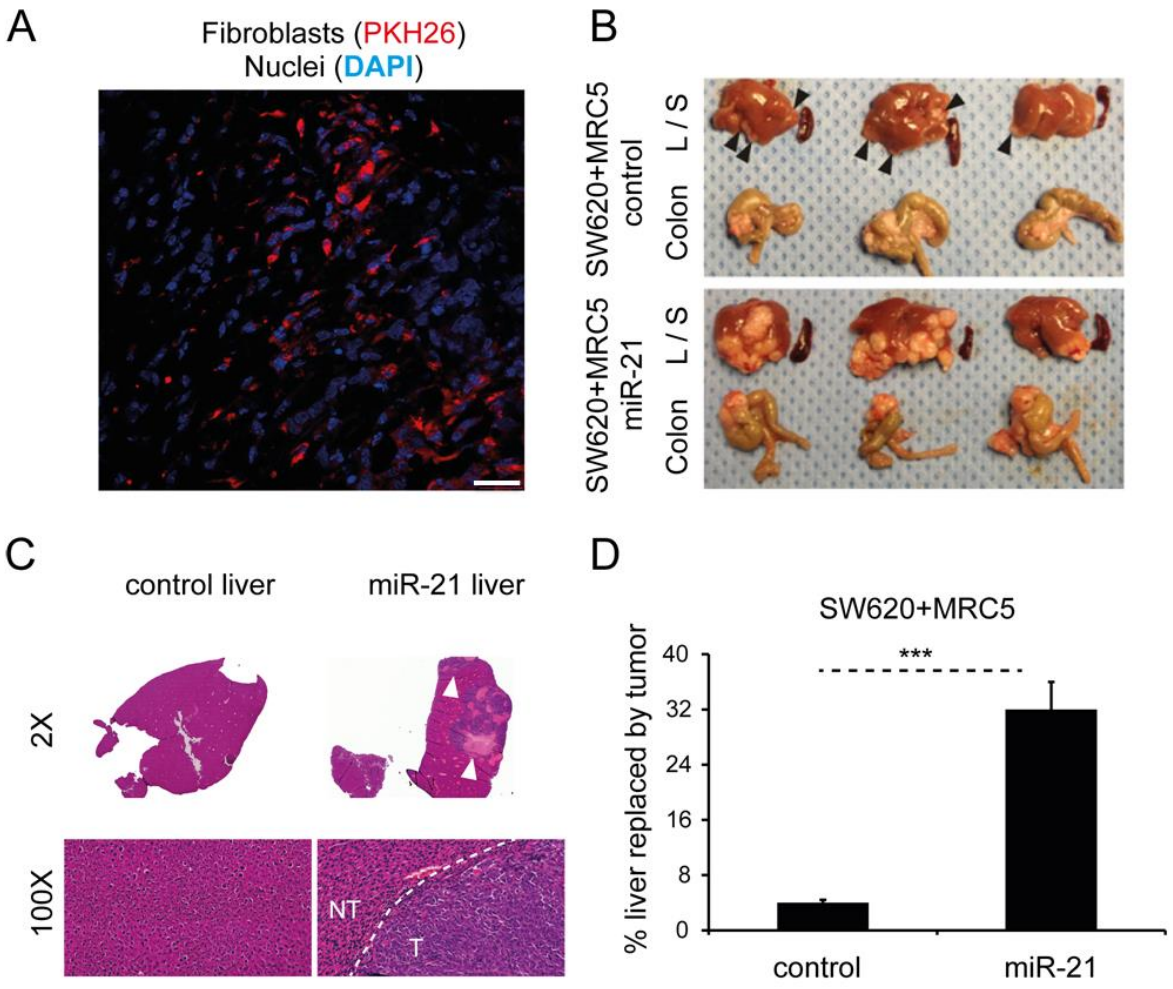

Figure 3-23. Stromal miR-21 leads to tumour progression in an *in vivo* orthotopic CRC model. (**A**) Confocal microscopy of tumour section generated by subcutaneous co-injection of PKH26-labelled MRC fibroblasts (red) and CRC cells, counterstained with DAPI (blue; 60x objective). Scale bar represents 25 µm. Representative of nine tissue sections (from three tumour xenografts). (**B**) Liver (L), spleen (S) and colon from mice orthotopically injected with SW620 CRC cells, and MRC5 control, or, miR-21-overexpressing fibroblasts. Arrowheads highlight liver metastases. The effect of miR-21-overexpressing cells was to increase the size and number of liver metastases. No splenic metastases were seen in either group. (**C**) Liver sections at 2x and 100x total magnification. Bulky hepatic metastases are evident in the SW620/MRC5-miR-21 liver (arrowheads; seen at 2x) with a clear histological demarcation between normal liver and metastatic tumour (NT – normal tissue, T – tumour; seen at 100x). Each image is representative of nine tissue sections (from three tumour xenografts). (**D**) Mean percentage liver replacement by metastatic tumour in SW620/MRC5-control (control) and SW620/MRC5-miR-21 (miR-21) mice

(calculated from nine individual tissue sections; three from each tumour xenograft). From *Bhome et al. (2017)* [481].

3.2.7 Discussion

A collection of paired NOFs and CAFs were isolated from human CRC specimens, and shown to be phenotypically distinct by their myofibroblastic marker expression, cytoskeletal actin density and surface area. Exosomes from NOF and CAF subcultures were subjected to NanoString miRNA array, with miR-329, -181a, -199b, -382, -215 and -21, found to be significantly more abundant in CAF exosomes than NOF exosomes. Of these, miR-21 was the focus of further study, because of its known stromal origin and oncogenic potential [427, 504, 506, 514]. Furthermore, miR-21 was shown to be enriched in CAF exosomes, compared to parental cells, suggesting that this miRNA might be selectively concentrated into exosomes. MiR-21-overexpressing fibroblasts were co-injected with CRC cells to generate orthotopic tumour xenografts in mice, resulting in a significantly greater burden of liver metastases, compared to tumours established with CRC cells and control fibroblasts.

Our group previously showed that the secretome of miR-21-overexpressing fibroblasts directly increases invasion of CRC cells [504]. Here, we focussed on exosomes as a specific component of the secretome. We showed in section **3.1**, that fibroblast exosomes can be transferred to CRC cells, leading to an increase in miR-21 (**Figure 3-5**, **Figure 3-7**). Taken together with the data presented here, we propose that miR-21 is a stromal signal, which is conveyed to CRC cells in exosomes, leading to greater CRC invasion and metastasis. These results add weight to the evidence implicating exomiRs in cancer progression, particularly pointing a spotlight on the actions of miR-21.

3.3 The role of exosomes in EMT-driven CAF phenotype

3.3.1 Introduction

It is important to note that fibroblast phenotype is associated with oncological outcome. In particular, myofibroblastic transdifferentiation is a marker of poor prognosis in several solid tumours, including but not limited to, prostate, colon, HNSCC and pancreas [515-518]. This has recently been meta-analysed by Liu and colleagues [519].

There are several reasons why myofibroblasts may influence tumour progression. From the viewpoint of cancer as a "wound that does not heal", myofibroblasts are thought to remain in a persistently activated state [50]. This results in upregulation of growth factors and pro-inflammatory cytokines, such as insulin-like growth factor (IGF)-1, EGF and VEGF, as well as their cognate receptors [520]. This impacts upon remodelling of the tumour stroma [521, 522], cancer cell migration [523] and induction of chemoresistance [524, 525].

Unsurprisingly then, a histological association between invasive (mesenchymal) carcinoma cells and myofibroblasts has been described, at the invasive front, in tumours such as HNSCC and CRC [526, 527]. However, the mechanisms behind this association are unclear. In the following section we sought to investigate whether EMT status of CRC cells was a determinant of myofibroblast phenotype, and whether exchange of exosomal cargo mediated the interplay between these cell types.

3.3.2 EMT models

In vitro models of EMT in CRC were utilized for this aspect of the project. Four established CRC cell lines (DLD1, HCT116, SW620 and SW480) with variable EMT status, were used. DLD1, HCT116 and SW620 cells all expressed E-cadherin, and were considered to be classically epithelial, whereas SW480 cells lacked E-cadherin, and was considered mesenchymal (**Figure 3-24**A). SW480 cells expressed relatively high amounts of the EMT transcription factor Zeb1, which was also detectable in HCT116 and SW620 cells, to a lesser extent. Both SW620 and SW480 cells expressed vimentin and it is worth noting that these isogenic, but epigenetically distinct cells, were derived from the same patient [528]. SW620 cells, although derived from a metastatic lymph node, were considered to have reverted back to a more epithelial state through the process of MET. Conversely, SW480 cells were thought to be invasive mesenchymal cells in the primary tumour, capable of metastasis. This is an important point to note and is often confused in the literature [529]. Unsurprisingly, all four CRC cell lines expressed keratins, in keeping with colorectal adenocarcinoma, with the highly epithelial DLD1 cells expressing the most.

SW480 Zeb1-KD (SW480 ZKD) cells were generated here as another isogenic EMT model with less epigenetic variation than the SW620/ SW480 pairing. SW480 ZKD cells lacked Zeb1, and expressed similar amounts of E-cadherin and keratins to HCT116 cells (**Figure 3-24**B). Using these biochemical parameters, SW480 ZKD cells were classed as an isogenic but epithelial counterpart to SW480 cells. To our knowledge SW480 ZKD cells have never previously been described in the literature.

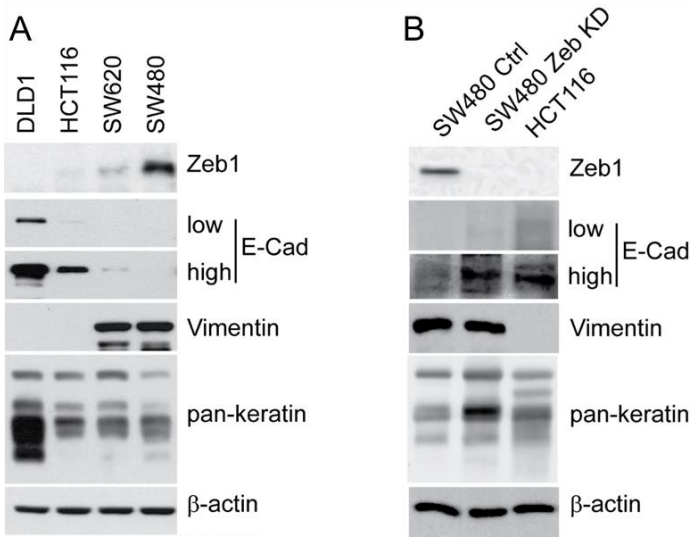

Figure 3-24. EMT status of CRC cell lines. (**A**) Four established CRC cell lines probed for epithelial (E-cadherin, pan-keratin) and mesenchymal (Zeb1, vimentin) markers by western blotting. β-actin was used as an equal loading control. (**B**) Generation of an isogenic EMT model by knocking down ZEB1 in SW480 cells. Notice the absence of Zeb1 protein and the increase in E-cadherin and pan-keratin in SW480 ZKD cells. Representative of two separate experiments.

3.3.3 Differing effects of epithelial and mesenchymal cell-derived exosomes on cellular signalling in fibroblasts

We next studied the effects of epithelial and mesenchymal CRC exosomes on MRC5 fibroblasts, initially with a focus on ERK and Akt pathways, which have wide ranging implications on cell fate, including proliferation, senescence and apoptosis [530-532]. Before conditioning fibroblasts with exosomes, we sought to document ERK and Akt activity in the donor CRC cells (**Figure 3-25**A). Conditioning of fibroblasts with epithelial (DLD1, HCT116 and SW620) but not mesenchymal (SW480) exosomes, attenuated ERK activity (reduced p-ERK 1/2) in fibroblasts, even at the lowest exosome concentration of 5 μg/ ml (**Figure 3-25**B). Interestingly, Akt activity in fibroblasts, increased in a dose-dependent manner with HCT116 and SW620 exosomes but not DLD1 or SW480 exosomes, therefore unrelated to CRC EMT status. Of note, cellular levels of ERK, Akt and their phosphorylated isoforms, in the donor CRC cells, did not predict the effect that their

exosomes had on the recipient fibroblasts. For example, phospho-Akt is relatively high in SW480 cells compared to other CRC cells but this was not conveyed to fibroblasts exposed to SW480 exosomes (**Figure 3-25**A, B). This is important because it suggests that the effects demonstrated on fibroblasts are unlikely to be because of direct protein or mRNA transfer, but other exosomal cargo.

Similarly, using the SW480 EMT model, epithelial exosomes from SW480 ZKD cells attenuated ERK activity in MRC5 fibroblasts (this time in a dose-dependent manner) but mesenchymal exosomes from SW480 control cells did not (**Figure 3-25**C, D). There was no consistent effect on fibroblast Akt activity with either SW480 control or ZKD exosomes. Again, ERK and Akt activity in donor SW480 control and ZKD cells did not determine the effect of their exosomes on fibroblast ERK and Akt activity.

Using the same experimental set up, several other cellular pathways were investigated, including ATM/ ATR (DNA damage response), protein kinase A (PKA), protein kinase C (PKC) and AMP-actvated protein kinase (AMPK). There was a clear difference between the effects of DLD1 and HCT116 exosomes compared to SW620 and SW480 exosomes, on these pathways. However, unlike what was shown with ERK, there was no clear link with CRC EMT status (**Figure 3-26**).

Taken together, this collection of western blots suggests that exosomes from epithelial and mesenchymal cells have differening effects on cellular pathways in fibroblasts. Considering that we were most interested in the survival advantage that mesenchymal (metastatic) carcinoma cells would confer to fibroblasts in the TME, we initially focused on the ERK pathway.

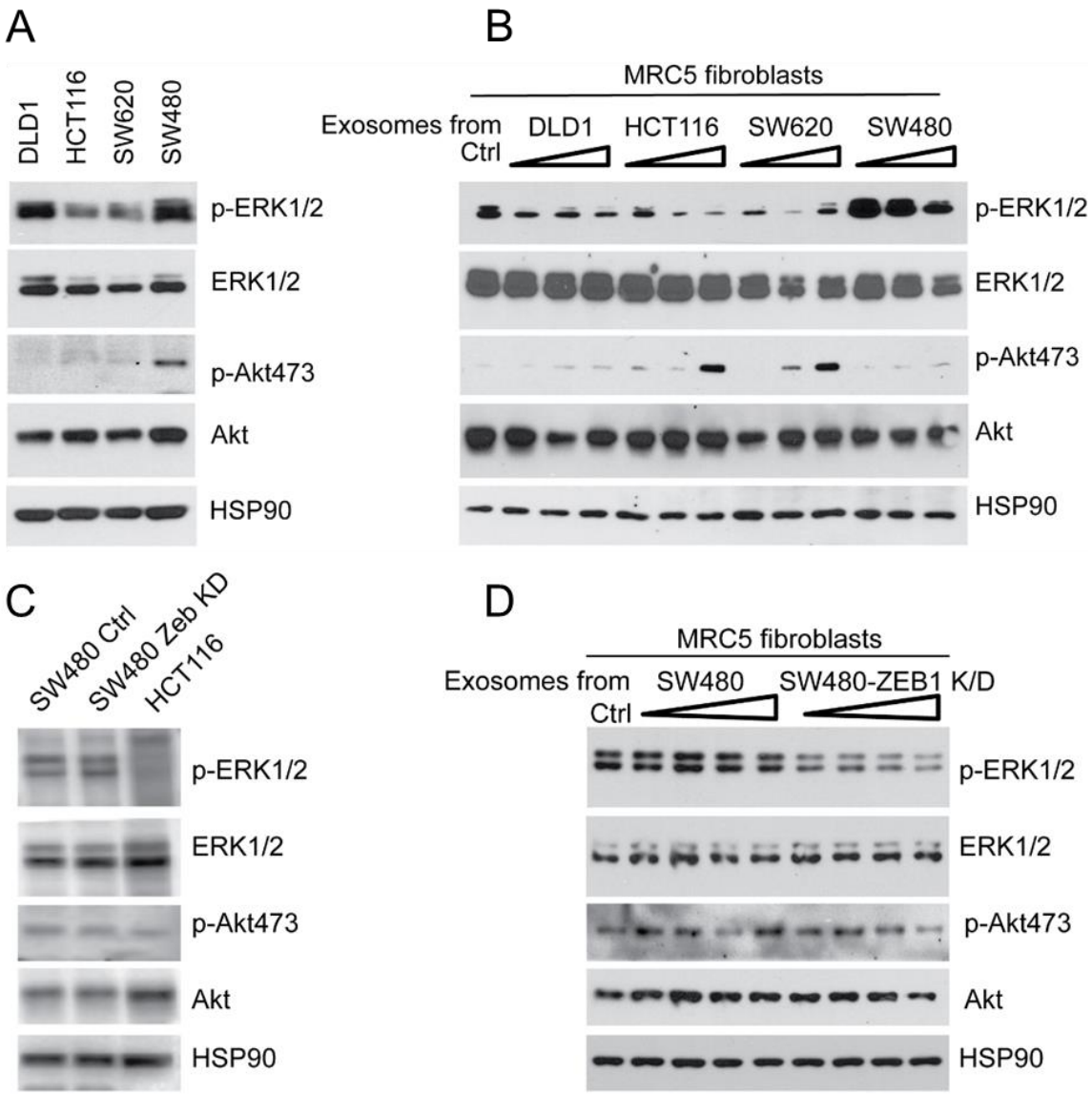

Figure 3-25. Fibroblasts conditioned with CRC exosomes: ERK and Akt activity. (**A**) Constitutive ERK and Akt activity in CRC cell lines. HSP90 was used as an equal loading control. (**B**) Conditioning of MRC5 fibroblasts with CRC exosomes at increasing doses (5, 15 and 45 µg/ml), with resultant effects on fibroblast ERK and Akt activity. (**C**) Constitutive ERK and Akt activity in SW480 control and SW480 ZKD cells (HCT116 shown as comparative control). (**D**) Conditioning of MRC5 fibroblasts with CRC exosomes at increasing doses (5, 10, 15 and 45 µg/ml), with resultant effects on fibroblast ERK and Akt activity. Representative of two separate experiments.

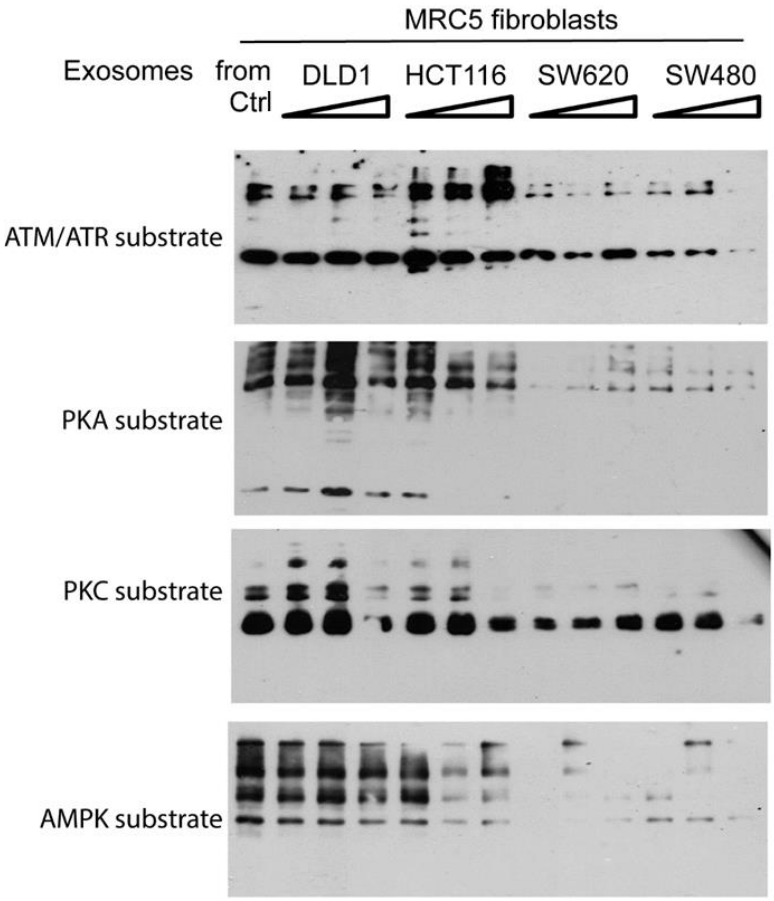

Figure 3-26. Fibroblasts conditioned with CRC exosomes: other cellular pathways. Conditioning of MRC5 fibroblasts with CRC exosomes at increasing doses (5, 15 and 45 μg/ml), with resultant effects on other pathways. Notice the clear difference in effect of DLD1/ HCT116 and SW620/ SW480 exosomes. Amount of lysate loaded for each sample is the same as in **Figure 3-25**B. Representative of two separate experiments.

3.3.4 Effect of CRC exosomes on fibroblast proliferation and cell cycle

To investigate the functional effect of CRC exosomes on fibroblast ERK activity, cell cycle and proliferation were assessed. There was very little difference in cell cycle profile between unconditioned (control), mesenchymal (SW480) exosome conditioned and epithelial (SW620) exosome conditioned fibroblasts on day 1 (**Figure 3-27**A), although the slight 1.8% reduction in G1 brought about by epithelial exosomes, compared to control, did reach significance (p=0.0067). There was no significant difference between control and mesenchymal exosome conditioning, or between mesenchymal and epithelial exosome conditioning. However, on day 4, fibroblasts conditioned with epithelial exosomes clearly showed a greater proportion of cells in G1, compared to those conditioned with mesenchymal exosomes (p<0.001) or control (p<0.001). Mesenchymal exosomes also induced an increase in G1 compared to control on day 4, but this effect was much smaller than with epithelial exosomes (p=0.002).

Cell cycle profiles were corroborated by growth characteristics, in that fibroblasts conditioned with epithelial exosomes, proliferated less between days 3 and 4 following exosome exposure, compared to those conditioned with epithelial exosomes ($p<0.001$) or control ($p<0.001$; **Figure 3-27**B). Fibroblasts conditioned with mesenchymal exosomes proliferated at the same rate as unconditioned fibroblasts ($p=0.26$). It should be noted that in this assay, fibroblasts were exposed to CRC exosomes for 24 h (day 0), after which they were allowed to grow in exosome-free conditions (days 1-4).

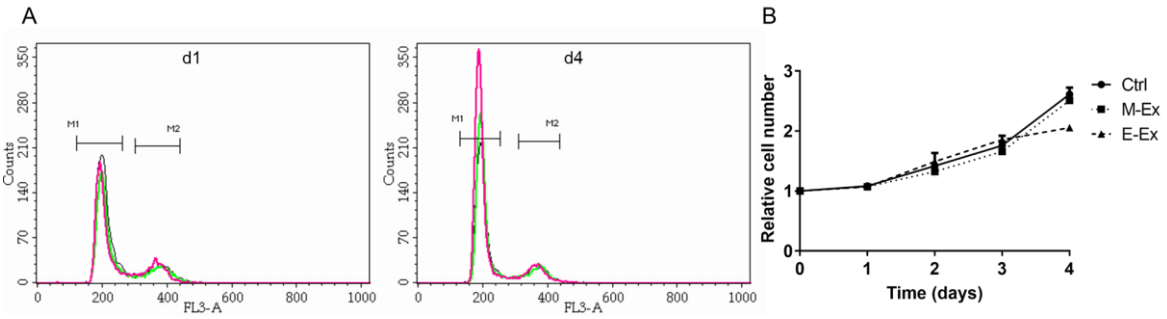

Figure 3-27. CRC exosomes alter fibroblast cell cycle and growth. (**A**) Cell cycle profile of MRC5 fibroblasts on day 1 (d1) and day 4 (d4) following exosome treatment. M1 represents G1 and M2 represents G2. Black, control; green, conditioned with (SW480) mesenchymal exosomes; pink, conditioned with (SW620) epithelial CRC exosomes. Representative of two separate experiments. (**B**) Growth curve of MRC5 fibroblasts conditioned with mesenchymal (SW480) exosomes (M-Ex), epithelial (SW620) exosomes (E-Ex), or untreated control (Ctrl). Cell number is relative to that on day 0. Representative of two separate experiments, each with four technical replicates.

3.3.5 MiRNA profiling of CRC cells and exosomes

As previously alluded to, miRNAs are one of the most stable of all exosome cargos. In addition, the effects seen on attenuating ERK activity, fit with the repressive function of miRNAs. Hence, the miRNA cargo of CRC exosomes and parent cells were assayed using the Quantimir™ miRNA array, which profiles 95 cancer-associated miRNAs [533]. Unbiased hierarchical clustering analysis revealed that CRC exosomes clustered according to EMT status of parent cells, even though the cells themselves did not cluster in this manner (**Figure 3-28**, **Figure 3-29**). This is in keeping with previous work, which shows that miRNA profiles of exosomes and parental cells can be dissimilar [335, 337]. It supports the idea that exosomes are not passively filled cytosolic fragments, rather that miRNAs may be selectively loaded into exosomes.

In terms of cellular miRNA expression, DLD1 and SW620 were closely related, with SW480 more distantly related to these two. However, HCT116 seems to be distinct from the others. The key distinguishing feature of HCT116 cells is their *TP53* wild type status, the others all bearing

mutations of this gene (**Table 2-2**). However, this is a small selected panel of CRC cells on which to make such inferences. In terms of CRC exosome profiles, DLD1 and HCT116 were closely related, with SW620 related to these two, and SW480 distinct from all of these. This closely mirrors the EMT spectrum of the parent cells, with DLD1 considered most epithelial (greatest E-cadherin expression), followed by HCT116 and SW620, and SW480 considered mesenchymal (absence of E-cadherin).

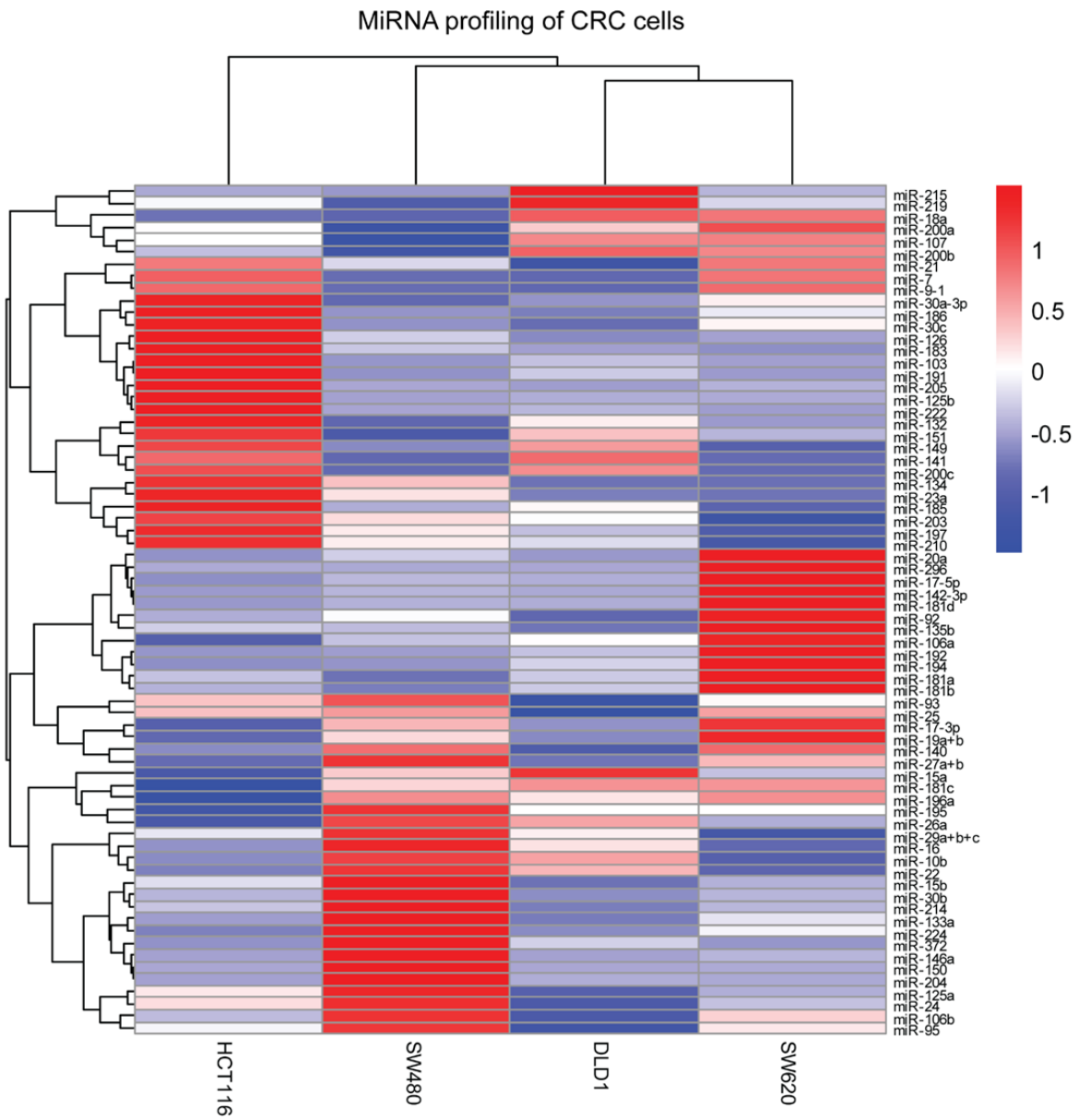

Figure 3-28. CRC cell miRNA profile. Unbiased hierarchical clustering analysis of 95 cancer-related miRNAs expressed by epithelial and mesenchymal CRC cells. Input values were the mean of two separate experiments. Values shown are mean $2^{-\Delta\Delta CT}$ from two separate experiments.

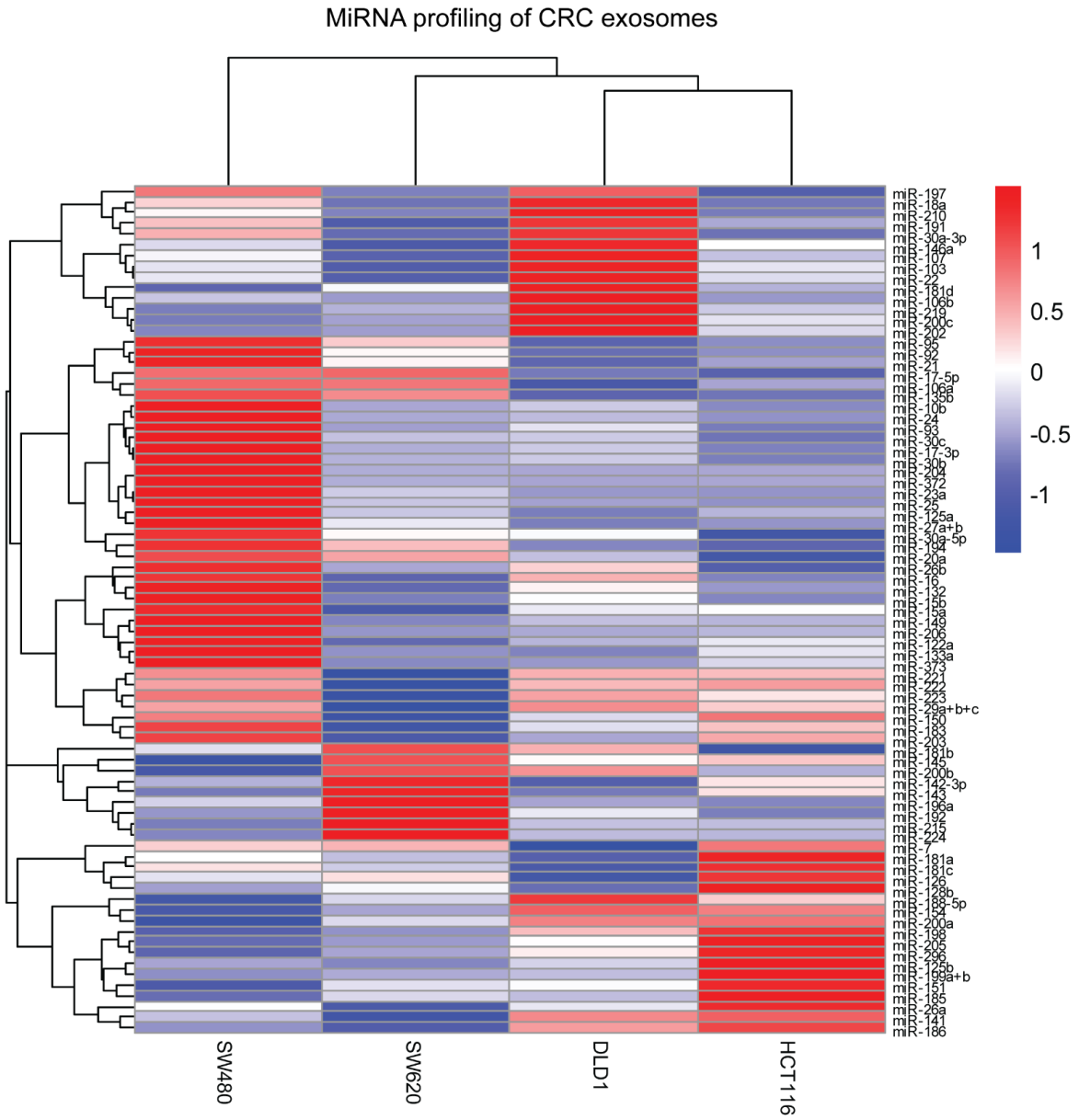

Figure 3-29. CRC exosome miRNA profile. Unbiased hierarchical clustering analysis of 95 cancer-related miRNAs present in exosomes derived from epithelial and mesenchymal CRC cells. Values shown are mean $2^{-\Delta\Delta CT}$ from two separate experiments.

The profiling data were interrogated to identify miRNAs which were consistently more abundant in epithelial compared to mesenchymal exosomes. This is because we sought to find a miRNA or group of miRNAs, which epithelial CRC cells could shuttle to the surrounding stroma, to reduce the accumulation of CAFs, in comparison to mesenchymal CRC cells, which would not exert such a repressive effect.

MiR-200 family members were consistently more abundant in epithelial compared to mesenchymal exosomes (**Figure 3-30**A). This was also true for exosomes isolated from SW480 control and SW480 ZKD cells (**Figure 3-30**B). The differences in miR-200 levels seen in different CRC exosomes were in keeping with differences seen in parent cells, but the relative fold changes

did not mirror one another exactly (**Figure 3-31**A-D). Exosomal miR-200 levels seemed to reflect EMT status better than cellular miR-200, in demonstrating the gradient between DLD1 (most epithelial) and SW480 (least epithelial). With regard to the SW480 ZKD model, exosomal miR-200 levels were consistently higher in ZKD (epithelial) compared to control (mesenchymal) exosomes (**Figure 3-30**B, **Figure 3-31**D) but this was not always the case for cellular miR-200 family members, as evidenced by miR-429 (**Figure 3-31**C).

A

miRNA	DLD1-Ex	HCT116-Ex	SW620-Ex	SW480-Ex
miR-200a	2.34	1.94	3.39	0.03
miR-200b	72.0	30.5	65.0	2.21
miR-200c	452	562	23.2	21.8
miR-141	1.78	1.95	0.27	0.96

B

miRNA	SW480 ctrl-Ex	SW480 ZKD-Ex
miR-200a	0.39	0.03
miR-200b	0.19	0.57
miR-200c	0.66	12.4
miR-141	0.31	0.43

Figure 3-30. Exosomal miR-200 fold changes from miRNA array. (**A**) Exosomes from CRC cell lines. (**B**) Exosomes from SW480 control and ZKD cells. Values shown are mean $2^{-\Delta\Delta CT}$ from two separate experiments. Red-blue scale is arbitrary, with red indicating higher and blue indicating lower abundance for each individual miRNA. Note that miR-429 was not assayed by the Quantimir™ array.

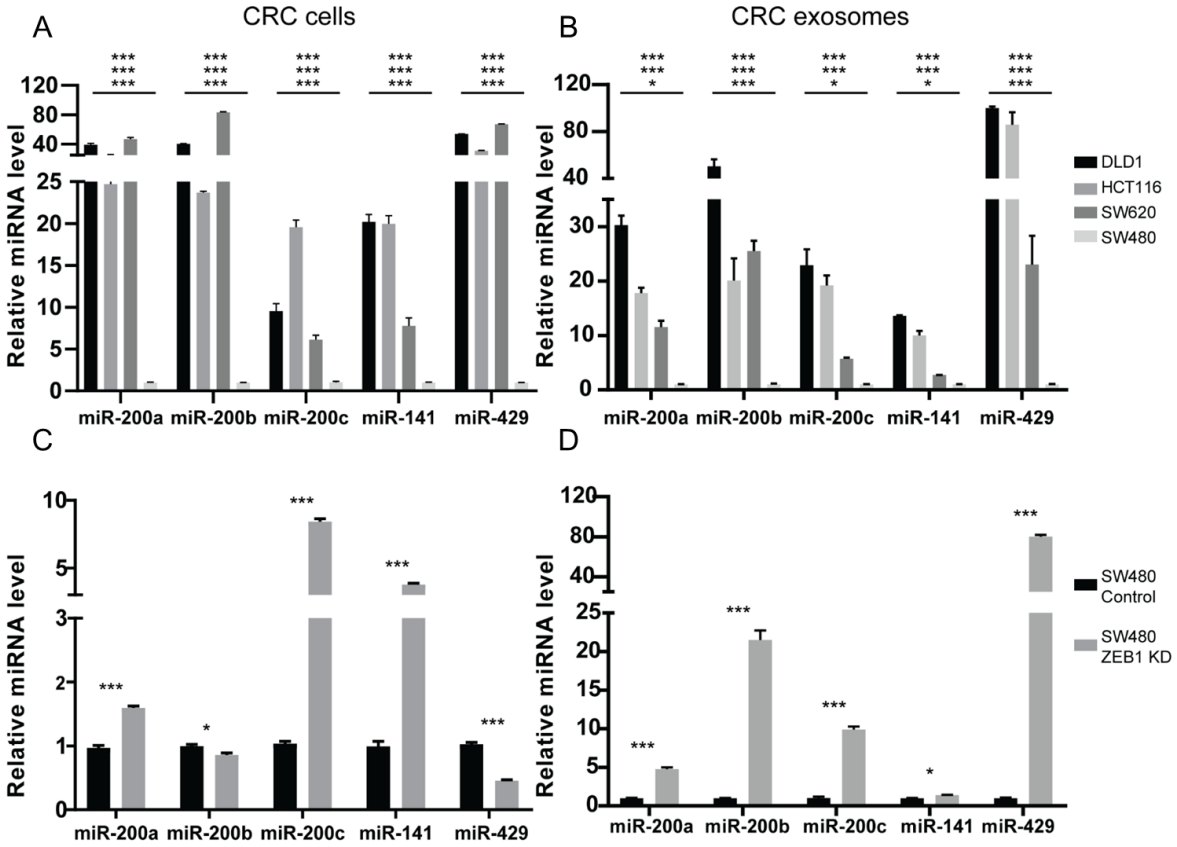

Figure 3-31. MiR-200 profiling of CRC cells and exosomes. (**A**) CRC cell lines. (**B**) Exosomes from CRC cell lines. (**C**) SW480 control and ZKD cells. (**D**) Exosomes from SW480 control and ZKD cells. MiR-200 levels were assayed in triplicate with mean values shown relative to SW480 cells or

exosomes, which were assigned the value "1". The stacked asterisks in (**A**) and (**B**) denote statistical significance for comparisons of DLD1, HCT116 and SW620 with SW480 (from top to bottom), respectively. Representative of two separate experiments.

3.3.6 MiR-200 targets ZEB1 in fibroblasts: 3'UTR luciferase reporter assays

The most well known target of miR-200 family members is *ZEB1*. Goodall's group demonstrated that miR-200 family members bind to the 3'UTR of *Zeb1* and *Zeb2* in MDCK (canine) cells, repressing their translation [458]. However, this has not been shown in the context of fibroblasts. To optimise the assay, readily transfectable HEK293T cells were used. Using constructs that were deposited by Goodall's group, we demonstrated that co-transfection of miR-200b mimic with *ZEB1* 3'UTR led to a decrease in luciferase activity of 58%, compared to scrambled control ($p<0.01$; **Figure 3-32**A). There was also a reduction in luciferase activity with miR-200c (21%), but this did not reach significance. However, when miR-200b was co-transfected with a mutant *ZEB1* 3'UTR (mutated at five putative miR-200b binding sites; see Appendix **B**), there was no significant reduction in luciferase activity. MiR-200c seemed to reduce luciferase activity in the presence of the mutant construct (32%) but the change did not reach statistical significance. Co-transfection of miR-200b and -200c with a control 3'UTR construct (*HNF4A*) caused no significant decrease in luciferase activity, with miR-200c actually increasing luciferase activity in this context.

In MRC5 fibroblasts, a similar pattern of results was demonstrated (**Figure 3-32**B). Both miR-200b and -200c significantly reduced luciferase activity in the presence of *ZEB1* 3'UTR, by 77% and 63% respectively ($p<0.001$). In the presence of the mutant 3'UTR construct, miR-200b had no effect on luciferase activity but miR-200c reduced activity by 20% ($p<0.05$). This was not unexpected because the mutant construct was created by site directed mutagenesis at putative miR-200b (not -200c) binding sites. Again, there was no significant decrease in luciferase activity when miR-200b or -200c were co-transfected with the control construct. As seen in HEK293T cells, luciferase activity actually increased when miR-200c was co-transfected with the control construct. These data show, for the first time, that miR-200b and -200c target *ZEB1* in fibroblasts.

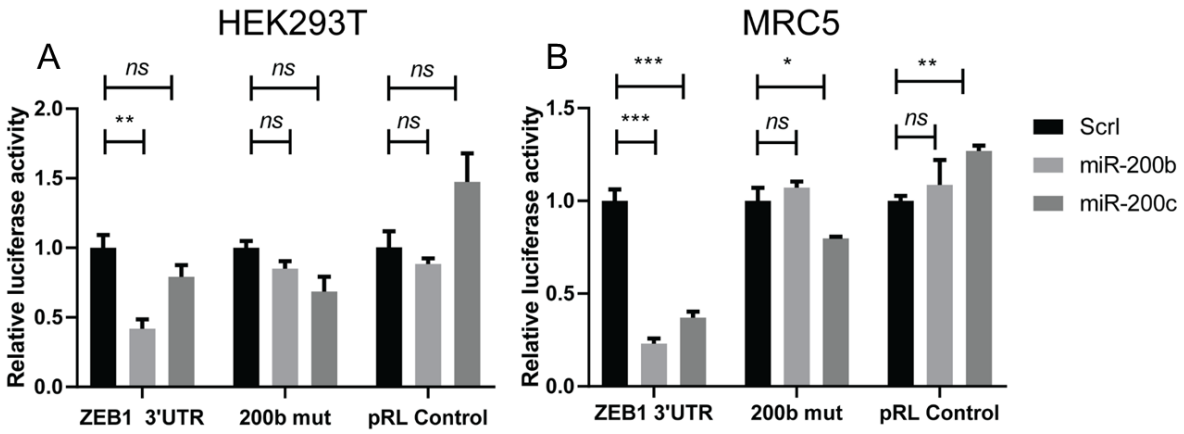

Figure 3-32. MiR-200 targets ZEB1 in fibroblasts. (A) 3' UTR luciferase reporter assay for miR-200b/c mimics or scrambled sequence control (scrl), binding to *ZEB1* 3'UTR, mutant 3'UTR (200b mutant) and control 3'UTR (pRL control) constructs in HEK293T cells. (B) The same oligonucleotides and 3'UTR constructs in MRC5 fibroblasts. Representative of two separate experiments, each with three technical replicates.

3.3.7 The effect of epithelial and mesenchymal exosomes on fibroblast to myofibroblast transdifferentiation

3.3.7.1 TGF-β treatment of different fibroblasts

TGF-β-mediated fibroblast to myofibroblast transdiffererentiation is a well established model, for recapitulating one of phenotypic effects which occurs in the TME, in a controlled manner, and has been previously used in our lab [54, 504, 534, 535]. To identify the most appropriate fibroblast line in which to assess TGF-β-mediated transdifferentiation, five different fibroblasts (IMR90, MRC5, primary normal colonic fibroblast (NOF), HFFF2 and primary colon CAF) were treated with 2 ng/ml TGF-β for 48 h, and changes in Zeb1, fibronectin and α-SMA expression were detected by western blotting (**Figure 3-33**). TGF-β increased Zeb1 protein level in IMR90, MRC5, HFFF2 and CAF. However, there was a reduction in Zeb1 in NOF. There was a marked increase in fibronectin in all fibroblasts with the exception of NOF, where the increase was quite subtle. α-SMA level increased in all fibroblasts but was again quite subtle in NOF. As expected, CAF had relatively high resting α-SMA, limiting the degree of α-SMA induction by TGF-β. Therefore, MRC5 was chosen as an appropriate model because it has almost no resting fibronectin and α-SMA, and both these myofibroblastic markers were induced by TGF-β, in parallel with Zeb1. This made it the ideal candidate to assess the effects of miR-200 on Zeb1-mediated myofibroblast transdifferentiation. Of note, NOF cells, although showing evidence of transdifferentiation upon TGF-β stimulation, actually reduced Zeb1 levels in its presence. This behaviour is inconsistent with all other

fibroblasts demonstrated here, and it does not seem to be a tissue-specific effect because Zeb1 was induced in CAF cells, which were also colonic.

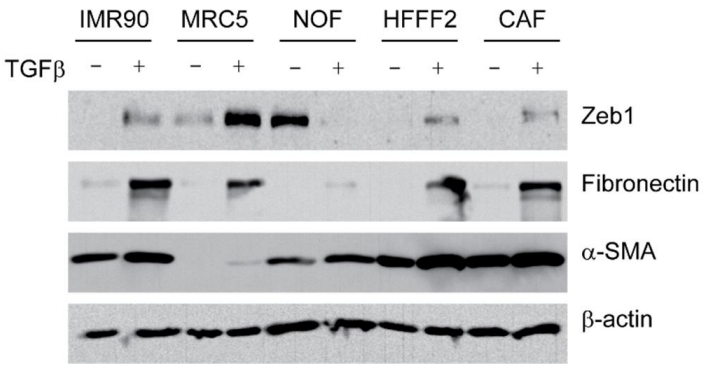

Figure 3-33. The effect of TGF-β on different fibroblasts. Zeb1, fibronectin and α-SMA expression in fibroblasts in the absence (-) and presence (+) of TGF-β (2 ng/ml for 48 h). β-actin was used as an equal loading control. Representative of two separate experiments.

3.3.7.2 Time course of TGF-β treatment in fibroblasts

To determine the optimal duration of TGF-β treatment, MRC5 fibroblasts were exposed to a constant dose of 2 ng/ml for varying durations (0-72h). With increasing duration of treatement, Zeb1 protein increased from 0-48 h, and then plateaued (**Figure 3-34**). For fibronectin and α-SMA, protein levels increased from 0-36 h, plateaued between 48-60 h, and fell at the final time point (72 h). 48 h was chosen as an optimal duration of TGF-β treatment because it gave maximally detectable induction of Zeb1, fibronectin and α-SMA.

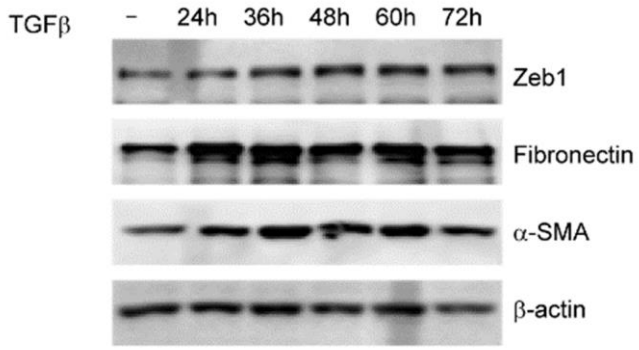

Figure 3-34. Extended duration of TGF-β fibroblast treatment. Zeb1, fibronectin and α-SMA expression in MRC5 fibroblasts, treated with TGF-β (2 ng/ml) for up to 72 h. Control fibroblasts (-) were untreated. β-actin was used as an equal loading control. Representative of two separate experiments.

3.3.7.3 The effect of CRC exosomes on myofibroblast transdifferentiation

Next, we asked whether CRC exosomes could alter miR-200 levels in recipient fibroblasts. Exosomes from mesenchymal (SW480 control) or epithelial (SW480 ZKD) cells were used to condition MRC5 fibroblasts for five days, in order to better simulate the *in vivo* situation. Epithelial but not mesenchymal exosomes increased miR-200 levels in recipient fibroblasts, at day 3 and day 5 (**Figure 3-35**A). This was true for all miR-200 family members. On day 3, the increases conveyed by epithelial exosomes were between 3-23 fold, relative to mesenchymal exosomes, the greatest increase being miR-429. Comparing day 3 to day 5, epithelial exosomes produced modest additional increases in miR-200a and -200b, a substantial additional increase in miR-200c (from 5 to 25 fold) and no additional increases in miR-141 and -429. The miRNA levels shwn here are all relative to fibroblasts treated with mesenchymal exosomes at day 3, showing clearly that there was no change whatsoever in fibroblast miR-200 levels from day 3 to day 5 in the presence of mesenchymal exosomes.

To investigate whether exosome mediated changes in miR-200 levels would influence fibroblast phenotype, we utilised the TGF-β-driven fibroblast to myofibroblast transdifferentiation model. Following five days of conditioning with either epithelial or mesenchymal exosomes, fibroblasts were switched to low serum conditions (0.1% FBS) for 24 h and then stimulated with TGF-β (2 ng/ml) for 48 h. This was similar to the method used by Yang et al. [491]. Low serum conditions were used because serum has been shown to influence fibroblast contractility and transdifferentiation in multiple models [536, 537]. Fibroblasts conditioned with mesenchymal exosomes (low miR-200) demonstrated marked upreguation of α-SMA and fibronectin upon TGF-β stimulation, consistent with myofibroblast transdifferentiation (**Figure 3-35**B). In these conditions, TGF-β induced Zeb1 expression in fibroblasts. Although this has not been shown before in fibroblasts, others have demonstrated the same effect in cells of epithelial lineage, such as NmuMG [538]. Furthermore, the link between Zeb1 and α-SMA has been demonstrated in smooth muscle cells, where Zeb1 activates the α-SMA gene promoter [539]. However, in the presence of epithelial exosomes (high miR-200), the TGF-β-mediated increase in α-SMA and fibronectin was clearly attenuated. In these conditions, Zeb1 was not induced by TGF-β, in fact, its expression went down (**Figure 3-35**B). Taken together, these data suggest that epithelial but not mesenchymal exosomes increase miR-200 levels in fibroblasts, preventing Zeb1 induction and myofibroblast transdifferentiation, upon TGF-β stimulation.

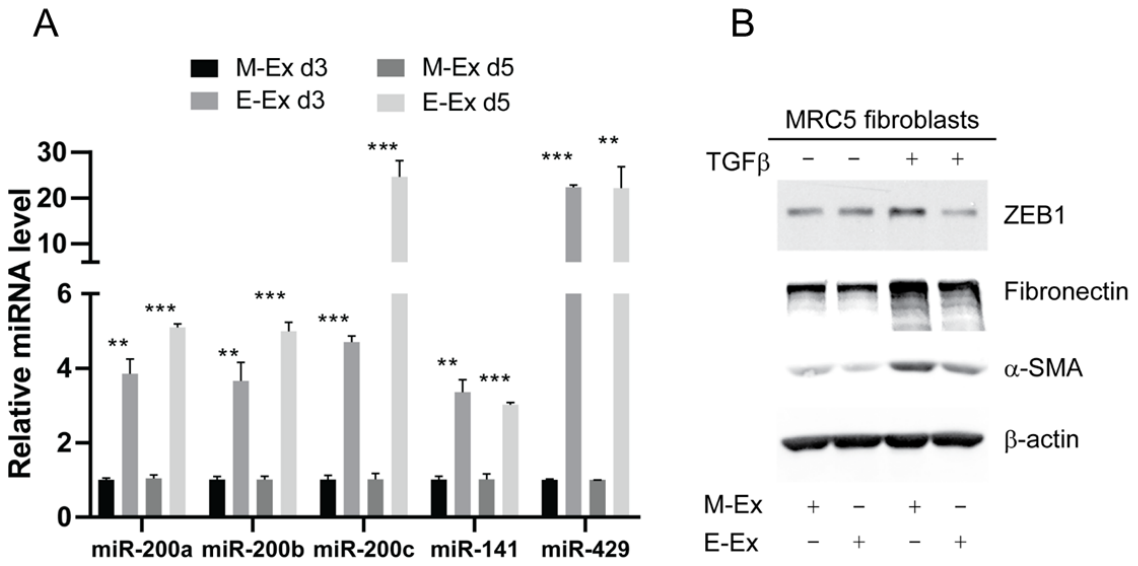

Figure 3-35. Differential effects of mesenchymal and epithelial CRC exosomes on fibroblast phenotype. (**A**) SW480 control (mesenchymal; M-Ex) or SW480 ZKD (epithelial; E-Ex) exosomes were used to condition MRC5 fibroblasts for five days. MiR-200 levels on day 3 (d3) and day 5 (d5) are shown, relative to M-Ex treated fibroblasts at day 3, which were assigned the value "1". Representative of two separate experiments, each with three technical replicates. (**B**) The effect of M-Ex and E-Ex conditioning on Zeb1, fibronectin and α-SMA, in the absence (-) and presence (+) of TGF-β. β-actin was used as an equal loading control. Representative of two separate experiments.

3.3.8 Confirming the effects of miR-200 and Zeb1 on myofibroblast transdifferentiation

To confirm the effects of miR-200 and Zeb1 on myofibroblast transdifferentiation, MRC5 fibroblasts were transfected with miR-200 mimics or ZEB1 siRNA (day 0), switched to low serum conditions (day 2), stimulated with TGF-β (day 3) and collected 48 h later (day 5). Transfection efficiency of miR-200 mimics was confirmed by RT-qPCR, where the relative level of miR-200b was increased >3000-fold by its mimic compared to scrambled sequence control, and miR-200c, 82-fold by its mimic (**Figure 3-36**A). Of note, the miR-200b mimic increased detectable miR-200c by 46-fold, and the miR-200c mimic increased detectable miR-200b by 7.9-fold, suggesting a degree of non-specificity in the assays.

As predicted, miR-200b and -200c reduced baseline Zeb1 expression in fibroblasts, and decreased its induction upon TGF-β stimulation (**Figure 3-36**B). This was associated with a reduction in baseline α-SMA and fibronectin expression, but strikingly, the induction of α-SMA and fibronectin upon TGF-β stimulation was markedly reduced.

Transfection efficiency of ZEB1 siRNA was confirmed by >50% reduction of protein level by western blotting (**Figure 3-36**C). Knock down of Zeb1 markedly reduced baseline and TGF-β-induced α-SMA and fibronectin expression (**Figure 3-36**C), mirroring the effects of miR-200 mimics.

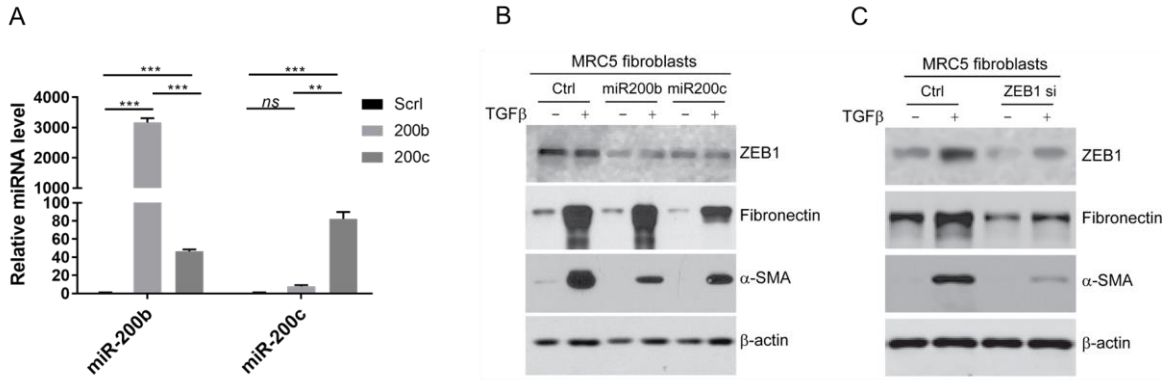

Figure 3-36. MiR-200/ Zeb1 axis determines myofibroblast transdifferentiation. (**A**) Transfection efficiency of miR-200 mimics in MRC5 fibroblasts. MiRNA levels are shown relative to scrl, which was assigned the value "1". Scrl - scrambled sequence control; 200b - miR-200b mimic; 200c - miR-200c mimic. Representative of two separate experiments, each with three technical replicates. (**B**) Zeb1, fibronectin and α-SMA expression in control (ctrl), miR-200b-and miR-200c-transfected MRC5 fibroblasts, in the absence (-) and presence (+) of TGF-β. (**C**) Zeb1, fibronectin and α-SMA expression in control (ctrl) and ZEB1 siRNA-transfected MRC5 fibroblasts, in the absence (-) and presence (+) of TGF-β. β-actin was used as an equal loading control. Representative of two separate experiments.

3.3.9 CRC EMT status determines fibroblast phenotype *in vivo*

SW480 control (mesenchymal) or ZKD (epithelial) cells were co-injected with MRC5-PKH fibroblasts subcutaneously into nude mice. Tumours were excised after 14 days, disaggregated into single cells and flow-sorted according to PKH-positivity. In mesenchymal tumours, 59.7% of viable single cells were classed as PKH-positive, and 13.3% as PKH-negative. In epthelial tumours, these proportions were 58.6% and 12.7%, respectively. The flow-sorting strategy and gate statistcis are shown in **Supplementary Figure 2**.

Haematoxylin and eosin (H&E) staining shows clear histological differences between mesenchymal and epithelial tumours (**Figure 3-37**). CRC cells are widely dispersed in mesenchymal tumours, whereas they form visible islands in epithelial tumours. This is consistent with differences in E-cadherin expression between SW480 control (E-cadherin-negative) and ZKD (E-cadherin-positive) cells. The demarcation between cancer and stromal compartments was

much clearer in ZKD tumours, whereas CRC cells and fibroblasts were interspersed in control tumours.

PKH-negative cells (CRC cells) from epithelial tumours were more abundant in miR-200a (39 fold; $p<0.001$), -200c (1.9 fold; $p<0.01$) and -141 (2.1 fold; $p<0.01$) but not significantly different in miR-200b or -429, compared to those from mesenchymal tumours (**Figure 3-38**A). Assuming that PKH-negative cells represent SW480 control cells (mesenchymal tumours) or SW480 ZKD cells (epithelial tumours), these relative miR-200 levels correspond with those seen *in vitro* (**Figure 3-31**C). PKH-positive cells (MRC5 fibroblasts) from epithelial tumours were more abundant in miR-200a (6.3 fold; $p<0.001$), -200b (33 fold; $p<0.01$), -200c (10 fold; $p<0.001$), -141 (8.0 fold; $p<0.001$) and -429 (>500 fold; $p<0.001$), compared to those from mesenchymal tumours (**Figure 3-38**B). Increases in miR-200 levels were associated with reciprocal decreases in α-SMA (*ACTA2*; 4.8 fold; $p<0.001$) and fibronectin (*FN1*; 2.2 fold; $p<0.001$) mRNA levels (**Figure 3-38**C). Immunohistochemical staining, to support these findings, showed characteristic nuclear Zeb1 in mesenchymal CRC cells (SW480 control) and absence of Zeb1 in epithelial CRC cells (SW480 ZKD; **Figure 3-39**A). Furthermore, stromal α-SMA staining was denser in mesenchymal compared to epithelial tumours (**Figure 3-39**B). Overall, these date demonstrate that EMT status of CRC cells determines fibroblast phenotype *in vivo*. More specifically, epithelial CRC cells are able to confer increased miR-200 on fibroblasts, reducing α-SMA and FN levels. In comparison, mesenchymal CRC cells do not increase fibroblast miR-200, allowing unrepressed myofibroblast transdifferentiation.

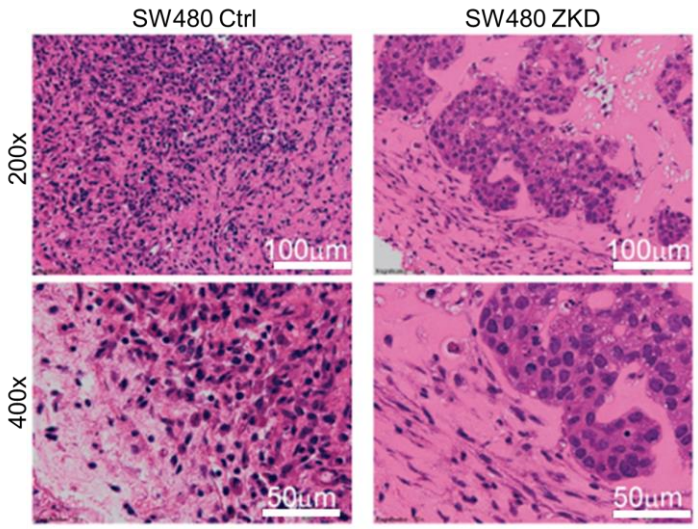

Figure 3-37. Histology of mesenchymal and epithelial tumours. H&E-stained sections of tumour xenografts established with mesenchymal (SW480 ctrl), or, epithelial (SW480 ZKD) CRC cells, with MRC5 fibroblasts. Epithelial (SW480 ZKD) CRC cells form organised tumour islands (surrounded by stromal fibroblasts), whereas mesenchymal (SW480 control) CRC cells were characteristically

disorganised. 200x and 400x denote total magnification obtained with 20x and 40x objective, respectively. Each image is representative of six tissue sections (three from each tumour xenograft).

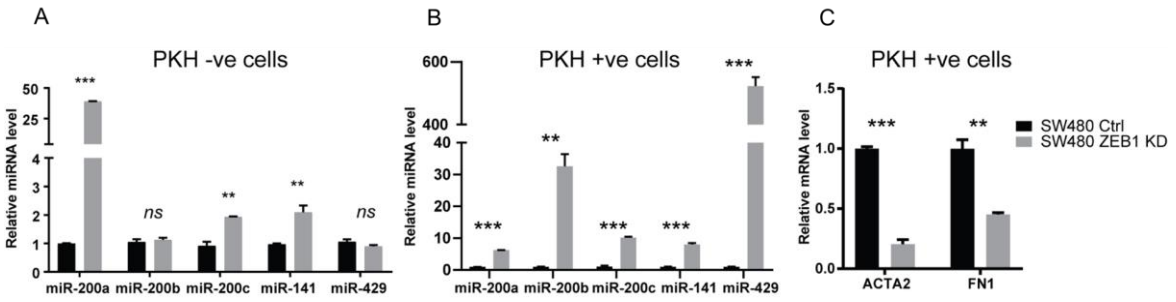

Figure 3-38. RNA profiles of CRC cells and fibroblasts from tumour xenografts. (**A**) MiR-200 levels in PKH-negative cells (CRC cells) extracted from SW480 control and ZKD tumours, relative to PKH-negative cells from SW480 control tumours, which were assigned the value "1". (**B**) MiR-200 levels in PKH-positive cells (MRC5 fibroblasts) extracted from SW480 control and ZKD tumours, relative to PKH-positive cells from SW480 control tumours, which were assigned the value "1". (**C**) *ACTA2* and *FN1* mRNA levels in PKH-positive cells extracted from SW480 control and ZKD tumours, relative to PKH-positive cells from SW480 control tumours, which were assigned the value "1". Values represent a single sample (pooled together from four tumour xenografts), with three technical replicates.

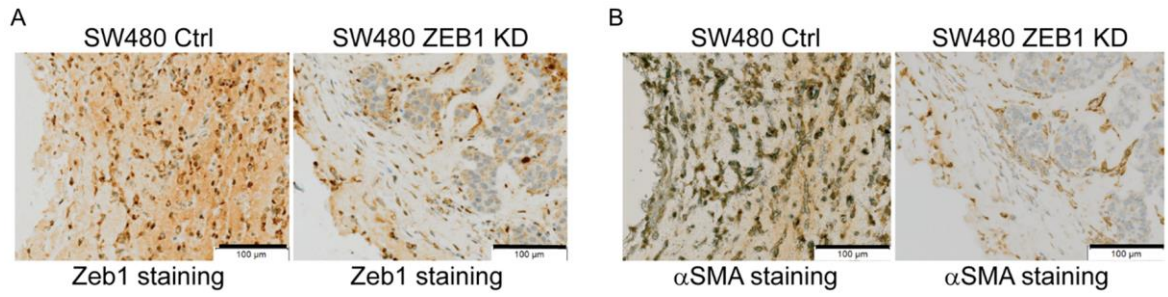

Figure 3-39. **Immunohistochemical staining of mesenchymal and epithelial tumours.** (**A**) Zeb1 staining of SW480 ctrl and ZKD tumour xenografts (20x objective). (**B**) α-SMA staining of SW480 ctrl and ZKD tumour xenografts (20x objective). Scale bars represent 100 µm. Each image is representative of six tissue sections (three from each tumour xenograft).

3.3.10 TGF-β production by SW480 control and SW480 ZKD cells

Having observed differences in myofibroblast transdifferentiation in epithelial and mesenchymal tumour xenografts, we wanted to ensure that these differences were not due to inherent differences in TGF-β production by SW480 control and ZKD cells. To test this, we used MLEC cells stably transfected with truncated PAI-1 promoter fused to firefly luciferase. Initially, MLEC cells

were incubated with different concentrations of TGF-β (0, 0.25, 0.5, 1 and 2 ng/ml) to produce a dose-response curve (**Figure 3-40**A). MLEC cells were then incubated with conditioned medium from SW480 control or SW480 ZKD cells. Although conditioned medium from both cell lines increased luciferase activity compared to untreated control (2.3 fold; $p<0.01$ and 2.6 fold; $p<0.001$, respectively) there was no difference between cell lines ($p=0.34$). This shows that SW480 control and SW480 ZKD produce similar quantities of TGF-β (**Figure 3-40**B).

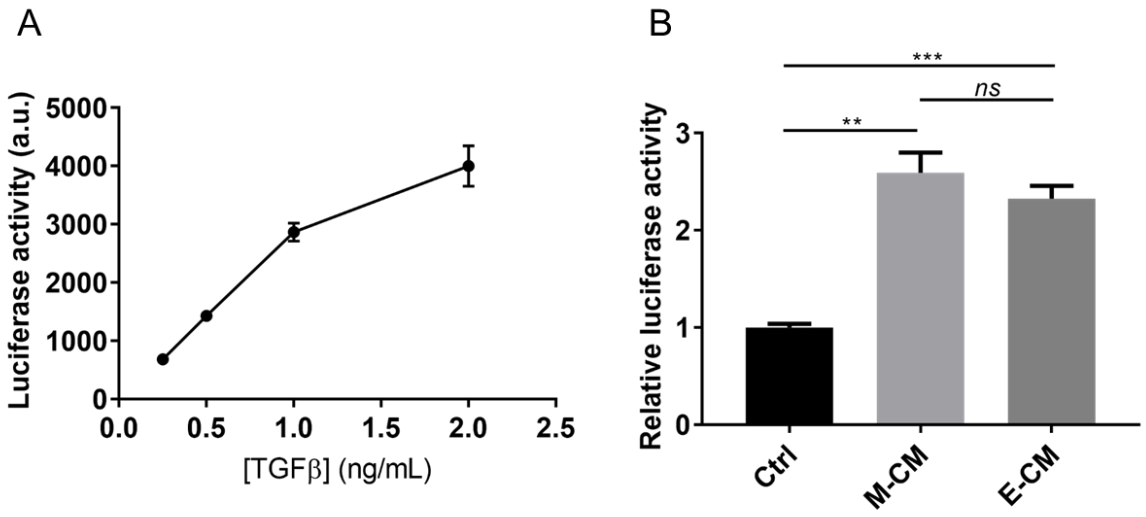

Figure 3-40. TGF-β production by SW480 control and ZKD cells. (**A**) Dose response curve for luciferase activity of MLEC cells treated with TGF-β. Luciferase activity normalised by total cellular protein concentration. Arbitrary units. (**B**) Luciferase activity of MLEC cells conditioned with medium from SW480 control cells (mesenchymal; M-CM), or, SW480 ZKD cells (epithelial; E-CM). Representative of two separate experiments, each with three technical replicates.

3.3.11 Discussion

In this section, CRC cells were classified according to EMT status, and exosomes were isolated from epithelial and mesenchymal cells. Epithelial but not mesenchymal exosomes attenuated ERK activity in fibroblasts, causing G1 arrest and reducing proliferation. This finding was validated by epithelial and mesenchymal exosomes from isogenic SW480 ZKD and SW480 control cells. To identify the exosome cargo which was responsible for differing effects of epithelial and mesenchymal exosomes, CRC exosomes were profiled for miRNAs. Epithelial exosomes were more abundant in miR-200 than mesenchymal exosomes. MiR-200 was shown to target the 3'UTR of *ZEB1* in fibroblasts. Conditioning of fibroblasts with epithelial exosomes increased miR-200 and reduced Zeb1, compared to mesenchymal exosomes. Importantly, this was associated with a reduction in TGF-β-induced myofibroblast transdifferentiation. To confirm that miR-200 and Zeb1 were responsible for the observed effects, miR-200 mimics or *ZEB1* siRNA were transfected into

fibroblasts. In both conditions, myofibroblast transdifferentiation was reduced. *In vivo*, epithelial and mesenchymal CRC xenografts were generated, containing labelled fibroblasts. Fibroblasts from epithelial xenografts expressed more miR-200 and less *ACTA2*/ *FN1*, than those from mesenchymal tumours. These data provide an explanation for the spatial distribution of myofibroblasts within tumours. We propose that epithelial CRC cells (predominantly in the core of a tumour), deliver miR-200 to fibroblasts in exosomes, reducing fibroblast Zeb1, and therefore decreasing their sensitivity to TGF-β, such that myofibroblastic transdifferentiation is reduced. Conversely, mesenchymal CRC cells (invasive front), convey to neighbouring fibroblasts, exosomes which are deplete in miR-200. Zeb1 level in these fibroblasts is maintained, allowing unrestricted myofibroblast transdifferentiation in the presence of TGF-β. This may explain why myofibroblastic CAFs accumulate at the invasive front of solid tumours. More generally, this may explain why metastatic tumours contain more myofibroblastic CAFs than non-metastatic tumours.

Chapter 4 Discussion

4.1 Overview

Although exosomes were first described over 30 years ago, it was Lotvall's group who reinvigorated research into this field, with the finding that exosomes convey functional cargo, which can alter the phenotype of recipient cells [46, 298]. In terms of their contents, exosomes have been shown to contain a greater proportion of small RNAs than parental cells, suggesting that miRNAs (and other small RNA species), may be selectively packaged into exosomes [334]. This is particularly important because miRNAs are known to be master regulators of the genome [286, 287]. Bearing this in mind, we were interested in identifying the role of exosomes in miRNA trafficking between cancer and stromal compartments of the TME. Identifying such signals is critically important in understanding the biological relationship between cancer and stroma. From a clinical perspective, it provides an opportunity to identify disease biomarkers and targets for therapeutic manipulation.

The work presented here focuses on the bidirectional flow of exomiRs between cancer and stromal compartments in CRC. Using patient-derived fibroblasts, we identified a panel of stromal miRNAs which were more abundant in CAF exosomes than NOF exosomes (**Figure 3-19**). Of these, miR-21 was relatively more abundant in exosomes than parental cells, suggesting that it is selectively loaded into CAF exosomes (**Figure 3-22**). Conditioning of CRC cells with fibroblast exosomes increased cellular miR-21 levels, suggesting that fibroblasts can transmit miR-21 to CRC cells via exosomes (**Figure 3-7**). Tumour xenografts established with miR-21-overexpressing fibroblasts and CRC cells led to eight times more liver metastases than those established with control fibroblasts and CRC cells, confirming the functional relevance of stromal miR-21 in CRC (**Figure 3-23**).

In parallel, we identified how cancer cell-derived exosomes regulate the phenotype of stromal fibroblasts. In particular, we showed that epithelial CRC cells produce exosomes rich in miR-200, which can be transferred to fibroblasts, repressing fibroblast *ZEB1*, and rendering them less sensitive to TGF-β-driven myofibroblast transdifferentiation. On the other hand, mesenchymal (metastatic) CRC cells produce exosomes with little miR-200, allowing fibroblasts to maintain Zeb1 levels, and readily transdifferentiate in the presence of TGF-β (**Figure 3-31**, **Figure 3-35**). This was confirmed *in vivo* by generating metastatic and non-metastatic CRC xenografts, and showing that metastatic tumours contained a greater proportion of myofibroblastic CAFs than non-metastatic tumours (**Figure 3-38**). This is especially important because it provides a mechanism for the histological association between metastatic cancer cells and activated CAFs.

Our work shows that there is a bidirectional flow of regulatory exomiRs between cancer and stromal cells in the TME. We have identified miR-21 as a stromal-derived signal which is conveyed to CRC cells, and miR-200 as a CRC cell signal which is conveyed to fibroblasts. These miRNAs have been reported to have multiple targets, across several tissue types. For example, miR-21 regulates IL-12 expression in allergic airway inflammation [540]. There are several reasons why miRNAs may have different functions in different tissues. Firstly, the abundance of miRNA targets varies between tissue types. Secondly, the presence of other miRNA species in a tissue can cooperate with or antagonise the actions of a particular miRNA [541]. Thirdly, competitive endogenous RNAs (miRNA sponges) may exist in different concentrations in different tissues [542]. Finally, the 3'UTR length of a given mRNA can be altered in different tissues, affecting the ability of a miRNA to repress its translation [543]. It is likely that multiple miRNAs, such as miR-21 and miR-200, are transferred between cancer and stromal compartments at the same time, with the sum total of these communications resulting in tumour progression or regression. However, the ability to dissect out single exomiRs, provides the opportunity to study their individual effects, assess their potential as biomarkers, and develop strategies to augment or antagonise their effects with novel therapeutics.

With regard to exosome-mediated therapy, Kalluri's group has shown that allogenic exosomes can be used to deliver *KRAS*-targeting siRNA to pancreatic cancer patients [544]. Exosomes are reported to be better than liposomal delivery systems, as they are less prone to accumulate in the liver, and less likely to be phagocytosed in the circulation [320]. Our data suggest that an exosome-delivered miR-21 antagonist or a miR-200 agonist, may be beneficial in CRC. However, delivering a tumour-specific siRNA (directed against mutant $KRAS^{G12D}$ for example), is quite different to delivering a miRNA agonist or antagonist. It is preferable for miRNA therapy to be targeted to the tissue or cell in question, because miRNAs have pleiotropic actions across a wide range of tissues. In this regard, it is possible that exosomes could be engineered to target particular cells, using a ligand-receptor or antigen-antibody approach. An alternative might be to generate exosomes with integrin patterns that promote homing to a particular tissue [283]. In this manner, exosomes could be utilised to improve delivery and reduce unintended effects of miRNA-based therapies.

4.2 CRC stromal exomiR panel

The identification of a stromal exomiR panel in CRC has important implications for biomarker development. Firstly, miRNA expression profiles effectively classify cancer into subtypes, and miRNAs have long been proposed as suitable diagnostic and prognostic biomarkers in various cancers [545]. Furthermore, existing biomarkers for CRC, such as CEA, are known to be poorly

sensitive, particularly in the diagnostic setting [546]. Secondly, the stroma is a key determinant of cancer development and progression [501, 502]. Our group and others, have demonstrated the value of stromal miRNAs as prognostic markers in CRC [427, 547]. In addition, the stromal compartment of a tumour is genetically more stable than the cancer compartment [34]. Therefore, there should be less variability in stromal miRNA profiles compared to cancer cell or whole tumour profiles, increasing reproducibility across patients. Lastly, exosome encapsulated miRNAs have proven to be representative of the tumour, protected from degradation, and disseminated in the circulation, which improves their utility as circulating biomarkers and liquid biopsy material [278, 295, 359, 548, 549].

The panel of stromal exomiRs proposed here (miR-329, -181a, -199b, -382, -215 and -21), consists of miRNAs which have all been implicated in human cancer biology. MiR-329 was initially highlighted as a tumor suppressive miRNA in glioblastoma [550, 551]. Xiao and co-coworkers first showed that miR-329 negatively regulates the oncogenic transcription factor E2F1, thereby reducing cyclin D1 levels, and attenuating cell proliferation [551]. Tissue analysis of human glioblastoma patients showed that higher miR-329/323 resulted in greater time to disease progression, corroborating the *in vitro* findings [550]. More recent studies have also highlighted tumor suppressive effects of miR-329, but in other cancer types, including gastric [552] and NSCLC, where it was shown to target the proto-oncogene *MET* [553].

MiR-181 more clearly exhibits a dual oncogenic and tumor suppressive function. Very early on, this miRNA was shown to influence differentiation of haematopoeitic cells towards the B cell lineage [554]. In B cell chronic lymphocytic leukaemia, Croce's group showed by co-transfection, that miR-181b downregulates the *TCL1* oncogene, which has a causal effect in aggressive disease [555]. However, miR-181a, the closely related sequence found in this study, has been shown to have oncogenic effects [556-558]. Furthermore, in oral squamous cell carcinoma, ectopic miR-181a/b expression resulted in greater cell migration, which may explain the higher intratumoral and plasma miR-181a/b levels seen in patients with metastasis [556]. In breast cancer, TGFβ-dependent miR-181a/b was shown to inhibit ataxia telangiectasia mutatated (ATM), increasing stem cell properties such as mammosphere formation [557]. Similarly, Ji et al. showed that all miR-181 family members (a-d) enrich the population of EpCAM+ stem/ progenitor cells in hepatocellular carcinoma (HCC) [558].

MiR-199 has clearly proved to be an important tumor suppressor in HCC [559-561]. In a study of more than 500 tissue specimens, categorized into normal liver, hepatitis B and HCC, nine miRNAs were shown to make up nearly 90% of the liver "miRNome", of which miR-199 was reduced in HCC [561]. This, and other studies, demonstrated a role for miR-199 in negatively regulating

pathways which converge on ERK, via Ras-dependent kinases [561], MET [559, 560] and mTOR [560]. Of significance to this current project, Kim et al showed that miR-199 expression is restricted to fibroblasts [559], giving credence to its place in a stromal panel. MiR-199 levels were also found to be reduced in several other cancer types, including breast cancer, CRC and NSCLC [562]. In NSCLC and osteosarcoma, miR-199 was shown to repress Axl, a key pro-survival and pro-migratory protein [562, 563].

MiR-382 has been shown to regulate the cancer hallmarks of angiogenesis and epithelial-EMT in solid tumors [564-566]. Seok and colleagues showed that in hypoxic conditions, HIF1α-induced miR-382 targets PTEN, unleashing Akt activity, and acting as an angiogenic switch [564]. With regard to EMT, there is contrasting evidence, with Kriegel and co-workers showing that TGF-β-induced miR-382 promotes loss of E-cadherin in renal epithelial cells [565], and Xu et al. showing attenuation of EMT, stemness and invasive properties in osteosarcoma [567].

There have been some important studies linking miR-215 with chemotherapy resistance in CRC [568, 569]. The anti-metabolite 5FU, a first line agent in the adjuvant/ neoadjuvant setting, and the most widely used chemotherapeutic in CRC, acts by inhibiting thymidylate synthase (TS). The miR-192/215 homologue was shown to repress TS, but unexpectedly, this did not increase sensitivity to 5FU. Mechanistic dissection revealed a double-edged sword, in that, coupled to loss of TS activity, miR-192/215 also slows cell cycle, reducing the proportion of cells in S phase, thereby reducing sensitivity to anti-metabolites [569]. Others have shown that in this context, miR-192/215 targets denticless protein homolog (DTL), a G2/M regulatory protein. Repression of DTL by miR-192/215 stabilizes P53 and leads to G2 arrest [568, 570]. This may explain our *in vitro* findings, where conditioning with fibroblast exosomes (albeit non-tumour-derived fibroblast exosomes) led to a reduction in CRC cell proliferation, and yet, greater chemoresistance (**Figure 3-14**). Furthermore, if G2 arrest was induced by exosomes in this manner, it may help explain why cell proliferation decreased in the presence of increased ERK activity.

From the profiling data, we were particularly interested in identifying miRNAs of stromal origin with relevance in CRC. Considering that we were looking for miRNAs which could be transmitted to cancer cells from the stroma, we focussed on those with oncogenic functions [483]. Additionally, the selected miRNAs had to be abundantly expressed in CAF exosomes such that significant amounts could be delivered to CRC cells. MiR-21 met these criteria.

MiR-21 is widely accepted to have oncogenic effects across several tumour types [506, 514]. Its most well described interactions are with the tumour suppressors *PTEN* and *PDCD4* [506, 514, 571-575]. In the context of CRC, Asangani and colleagues demonstrated an inverse correlation between miR-21 and *PDCD4* in multiple CRC cell lines, with direct binding to its 3'UTR, leading to

increased invasive capability [506]. We and others, have previously demonstrated that miR-21 is a stromal signal in CRC, using techniques such as *in situ* hybridization and laser capture microdissection [427, 504, 576]. This seems to be a generalisable finding spanning different solid tumours [489, 577].

Interestingly, Yeung et al. recently demonstrated the role of stroma-derived miR-21 in promoting chemoresistance in ovarian cancer [577]. In this study, exosomes derived from miR-21-overexpressing MEFs (miR-21-MEFs) were transferred to ovarian cancer cells, showing that miR-21 is delivered by exosomes. Subcutaneous ovarian cancer xenografts were then established in mice by co-injection of cancer cells and miR-21-MEFs. Intratumoral taxol injection had significantly less effect on tumour burden in xenografts containing miR-21-MEFs compared to control. We took a similar approach in CRC but used orthotopic xenografts, which provide a more reproducible metastatic model of CRC [578, 579].

The stromal exomiRs identified here, play important roles in cancer biology, with multiple experimentally-validated targets having been identified. This was confirmed by KEGG pathway enrichment analysis, which highlighted "colorectal cancer" genes, such as BRAF, KRAS and MSH6, as significant targets. Furthermore, the stromal origin of miRNAs in the signature is reiterated by enrichment of target genes in "ECM-receptor interaction" and "proteoglycans in cancer" pathways (**Figure 3-21**). Interestingly, miRNAs in our signature are predicted to regulate the PI3K-Akt pathway, which is in keeping with our finding that fibroblast exosomes increase Akt phosphorylation in CRC cells. As miRNAs are negative regulators, we would attribute the exosome-mediated Akt phosphorylation to the inhibition of a phosphatase. Fitting with this, *PHLPP2* which encodes for a phosphatase acting specifically at serine 473 on AKT [580], is a common target of miR-329, -181 and -199. Increased Akt activation by this mechanism leads directly to Bad phosphorylation (**Figure 3-14**). Bad, known as Bcl-2 death promoter, binds with Bcl-2 in its dephosphorylayed form. Once phosphorylated by Akt, it forms a heterodimer, and frees up Bcl2 to inhibit the pro-apoptotic protein Bax. This may account for the increased resistance to chemotherapy-induced apoptosis demonstrated by CRC cells conditioned with fibroblast exosomes (**Figure 3-14**, **Figure 3-15**).

4.3 MiR-200/ Zeb1 signalling in fibroblasts

EMT TFs (Snail, Twist, Zeb1) were initially described as key regulators of embryogenesis and development [581]. Several studies have since highlighted their roles in stemness, invasion and metastasis of cancer cells [582, 583]. There is a large body of information regarding the roles of EMT TFs in epithelial cells, but comparatively, very little is known about their roles in fibroblasts.

Nonetheless, it is becoming more apparent that EMT TFs are associated with the CAF phenotype [584].

Franci and colleagues showed in cervical and colonic carcinomas, that Snail expression was limited to fibroblasts in close proximity to tumour cells, and that these tumour cells were also Snail positive [585]. Furthermore, Baulida's group showed that Snail expression by CAFs determined their ability to stiffen the ECM, through a Snail1/RhoA/α-SMA axis, and that loss of Snail, reduced the ability of TGF-β to activate this pathway [586]. In parallel with this, depletion of Snail1 in CAFs, produced less invasive tumour xenografts than control cells, when co-injected with breast cancer cells [587].

Sung et al. investigated Twist expression in gastric cancer stroma using an immunohistochemical approach [588]. Twist1-positive fibroblasts also stained positive for myofibroblastic markers such as FSP-1, suggesting an association between Twist and CAF activation. Moreover, stromal Twist1 positivity was associated with increased tumour invasion and metastasis. In a follow up study, the mechanism of CAF activation was shown to be through IL-6/ STAT3 [589].

The importance of Zeb1 was highlighted by Bronsert and colleagues, who showed that stromal Zeb1 was the only independent marker of prognosis in patients who has undergone resection for pancreatic ductal adenocarcinoma [590]. However, this study made no mechanistic association between Zeb1 and CAF phenotype. In the same year, Chang et al. showed that Zeb1 binds the α-SMA promoter, increasing its expression [591].

The most well-known target of miR-200 is the Zeb family of transcription factors (Zeb 1/ 2), a relationship first described by Gregory et al. [458]. However, when showing this relationship, the majority of studies have focussed on cells of epithelial origin, including carcinoma cells [458, 592, 593]. In this project, the miR-200/ Zeb1 axis was elucidated in fibroblasts. Here, miR-200b/c were shown to target the 3'UTR of *ZEB1* in MRC5 fibroblasts (**Figure 3-32**). Upregulation of miR-200b/c in fibroblasts resulted in a decrease in resting Zeb1, and prevented induction of Zeb1, upon TGF-β stimulation (**Figure 3-36**B). The consequence of this was to prevent TGF-β-induced myofibroblastic transdifferentiation, as evidenced by the inability to upregulate α-SMA and fibronectin (**Figure 3-36**B).

Tang et al. showed the importance of miR-200 in breast cancer stroma [594]. In this study, primary NOFs and CAFs were derived from breast tumours, and profiled for miR-200. NOFs consistently expressed more miR-200a/b/c, -141 and -429, than CAFs. Overexpression of miR-200 family in CAFs, resulted in a decrease in α-SMA. Conversely, knock down of miR-200 in NOFs, resulted in increased α-SMA levels. MiR-200 was shown to target *FLI1* and *TCF12* (expressing ECM

remodelling proteins), which were relatively overexpressed in CAFs. Similarly, Yang and colleagues showed that miR-200 regulates activation of myofibroblasts in pulmonary fibrosis [491]. Using a bleomycin-induced mouse model of pulmonary fibrosis, they showed that fibrotic lungs expressed less miR-200a/b/c than controls, which was also true in patients with idiopathic pulmonary fibrosis. Furthermore, primary mouse fibroblasts from fibrotic lungs (activated), expressed more α-SMA and fibronectin than those from control lungs. Overexpression of miR-200b/c in activated fibroblasts, reduced α-SMA expression. Using MRC5 fibroblasts, it was shown that miR-200b/c overexpression reduced TGF-β-induced myofibroblast transdifferentiation, an experiment which has been reproduced here. Strikingly, the administration of miR-200c mimic with bleomycin, reduced the extent of collagen deposition in the lungs, suggesting that miR-200 can reduce fibrogenic capacity of pulmonary fibroblasts. These studies were critical in identifying the role of miR-200 in myofibroblast transdifferentiation, however, neither addressed the source of miR-200 in fibroblasts, or how miR-200 levels were altered.

In a recent study from our institution, paracrine signalling between alveolar type II epithelial cells (ATII) and lung fibroblasts, was shown to influence fibroblast phenotype [595]. Here, $ATII^{ER:KRASV12}$ cells were used as an inducible Ras-mediated EMT model. Induction with 4-hydroxytamoxifen, led to reduction in E-cadherin and upregulation of Zeb1. Conditioned media from induced ATII (mesenchymal) cells, allowed uninhibited TGF-β-mediated myofibroblast transdifferentiation (α-SMA upregulation) of MRC5 fibroblasts, but this was attenuated in the presence of conditioned media from uninduced (epithelial) ATII cells. In sections from fibrotic lungs, nuclear Zeb1 expression was identified in fibroblastic foci and adjacent alveolar epithelial cells, further suggesting that Zeb1 mediates the crosstalk between epithelial cells and fibroblasts in this disease. Furthermore, proteomic analysis of the conditioned media from epithelial and mesenchymal alvealoar cells, combined with chromatin immunoprecipitation assays, revealed that Zeb1 regulates the *PLAT* gene promoter in alveolar cells, increasing tissue plasminogen activator (tPA) expression in alveolar cells. tPA was shown to enhance TGF-β-mediated myofibroblast transdifferentiation.

There are several parallels between this study and the work presented in this thesis. In both cases, it was shown that the epithelial compartment can alter phenotype of the stromal compartment, through paracrine mechanisms, and that this is determined by EMT status of the epithelial cells. Furthermore, the importance of *ZEB1* in regulating fibroblast phenotype was highlighted in both cases. In this thesis, it was shown that Zeb1-low (epithelial) CRC cells, release exosomes which are rich in miR-200, and are able to increase miR-200 levels in fibroblasts, resulting in the repression of fibroblast *ZEB1*, and reduced sensitivity to TGF-β-mediated myofibroblast transdifferentiation. The converse was true for Zeb-1-high (mesenchymal) cells,

which allowed the maintenance of a myofibroblastic phenotype in surrounding fibroblasts. Yao et al. identified a soluble factor, tPA, as an important constituent of the secretome of mesenchymal but not epithelial alveolar cells, which increased responsiveness of surrounding fibroblasts to TGF-β [595]. Their study identified Zeb1-high fibroblasts adjacent to Zeb1-high alveolar cells in tissue sections of pulmonary fibrosis, similar to the relationship between Zeb1-high CRC cells and Zeb1-high myofibroblasts in tumour xenografts shown here (**Figure 3-39**). However, despite providing an in-depth analysis of the alveolar cell secretome, they failed to explain how Zeb1 is regulated in fibroblasts. We showed that CRC cell-derived exosomal miR-200 is critical in this process.

4.4 Technical considerations of exosome work

4.4.1 Exosome nomenclature

Throughout this project, the term “exosome” has been used to describe particular EVs, isolated and characterised by the techniques described here. In this context, “exosome” refers to EVs in the order of 100 nm, which are enriched for endosomal markers (Alix, TSG101), suggesting that they originate from endosomes.This distinguishes them from larger vesicles (microparticles, microvesicles, large oncosomes) and membrane-derived shedding vesicles. However, following extensive proteomic profiling of EV subpopulations, Thery’s group has suggested that bona fide exosomes are a subpopulation of small EVs which should be immune-precipitated using a combination of CD63, CD81 and CD9 antibody-conjugated beads [596]. To avoid misleading the reader, ISEV recommends use of the term “EV” for all preparations. However, this all-encompassing term may be too broad, describing exosomes, microparticles and oncosomes [306].

The field now tends to reserve the term “exosome” for preparations isolated by second generation methodologies, such as SEC, density gradient centrifugation and immunoaffinity capture [596-598]. However, these methods are not suitable for all experiments, as discussed below (section **4.4.2**). Clearly, use of differing nomenclature is a problem in the field. The important thing is to clearly describe the techniques used to isolate and characterise the EVs of interest, so that data can be reproduced by independent researchers. In this thesis, dUC has been used throughout for isolation, and extensive characterisation of preparations has been shown by multiple techniques (western blotting, TEM, NTA). Hence, readers should be in no doubt as to the definition of the term “exosome” used here.

4.4.2 Exosome isolation techniques

There are several methods for exosome isolation based on size (dUC, SEC), density (density gradient centrifugation) and surface markers (immunoaffinity binding) [299, 326, 599, 600]. The optimal method depends on the starting material (e.g. conditioned culture medium, plasma, urine), experimental question and resources available. Nonetheless, the principle is to produce a homogenous preparation of vesicles without protein contamination. In this project, dUC was used, producing homogenous and appropriately sized vesicles (40-120 nm), as shown by TEM and NTA (e.g. **Figure 3-1**). This methodology meets ISEV criteria for exosome isolation and was assigned an EV metric in the 99th percentile when submitted to the EV Track consortium [306, 330].

For dUC, the isolation of exosomes is a binary phenomenon: exosomes are pelleted and non-exosomal material remains in the supernatant. This is not the case for SEC and density gradient separation. In SEC, samples (typically plasma and urine) are passed through a column of porous sepharose CL-2B beads, with pore size of 75 nm. Larger vesicles exceed the size of the pores, and rapidly pass through the column, being collected in early fractions (1-8). Exosome-sized vesicles take a tortuous route through the pores and are collected in fractions 9-11. The passage of smaller material, such as proteins, is more extensively retarded by the beads, such that they are found in later fractions (>11) [325]. In density gradient centrifugation, concentrated vesicles are floated on a sucrose or Optiprep^{TM} (iodixanol) gradient, and ultracentrifuged for 16 h. Similar to SEC, this produces multiple fractions, each enriched for a characteristic population of particles, with exosomes most frequently found in fractions 6-7 [326, 600].

DUC is intrinsically limited in its ability to remove protein contaminants from the exosome preparation. Although the majority of cell-secreted proteins remain in the supernatant after dUC, the exosome pellet will have a significant amount of protein contamination. This is particularly important to consider in the study of exomiRs, because miRNAs are known to bind with certain chaperone proteins, such as Ago2, which can carry miRNAs independently of exosomes [601]. MiRNAs which were considered exomiRs, may actually have been Ago2-bound, and pulled down with protein aggregates. Bearing this in mind, it would have been useful to probe for Ago2 in exsomes and and equivalent volume of exosome-depleted medium, by western blotting, to check the extent of Ago2 contamination.

However, SEC and density gradient centrifugation, although improving purity of vesicle preparations, have their own constraints. SEC is costly due to the requirement for sepharose beads, which need replacing after each sample. Furthermore, the volume of starting material is typically 1-2 ml, which requires the sample to be highly concentrated. For this reason, SEC is more

suitable for isolation of exosomes from biological fluids rather than conditioned medium. Density gradient centrifugation takes much longer than dUC or SEC because of the overnight (16 h) centrifugation step, and when isolating exosomes from multiple samples, this is a limitation which needs to be considered. Duration is further increased by the need to concentrate large volumes of starting material (e.g. conditioned medium). Furthermore, sucrose is often used to generate a denisty gradient, creating a highly viscous and hyper-osmotic environment, which can alter water content of organelles [602]. Iodixanol is better in this regard due to its iso-osmolarity.

In terms of purity, one study has shown that immunoafinity capture of exosomes is better than SEC and density gradient centrifugation [599]. In this study, EpCAM-conjugated magnetic microbeads were used to capture exosomes from CRC cells, and compared with preparations from dUC and density gradient centrifugation, by proteomic profiling of exosomal markers. Despite the specificty of exosomal capture, the major disadvantage of the immunoaffinity technique is that exosomes require elution from the antibody before any downstream experiments can be done, which can impair their structure and function [603].

It was noticeable in this study, particularly for fibroblasts, that a large amount of starting material (cell culture medium) was required, to isolate enough exosomes for downstream analysis (**Table 3-1**). Fibroblasts were shown to produce in the order of 1000 exosomes per cell, equating to less than 100 µg exosome protein-equivalent from 10^8 cells. When considering the therapeutic applications of exosomes, a much more efficient culture system is needed. Watson et al. demonstrated the use of a hollow fibre bioreactor to grow cells on a large scale [604]. In this system, a cylindrical tank composed of hollow tubes, is seeded with cells. Cells attach to the surfaces of the internal tubes, and medium is pumped through the hollow cores. Gas and nutrient exchange occurs through 20 Kd pores on the surface of the tubes, and larger particles, such as vesicles, collect in the extracellular space. Exosomes can then be isolated from the extracellular medium by dUC. The Kalluri group has used a similar method to generate clinical grade exosomes from MSCs [544].

Several kit-based methods for exosome isolation exist, based on the principle of precipitation, where water-excluding polymers such as polyethylene glycol force exosomes out of solution [605]. Kits are being used more commonly, especially for clinical applications, where there are high numbers of samples [606]. In this respect, kits are advantageous because they require small input volumes of biological fluids, and can produce exosomes in a rapid and simple manner. However, despite kits being highly efficient, there are concerns about increased protein contamination, and alteration in resulting RNA profile [607-609]. Furthermore, the cost of such kits can be prohibitive.

Given that the exosome isolation protocol used in this project meets current guidelinesexo, and the requirement to produce relatively small quantities of exosomes on a regular basis, dUC was used throughout. Nonetheless, data shown here, could potentially be validated, using any of the other exosome isolation methods described.

4.4.3 Exosomal RNA

Differences in the composition of cellular and exosomal RNA suggest that typically used reference genes such as *U6*, *GAPDH* and *ACTB*, may not be appropriate for normalisation of exosomal RNA data. Certainly, at the protein level, β-actin does not seem as representative of total protein concentration in exosomes, as it does in cells. For example, the ratio of cellular to exosomal β-actin in MDA231 cells and CRC organoids is markedly different (**Figure 3-2**, **Figure 3-3**). Added to this, is the variability of exosomes derived from different tissues, which has led to certain reference genes being reported in a tissue-specific manner [610]. The small nuclear fragment U6 (snU6) is often used as a normaliser in miRNA studies [476, 504]. However, recent studies have suggested that it may not be suitable in all situations, particularly in samples from diseased tissues [611]. In this project, the Quantimir™ miRNA array that was used to profile exosomal miRNAs, recommends the use of snU6 to normalise CT values. However, snU6 CT values varied markedly between samples, despite them all being exosomes, derived from CRC cell lines. For this reason the global mean of all CT values was used to normalise each individual miRNA, as it is thought to give "better reduction of technical variation and more accurate appreciation of biological changes" [612]. However, this was not possible for RT-qPCR where a small number of miRNAs were being assayed at one time. The manufacturer recommends a number of endogenous controls, such as miR-423-5p, -26a-5p and -361-5p for Taqman Advanced miRNA assays. These were assessed for primary fibroblast exosomes in the NanoString dataset, and CRC exosomes in the Quantimir™ dataset. MiR-423-5p gave least variability between samples and was used as the reference gene of choice.

4.5 Limitations

4.5.1 Exosome quantification

The size of exosomes limits the techniques by which they can be quantified. For example, at up to 100 nm in size, they are too small to be detected, or counted, by light microscopy. Electron microscopy, including TEM, enables excellent visualisation of exosome size and morphology, but counting by this technique is time consuming and impractical. Flow cytometry offers the possibility of resolving subcellular structures, however, studies have commented on multiple

exosomes being simultaneously illuminated by the laser beam, resulting in “swarm” detection [613]. Additional technical problems include the wide size distribution and low refractive index [614].

One of the earliest, fastest and simplest methods to quantify exosomes, was to use protein concentration as a surrogate for exosome number [299, 615]. Typically, BCA or Bradford assay is used to determine protein concentration of lysed or unlysed exosomes, from which particle number is inferred. There are several drawbacks to this method, however. Firstly, the relationship between protein concentration and particle number is not the same for exosomes from different cell types. Secondly, as alluded to above, exosome preparations can be contaminated with protein aggregates, which will apportion a higher protein concentration to exosomes than is actually the case.

NTA has become the most popular exosome quantification technique in recent years. This light scattering technique is based on the correlation between particle size and rate of Brownian motion (Stokes-Einstein equation), but it also enables quantification using frame-by-frame analysis of exosome movements [616]. This technique is advantageous because it does not require any sample treatment prior to analysis, allows real-time tracking of exosomes, and is comparably fast compared to protein quantification. However, NTA requires several adjustments for optimisation of different samples (e.g. serial dilutions, syringe pump) [328].

More recently, a range of existing techniques have been applied to exosome quantification. Enzyme-linked immunosorbent assay (ELISA) can be used to detect tetraspanin markers such as CD63, enabling quantification of a specific subset of EVs [617]. Turnable resistive pulse sensing (TRPS) detects the passage of exosomes through a membrane, as momentary changes in current, the frequency of which indicate exosome concentration [618]. Another technique, surface plasmon resonance (SPR) detects exosome binding by detecting changes in the optical properties of the surface to which they bind [619]. ELISA is prohibitively time consuming for repeated quantification measurements, and plates are expensive if acquired commercially. TRPS and SPR both require access to specialised equipment. For these reasons, a combination of protein quantification and NTA were used in this project.

NTA was not available in our department, but samples were routinely sent to the DeWever lab (Ghent University) for quantification. With this information, the relationship between particle number and protein concentration was determined for exosomes from different cell types (**Table 3-1**). Generally, particle concentration correlated with protein concentration for tumour and stromal exosomes. Importantly, there was little difference in exosome production (particles/ cell)

between epithelial and mesenchymal CRC cells, which argues against the differential effect on fibroblast phenotype being due to exosome production.

4.5.2 Exosomal miRNA transfer

During the course of this project, it was shown for both stromal and CRC exosomes, that: (i) exosomes contain miRNA (**Figure 3-17**, **Figure 3-29**); (ii) exosomes can be taken up by recipient cells (**Figure 3-5**), and; (iii) miRNA levels increase in recipient cells upon exosome transfer (**Figure 3-7**). This suggests that exosomes deliver miRNAs of interest (miR-21, miR-200) to recipient cells. However, there is the possibility that recipient cells upregulate endogenous miRNA levels in response to exosomes. Although this in itself does not detract from the findings (exosomes still play a role in CRC progression regardless), it was important to investigate.

In order to address this, miR-200c knock out mouse ES cells were procured, and conditioned with human CRC exosomes. The aim was to show the presence of (human) miR-200c in the knock out cells. However, Taqman qPCR assay showed the control (untreated) ES cells to be abundant in miR-200c (**Figure 3-9**). This suggests that either the qPCR assay was non-specific (detecting other miR-200 family members), or, the cells were not genuinely deficient in miR-200c. One approach to answering this question, is to design primers for the miR-200c primary transcript (pri-mir). Pri-mir sequences are longer and more distinct between family members, compared to mature sequences. Absence of pri-mir will identify whether the *MIR200C* gene is actually knocked out in the ES cells.

Another approach that was attempted, was to use fluorescently labelled miR-200c. Here, miR-200c-FAM (miRCURY LNA miRNA mimic; cat no. YM00471150-ADB; Qiagen) was transfected into SW480 cells, with a plan to isolate exosomes, deliver them to fibroblasts, and detect FAM signal in the recipient cells. However, although miR-200c levels were significantly increased in the transfected cells, no fluorescent signal was detectable, suggesting that the label was not properly conjugated to the miRNA. The same result was obtained with two iterations of replacement constructs, provided by the supplier. Alternative fluorescent dyes include Cy3 and Cy5. However, a recent study suggests that labelled miRNAs non-specifically bind to cells, with the majority remaining attached to the cell membrane in some cases [620]. This will negatively skew the proportion of miRNAs in exosomes, compared to miRNAs in shedding vesicles, for example. For these reasons, this approach was abandoned.

An elegant method of detecting miRNA transfer in exosomes was recently shown by Probert et al. [470]. Nascent RNA was labelled with 5-ethynyl uridine (5EU), and exosomes from these cells delivered to recipient cells. 5EU-labelled RNA was affinity captured in the recipient cells, and

probed for miRNAs of interest. This approach definitively demonstrates whether miRNAs in the recipient cell have originated from exosomes. Time constraints prevented the application of this method here, but prior to publishing this work, a similar approach with CRC cells and fibroblasts could be employed.

4.5.3 Attributing *in vivo* effects to exosomes

In this project, stromal miR-21 was responsible for increased CRC metastasis *in vivo* (**Figure 3-23**). In terms of a mechanism, our group previously demonstrated that the secretome of miR-21-overexpressing fibroblasts directly increases proliferative and invasive capacity of CRC cells [504]. Evidence presented here suggests that one component of the secretome, exosomes, are abundant and enriched in miR-21. Furthermore, transfer of CAF exosomes results in increased miR-21 in recipient CRC cells (**Figure 3-7**B). Based on these observations, we propose that in the CRC microenvironment, CAFs deliver miR-21 to cancer cells in exosomes, promoting metastatic cancer progression. Of course, this is one mechanism of stromal-tumour crosstalk and others may exist in parallel, such as CAF-derived soluble factors (e.g. TGF-β, SDF-1) and juxtacrine signalling [59, 76, 86].

Similarly, mesenchymal CRC cells were shown to allow CAF activation *in vivo*, a process which was attenuated in epithelial tumours (**Figure 3-38**). *In vitro*, it was shown that CRC exosomes directly regulate TGF-β-mediated myofibroblast transdifferentiation, through changes in fibroblast miR-200/ Zeb1 signalling (**Figure 3-34**). Futhermore, CRC cells were shown to transmit exosomes to fibroblasts *in vivo* (**Figure 3-13**). Despite the inference, it was not proven definitively that *in vivo* effects on fibroblast phenotype were due to CRC exosomes. Again, soluble factors and contact signalling may play a part. However, the fact that SW480 control and ZKD cells (which formed the xenografts), produce similar amounts of TGF-β, goes against this theory (**Figure 3-40**).

To show that the observed effects in the two animal studies are exosome-dependent, is experimentally difficult. One option is to knock down Rab27 (Rab GTPase involved in exosome release) in cells of interest, such that they produce less exosomes [313]. In the first study, this would be the miR-21-overexpressing MRC5 fibroblast (co-injected with SW620 cells), and in the second study, this would be the SW480 ZKD cell (co-injected with MRC5 fibroblasts). In both cases, this would involve transducing an already-modified cell line, which may prove challenging (e.g. development of fibroblast senescence, requirement for multiple antibiotic selection genes). Another option is to dose animals with the nMase-2 inhibitor GW4869, which both reduces miRNA loading into exosomes and reduces exosome production [340]. However, systemic delivery

of this drug may result in significant non-specific effects on both fibroblasts and cancer cells [621, 622].

4.6 Conclusion

There exists a dynamic crosstalk between cancer and stroma, which facilitates progression of solid tumours, including CRC. As a means of cross communication between these compartments, exosomes are critical messengers in the TME. This thesis has examined the bidirectional transfer of exosomes from stroma to tumour and *vice versa*. Exosomal cargo has been interrogated, and exomiRs have been identified, which play key roles in CRC progression. Stromal miR-21, enriched in CAF exosomes, was shown to directly increase CRC metastasis. MiR-200, deliverable by CRC exosomes to fibroblasts, was shown to regulate myofibroblastic phenotype. A better understanding of the molecular mechanisms that underlie crosstalk between cancer and stroma, through studies such as these, provide incremental gains, in the quest to identify better markers of disease progression, and novel targets for drug discovery.

Appendix A TNM staging of colorectal cancer

The American Joint Committee on Cancer and the International Union for Cancer Control TNM cancer staging system (from 1st January 2010) [623].

T stage	Definition
Tx	Primary tumour cannot be assessed
T0	No evidence of primary tumour
T_{is}	Carcinoma in situ: intraepithelial or invasion of lamina propria
T1	Tumour invades submucosa
T2	Tumour invades muscularis propria
T3	Tumour invades through the muscularis propria into pericolorectal tissues
T4a	Tumour penetrates to the surface of the visceral peritoneum
T4b	Tumour directly invades or is adherent to other organs or structures

N stage	Definition
Nx	Regional lymph nodes cannot be assessed
N0	No regional lymph node metastasis
N1	Metastasis in 1–3 regional lymph nodes
N1a	Metastasis in one regional lymph node
N1b	Metastasis in 2–3 regional lymph nodes
N1c	Tumour deposit(s) in the subserosa, mesentery, or nonperitonealised pericolic or perirectal tissues without regional nodal metastasis
N2	Metastasis in 4 or more regional lymph nodes
N2a	Metastasis in 4–6 regional lymph nodes
N2b	Metastasis in 7 or more regional lymph nodes

M stage	Definition
M0	No distant metastasis
M1	Distant metastasis
M1a	Metastasis confined to one organ or site (for example, liver, lung, ovary, non-regional node)
M1b	Metastases in more than one organ/site or the peritoneum

Appendix B Supplementary Methods

B.1 Recipies for resolving SDS-PAGE gels used in western blotting

10 ml Resolving Gels

Constituent	8%	10%	12%	15%
dH_2O (ml)	4.6	4.0	3.3	2.3
30% acrylamide mix (ml)	2.7	3.3	4.0	5.0
1.5M Tris (pH 8.8) (ml)	2.5	2.5	2.5	2.6
10% SDS (w/v) (µl)	100	100	100	100
10% Ammonium persulphate (w/v) (µl)	100	100	100	100
TEMED (µl)	6	4	4	4

4 ml Stacking Gel

Constituent	
dH_2O (ml)	2.7
30% acrylamide mix (ml)	0.67
1.5M Tris (pH 8.8) (ml)	0.5
10% SDS (w/v) (µl)	40
10% Ammonium persulphate (w/v) (µl)	40
TEMED (µl)	4

B.2 Buffers used in western blotting

Buffer	Components
Laemmli Buffer (lysis)	4% SDS; 20% Glycerol; 0.125 mM Tris-HCl (pH 6.8) 10 ml of working solution (2X): 4 ml 10% SDS; 2 ml Glycerol; 1.2 ml 1M Tris-HCl (pH 6.8); 2.8 ml dH_2O
SDS loading buffer (5X)	10% SDS; 50% Glycerol; 0.25 mM Tris-HCl (pH 6.8); 0.25% Bromophenol blue; 10% β-mercaptoethanol 20 ml of working solution (5X): 2 g SDS; 10 ml Glycerol; 2.5 ml 2M Tris-HCl (pH 6.8); 50 µl Bromophenol blue; 200 µl β-mercaptoethanol; 7.25 ml dH_2O
Running Buffer	25 mM Tris, 190 mM Glycine, 0.1% SDS 5L of 10X stock: 150 g Tris Base; 720 g Glycine; 50 g SDS (in 5L dH_2O) 1L of working buffer: 100 ml 10X stock; 900 ml dH_2O
Transfer Buffer	25 mM Tris; 190 mM Glycine; 20% Methanol 5L of 10X stock: 150 g Tris Base; 720 g Glycine (in 5L dH_2O) 1L of working buffer: 100 ml 10X stock; 700 ml dH_2O; 200 ml Methanol
TBS-T	20 mM Tris, pH 7.5; 150 mM NaCl; 0.1% Tween 20 1L of 10X TBS stock: 61 g Tris; 88 g NaCl (in 1L dH_2O; pH adjusted to 7.5 with 1M HCl) 1L of working buffer: 100 ml 10X stock; 900 ml dH_2O; 1 ml Tween 20

B.3 Primary antibodies used in western blotting

Antibody	Clone/ Variant	Manufacturer	Polyclonal/Monoclonal	Host	Dilution
Alix	3A9	Abcam	Monoclonal	Mouse	1:500
TSG101	4A10	Abcam	Monoclonal	Mouse	1:500
CD63	Ts63	ThermoFisher	Monoclonal	Mouse	1:500
CD81	1.3.3.22	ThermoFisher	Monoclonal	Mouse	1:500
GM130	35/GM130	BD	Monoclonal	Mouse	1:500
Cytochrome C	N/A	CST	Polyclonal	Rabbit	1:1000
β-actin	C4	BD	Monoclonal	Mouse	1:5000
GFP	D5.1	CST	Monoclonal	Rabbit	1:1000
HSP90	68/Hsp90	BD	Monoclonal	Mouse	1:1000
p44/42 (ERK1/2)	137F5	CST	Monoclonal	Rabbit	1:2000
phospho-p44/42 MAPK (ERK1/2)	D13.14.4E	CST	Monoclonal	Rabbit	1:1000
Akt	C67E7	CST	Monoclonal	Rabbit	1:1000
phospho-AKT (Ser473)	D9E	CST	Monoclonal	Rabbit	1:500
Bad	11E3	CST	Monoclonal	Rabbit	1:1000
phospho-Bad (Ser136)	D25H8	CST	Monoclonal	Rabbit	1:500
α-SMA	1A4	Sigma	Monoclonal	Mouse	1:2000
Fibronectin	MAB1940	Merck Millipore	Monoclonal	Mouse	1:2000
Palladin	1E6	Novus	Monoclonal	Mouse	1:1000
Vimentin	3B4	Dako	Monoclonal	Mouse	1:1000
HSC-70	B-6	Santa Cruz	Monoclonal	Mouse	1:2000
Zeb1	N/A	Santa Cruz	Polyclonal	Rabbit	1:500
E-cadherin	36	BD	Monoclonal	Mouse	1:1000
Pan cytokeratin	C11	CST	Monoclonal	Mouse	1:10000

B.4 Secondary antibodies used in western blotting

Antibody	Clone/ Variant	Manufacturer	Polyclonal/Monoclonal	Host	Dilution
Mouse-HRP	N/A	Dako	Polyclonal	Goat	1:3000-1:4000
Rabbit-HRP	N/A	Dako	Polyclonal	Swine	1:3000-1:4000

B.5 Mature sequences of miRNAs detected using Taqman Advanced miRNA assays

MiRNA	Assay ID	Catalogue number	Mature sequence
miR-329-3p	478029_mir	A25576	AACACACCCAGCUAACCUUUUU
miR-181a-3p	479405_mir	A25576	ACCAUCGACCGUUGAUUGUACC
miR-199b-5p	478486_mir	A25576	CCCAGUGUUUAGACUAUCUGUUC
miR-382-5p	478078_mir	A25576	GAAGUUGUUCGUGGUGGAUUCG
miR-215-5p	478516_mir	A25576	AUGACCUAUGAAUUGACAGAC
miR-21-5p	477975_mir	A25576	UAGCUUAUCAGACUGAUGUUGA
miR-200a-3p	478490_mir	A25576	UAACACUGUCUGGUAACGAUGU
miR-200b-3p	477963_mir	A25576	UAAUACUGCCUGGUAAUGAUGA
miR-200c-3p	478351_mir	A25576	UAAUACUGCCGGGUAAUGAUGGA
miR-141-3p	478501_mir	A25576	UAACACUGUCUGGUAAAGAUGG
miR-429	477849_mir	A25576	UAAUACUGUCUGGUAAAACCGU
miR-423-5p	478090_mir	A25576	UGAGGGGCAGAGAGCGAGACUUU

B.6 Cell lines

Cell line	Species	Cell type	Morphology	Tissue	Growth type	Growth medium	Subculture routine
DLD1	Human	Adenocarcinoma	Epithelial	Colorectal	Monolayer	DMEM/ 10% FBS	1:6 – 1:9
HCT116	Human	Adenocarcinoma	Borderline	Colorectal	Monolayer	DMEM/ 10% FBS	1:6 – 1:9
SW620	Human	Adenocarcinoma	Borderline	Colorectal	Monolayer	DMEM/ 10% FBS	1:6 – 1:9
SW480	Human	Adenocarcinoma	Mesenchymal	Colorectal	Monolayer	DMEM/ 10% FBS	1:6 – 1:9
MRC5	Human	Fibroblast	Mesenchymal	Lung	Monolayer	DMEM/ 10% FBS	1:3 – 1:6
HFFF2	Human	Fibroblast	Mesenchymal	Foreskin	Monolayer	DMEM/ 10% FBS	1:3 – 1:6
IMR90	Human	Fibroblast	Mesenchymal	Lung	Monolayer	DMEM/ 10% FBS	1:3
PCF	Human	Fibroblast	Mesenchymal	Colon	Monolayer	DMEM/ 10% FBS	1:3 – 1:6
MEF	Mouse	Embryonic fibroblast	Mesenchymal	Embryo	Monolayer	DMEM/ 10% FBS	1:3 – 1:6
SCC7	Mouse	Squamous cell carcinoma	Epithelial	Head and neck	Monolayer	DMEM/ 10% FBS	1:6 – 1:9
Mirko_11A2	Mouse	Embryonic stem cell	Epithelial	Embryo	Monolayer	KO DMEM/ 15% FBS	1:3 – 1:6

B.7 Partial sequences of 3'UTR constructs used in luciferase reporter assays

pCI-neo-RL-ZEB1

Leading primer: > RenLuc3F 5'-GTACATCAAGAGCTTCGTGG-3'

AATCCGGGTGTGCCTGAACCTCAGACCTAGTAATTTTTCATGCAGTTTTCAAAGTTAGGAACAAGTTTGT
AACATGCAGCAGATTAGAAAACCTTAATGACTCAGAGAGCAACAATACAAGAGGTTAAAGGAAGCTGATT
AATTAGATATGCATCTGGCATTGTTTTATCTTATCAGTATTATCACTCTTATGTTGGTTTATTCTTAAGC
TGTACAATTGGGAGAAATTTTATAATTTTTTATTGGTAAACATATGCTAAATCCGCTTCAGTATTTTATT
ATGTTTTTTAAAATGTGAGAACTTCTGCACTACAAAATTCCCTTCACAGAGAAGTATAATGTAGTTCCAA
CCCGTGCTAACTACCTTTTATAAATTCAGTCTAGAAGGTAGTAATTTCTAATATTTAGATGTCTTAGTAG
AGCGTATTATCATTTAAAGTGTATTGTTAGCCTTAAGAAAGCAGCTGATAGAAGAACTGAAGTTTCTTAC
TCACGTGGTTTAAAATGGAGTTCAAAAGATTGCCATTGAGTTCTGATTGCAGGGACTAACAATGTTAATC
TGATAAGGACAGCAAAATCATCAGAATCAGTGTTTGTGATTGTGTTTGAATATGTGGTAACATATGAAGG
ATATGACATGAAGCTTTGTATCTCCTTTGGCCTTAAGCAAGACCTGTGTGCTGTAAGTGCCATTTCTCAG
TATTTTCAAGGCTCTAACCCGCCTTCATCCAATGTGTGGCCTACAATAACTAGCATTTGTTGATTTGTCT
CTTGTATCAAAATTCCCAAATAAAACTTAAAACCACTGACTCTGTCAGAGAAACTGAAACACTGGGACAT
TTCATCC

pCI-neo-RL-ZEB1 200bmutx5

Leading primer: > RenLuc3F 5'-GTACATCAAGAGCTTCGTGG-3'

TTCTAGTCAAAATAAATCCGGGTGTGCCTGAACCTCAGACCTAGTAATTTTTCATGCAGTTTTCAAAGTT
AGGAACAAGTTTGTAACATGCAGCAGATTAGAAAACCTTAATGACTCAGAGAGCAACAATACAAGAGGTT
AAAGGAAGCTGATTAATTAGATATGCATCTGGCATTGTTTTATCTTATCAGGACTATCACTCTTATGTTG
GTTTATTCTTAAGCTGTACAATTGGGAGAAATTTTATAATTTTTTATTGGTAAACATATGCTAAATCCGC
TTCAGGACTTTATTATGTTTTTTAAAATGTGAGAACTTCTGCACTACAAAATTCCCTTCACAGAGAAGTA
TAATGTAGTTCCAACCCGTGCTAACTACCTTTTATAAATTCAGTCTAGAAGGTAGTAATTTCTAATATTT
AGATGTCTTAGTAGAGCGTATTATCATTTAAAGTGTATTGTTAGCCTTAAGAAAGCAGCTGATAGAAGAA
CTGAAGTTTCTTACTCACGTGGTTTAAAATGGAGTTCAAAAGATTGCCATTGAGTTCTGATTGCAGGGAC
TAACAATGTTAATCTGATAAGGACAGCAAAATCATCAGAATCAGTGTTTGTGATTGTGTTTGAATATGTG
GTAACATATGAAGGATATGACATGAAGCTTTGTATCTCCTTTGGCCTTAAGCAAGACCTGTGTGCTGTAA
GTGCCATTTCTCAGGACTTTCAAGGCTCTAACCCGCCTTCATCCAATGTGTGGCCTACAATAACTAGCAT
TTGTTGATTTGTCTCTTGTATCAAA

pRLCon1-1746

Leading primer: > EBV-rev 5'-GTGGTTTGTCCAAACTCATC-3'

CNCNACNTACCCTCACTAaAGGGAAGCGGCCGCGAGAAAAGCTGTCAAGAGTCATGAATTCTCCTTAATA
TTTATCAGCAAACAGGATGCTCGACCCTAAGTGAATTTTAGTGCAGCCTCAGGCCAATCTTGGTCCTGGG

AGTGGGCAGGGTTCCCAGAAGAACGAGTCTGGTTTCTGAGGCTGTAGAAGGGAGCCGGAAGCCCCTCAC

TTGATCACGGTGAGAACACAGGGAGCCTTTGGAGAAGCTATTCAGCCACTGTAGTTAAGAGCTCCTGTTC

TGATCCAGGGAGACCTGGGTTCAAGTCCTGACTCAGCCACTTCCTAGTTGTGTGAGTTTCAGAAAAAAAA

TCACTTCACCTCTTAGAACGCAATTTCAGCTTCTGTAACAATCTCTAGGTTAGGAGGGAGTGGGGCGGGT

GAGGGCGGGGAGGGAGGAGGAGAATAAAAAACAAAAACAATCTCTAGGTTAATAGGGAGGAAGGGAGA

TTAAATGAGATGATGCATGTCAGATGCCTTAAGACAGTGCCTGGGAGTAAGGAAGAGCTTGAGACAGGCC

CTGGGAGCTTATTCCTCCTGGATGTCACTCTGATGTGAGGGTTTACCCATCTTGTCCTCTCCAGCCCCAAG

CCTCATTACTCTCACCCACATTATATCATCCACCCCACCTGACCTCCCAGCTTCCAGCCTCCCGTCCTCT

GCAGAACTGCTGTGTTCATTTTCTGGAAGCCCAGCTCCCTGCATACTCCTTGAAGCTGATCAGGACCTCA

GCCTGGTGTTCCAGACCCTATGCTCTCCAGCAGGCCCTCTCTCTCTTCATCATCCCTCTCcCACACcATT

CTTCCTCaATTCTTGCTAGATtCTtACTACCACTAGGCCTTGGCTCAGGCTGTTCtTTGGaATGTCcCAT

CTCACCTGCTCTACcAGCCAGAATTCTACCCTTCTC

Appendix C Supplementary Data

C.1 KEGG pathway and miRNA-small molecule network analyses

Supplementary Table 1. KEGG pathway analysis combining gene targets of miR-329-3p, miR-181a-3p, miR-199b-5p, miR-382-5p, miR-215-5p and miR-21-5p.

KEGG Pathway	*p*-value	Genes	MiRNAs
MicroRNAs in cancer	9.24E-30	54	4
ECM-receptor interaction	4.32E-21	19	4
Prion diseases	1.20E-16	7	2
Proteoglycans in cancer	2.58E-09	52	4
Glioma	4.67E-08	24	4
Colorectal cancer	3.86E-06	23	4
Hepatitis B	9.78E-06	39	4
Non-small cell lung cancer	1.91E-04	20	4
Pathways in cancer	1.91E-04	79	4
Bladder cancer	3.54E-04	18	4
Endometrial cancer	3.54E-04	19	4
Pancreatic cancer	4.51E-04	24	4
Lysine degradation	5.24E-04	14	2
FoxO signalling pathway	1.01E-03	38	4
Fatty acid elongation	1.04E-04	7	2
PI3K-Akt signalling pathway	1.22E-03	71	4
Focal adhesion	1.31E-03	52	4
Central carbon metabolism in cancer	1.39E-03	20	4
Chronic myeloid leukemia	1.50E-03	24	4
Melanoma	1.63E-03	22	4

KEGG Pathway	*p*-value	Genes	MiRNAs
Thyroid hormone signalling pathway	3.61E-03	29	4
ErbB signalling pathway	3.97E-03	23	4
Prostate cancer	4.21E-03	27	4
Small cell lung cancer	4.21E-03	25	4
Thyroid cancer	6.83E-03	10	4
HIF-1 signalling pathway	7.72E-03	29	3
Amoebiasis	1.23E-02	26	4
mTOR signalling pathway	1.65E-02	19	4
Renal cell carcinoma	1.95E-02	19	4
Hippo signalling pathway	3.11E-02	29	4
Prolactin signalling pathway	3.17E-02	18	4
Choline metabolism in cancer	4.39E-02	25	4
Adherens junction	4.46E-02	18	3
MAPK signalling pathway	4.46E-02	51	4
Cell cycle	4.90E-02	27	4

From *Bhome et al. (2017)* [481]

Supplementary Table 2. Network analytics for miRNA-small molecule interactions for miR-329-3p, miR-181a-3p, miR-199b-5p, miR-382-5p, miR-215-5p and miR-21-5p.

MiRNA	Molecule	Pubchem ID	Experiment	Pubmed ID
hsa-mir-21-5p	5-fluorouracil	3385	Microarray	21506117
hsa-mir-21-5p	5-aza-2'-deoxycytidine (5-Aza-CdR)	451668	Microarray	22076154
hsa-mir-21-5p	17beta-estradiol (E2)	5757	Microarray	22403704
hsa-mir-21-5p	5-fluorouracil	3385	qRT-PCR	17702597
hsa-mir-21-5p	17beta-estradiol (E2)	5757	Microarray	19528081
hsa-mir-21-5p	3,3'-diindolylmethane (BR-DIM)	3071	qRT-PCR	20724916
hsa-mir-21-5p	5-aza-2'-deoxycytidine (5-Aza-CdR)	451668	Microarray	22076154
hsa-mir-21-5p	17beta-estradiol (E2)	5757	qRT-PCR	22403704
hsa-mir-21-5p	CDF (analogues of curcumin) + gemcitabine	N/A	qRT-PCR	20388782
hsa-mir-21-5p	Cisplatin	84093	qRT-PCR	22475935
hsa-mir-21-5p	Curcumin	969516	Microarray	18347134
hsa-mir-21-5p	Curcumin	969516	qRT-PCR	22363450
hsa-mir-21-5p	Diazobenzene and its derivatives	N/A	Luciferase reporter assay	18712719
hsa-mir-21-5p	17beta-estradiol (E2)	5757	qRT-PCR	19264808
hsa-mir-21-5p	Curcumin	969516	qRT-PCR	20815812
hsa-mir-21-5p	Bisphenol A	6623	Microarray	20417706
hsa-mir-21-5p	Bisphenol A	6623	Microarray	20417706
hsa-mir-21-5p	Bisphenol A	6623	Microarray	22403704
hsa-mir-21-5p	Caudatin	21633059	qRT-PCR	23708208
hsa-mir-21-5p	CDF (analogues of curcumin)	N/A	qRT-PCR	20388782
hsa-mir-21-5p	Gemcitabine	60750	qRT-PCR	24460329
hsa-mir-21-5p	Gemcitabine	60750	qRT-PCR	21738581
hsa-mir-21-5p	Ginsenoside Rh2	119307	Microarray	21372826
hsa-mir-21-5p	Ginsenoside Rh2	119307	qRT-PCR	21372826

MiRNA	Molecule	Pubchem ID	Experiment	Pubmed ID
hsa-mir-21-5p	Ginsenoside Rh2	119307	Microarray	23152132
hsa-mir-21-5p	Glossy ganoderma spore oil	N/A	qRT-PCR	21842656
hsa-mir-21-5p	Dihydrotestosterone (DHT)	10635	Microarray	20945501
hsa-mir-21-5p	17beta-estradiol (E2)	5757	qRT-PCR	19528081
hsa-mir-21-5p	Hydroxamic acid HDACi LAQ824	N/A	Microarray	16452179
hsa-mir-21-5p	Hydroxychloroquine	3652	Microarray	24121037
hsa-mir-21-5p	Hydroxychloroquine	3652	qRT-PCR	24121037
hsa-mir-21-5p	Marine fungal metabolite 1386A	N/A	Microarray	22159329
hsa-mir-21-5p	Gemcitabine	60750	Northern blot	16762633
hsa-mir-21-5p	Microcystin-LR (MC-LR)	445434	qRT-PCR	22265967
hsa-mir-21-5p	Nicotine	89594	qRT-PCR	24756761
hsa-mir-21-5p	Nicotine	89594	qRT-PCR	21081469
hsa-mir-21-5p	N-methyl-N-nitro-N'-nitrosogua nidine (MNNG)	9576410	qRT-PCR	24821435
hsa-mir-21-5p	5-fluorouracil	3385	qRT-PCR	21506117
hsa-mir-21-5p	All-trans-retinoic acid (ATRA)	444795	Microarray	21131358
hsa-mir-21-5p	Glucocorticoid	N/A	qRT-PCR	22815788
hsa-mir-21-5p	Glucocorticoid	N/A	TaqMan low-density array	22815788
hsa-mir-21-5p	Arsenite	544	qRT-PCR	24004609
hsa-mir-21-5p	Sulindac sulfide	5352624	qRT-PCR	22286762
hsa-mir-21-5p	Sunitinib	5329102	qRT-PCR	25061297
hsa-mir-21-5p	Temozolomide	5394	qRT-PCR	22753745
hsa-mir-21-5p	Matrine	91466	qRT-PCR	22832383
hsa-mir-21-5p	Trastuzumab	N/A	qRT-PCR	22384020
hsa-mir-21-5p	Trastuzumab	N/A	Microarray	22384020
hsa-mir-21-5p	Trichostatin A (TSA)	444732	Microarray	19112422
hsa-mir-21-5p	Trichostatin A (TSA)	444732	Northern blot	19112422
hsa-mir-21-5p	Trimetazidine (TMZ)	21109	qRT-PCR	22842854

MiRNA	Molecule	Pubchem ID	Experiment	Pubmed ID
hsa-mir-21-5p	Triptolide	107985	qRT-PCR	22957792
hsa-mir-21-5p	Trypaflavine	N/A	qRT-PCR	20529860
hsa-mir-21-5p	Valproate	3121	qRT-PCR	20427269
hsa-mir-21-5p	Dihydrotestosterone (DHT)	10635	qRT-PCR	20945501
hsa-mir-21-5p	Doxorubicin	31703	Microarray	19237188
hsa-mir-21-5p	Enoxacin	3229	qRT-PCR	21368194
hsa-mir-21-5p	Etoposide	36462	Microarray	19633716
hsa-mir-21-5p	Trastuzumab	N/A	Microarray	22384020
hsa-mir-21-5p	Formaldehyde	712	Microarray	21147603
hsa-mir-21-5p	Progesterone	5994	Microarray	22543862
hsa-mir-21-5p	CDF (analogues of curcumin) + gemcitabine	N/A	qRT-PCR	21408027
hsa-mir-21-5p	All-trans-retinoic acid (ATRA)	444795	qRT-PCR	21131358
hsa-mir-21-5p	Arsenic trioxide	14888	qRT-PCR	22072212
hsa-mir-21-5p	O,p'-dichlorodiphenyltrichlo-roethane (DDT)	13089	Microarray	22403704
hsa-mir-21-5p	Prednisone	5865	qRT-PCR	24121037
hsa-mir-21-5p	Morphine	5288826	Microarray	20564181
hsa-mir-21-5p	CDF (analogues of curcumin)	N/A	qRT-PCR	21408027
hsa-mir-21-5p	Prednisone	5865	Microarray	24121037
hsa-mir-21-5p	Polylysine	162282	qRT-PCR	20529860
hsa-mir-199b-5p	Imatinib mesylate	123596	qRT-PCR	20460641
hsa-mir-199b-5p	Imatinib mesylate	123596	TaqMan low-density array	20460641
hsa-mir-199b-5p	Glucose	5793	qRT-PCR	24394957
hsa-mir-199b-5p	4-hydroxynonenal	5283344	Microarray	19022373
hsa-mir-199b-5p	Enoxacin	3229	qRT-PCR	18641635
hsa-mir-181a-3p	Gemcitabine	60750	Microarray	19237188
hsa-mir-181a-3p	Curcumin	969516	qRT-PCR	22510010

MiRNA	Molecule	Pubchem ID	Experiment	Pubmed ID
hsa-mir-181a-3p	Doxorubicin	31703	Microarray	19237188
hsa-mir-181a-3p	Gemcitabine	60750	Northern blot	16762633
hsa-mir-181a-3p	4-hydroxynonenal	5283344	Microarray	19022373
hsa-mir-181a-3p	Diethylstilbestrol	448537	Microarray	19549897
hsa-mir-215-5p	Trichostatin A (TSA)	444732	Microarray	21971930
hsa-mir-215-5p	Formaldehyde	712	Microarray	21147603
hsa-mir-215-5p	Arsenic trioxide	14888	qRT-PCR	22072212
hsa-mir-382-5p	Morphine	5288826	qRT-PCR	21224041
hsa-mir-382-5p	Vorinostat (SAHA)	5311	Microarray	19513533
hsa-mir-329-3p	Glucose	5793	Microarray	24394957
hsa-mir-329-3p	Gemcitabine	60750	Northern blot	16762633

From *Bhome et al. (2017)* [481].

C.2 Flow sorting of PKH-labelled fibroblasts

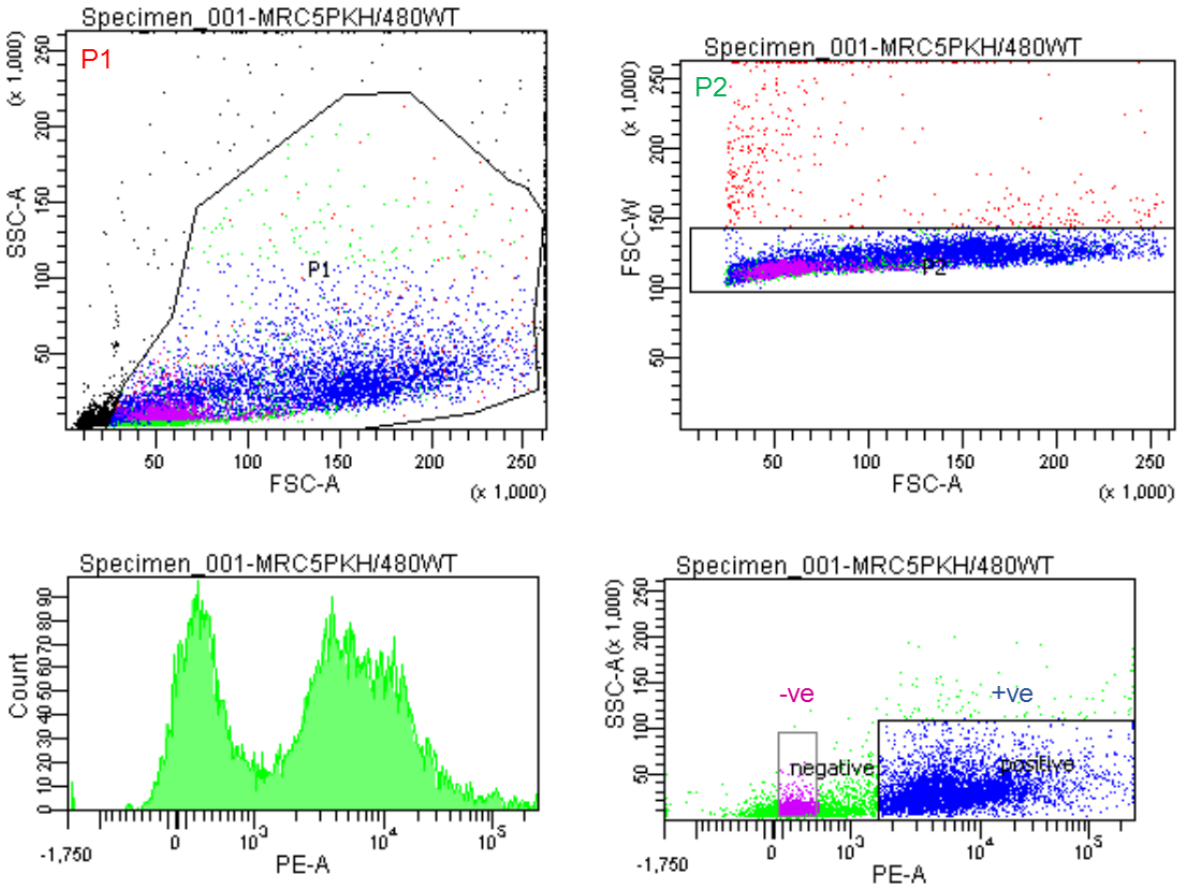

Tube: MRC5PKH/480WT

Population	#Events	%Parent	%Total
All Events	10,000	####	100.0
P1	8,131	81.3	81.3
P2	7,732	95.1	77.3
positive	4,617	59.7	46.2
negative	1,032	13.3	10.3

Supplementary Figure 1. Flow-sorting strategy for SW480 ctrl/ MR5-PKH (mesenchymal) tumour xenografts. P1 includes all viable cells. P2 includes viable single cells (duplet exclusion). Cells were resolved in the PE channel into PHK-positive and -negative. Gate statistics are shown for 10 000 events. “480WT” refers to SW480 ctrl.

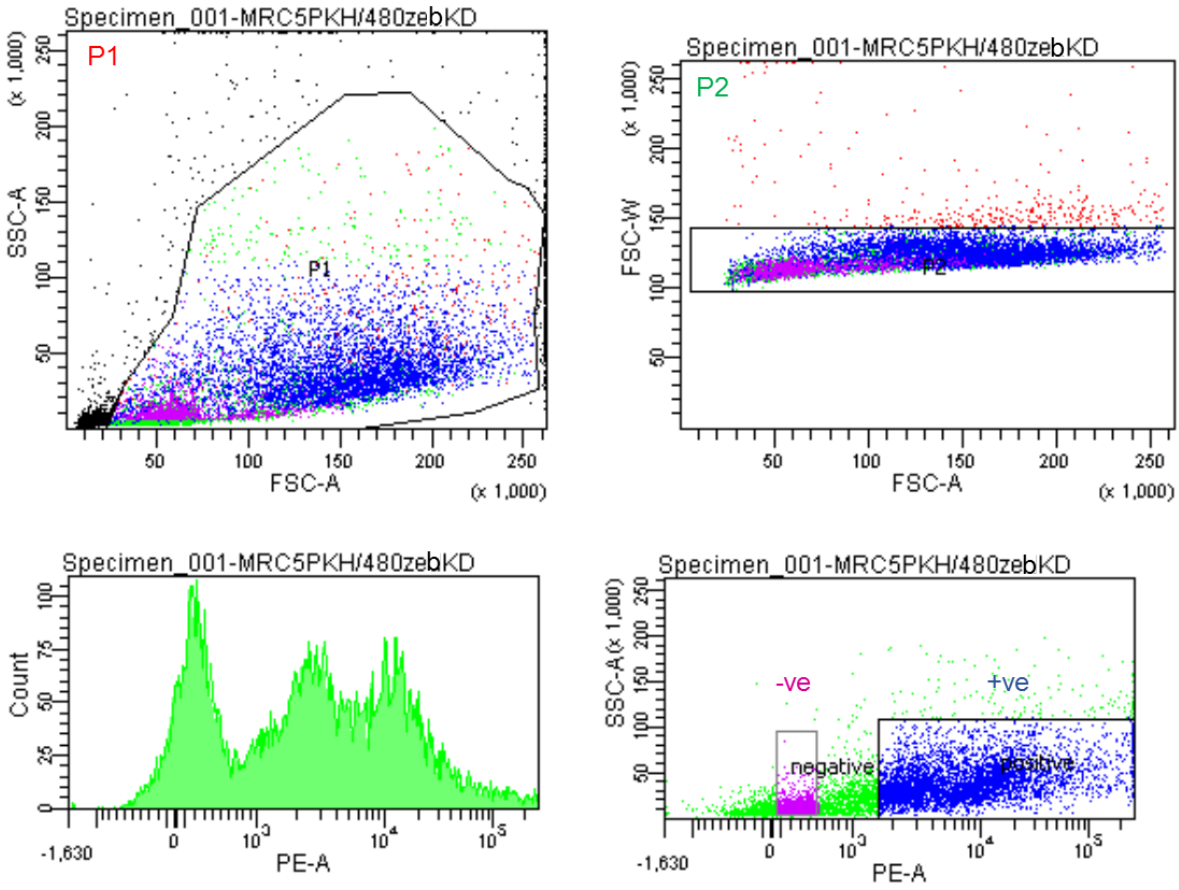

Tube: MRC5PKH/480zebKD

Population	#Events	%Parent	%Total
All Events	10,000	####	100.0
P1	8,860	88.6	88.6
P2	8,520	96.2	85.2
positive	4,995	58.6	50.0
negative	1,078	12.7	10.8

Supplementary Figure 2. Flow-sorting strategy for SW480 ZKD/ MRC5-PKH (epithelial) tumour xenografts. P1 includes all viable cells. P2 includes viable single cells (duplet exclusion). Cells were resolved in the PE channel into PKH-positive and -negative. Gate statistics are shown for 10 000 events.

List of References

1. Arnold, M., et al., *Global patterns and trends in colorectal cancer incidence and mortality.* Gut, 2017. **66**(4): p. 683-691.
2. Luengo-Fernandez, R., et al., *Economic burden of cancer across the European Union: a population-based cost analysis.* Lancet Oncol, 2013. **14**(12): p. 1165-74.
3. Simmonds, P.C., *Palliative chemotherapy for advanced colorectal cancer: systematic review and meta-analysis. Colorectal Cancer Collaborative Group.* BMJ, 2000. **321**(7260): p. 531-5.
4. Johnson, C.M., et al., *Meta-analyses of colorectal cancer risk factors.* Cancer Causes Control, 2013. **24**(6): p. 1207-22.
5. Wei, E.K., et al., *A Comprehensive Model of Colorectal Cancer by Risk Factor Status and Subsite Using Data From the Nurses' Health Study.* Am J Epidemiol, 2017. **185**(3): p. 224-237.
6. Fearon, E.R. and B. Vogelstein, *A genetic model for colorectal tumorigenesis.* Cell, 1990. **61**(5): p. 759-67.
7. Leslie, A., et al., *The colorectal adenoma-carcinoma sequence.* Br J Surg, 2002. **89**(7): p. 845-60.
8. Vasen, H.F., et al., *Guidelines for the clinical management of familial adenomatous polyposis (FAP).* Gut, 2008. **57**(5): p. 704-13.
9. Lynch, H.T., et al., *Attenuated familial adenomatous polyposis (AFAP). A phenotypically and genotypically distinctive variant of FAP.* Cancer, 1995. **76**(12): p. 2427-33.
10. Knudsen, A.L., M.L. Bisgaard, and S. Bulow, *Attenuated familial adenomatous polyposis (AFAP). A review of the literature.* Fam Cancer, 2003. **2**(1): p. 43-55.
11. Hampel, H., et al., *Cancer risk in hereditary nonpolyposis colorectal cancer syndrome: later age of onset.* Gastroenterology, 2005. **129**(2): p. 415-21.
12. Vasen, H.F., et al., *New clinical criteria for hereditary nonpolyposis colorectal cancer (HNPCC, Lynch syndrome) proposed by the International Collaborative group on HNPCC.* Gastroenterology, 1999. **116**(6): p. 1453-6.
13. Giardiello, F.M., et al., *Guidelines on genetic evaluation and management of Lynch syndrome: a consensus statement by the US Multi-society Task Force on colorectal cancer.* Am J Gastroenterol, 2014. **109**(8): p. 1159-79.
14. Sieber, O.M., et al., *Multiple colorectal adenomas, classic adenomatous polyposis, and germ-line mutations in MYH.* N Engl J Med, 2003. **348**(9): p. 791-9.
15. Sampson, J.R., et al., *Autosomal recessive colorectal adenomatous polyposis due to inherited mutations of MYH.* Lancet, 2003. **362**(9377): p. 39-41.
16. Jasperson, K.W., W.S. Samowitz, and R.W. Burt, *Constitutional mismatch repair-deficiency syndrome presenting as colonic adenomatous polyposis: clues from the skin.* Clin Genet, 2011. **80**(4): p. 394-7.
17. Brosens, L.A., et al., *Risk of colorectal cancer in juvenile polyposis.* Gut, 2007. **56**(7): p. 965-7.
18. Knudson, A.G., Jr., *Mutation and cancer: statistical study of retinoblastoma.* Proc Natl Acad Sci U S A, 1971. **68**(4): p. 820-3.
19. Garman, K.S., et al., *A genomic approach to colon cancer risk stratification yields biologic insights into therapeutic opportunities.* Proc Natl Acad Sci U S A, 2008. **105**(49): p. 19432-7.
20. Lal, N., et al., *An immunogenomic stratification of colorectal cancer: Implications for development of targeted immunotherapy.* Oncoimmunology, 2015. **4**(3): p. e976052.
21. Guinney, J., et al., *The consensus molecular subtypes of colorectal cancer.* Nat Med, 2015. **21**(11): p. 1350-6.
22. Isella, C., et al., *Selective analysis of cancer-cell intrinsic transcriptional traits defines novel clinically relevant subtypes of colorectal cancer.* Nat Commun, 2017. **8**: p. 15107.
23. Logan, R.F., et al., *Outcomes of the Bowel Cancer Screening Programme (BCSP) in England after the first 1 million tests.* Gut, 2012. **61**(10): p. 1439-46.

24. Young, G.P., et al., *Advances in Fecal Occult Blood Tests: the FIT revolution.* Dig Dis Sci, 2015. **60**(3): p. 609-22.
25. Atkin, W.S., et al., *Once-only flexible sigmoidoscopy screening in prevention of colorectal cancer: a multicentre randomised controlled trial.* Lancet, 2010. **375**(9726): p. 1624-33.
26. Moran, B., S. Karandikar, and I. Geh, *Association of Coloproctology of Great Britain & Ireland (ACPGBI): Guidelines for the Management of Cancer of the Colon, Rectum and Anus (2017) - Introduction.* Colorectal Dis, 2017. **19 Suppl 1**: p. 6-8.
27. Lam, A.K., S.S. Chan, and M. Leung, *Synchronous colorectal cancer: clinical, pathological and molecular implications.* World J Gastroenterol, 2014. **20**(22): p. 6815-20.
28. Puppa, G., et al., *TNM staging system of colorectal carcinoma: a critical appraisal of challenging issues.* Arch Pathol Lab Med, 2010. **134**(6): p. 837-52.
29. Dukes, C.E., *The classification of cancer of the rectum.* The Journal of Pathology and Bacteriology, 1932. **35**(3): p. 323-332.
30. Foxtrot Collaborative, G., *Feasibility of preoperative chemotherapy for locally advanced, operable colon cancer: the pilot phase of a randomised controlled trial.* Lancet Oncol, 2012. **13**(11): p. 1152-60.
31. Bhome, R., et al., *Translational aspects in targeting the stromal tumour microenvironment: from bench to bedside.* New Horiz Transl Med, 2016. **3**(1): p. 9-21.
32. Hill, R., et al., *Selective evolution of stromal mesenchyme with p53 loss in response to epithelial tumorigenesis.* Cell, 2005. **123**(6): p. 1001-11.
33. Boehm, T., et al., *Antiangiogenic therapy of experimental cancer does not induce acquired drug resistance.* Nature, 1997. **390**(6658): p. 404-7.
34. Allinen, M., et al., *Molecular characterization of the tumor microenvironment in breast cancer.* Cancer Cell, 2004. **6**(1): p. 17-32.
35. Qiu, W., et al., *No evidence of clonal somatic genetic alterations in cancer-associated fibroblasts from human breast and ovarian carcinomas.* Nat Genet, 2008. **40**(5): p. 650-5.
36. Witz, I.P., *The tumor microenvironment: the making of a paradigm.* Cancer Microenviron, 2009. **2 Suppl 1**: p. 9-17.
37. Paget, S., *The distribution of secondary growths in cancer of the breast. 1889.* Cancer Metastasis Rev, 1989. **8**(2): p. 98-101.
38. Folkman, J., et al., *Isolation of a tumor factor responsible for angiogenesis.* J Exp Med, 1971. **133**(2): p. 275-88.
39. Hersh, E.M., et al., *Mononuclear cell content of human solid tumors.* Med Pediatr Oncol, 1976. **2**(1): p. 1-9.
40. Russel, S.W., W.F. Doe, and C.G. Cochrane, *Number of macrophages and distribution of mitotic activity in regressing and progressing Moloney sarcomas.* J Immunol, 1976. **116**(1): p. 164-6.
41. Jones, P.A. and Y.A. DeClerck, *Destruction of extracellular matrices containing glycoproteins, elastin, and collagen by metastatic human tumor cells.* Cancer Res, 1980. **40**(9): p. 3222-7.
42. Moses, H.L., et al., *Transforming growth factor production by chemically transformed cells.* Cancer Res, 1981. **41**(7): p. 2842-8.
43. Nickell, K.A., J. Halper, and H.L. Moses, *Transforming growth factors in solid human malignant neoplasms.* Cancer Res, 1983. **43**(5): p. 1966-71.
44. Delinassios, J.G. and S.D. Kottaridis, *Interactions between human fibroblasts and HeLa cells in vitro.* Biol Cell, 1984. **50**(1): p. 9-16.
45. Roskelley, C.D., P.Y. Desprez, and M.J. Bissell, *Extracellular matrix-dependent tissue-specific gene expression in mammary epithelial cells requires both physical and biochemical signal transduction.* Proc Natl Acad Sci U S A, 1994. **91**(26): p. 12378-82.
46. Valadi, H., et al., *Exosome-mediated transfer of mRNAs and microRNAs is a novel mechanism of genetic exchange between cells.* Nat Cell Biol, 2007. **9**(6): p. 654-9.
47. Bhome, R., et al., *A top-down view of the tumor microenvironment: structure, cells and signaling.* Front Cell Dev Biol, 2015. **3**: p. 33.

48. Cortez, E., P. Roswall, and K. Pietras, *Functional subsets of mesenchymal cell types in the tumor microenvironment.* Semin Cancer Biol, 2014. **25**: p. 3-9.
49. Kalluri, R., *The biology and function of fibroblasts in cancer.* Nat Rev Cancer, 2016. **16**(9): p. 582-98.
50. Dvorak, H.F., *Tumors: wounds that do not heal. Similarities between tumor stroma generation and wound healing.* N Engl J Med, 1986. **315**(26): p. 1650-9.
51. Marsh, T., K. Pietras, and S.S. McAllister, *Fibroblasts as architects of cancer pathogenesis.* Biochim Biophys Acta, 2013. **1832**(7): p. 1070-8.
52. Cirri, P. and P. Chiarugi, *Cancer associated fibroblasts: the dark side of the coin.* Am J Cancer Res, 2011. **1**(4): p. 482-97.
53. Ronnov-Jessen, L. and O.W. Petersen, *Induction of alpha-smooth muscle actin by transforming growth factor-beta 1 in quiescent human breast gland fibroblasts. Implications for myofibroblast generation in breast neoplasia.* Lab Invest, 1993. **68**(6): p. 696-707.
54. Desmouliere, A., et al., *Transforming growth factor-beta 1 induces alpha-smooth muscle actin expression in granulation tissue myofibroblasts and in quiescent and growing cultured fibroblasts.* J Cell Biol, 1993. **122**(1): p. 103-11.
55. Lohr, M., et al., *Transforming growth factor-beta1 induces desmoplasia in an experimental model of human pancreatic carcinoma.* Cancer Res, 2001. **61**(2): p. 550-5.
56. Kalluri, R. and M. Zeisberg, *Fibroblasts in cancer.* Nat Rev Cancer, 2006. **6**(5): p. 392-401.
57. Augsten, M., *Cancer-associated fibroblasts as another polarized cell type of the tumor microenvironment.* Front Oncol, 2014. **4**: p. 62.
58. De Wever, O., et al., *Carcinoma-associated fibroblasts provide operational flexibility in metastasis.* Semin Cancer Biol, 2014. **25**: p. 33-46.
59. Kojima, Y., et al., *Autocrine TGF-beta and stromal cell-derived factor-1 (SDF-1) signaling drives the evolution of tumor-promoting mammary stromal myofibroblasts.* Proc Natl Acad Sci U S A, 2010. **107**(46): p. 20009-14.
60. Mitra, A.K., et al., *MicroRNAs reprogram normal fibroblasts into cancer-associated fibroblasts in ovarian cancer.* Cancer Discov, 2012. **2**(12): p. 1100-8.
61. Elkabets, M., et al., *Human tumors instigate granulin-expressing hematopoietic cells that promote malignancy by activating stromal fibroblasts in mice.* J Clin Invest, 2011. **121**(2): p. 784-99.
62. Quante, M., et al., *Bone marrow-derived myofibroblasts contribute to the mesenchymal stem cell niche and promote tumor growth.* Cancer Cell, 2011. **19**(2): p. 257-72.
63. Jotzu, C., et al., *Adipose tissue-derived stem cells differentiate into carcinoma-associated fibroblast-like cells under the influence of tumor-derived factors.* Anal Cell Pathol (Amst), 2010. **33**(2): p. 61-79.
64. Iwano, M., et al., *Evidence that fibroblasts derive from epithelium during tissue fibrosis.* J Clin Invest, 2002. **110**(3): p. 341-50.
65. Zeisberg, E.M., et al., *Endothelial-to-mesenchymal transition contributes to cardiac fibrosis.* Nat Med, 2007. **13**(8): p. 952-61.
66. Zeisberg, E.M., et al., *Discovery of endothelial to mesenchymal transition as a source for carcinoma-associated fibroblasts.* Cancer Res, 2007. **67**(21): p. 10123-8.
67. Hosaka, K., et al., *Pericyte-fibroblast transition promotes tumor growth and metastasis.* Proc Natl Acad Sci U S A, 2016. **113**(38): p. E5618-27.
68. LeBleu, V.S. and R. Kalluri, *A peek into cancer-associated fibroblasts: origins, functions and translational impact.* Dis Model Mech, 2018. **11**(4).
69. Sugimoto, H., et al., *Identification of fibroblast heterogeneity in the tumor microenvironment.* Cancer Biol Ther, 2006. **5**(12): p. 1640-6.
70. Fischer, K.R., et al., *Epithelial-to-mesenchymal transition is not required for lung metastasis but contributes to chemoresistance.* Nature, 2015. **527**(7579): p. 472-6.
71. Hayward, S.W., et al., *Malignant transformation in a nontumorigenic human prostatic epithelial cell line.* Cancer Res, 2001. **61**(22): p. 8135-42.

72. Olumi, A.F., et al., *Carcinoma-associated fibroblasts direct tumor progression of initiated human prostatic epithelium.* Cancer Res, 1999. **59**(19): p. 5002-11.
73. Jue, S.F., et al., *The mouse Wnt-1 gene can act via a paracrine mechanism in transformation of mammary epithelial cells.* Mol Cell Biol, 1992. **12**(1): p. 321-8.
74. Kuperwasser, C., et al., *Reconstruction of functionally normal and malignant human breast tissues in mice.* Proc Natl Acad Sci U S A, 2004. **101**(14): p. 4966-71.
75. Bonnans, C., J. Chou, and Z. Werb, *Remodelling the extracellular matrix in development and disease.* Nat Rev Mol Cell Biol, 2014. **15**(12): p. 786-801.
76. Levental, K.R., et al., *Matrix crosslinking forces tumor progression by enhancing integrin signaling.* Cell, 2009. **139**(5): p. 891-906.
77. Nishioka, T., A. Eustace, and C. West, *Lysyl oxidase: from basic science to future cancer treatment.* Cell Struct Funct, 2012. **37**(1): p. 75-80.
78. Chen, L.C., et al., *Human breast cancer cell metastasis is attenuated by lysyl oxidase inhibitors through down-regulation of focal adhesion kinase and the paxillin-signaling pathway.* Breast Cancer Res Treat, 2012. **134**(3): p. 989-1004.
79. Yang, X., et al., *Inactivation of lysyl oxidase by beta-aminopropionitrile inhibits hypoxia-induced invasion and migration of cervical cancer cells.* Oncol Rep, 2013. **29**(2): p. 541-8.
80. Bondareva, A., et al., *The lysyl oxidase inhibitor, beta-aminopropionitrile, diminishes the metastatic colonization potential of circulating breast cancer cells.* PLoS One, 2009. **4**(5): p. e5620.
81. Pietras, K., et al., *Functions of paracrine PDGF signaling in the proangiogenic tumor stroma revealed by pharmacological targeting.* PLoS Med, 2008. **5**(1): p. e19.
82. Ito, T.K., et al., *The VEGF angiogenic switch of fibroblasts is regulated by MMP-7 from cancer cells.* Oncogene, 2007. **26**(51): p. 7194-203.
83. Allen, E., I.B. Walters, and D. Hanahan, *Brivanib, a dual FGF/VEGF inhibitor, is active both first and second line against mouse pancreatic neuroendocrine tumors developing adaptive/evasive resistance to VEGF inhibition.* Clin Cancer Res, 2011. **17**(16): p. 5299-310.
84. Huynh, H., et al., *Brivanib alaninate, a dual inhibitor of vascular endothelial growth factor receptor and fibroblast growth factor receptor tyrosine kinases, induces growth inhibition in mouse models of human hepatocellular carcinoma.* Clin Cancer Res, 2008. **14**(19): p. 6146-53.
85. Lieu, C.H., et al., *The association of alternate VEGF ligands with resistance to anti-VEGF therapy in metastatic colorectal cancer.* PLoS One, 2013. **8**(10): p. e77117.
86. Orimo, A., et al., *Stromal fibroblasts present in invasive human breast carcinomas promote tumor growth and angiogenesis through elevated SDF-1/CXCL12 secretion.* Cell, 2005. **121**(3): p. 335-48.
87. Brabletz, T., et al., *EMT in cancer.* Nat Rev Cancer, 2018. **18**(2): p. 128-134.
88. Yu, Y., et al., *Cancer-associated fibroblasts induce epithelial-mesenchymal transition of breast cancer cells through paracrine TGF-beta signalling.* Br J Cancer, 2014. **110**(3): p. 724-32.
89. Zhou, B., et al., *A role for cancer-associated fibroblasts in inducing the epithelial-to-mesenchymal transition in human tongue squamous cell carcinoma.* J Oral Pathol Med, 2014. **43**(8): p. 585-92.
90. Xu, Z., et al., *Role of pancreatic stellate cells in pancreatic cancer metastasis.* Am J Pathol, 2010. **177**(5): p. 2585-96.
91. Labernadie, A., et al., *A mechanically active heterotypic E-cadherin/N-cadherin adhesion enables fibroblasts to drive cancer cell invasion.* Nature Cell Biology, 2017. **19**(3): p. 224-237.
92. Coppe, J.P., et al., *The senescence-associated secretory phenotype: the dark side of tumor suppression.* Annu Rev Pathol, 2010. **5**: p. 99-118.
93. Mellone, M., et al., *Induction of fibroblast senescence generates a non-fibrogenic myofibroblast phenotype that differentially impacts on cancer prognosis.* Aging (Albany NY), 2016. **9**(1): p. 114-132.

94. Ozdemir, B.C., et al., *Depletion of carcinoma-associated fibroblasts and fibrosis induces immunosuppression and accelerates pancreas cancer with reduced survival.* Cancer Cell, 2014. **25**(6): p. 719-34.
95. Carstens, J.L., et al., *Spatial computation of intratumoral T cells correlates with survival of patients with pancreatic cancer.* Nat Commun, 2017. **8**: p. 15095.
96. Harper, J. and R.C. Sainson, *Regulation of the anti-tumour immune response by cancer-associated fibroblasts.* Semin Cancer Biol, 2014. **25**: p. 69-77.
97. Dominici, M., et al., *Minimal criteria for defining multipotent mesenchymal stromal cells. The International Society for Cellular Therapy position statement.* Cytotherapy, 2006. **8**(4): p. 315-7.
98. Mishra, P.J., et al., *Carcinoma-associated fibroblast-like differentiation of human mesenchymal stem cells.* Cancer Res, 2008. **68**(11): p. 4331-9.
99. Karnoub, A.E., et al., *Mesenchymal stem cells within tumour stroma promote breast cancer metastasis.* Nature, 2007. **449**(7162): p. 557-63.
100. Bai, H., et al., *CCL5 secreted from bone marrow stromal cells stimulates the migration and invasion of Huh7 hepatocellular carcinoma cells via the PI3K-Akt pathway.* Int J Oncol, 2014. **45**(1): p. 333-43.
101. Kuo, C.H., et al., *17beta-estradiol inhibits mesenchymal stem cells-induced human AGS gastric cancer cell mobility via suppression of CCL5- Src/Cas/Paxillin signaling pathway.* Int J Med Sci, 2014. **11**(1): p. 7-16.
102. Chen, K., et al., *Human MSCs promotes colorectal cancer epithelial-mesenchymal transition and progression via CCL5/beta-catenin/Slug pathway.* Cell Death Dis, 2017. **8**(5): p. e2819.
103. Sicoli, D., et al., *CCR5 receptor antagonists block metastasis to bone of v-Src oncogene-transformed metastatic prostate cancer cell lines.* Cancer Res, 2014. **74**(23): p. 7103-14.
104. Vesely, M.D., et al., *Natural innate and adaptive immunity to cancer.* Annu Rev Immunol, 2011. **29**: p. 235-71.
105. Verbeke, H., et al., *The expression and role of CXC chemokines in colorectal cancer.* Cytokine Growth Factor Rev, 2011. **22**(5-6): p. 345-58.
106. Baxevanis, C.N. and M. Papamichail, *Characterization of the anti-tumor immune response in human cancers and strategies for immunotherapy.* Crit Rev Oncol Hematol, 1994. **16**(3): p. 157-79.
107. Taylor, R.C., et al., *Tumor-infiltrating lymphocytes predict sentinel lymph node positivity in patients with cutaneous melanoma.* J Clin Oncol, 2007. **25**(7): p. 869-75.
108. Zhang, L., et al., *Intratumoral T cells, recurrence, and survival in epithelial ovarian cancer.* N Engl J Med, 2003. **348**(3): p. 203-13.
109. Galon, J., et al., *Type, density, and location of immune cells within human colorectal tumors predict clinical outcome.* Science, 2006. **313**(5795): p. 1960-4.
110. Mahmoud, S.M., et al., *Tumor-infiltrating CD8+ lymphocytes predict clinical outcome in breast cancer.* J Clin Oncol, 2011. **29**(15): p. 1949-55.
111. Ward, M.J., et al., *Tumour-infiltrating lymphocytes predict for outcome in HPV-positive oropharyngeal cancer.* Br J Cancer, 2014. **110**(2): p. 489-500.
112. Rosenberg, S.A., et al., *Use of tumor-infiltrating lymphocytes and interleukin-2 in the immunotherapy of patients with metastatic melanoma. A preliminary report.* N Engl J Med, 1988. **319**(25): p. 1676-80.
113. Dudley, M.E., et al., *Adoptive cell transfer therapy following non-myeloablative but lymphodepleting chemotherapy for the treatment of patients with refractory metastatic melanoma.* J Clin Oncol, 2005. **23**(10): p. 2346-57.
114. Morgan, R.A., et al., *Cancer regression in patients after transfer of genetically engineered lymphocytes.* Science, 2006. **314**(5796): p. 126-9.
115. Yvon, E., et al., *Immunotherapy of metastatic melanoma using genetically engineered GD2-specific T cells.* Clin Cancer Res, 2009. **15**(18): p. 5852-60.
116. Kershaw, M.H., et al., *A phase I study on adoptive immunotherapy using gene-modified T cells for ovarian cancer.* Clin Cancer Res, 2006. **12**(20 Pt 1): p. 6106-15.

117. Krause, A., et al., *Antigen-dependent CD28 signaling selectively enhances survival and proliferation in genetically modified activated human primary T lymphocytes.* J Exp Med, 1998. **188**(4): p. 619-26.
118. Maher, J., et al., *Human T-lymphocyte cytotoxicity and proliferation directed by a single chimeric TCRzeta /CD28 receptor.* Nat Biotechnol, 2002. **20**(1): p. 70-5.
119. Grupp, S.A., et al., *Chimeric antigen receptor-modified T cells for acute lymphoid leukemia.* N Engl J Med, 2013. **368**(16): p. 1509-1518.
120. Kochenderfer, J.N., et al., *Eradication of B-lineage cells and regression of lymphoma in a patient treated with autologous T cells genetically engineered to recognize CD19.* Blood, 2010. **116**(20): p. 4099-102.
121. Brown, C.E., et al., *Regression of Glioblastoma after Chimeric Antigen Receptor T-Cell Therapy.* N Engl J Med, 2016. **375**(26): p. 2561-9.
122. Beatty, G.L., et al., *Activity of Mesothelin-Specific Chimeric Antigen Receptor T Cells Against Pancreatic Carcinoma Metastases in a Phase 1 Trial.* Gastroenterology, 2018. **155**(1): p. 29-32.
123. Pardoll, D.M., *The blockade of immune checkpoints in cancer immunotherapy.* Nat Rev Cancer, 2012. **12**(4): p. 252-64.
124. Schwartz, R.H., *Costimulation of T lymphocytes: the role of CD28, CTLA-4, and B7/BB1 in interleukin-2 production and immunotherapy.* Cell, 1992. **71**(7): p. 1065-8.
125. Keir, M.E., et al., *Tissue expression of PD-L1 mediates peripheral T cell tolerance.* J Exp Med, 2006. **203**(4): p. 883-95.
126. Leach, D.R., M.F. Krummel, and J.P. Allison, *Enhancement of antitumor immunity by CTLA-4 blockade.* Science, 1996. **271**(5256): p. 1734-6.
127. Hodi, F.S., et al., *Improved survival with ipilimumab in patients with metastatic melanoma.* N Engl J Med, 2010. **363**(8): p. 711-23.
128. Larkin, J., et al., *Combined Nivolumab and Ipilimumab or Monotherapy in Untreated Melanoma.* N Engl J Med, 2015. **373**(1): p. 23-34.
129. Herbst, R.S., et al., *Predictive correlates of response to the anti-PD-L1 antibody MPDL3280A in cancer patients.* Nature, 2014. **515**(7528): p. 563-7.
130. Powles, T., et al., *MPDL3280A (anti-PD-L1) treatment leads to clinical activity in metastatic bladder cancer.* Nature, 2014. **515**(7528): p. 558-62.
131. Fehrenbacher, L., et al., *Atezolizumab versus docetaxel for patients with previously treated non-small-cell lung cancer (POPLAR): a multicentre, open-label, phase 2 randomised controlled trial.* Lancet, 2016. **387**(10030): p. 1837-46.
132. Robert, C., et al., *Pembrolizumab versus Ipilimumab in Advanced Melanoma.* N Engl J Med, 2015. **372**(26): p. 2521-32.
133. Garon, E.B., et al., *Pembrolizumab for the treatment of non-small-cell lung cancer.* N Engl J Med, 2015. **372**(21): p. 2018-28.
134. Le, D.T., et al., *PD-1 Blockade in Tumors with Mismatch-Repair Deficiency.* N Engl J Med, 2015. **372**(26): p. 2509-20.
135. Shevach, E.M., *Certified professionals: CD4(+)CD25(+) suppressor T cells.* J Exp Med, 2001. **193**(11): p. F41-6.
136. Fontenot, J.D., M.A. Gavin, and A.Y. Rudensky, *Foxp3 programs the development and function of CD4+CD25+ regulatory T cells.* Nat Immunol, 2003. **4**(4): p. 330-6.
137. Curiel, T.J., et al., *Specific recruitment of regulatory T cells in ovarian carcinoma fosters immune privilege and predicts reduced survival.* Nat Med, 2004. **10**(9): p. 942-9.
138. Bates, G.J., et al., *Quantification of regulatory T cells enables the identification of high-risk breast cancer patients and those at risk of late relapse.* J Clin Oncol, 2006. **24**(34): p. 5373-80.
139. Kono, K., et al., *CD4(+)CD25high regulatory T cells increase with tumor stage in patients with gastric and esophageal cancers.* Cancer Immunol Immunother, 2006. **55**(9): p. 1064-71.
140. Kobayashi, N., et al., *FOXP3+ regulatory T cells affect the development and progression of hepatocarcinogenesis.* Clin Cancer Res, 2007. **13**(3): p. 902-11.

141. Ohmura, Y., et al., *Combinations of tumor-specific CD8+ CTLs and anti-CD25 mAb provide improved immunotherapy.* Oncol Rep, 2008. **19**(5): p. 1265-70.
142. Rech, A.J., et al., *CD25 blockade depletes and selectively reprograms regulatory T cells in concert with immunotherapy in cancer patients.* Sci Transl Med, 2012. **4**(134): p. 134ra62.
143. Ahmad, S., et al., *Differential PI3Kdelta Signaling in CD4(+) T-cell Subsets Enables Selective Targeting of T Regulatory Cells to Enhance Cancer Immunotherapy.* Cancer Res, 2017. **77**(8): p. 1892-1904.
144. Ali, K., et al., *Inactivation of PI(3)K p110delta breaks regulatory T-cell-mediated immune tolerance to cancer.* Nature, 2014. **510**(7505): p. 407-11.
145. Knutson, K.L. and M.L. Disis, *Tumor antigen-specific T helper cells in cancer immunity and immunotherapy.* Cancer Immunol Immunother, 2005. **54**(8): p. 721-8.
146. Surman, D.R., et al., *Cutting edge: CD4+ T cell control of CD8+ T cell reactivity to a model tumor antigen.* J Immunol, 2000. **164**(2): p. 562-5.
147. Haabeth, O.A., et al., *Inflammation driven by tumour-specific Th1 cells protects against B-cell cancer.* Nat Commun, 2011. **2**: p. 240.
148. Tatsumi, T., et al., *Disease-associated bias in T helper type 1 (Th1)/Th2 CD4(+) T cell responses against MAGE-6 in HLA-DRB10401(+) patients with renal cell carcinoma or melanoma.* J Exp Med, 2002. **196**(5): p. 619-28.
149. Tatsumi, T., et al., *Disease stage variation in CD4+ and CD8+ T-cell reactivity to the receptor tyrosine kinase EphA2 in patients with renal cell carcinoma.* Cancer Res, 2003. **63**(15): p. 4481-9.
150. Sprent, J., *Antigen-presenting cells. Professionals and amateurs.* Curr Biol, 1995. **5**(10): p. 1095-7.
151. Chaux, P., et al., *Tumor-infiltrating dendritic cells are defective in their antigen-presenting function and inducible B7 expression in rats.* Int J Cancer, 1997. **72**(4): p. 619-24.
152. Menetrier-Caux, C., et al., *Inhibition of the differentiation of dendritic cells from CD34(+) progenitors by tumor cells: role of interleukin-6 and macrophage colony-stimulating factor.* Blood, 1998. **92**(12): p. 4778-91.
153. Bharadwaj, U., et al., *Elevated interleukin-6 and G-CSF in human pancreatic cancer cell conditioned medium suppress dendritic cell differentiation and activation.* Cancer Res, 2007. **67**(11): p. 5479-88.
154. Almand, B., et al., *Increased production of immature myeloid cells in cancer patients: a mechanism of immunosuppression in cancer.* J Immunol, 2001. **166**(1): p. 678-89.
155. Cortez-Retamozo, V., et al., *Origins of tumor-associated macrophages and neutrophils.* Proc Natl Acad Sci U S A, 2012. **109**(7): p. 2491-6.
156. Sadelain, M., I. Riviere, and R. Brentjens, *Targeting tumours with genetically enhanced T lymphocytes.* Nat Rev Cancer, 2003. **3**(1): p. 35-45.
157. Kim, J.V., et al., *The ABCs of artificial antigen presentation.* Nat Biotechnol, 2004. **22**(4): p. 403-10.
158. Mitchell, M.S., et al., *Phase I trial of adoptive immunotherapy with cytolytic T lymphocytes immunized against a tyrosinase epitope.* J Clin Oncol, 2002. **20**(4): p. 1075-86.
159. Latouche, J.B. and M. Sadelain, *Induction of human cytotoxic T lymphocytes by artificial antigen-presenting cells.* Nat Biotechnol, 2000. **18**(4): p. 405-9.
160. Maus, M.V., et al., *Ex vivo expansion of polyclonal and antigen-specific cytotoxic T lymphocytes by artificial APCs expressing ligands for the T-cell receptor, CD28 and 4-1BB.* Nat Biotechnol, 2002. **20**(2): p. 143-8.
161. Levine, B.L., et al., *Effects of CD28 costimulation on long-term proliferation of CD4+ T cells in the absence of exogenous feeder cells.* J Immunol, 1997. **159**(12): p. 5921-30.
162. Raposo, G., et al., *B lymphocytes secrete antigen-presenting vesicles.* J Exp Med, 1996. **183**(3): p. 1161-72.
163. Butler, M.O., et al., *Establishment of antitumor memory in humans using in vitro-educated CD8+ T cells.* Sci Transl Med, 2011. **3**(80): p. 80ra34.

164. Mantovani, A., et al., *Macrophage polarization: tumor-associated macrophages as a paradigm for polarized M2 mononuclear phagocytes.* Trends Immunol, 2002. **23**(11): p. 549-55.
165. Sica, A. and A. Mantovani, *Macrophage plasticity and polarization: in vivo veritas.* J Clin Invest, 2012. **122**(3): p. 787-95.
166. Solinas, G., et al., *Tumor-associated macrophages (TAM) as major players of the cancer-related inflammation.* J Leukoc Biol, 2009. **86**(5): p. 1065-73.
167. Mills, C.D., et al., *M-1/M-2 macrophages and the Th1/Th2 paradigm.* J Immunol, 2000. **164**(12): p. 6166-73.
168. Kuang, D.M., et al., *Activated monocytes in peritumoral stroma of hepatocellular carcinoma foster immune privilege and disease progression through PD-L1.* J Exp Med, 2009. **206**(6): p. 1327-37.
169. Leek, R.D., et al., *Association of macrophage infiltration with angiogenesis and prognosis in invasive breast carcinoma.* Cancer Res, 1996. **56**(20): p. 4625-9.
170. Wyckoff, J.B., et al., *Direct visualization of macrophage-assisted tumor cell intravasation in mammary tumors.* Cancer Res, 2007. **67**(6): p. 2649-56.
171. Chen, P., et al., *Tumor-associated macrophages promote angiogenesis and melanoma growth via adrenomedullin in a paracrine and autocrine manner.* Clin Cancer Res, 2011. **17**(23): p. 7230-9.
172. Yang, M., et al., *Microvesicles secreted by macrophages shuttle invasion-potentiating microRNAs into breast cancer cells.* Mol Cancer, 2011. **10**: p. 117.
173. Takanami, I., K. Takeuchi, and S. Kodaira, *Tumor-associated macrophage infiltration in pulmonary adenocarcinoma: association with angiogenesis and poor prognosis.* Oncology, 1999. **57**(2): p. 138-42.
174. Salvesen, H.B. and L.A. Akslen, *Significance of tumour-associated macrophages, vascular endothelial growth factor and thrombospondin-1 expression for tumour angiogenesis and prognosis in endometrial carcinomas.* Int J Cancer, 1999. **84**(5): p. 538-43.
175. Ryder, M., et al., *Increased density of tumor-associated macrophages is associated with decreased survival in advanced thyroid cancer.* Endocr Relat Cancer, 2008. **15**(4): p. 1069-74.
176. Zhang, Q.W., et al., *Prognostic significance of tumor-associated macrophages in solid tumor: a meta-analysis of the literature.* PLoS One, 2012. **7**(12): p. e50946.
177. Luo, Y., et al., *Targeting tumor-associated macrophages as a novel strategy against breast cancer.* J Clin Invest, 2006. **116**(8): p. 2132-2141.
178. Ries, C.H., et al., *Targeting tumor-associated macrophages with anti-CSF-1R antibody reveals a strategy for cancer therapy.* Cancer Cell, 2014. **25**(6): p. 846-59.
179. Cassier, P.A., et al., *CSF1R inhibition with emactuzumab in locally advanced diffuse-type tenosynovial giant cell tumours of the soft tissue: a dose-escalation and dose-expansion phase 1 study.* Lancet Oncol, 2015. **16**(8): p. 949-56.
180. Schiavoni, G., L. Gabriele, and F. Mattei, *The tumor microenvironment: a pitch for multiple players.* Front Oncol, 2013. **3**: p. 90.
181. Karre, K., et al., *Selective rejection of H-2-deficient lymphoma variants suggests alternative immune defence strategy.* Nature, 1986. **319**(6055): p. 675-8.
182. Smyth, M.J., et al., *Activation of NK cell cytotoxicity.* Mol Immunol, 2005. **42**(4): p. 501-10.
183. Lanier, L.L., *Evolutionary struggles between NK cells and viruses.* Nat Rev Immunol, 2008. **8**(4): p. 259-68.
184. Vivier, E., et al., *Innate or adaptive immunity? The example of natural killer cells.* Science, 2011. **331**(6013): p. 44-9.
185. Moretta, A., *Natural killer cells and dendritic cells: rendezvous in abused tissues.* Nat Rev Immunol, 2002. **2**(12): p. 957-64.
186. Moretta, A., et al., *P58 molecules as putative receptors for major histocompatibility complex (MHC) class I molecules in human natural killer (NK) cells. Anti-p58 antibodies reconstitute lysis of MHC class I-protected cells in NK clones displaying different specificities.* J Exp Med, 1993. **178**(2): p. 597-604.

187. Wilson, E.B., et al., *Human tumour immune evasion via TGF-beta blocks NK cell activation but not survival allowing therapeutic restoration of anti-tumour activity.* PLoS One, 2011. **6**(9): p. e22842.
188. Roberti, M.P., et al., *IL-2- or IL-15-activated NK cells enhance Cetuximab-mediated activity against triple-negative breast cancer in xenografts and in breast cancer patients.* Breast Cancer Res Treat, 2012. **136**(3): p. 659-71.
189. Gillard-Bocquet, M., et al., *Lung tumor microenvironment induces specific gene expression signature in intratumoral NK cells.* Front Immunol, 2013. **4**: p. 19.
190. Eguizabal, C., et al., *Natural killer cells for cancer immunotherapy: pluripotent stem cells-derived NK cells as an immunotherapeutic perspective.* Front Immunol, 2014. **5**: p. 439.
191. Atkins, M.B., et al., *High-dose recombinant interleukin 2 therapy for patients with metastatic melanoma: analysis of 270 patients treated between 1985 and 1993.* J Clin Oncol, 1999. **17**(7): p. 2105-16.
192. Fisher, R.I., S.A. Rosenberg, and G. Fyfe, *Long-term survival update for high-dose recombinant interleukin-2 in patients with renal cell carcinoma.* Cancer J Sci Am, 2000. **6 Suppl 1**: p. S55-7.
193. Ishikawa, E., et al., *Autologous natural killer cell therapy for human recurrent malignant glioma.* Anticancer Res, 2004. **24**(3b): p. 1861-71.
194. Iliopoulou, E.G., et al., *A phase I trial of adoptive transfer of allogeneic natural killer cells in patients with advanced non-small cell lung cancer.* Cancer Immunol Immunother, 2010. **59**(12): p. 1781-9.
195. Tonn, T., et al., *Treatment of patients with advanced cancer with the natural killer cell line NK-92.* Cytotherapy, 2013. **15**(12): p. 1563-70.
196. Bock, A.M., D. Knorr, and D.S. Kaufman, *Development, expansion, and in vivo monitoring of human NK cells from human embryonic stem cells (hESCs) and and induced pluripotent stem cells (iPSCs).* J Vis Exp, 2013(74): p. e50337.
197. Dancey, J.T., et al., *Neutrophil kinetics in man.* J Clin Invest, 1976. **58**(3): p. 705-15.
198. Sawanobori, Y., et al., *Chemokine-mediated rapid turnover of myeloid-derived suppressor cells in tumor-bearing mice.* Blood, 2008. **111**(12): p. 5457-66.
199. Colotta, F., et al., *Modulation of granulocyte survival and programmed cell death by cytokines and bacterial products.* Blood, 1992. **80**(8): p. 2012-20.
200. Templeton, A.J., et al., *Prognostic role of neutrophil-to-lymphocyte ratio in solid tumors: a systematic review and meta-analysis.* J Natl Cancer Inst, 2014. **106**(6): p. dju124.
201. Wculek, S.K. and I. Malanchi, *Neutrophils support lung colonization of metastasis-initiating breast cancer cells.* Nature, 2015. **528**(7582): p. 413-7.
202. Coffelt, S.B., et al., *IL-17-producing gammadelta T cells and neutrophils conspire to promote breast cancer metastasis.* Nature, 2015. **522**(7556): p. 345-348.
203. Ocana, A., et al., *Neutrophils in cancer: prognostic role and therapeutic strategies.* Mol Cancer, 2017. **16**(1): p. 137.
204. Carmeliet, P. and R.K. Jain, *Principles and mechanisms of vessel normalization for cancer and other angiogenic diseases.* Nat Rev Drug Discov, 2011. **10**(6): p. 417-27.
205. Casazza, A., et al., *Tumor stroma: a complexity dictated by the hypoxic tumor microenvironment.* Oncogene, 2014. **33**(14): p. 1743-54.
206. Dore-Duffy, P. and J.C. LaManna, *Physiologic angiodynamics in the brain.* Antioxid Redox Signal, 2007. **9**(9): p. 1363-71.
207. Morikawa, S., et al., *Abnormalities in pericytes on blood vessels and endothelial sprouts in tumors.* Am J Pathol, 2002. **160**(3): p. 985-1000.
208. Bergers, G., et al., *Benefits of targeting both pericytes and endothelial cells in the tumor vasculature with kinase inhibitors.* J Clin Invest, 2003. **111**(9): p. 1287-95.
209. Cooke, V.G., et al., *Pericyte depletion results in hypoxia-associated epithelial-to-mesenchymal transition and metastasis mediated by met signaling pathway.* Cancer Cell, 2012. **21**(1): p. 66-81.
210. Gerhardt, H., et al., *VEGF guides angiogenic sprouting utilizing endothelial tip cell filopodia.* J Cell Biol, 2003. **161**(6): p. 1163-77.

211. Hurwitz, H., et al., *Bevacizumab plus irinotecan, fluorouracil, and leucovorin for metastatic colorectal cancer.* N Engl J Med, 2004. **350**(23): p. 2335-42.
212. Sandler, A., et al., *Paclitaxel-carboplatin alone or with bevacizumab for non-small-cell lung cancer.* N Engl J Med, 2006. **355**(24): p. 2542-50.
213. Escudier, B., et al., *Bevacizumab plus interferon alfa-2a for treatment of metastatic renal cell carcinoma: a randomised, double-blind phase III trial.* Lancet, 2007. **370**(9605): p. 2103-11.
214. Perren, T.J., et al., *A phase 3 trial of bevacizumab in ovarian cancer.* N Engl J Med, 2011. **365**(26): p. 2484-96.
215. Tewari, K.S., et al., *Improved survival with bevacizumab in advanced cervical cancer.* N Engl J Med, 2014. **370**(8): p. 734-43.
216. Kerbel, R.S., *Tumor angiogenesis.* N Engl J Med, 2008. **358**(19): p. 2039-49.
217. Fan, F., et al., *Chronic exposure of colorectal cancer cells to bevacizumab promotes compensatory pathways that mediate tumour cell migration.* Br J Cancer, 2011. **104**(8): p. 1270-7.
218. Jain, R.K., *Normalization of tumor vasculature: an emerging concept in antiangiogenic therapy.* Science, 2005. **307**(5706): p. 58-62.
219. Fuchs, C.S., et al., *Ramucirumab monotherapy for previously treated advanced gastric or gastro-oesophageal junction adenocarcinoma (REGARD): an international, randomised, multicentre, placebo-controlled, phase 3 trial.* Lancet, 2014. **383**(9911): p. 31-9.
220. Wilke, H., et al., *Ramucirumab plus paclitaxel versus placebo plus paclitaxel in patients with previously treated advanced gastric or gastro-oesophageal junction adenocarcinoma (RAINBOW): a double-blind, randomised phase 3 trial.* Lancet Oncol, 2014. **15**(11): p. 1224-35.
221. Keating, G.M. and A. Santoro, *Sorafenib: a review of its use in advanced hepatocellular carcinoma.* Drugs, 2009. **69**(2): p. 223-40.
222. Escudier, B., et al., *Sorafenib in advanced clear-cell renal-cell carcinoma.* N Engl J Med, 2007. **356**(2): p. 125-34.
223. Llovet, J.M., et al., *Sorafenib in advanced hepatocellular carcinoma.* N Engl J Med, 2008. **359**(4): p. 378-90.
224. Brose, M.S., et al., *Sorafenib in radioactive iodine-refractory, locally advanced or metastatic differentiated thyroid cancer: a randomised, double-blind, phase 3 trial.* Lancet, 2014. **384**(9940): p. 319-28.
225. Denekamp, J., *Vascular attack as a therapeutic strategy for cancer.* Cancer Metastasis Rev, 1990. **9**(3): p. 267-82.
226. Thorpe, P.E., *Vascular targeting agents as cancer therapeutics.* Clin Cancer Res, 2004. **10**(2): p. 415-27.
227. West, C.M. and P. Price, *Combretastatin A4 phosphate.* Anticancer Drugs, 2004. **15**(3): p. 179-87.
228. Mooney, C.J., et al., *A phase II trial of fosbretabulin in advanced anaplastic thyroid carcinoma and correlation of baseline serum-soluble intracellular adhesion molecule-1 with outcome.* Thyroid, 2009. **19**(3): p. 233-40.
229. Zweifel, M., et al., *Phase II trial of combretastatin A4 phosphate, carboplatin, and paclitaxel in patients with platinum-resistant ovarian cancer.* Ann Oncol, 2011. **22**(9): p. 2036-41.
230. Mohamedali, K.A., et al., *Inhibition of prostate tumor growth and bone remodeling by the vascular targeting agent VEGF121/rGel.* Cancer Res, 2006. **66**(22): p. 10919-28.
231. Mohamedali, K.A., et al., *The vascular-targeting fusion toxin VEGF121/rGel inhibits the growth of orthotopic human bladder carcinoma tumors.* Neoplasia, 2005. **7**(10): p. 912-20.
232. Ran, S., et al., *The vascular-ablative agent VEGF(121)/rGel inhibits pulmonary metastases of MDA-MB-231 breast tumors.* Neoplasia, 2005. **7**(5): p. 486-96.
233. Wong, B.W., et al., *Emerging novel functions of the oxygen-sensing prolyl hydroxylase domain enzymes.* Trends Biochem Sci, 2013. **38**(1): p. 3-11.
234. Tang, N., et al., *Loss of HIF-1alpha in endothelial cells disrupts a hypoxia-driven VEGF autocrine loop necessary for tumorigenesis.* Cancer Cell, 2004. **6**(5): p. 485-95.

235. Skuli, N., et al., *Endothelial deletion of hypoxia-inducible factor-2alpha (HIF-2alpha) alters vascular function and tumor angiogenesis.* Blood, 2009. **114**(2): p. 469-77.
236. Branco-Price, C., et al., *Endothelial cell HIF-1alpha and HIF-2alpha differentially regulate metastatic success.* Cancer Cell, 2012. **21**(1): p. 52-65.
237. Zhang, H., et al., *Digoxin and other cardiac glycosides inhibit HIF-1alpha synthesis and block tumor growth.* Proc Natl Acad Sci U S A, 2008. **105**(50): p. 19579-86.
238. Venning, F.A., L. Wullkopf, and J.T. Erler, *Targeting ECM Disrupts Cancer Progression.* Front Oncol, 2015. **5**: p. 224.
239. Frantz, C., K.M. Stewart, and V.M. Weaver, *The extracellular matrix at a glance.* J Cell Sci, 2010. **123**(Pt 24): p. 4195-200.
240. Daley, W.P., S.B. Peters, and M. Larsen, *Extracellular matrix dynamics in development and regenerative medicine.* J Cell Sci, 2008. **121**(Pt 3): p. 255-64.
241. Butcher, D.T., T. Alliston, and V.M. Weaver, *A tense situation: forcing tumour progression.* Nat Rev Cancer, 2009. **9**(2): p. 108-22.
242. Paszek, M.J., et al., *Tensional homeostasis and the malignant phenotype.* Cancer Cell, 2005. **8**(3): p. 241-54.
243. De Wever, O., et al., *Stromal myofibroblasts are drivers of invasive cancer growth.* Int J Cancer, 2008. **123**(10): p. 2229-38.
244. Halvorsen, T.B. and E. Seim, *Association between invasiveness, inflammatory reaction, desmoplasia and survival in colorectal cancer.* J Clin Pathol, 1989. **42**(2): p. 162-6.
245. Pandol, S., et al., *Desmoplasia of pancreatic ductal adenocarcinoma.* Clin Gastroenterol Hepatol, 2009. **7**(11 Suppl): p. S44-7.
246. Kessenbrock, K., V. Plaks, and Z. Werb, *Matrix metalloproteinases: regulators of the tumor microenvironment.* Cell, 2010. **141**(1): p. 52-67.
247. Mariyama, M., et al., *The alpha 4(IV) chain of basement membrane collagen. Isolation of cDNAs encoding bovine alpha 4(IV) and comparison with other type IV collagens.* J Biol Chem, 1992. **267**(2): p. 1253-8.
248. Ohlund, D., et al., *Type IV collagen stimulates pancreatic cancer cell proliferation, migration, and inhibits apoptosis through an autocrine loop.* BMC Cancer, 2013. **13**: p. 154.
249. Rabinovich, G.A., *Galectin-1 as a potential cancer target.* Br J Cancer, 2005. **92**(7): p. 1188-92.
250. Vlodavsky, I., et al., *The impact of heparanese and heparin on cancer metastasis and angiogenesis.* Pathophysiol Haemost Thromb, 2006. **35**(1-2): p. 116-27.
251. Ben-Izhak, O., et al., *Heparanase expression in malignant salivary gland tumors inversely correlates with long-term survival.* Neoplasia, 2006. **8**(10): p. 879-84.
252. Hynes, R.O., *Integrins: bidirectional, allosteric signaling machines.* Cell, 2002. **110**(6): p. 673-87.
253. Ioachim, E., et al., *Immunohistochemical expression of extracellular matrix components tenascin, fibronectin, collagen type IV and laminin in breast cancer: their prognostic value and role in tumour invasion and progression.* Eur J Cancer, 2002. **38**(18): p. 2362-70.
254. Nam, J.M., et al., *Breast cancer cells in three-dimensional culture display an enhanced radioresponse after coordinate targeting of integrin alpha5beta1 and fibronectin.* Cancer Res, 2010. **70**(13): p. 5238-48.
255. Toole, B.P., *Hyaluronan promotes the malignant phenotype.* Glycobiology, 2002. **12**(3): p. 37R-42R.
256. Singha, N.C., et al., *Tumor-associated hyaluronan limits efficacy of monoclonal antibody therapy.* Mol Cancer Ther, 2015. **14**(2): p. 523-32.
257. Hingorani, S.R., et al., *Phase Ib Study of PEGylated Recombinant Human Hyaluronidase and Gemcitabine in Patients with Advanced Pancreatic Cancer.* Clin Cancer Res, 2016. **22**(12): p. 2848-54.
258. Gillan, L., et al., *Periostin secreted by epithelial ovarian carcinoma is a ligand for alpha(V)beta(3) and alpha(V)beta(5) integrins and promotes cell motility.* Cancer Res, 2002. **62**(18): p. 5358-64.

259. Underwood, T.J., et al., *Cancer-associated fibroblasts predict poor outcome and promote periostin-dependent invasion in oesophageal adenocarcinoma.* J Pathol, 2015. **235**(3): p. 466-77.
260. Tai, I.T., M. Dai, and L.B. Chen, *Periostin induction in tumor cell line explants and inhibition of in vitro cell growth by anti-periostin antibodies.* Carcinogenesis, 2005. **26**(5): p. 908-15.
261. Zhu, M., et al., *Neutralizing monoclonal antibody to periostin inhibits ovarian tumor growth and metastasis.* Mol Cancer Ther, 2011. **10**(8): p. 1500-8.
262. Salomaki, H.H., et al., *Differential expression of decorin by human malignant and benign vascular tumors.* J Histochem Cytochem, 2008. **56**(7): p. 639-46.
263. Grant, D.S., et al., *Decorin suppresses tumor cell-mediated angiogenesis.* Oncogene, 2002. **21**(31): p. 4765-77.
264. Xu, W., et al., *The systemic delivery of an oncolytic adenovirus expressing decorin inhibits bone metastasis in a mouse model of human prostate cancer.* Gene Ther, 2015. **22**(3): p. 247-56.
265. Pas, J., et al., *Analysis of structure and function of tenascin-C.* Int J Biochem Cell Biol, 2006. **38**(9): p. 1594-602.
266. Reardon, D.A., et al., *Phase II trial of murine (131)I-labeled antitenascin monoclonal antibody 81C6 administered into surgically created resection cavities of patients with newly diagnosed malignant gliomas.* J Clin Oncol, 2002. **20**(5): p. 1389-97.
267. Wyszko, E., et al., *A multivariate analysis of patients with brain tumors treated with ATN-RNA.* Acta Pol Pharm, 2008. **65**(6): p. 677-84.
268. McCawley, L.J. and L.M. Matrisian, *Matrix metalloproteinases: multifunctional contributors to tumor progression.* Mol Med Today, 2000. **6**(4): p. 149-56.
269. Recklies, A.D., et al., *Secretion of proteinases from malignant and nonmalignant human breast tissue.* Cancer Res, 1980. **40**(3): p. 550-6.
270. Gonzalez-Villasana, V., et al., *Rac1/Pak1/p38/MMP-2 axis regulates angiogenesis in ovarian cancer.* Clin Cancer Res, 2015.
271. Che, Y.L., et al., *The C3G/Rap1 pathway promotes secretion of MMP-2 and MMP-9 and is involved in serous ovarian cancer metastasis.* Cancer Lett, 2015.
272. Gu, X., et al., *TIMP-3 Expression Associates with Malignant Behaviors and Predicts Favorable Survival in HCC.* PLoS One, 2014. **9**(8): p. e106161.
273. Anand-Apte, B., et al., *A review of tissue inhibitor of metalloproteinases-3 (TIMP-3) and experimental analysis of its effect on primary tumor growth.* Biochem Cell Biol, 1996. **74**(6): p. 853-62.
274. Gu, P., et al., *Frequent loss of TIMP-3 expression in progression of esophageal and gastric adenocarcinomas.* Neoplasia, 2008. **10**(6): p. 563-72.
275. Qi, J.H., et al., *A novel function for tissue inhibitor of metalloproteinases-3 (TIMP3): inhibition of angiogenesis by blockage of VEGF binding to VEGF receptor-2.* Nat Med, 2003. **9**(4): p. 407-15.
276. Kudo, M., et al., *Brivanib as adjuvant therapy to transarterial chemoembolization in patients with hepatocellular carcinoma: A randomized phase III trial.* Hepatology, 2014. **60**(5): p. 1697-707.
277. Kozono, S., et al., *Pirfenidone inhibits pancreatic cancer desmoplasia by regulating stellate cells.* Cancer Res, 2013. **73**(7): p. 2345-56.
278. Ogata-Kawata, H., et al., *Circulating exosomal microRNAs as biomarkers of colon cancer.* PLoS One, 2014. **9**(4): p. e92921.
279. Corcoran, C., S. Rani, and L. O'Driscoll, *miR-34a is an intracellular and exosomal predictive biomarker for response to docetaxel with clinical relevance to prostate cancer progression.* Prostate, 2014. **74**(13): p. 1320-34.
280. Alegre, E., et al., *Circulating melanoma exosomes as diagnostic and prognosis biomarkers.* Clin Chim Acta, 2016. **454**: p. 28-32.
281. Peinado, H., et al., *Melanoma exosomes educate bone marrow progenitor cells toward a pro-metastatic phenotype through MET.* Nat Med, 2012. **18**(6): p. 883-91.

282. Costa-Silva, B., et al., *Pancreatic cancer exosomes initiate pre-metastatic niche formation in the liver.* Nat Cell Biol, 2015. **17**(6): p. 816-26.
283. Hoshino, A., et al., *Tumour exosome integrins determine organotropic metastasis.* Nature, 2015. **527**(7578): p. 329-35.
284. Boelens, M.C., et al., *Exosome transfer from stromal to breast cancer cells regulates therapy resistance pathways.* Cell, 2014. **159**(3): p. 499-513.
285. Lee, R.C., R.L. Feinbaum, and V. Ambros, *The C. elegans heterochronic gene lin-4 encodes small RNAs with antisense complementarity to lin-14.* Cell, 1993. **75**(5): p. 843-54.
286. Hobert, O., *Gene regulation by transcription factors and microRNAs.* Science, 2008. **319**(5871): p. 1785-6.
287. Ebert, M.S. and P.A. Sharp, *Roles for microRNAs in conferring robustness to biological processes.* Cell, 2012. **149**(3): p. 515-24.
288. Calin, G.A., et al., *Frequent deletions and down-regulation of micro- RNA genes miR15 and miR16 at 13q14 in chronic lymphocytic leukemia.* Proc Natl Acad Sci U S A, 2002. **99**(24): p. 15524-9.
289. Hayashita, Y., et al., *A polycistronic microRNA cluster, miR-17-92, is overexpressed in human lung cancers and enhances cell proliferation.* Cancer Res, 2005. **65**(21): p. 9628-32.
290. Zhang, L., et al., *microRNAs exhibit high frequency genomic alterations in human cancer.* Proc Natl Acad Sci U S A, 2006. **103**(24): p. 9136-41.
291. Esquela-Kerscher, A. and F.J. Slack, *Oncomirs - microRNAs with a role in cancer.* Nat Rev Cancer, 2006. **6**(4): p. 259-69.
292. Peng, Y. and C.M. Croce, *The role of MicroRNAs in human cancer.* Signal Transduct Target Ther, 2016. **1**: p. 15004.
293. Rabinowits, G., et al., *Exosomal microRNA: a diagnostic marker for lung cancer.* Clin Lung Cancer, 2009. **10**(1): p. 42-6.
294. Jin, X., et al., *Evaluation of Tumor-Derived Exosomal miRNA as Potential Diagnostic Biomarkers for Early-Stage Non-Small Cell Lung Cancer Using Next-Generation Sequencing.* Clin Cancer Res, 2017. **23**(17): p. 5311-5319.
295. Matsumura, T., et al., *Exosomal microRNA in serum is a novel biomarker of recurrence in human colorectal cancer.* Br J Cancer, 2015. **113**(2): p. 275-81.
296. Bhome, R., et al., *Exosomal microRNAs (exomiRs): Small molecules with a big role in cancer.* Cancer Lett, 2018. **420**: p. 228-235.
297. Johnstone, R.M., et al., *Vesicle formation during reticulocyte maturation. Association of plasma membrane activities with released vesicles (exosomes).* J Biol Chem, 1987. **262**(19): p. 9412-20.
298. Trams, E.G., et al., *Exfoliation of membrane ecto-enzymes in the form of micro-vesicles.* Biochim Biophys Acta, 1981. **645**(1): p. 63-70.
299. Thery, C., et al., *Isolation and characterization of exosomes from cell culture supernatants and biological fluids.* Curr Protoc Cell Biol, 2006. **Chapter 3**: p. Unit 3 22.
300. Zhang, H., et al., *Identification of distinct nanoparticles and subsets of extracellular vesicles by asymmetric flow field-flow fractionation.* Nat Cell Biol, 2018. **20**(3): p. 332-343.
301. Heijnen, H.F., et al., *Activated platelets release two types of membrane vesicles: microvesicles by surface shedding and exosomes derived from exocytosis of multivesicular bodies and alpha-granules.* Blood, 1999. **94**(11): p. 3791-9.
302. Jaiswal, R., et al., *Microparticle-associated nucleic acids mediate trait dominance in cancer.* FASEB J, 2012. **26**(1): p. 420-9.
303. Stein, J.M. and J.P. Luzio, *Ectocytosis caused by sublytic autologous complement attack on human neutrophils. The sorting of endogenous plasma-membrane proteins and lipids into shed vesicles.* Biochem J, 1991. **274 (Pt 2)**: p. 381-6.
304. Thery, C., M. Ostrowski, and E. Segura, *Membrane vesicles as conveyors of immune responses.* Nat Rev Immunol, 2009. **9**(8): p. 581-93.
305. Al-Nedawi, K., et al., *Intercellular transfer of the oncogenic receptor EGFRvIII by microvesicles derived from tumour cells.* Nat Cell Biol, 2008. **10**(5): p. 619-24.

306. Lotvall, J., et al., *Minimal experimental requirements for definition of extracellular vesicles and their functions: a position statement from the International Society for Extracellular Vesicles.* J Extracell Vesicles, 2014. **3**: p. 26913.
307. Zitvogel, L., et al., *Eradication of established murine tumors using a novel cell-free vaccine: dendritic cell-derived exosomes.* Nat Med, 1998. **4**(5): p. 594-600.
308. Mobius, W., et al., *Immunoelectron microscopic localization of cholesterol using biotinylated and non-cytolytic perfringolysin O.* J Histochem Cytochem, 2002. **50**(1): p. 43-55.
309. Thery, C., et al., *Proteomic analysis of dendritic cell-derived exosomes: a secreted subcellular compartment distinct from apoptotic vesicles.* J Immunol, 2001. **166**(12): p. 7309-18.
310. Raiborg, C. and H. Stenmark, *The ESCRT machinery in endosomal sorting of ubiquitylated membrane proteins.* Nature, 2009. **458**(7237): p. 445-52.
311. Stuffers, S., et al., *Multivesicular endosome biogenesis in the absence of ESCRTs.* Traffic, 2009. **10**(7): p. 925-37.
312. Savina, A., et al., *Exosome release is regulated by a calcium-dependent mechanism in K562 cells.* J Biol Chem, 2003. **278**(22): p. 20083-90.
313. Ostrowski, M., et al., *Rab27a and Rab27b control different steps of the exosome secretion pathway.* Nat Cell Biol, 2010. **12**(1): p. 19-30; sup pp 1-13.
314. Rao, S.K., et al., *Identification of SNAREs involved in synaptotagmin VII-regulated lysosomal exocytosis.* J Biol Chem, 2004. **279**(19): p. 20471-9.
315. Savina, A., et al., *Rab11 promotes docking and fusion of multivesicular bodies in a calcium-dependent manner.* Traffic, 2005. **6**(2): p. 131-43.
316. Hsu, C., et al., *Regulation of exosome secretion by Rab35 and its GTPase-activating proteins TBC1D10A-C.* J Cell Biol, 2010. **189**(2): p. 223-32.
317. Escrevente, C., et al., *Interaction and uptake of exosomes by ovarian cancer cells.* BMC Cancer, 2011. **11**: p. 108.
318. Nanbo, A., et al., *Exosomes derived from Epstein-Barr virus-infected cells are internalized via caveola-dependent endocytosis and promote phenotypic modulation in target cells.* J Virol, 2013. **87**(18): p. 10334-47.
319. Izquierdo-Useros, N., et al., *Capture and transfer of HIV-1 particles by mature dendritic cells converges with the exosome-dissemination pathway.* Blood, 2009. **113**(12): p. 2732-41.
320. Kamerkar, S., et al., *Exosomes facilitate therapeutic targeting of oncogenic KRAS in pancreatic cancer.* Nature, 2017. **546**(7659): p. 498-503.
321. Feng, D., et al., *Cellular internalization of exosomes occurs through phagocytosis.* Traffic, 2010. **11**(5): p. 675-87.
322. Parolini, I., et al., *Microenvironmental pH is a key factor for exosome traffic in tumor cells.* J Biol Chem, 2009. **284**(49): p. 34211-22.
323. Svensson, K.J., et al., *Exosome uptake depends on ERK1/2-heat shock protein 27 signaling and lipid Raft-mediated endocytosis negatively regulated by caveolin-1.* J Biol Chem, 2013. **288**(24): p. 17713-24.
324. Bhome, R., et al., *Profiling the MicroRNA Payload of Exosomes Derived from Ex Vivo Primary Colorectal Fibroblasts.* Methods Mol Biol, 2017. **1509**: p. 115-122.
325. Boing, A.N., et al., *Single-step isolation of extracellular vesicles by size-exclusion chromatography.* J Extracell Vesicles, 2014. **3**.
326. Lobb, R.J., et al., *Optimized exosome isolation protocol for cell culture supernatant and human plasma.* J Extracell Vesicles, 2015. **4**: p. 27031.
327. Dragovic, R.A., et al., *Sizing and phenotyping of cellular vesicles using Nanoparticle Tracking Analysis.* Nanomedicine, 2011. **7**(6): p. 780-8.
328. van der Pol, E., et al., *Particle size distribution of exosomes and microvesicles determined by transmission electron microscopy, flow cytometry, nanoparticle tracking analysis, and resistive pulse sensing.* J Thromb Haemost, 2014. **12**(7): p. 1182-92.
329. Witwer, K.W., et al., *Updating the MISEV minimal requirements for extracellular vesicle studies: building bridges to reproducibility.* J Extracell Vesicles, 2017. **6**(1): p. 1396823.

330. Consortium, E.-T., et al., *EV-TRACK: transparent reporting and centralizing knowledge in extracellular vesicle research.* Nat Methods, 2017. **14**(3): p. 228-232.
331. Mittelbrunn, M., et al., *Unidirectional transfer of microRNA-loaded exosomes from T cells to antigen-presenting cells.* Nat Commun, 2011. **2**: p. 282.
332. Alexander, M., et al., *Exosome-delivered microRNAs modulate the inflammatory response to endotoxin.* Nat Commun, 2015. **6**: p. 7321.
333. Challagundla, K.B., et al., *Exosome-mediated transfer of microRNAs within the tumor microenvironment and neuroblastoma resistance to chemotherapy.* J Natl Cancer Inst, 2015. **107**(7).
334. Goldie, B.J., et al., *Activity-associated miRNA are packaged in Map1b-enriched exosomes released from depolarized neurons.* Nucleic Acids Res, 2014. **42**(14): p. 9195-208.
335. Guduric-Fuchs, J., et al., *Selective extracellular vesicle-mediated export of an overlapping set of microRNAs from multiple cell types.* BMC Genomics, 2012. **13**: p. 357.
336. Skog, J., et al., *Glioblastoma microvesicles transport RNA and proteins that promote tumour growth and provide diagnostic biomarkers.* Nat Cell Biol, 2008. **10**(12): p. 1470-6.
337. Cha, D.J., et al., *KRAS-dependent sorting of miRNA to exosomes.* Elife, 2015. **4**: p. e07197.
338. Gibbings, D.J., et al., *Multivesicular bodies associate with components of miRNA effector complexes and modulate miRNA activity.* Nat Cell Biol, 2009. **11**(9): p. 1143-9.
339. Lee, Y.S., et al., *Silencing by small RNAs is linked to endosomal trafficking.* Nat Cell Biol, 2009. **11**(9): p. 1150-6.
340. Kosaka, N., et al., *Secretory mechanisms and intercellular transfer of microRNAs in living cells.* J Biol Chem, 2010. **285**(23): p. 17442-52.
341. Villarroya-Beltri, C., et al., *Sumoylated hnRNPA2B1 controls the sorting of miRNAs into exosomes through binding to specific motifs.* Nat Commun, 2013. **4**: p. 2980.
342. Santangelo, L., et al., *The RNA-Binding Protein SYNCRIP Is a Component of the Hepatocyte Exosomal Machinery Controlling MicroRNA Sorting.* Cell Rep, 2016. **17**(3): p. 799-808.
343. Burroughs, A.M., et al., *A comprehensive survey of 3' animal miRNA modification events and a possible role for 3' adenylation in modulating miRNA targeting effectiveness.* Genome Res, 2010. **20**(10): p. 1398-410.
344. Koppers-Lalic, D., et al., *Nontemplated nucleotide additions distinguish the small RNA composition in cells from exosomes.* Cell Rep, 2014. **8**(6): p. 1649-1658.
345. Squadrito, M.L., et al., *Endogenous RNAs modulate microRNA sorting to exosomes and transfer to acceptor cells.* Cell Rep, 2014. **8**(5): p. 1432-46.
346. Heil, F., et al., *Species-specific recognition of single-stranded RNA via toll-like receptor 7 and 8.* Science, 2004. **303**(5663): p. 1526-9.
347. Fabbri, M., et al., *MicroRNAs bind to Toll-like receptors to induce prometastatic inflammatory response.* Proc Natl Acad Sci U S A, 2012. **109**(31): p. E2110-6.
348. O'Brien, K., et al., *Exosomes from triple-negative breast cancer cells can transfer phenotypic traits representing their cells of origin to secondary cells.* Eur J Cancer, 2013. **49**(8): p. 1845-59.
349. Le, M.T., et al., *miR-200-containing extracellular vesicles promote breast cancer cell metastasis.* J Clin Invest, 2014. **124**(12): p. 5109-28.
350. Donnarumma, E., et al., *Cancer-associated fibroblasts release exosomal microRNAs that dictate an aggressive phenotype in breast cancer.* Oncotarget, 2017. **8**(12): p. 19592-19608.
351. Ono, M., et al., *Exosomes from bone marrow mesenchymal stem cells contain a microRNA that promotes dormancy in metastatic breast cancer cells.* Sci Signal, 2014. **7**(332): p. ra63.
352. Taylor, D.D. and C. Gercel-Taylor, *MicroRNA signatures of tumor-derived exosomes as diagnostic biomarkers of ovarian cancer.* Gynecol Oncol, 2008. **110**(1): p. 13-21.
353. Liu, R., et al., *A five-microRNA signature identified from genome-wide serum microRNA expression profiling serves as a fingerprint for gastric cancer diagnosis.* Eur J Cancer, 2011. **47**(5): p. 784-91.
354. Hu, Z., et al., *Serum microRNA signatures identified in a genome-wide serum microRNA expression profiling predict survival of non-small-cell lung cancer.* J Clin Oncol, 2010. **28**(10): p. 1721-6.

355. Yan, L.X., et al., *MicroRNA miR-21 overexpression in human breast cancer is associated with advanced clinical stage, lymph node metastasis and patient poor prognosis.* RNA, 2008. **14**(11): p. 2348-60.
356. Nair, V.S., L.S. Maeda, and J.P. Ioannidis, *Clinical outcome prediction by microRNAs in human cancer: a systematic review.* J Natl Cancer Inst, 2012. **104**(7): p. 528-40.
357. Iorio, M.V., et al., *MicroRNA signatures in human ovarian cancer.* Cancer Res, 2007. **67**(18): p. 8699-707.
358. Lu, J., et al., *MicroRNA expression profiles classify human cancers.* Nature, 2005. **435**(7043): p. 834-8.
359. Mitchell, P.S., et al., *Circulating microRNAs as stable blood-based markers for cancer detection.* Proc Natl Acad Sci U S A, 2008. **105**(30): p. 10513-8.
360. Xi, Y., et al., *Systematic analysis of microRNA expression of RNA extracted from fresh frozen and formalin-fixed paraffin-embedded samples.* RNA, 2007. **13**(10): p. 1668-74.
361. Andre, F., et al., *Malignant effusions and immunogenic tumour-derived exosomes.* Lancet, 2002. **360**(9329): p. 295-305.
362. Valenti, R., et al., *Human tumor-released microvesicles promote the differentiation of myeloid cells with transforming growth factor-beta-mediated suppressive activity on T lymphocytes.* Cancer Res, 2006. **66**(18): p. 9290-8.
363. Cheng, L., et al., *Exosomes provide a protective and enriched source of miRNA for biomarker profiling compared to intracellular and cell-free blood.* J Extracell Vesicles, 2014. **3**.
364. Ge, Q., et al., *miRNA in plasma exosome is stable under different storage conditions.* Molecules, 2014. **19**(2): p. 1568-75.
365. Cohen, J.D., et al., *Detection and localization of surgically resectable cancers with a multi-analyte blood test.* Science, 2018.
366. Turchinovich, A., et al., *Characterization of extracellular circulating microRNA.* Nucleic Acids Res, 2011. **39**(16): p. 7223-33.
367. Chevillet, J.R., et al., *Quantitative and stoichiometric analysis of the microRNA content of exosomes.* Proc Natl Acad Sci U S A, 2014. **111**(41): p. 14888-93.
368. Hannafon, B.N., et al., *Plasma exosome microRNAs are indicative of breast cancer.* Breast Cancer Res, 2016. **18**(1): p. 90.
369. Eichelser, C., et al., *Increased serum levels of circulating exosomal microRNA-373 in receptor-negative breast cancer patients.* Oncotarget, 2014. **5**(20): p. 9650-63.
370. Li, Z., et al., *Exosomal microRNA-141 is upregulated in the serum of prostate cancer patients.* Onco Targets Ther, 2016. **9**: p. 139-48.
371. Huang, X., et al., *Exosomal miR-1290 and miR-375 as prognostic markers in castration-resistant prostate cancer.* Eur Urol, 2015. **67**(1): p. 33-41.
372. Bryant, R.J., et al., *Changes in circulating microRNA levels associated with prostate cancer.* Br J Cancer, 2012. **106**(4): p. 768-74.
373. Mateescu, B., et al., *Obstacles and opportunities in the functional analysis of extracellular vesicle RNA - an ISEV position paper.* J Extracell Vesicles, 2017. **6**(1): p. 1286095.
374. Jackson, R.J. and N. Standart, *How do microRNAs regulate gene expression?* Sci STKE, 2007. **2007**(367): p. re1.
375. Evans, J.R., F.Y. Feng, and A.M. Chinnaiyan, *The bright side of dark matter: lncRNAs in cancer.* J Clin Invest, 2016. **126**(8): p. 2775-82.
376. Kapranov, P., et al., *RNA maps reveal new RNA classes and a possible function for pervasive transcription.* Science, 2007. **316**(5830): p. 1484-8.
377. Assumpcao, C.B., et al., *The role of piRNA and its potential clinical implications in cancer.* EPIGENOMICS, 2015. **7**(6): p. 975-984.
378. Heyns, M. and O. Kovalchuk, *Non-coding RNAs including miRNAs, piRNAs, and tRNAs in human cancer.* Oncotarget, 2015. **6**(27): p. 23055-7.
379. Bhome R, H.L., Emo K, Sayan AE, Mirnezami AH, *Clinical Relevance, Prognostic Potential, and Therapeutic Strategies of Noncoding RNAs in Cancer*, in *Cancer and Noncoding RNAs*, C.J.a.M. S, Editor. 2018, Elsevier: Amsterdam. p. 576.
380. Ambros, V., et al., *A uniform system for microRNA annotation.* RNA, 2003. **9**(3): p. 277-9.

381. Griffiths-Jones, S., et al., *miRBase: microRNA sequences, targets and gene nomenclature.* Nucleic Acids Res, 2006. **34**(Database issue): p. D140-4.
382. Yang, J.S., et al., *Widespread regulatory activity of vertebrate microRNA* species.* RNA, 2011. **17**(2): p. 312-26.
383. Griffiths-Jones, S., et al., *MicroRNA evolution by arm switching.* EMBO Rep, 2011. **12**(2): p. 172-7.
384. Wright, M.W., *A short guide to long non-coding RNA gene nomenclature.* Hum Genomics, 2014. **8**: p. 7.
385. Sai Lakshmi, S. and S. Agrawal, *piRNABank: a web resource on classified and clustered Piwi-interacting RNAs.* Nucleic Acids Res, 2008. **36**(Database issue): p. D173-7.
386. Wightman, B., I. Ha, and G. Ruvkun, *Posttranscriptional regulation of the heterochronic gene lin-14 by lin-4 mediates temporal pattern formation in C. elegans.* Cell, 1993. **75**(5): p. 855-62.
387. Reinhart, B.J., et al., *The 21-nucleotide let-7 RNA regulates developmental timing in Caenorhabditis elegans.* Nature, 2000. **403**(6772): p. 901-6.
388. Slack, F.J., et al., *The lin-41 RBCC gene acts in the C. elegans heterochronic pathway between the let-7 regulatory RNA and the LIN-29 transcription factor.* Mol Cell, 2000. **5**(4): p. 659-69.
389. Brannan, C.I., et al., *The product of the H19 gene may function as an RNA.* Mol Cell Biol, 1990. **10**(1): p. 28-36.
390. Brown, C.J., et al., *The human XIST gene: analysis of a 17 kb inactive X-specific RNA that contains conserved repeats and is highly localized within the nucleus.* Cell, 1992. **71**(3): p. 527-42.
391. Brockdorff, N., et al., *The product of the mouse Xist gene is a 15 kb inactive X-specific transcript containing no conserved ORF and located in the nucleus.* Cell, 1992. **71**(3): p. 515-26.
392. Huttenhofer, A., P. Schattner, and N. Polacek, *Non-coding RNAs: hope or hype?* Trends Genet, 2005. **21**(5): p. 289-97.
393. Kapranov, P., et al., *Large-scale transcriptional activity in chromosomes 21 and 22.* Science, 2002. **296**(5569): p. 916-9.
394. Kapranov, P., et al., *Examples of the complex architecture of the human transcriptome revealed by RACE and high-density tiling arrays.* Genome Res, 2005. **15**(7): p. 987-97.
395. Girard, A., et al., *A germline-specific class of small RNAs binds mammalian Piwi proteins.* Nature, 2006. **442**(7099): p. 199-202.
396. Aravin, A., et al., *A novel class of small RNAs bind to MILI protein in mouse testes.* Nature, 2006. **442**(7099): p. 203-7.
397. Lau, N.C., et al., *Characterization of the piRNA complex from rat testes.* Science, 2006. **313**(5785): p. 363-7.
398. Saito, K., et al., *Specific association of Piwi with rasiRNAs derived from retrotransposon and heterochromatic regions in the Drosophila genome.* Genes Dev, 2006. **20**(16): p. 2214-22.
399. Aravin, A.A., et al., *The small RNA profile during Drosophila melanogaster development.* Dev Cell, 2003. **5**(2): p. 337-50.
400. Carmell, M.A., et al., *MIWI2 is essential for spermatogenesis and repression of transposons in the mouse male germline.* Dev Cell, 2007. **12**(4): p. 503-14.
401. Bartel, D.P. and C.Z. Chen, *Micromanagers of gene expression: the potentially widespread influence of metazoan microRNAs.* Nat Rev Genet, 2004. **5**(5): p. 396-400.
402. Kim, V.N. and J.W. Nam, *Genomics of microRNA.* Trends Genet, 2006. **22**(3): p. 165-73.
403. Mirnezami, A.H., et al., *MicroRNAs: key players in carcinogenesis and novel therapeutic targets.* Eur J Surg Oncol, 2009. **35**(4): p. 339-47.
404. Ipsaro, J.J., et al., *The structural biochemistry of Zucchini implicates it as a nuclease in piRNA biogenesis.* Nature, 2012. **491**(7423): p. 279-83.
405. Ross, R.J., M.M. Weiner, and H. Lin, *PIWI proteins and PIWI-interacting RNAs in the soma.* Nature, 2014. **505**(7483): p. 353-9.

406. Meister, G., *Argonaute proteins: functional insights and emerging roles.* Nat Rev Genet, 2013. **14**(7): p. 447-59.
407. Luteijn, M.J. and R.F. Ketting, *PIWI-interacting RNAs: from generation to transgenerational epigenetics.* Nat Rev Genet, 2013. **14**(8): p. 523-34.
408. Siomi, M.C., et al., *PIWI-interacting small RNAs: the vanguard of genome defence.* Nat Rev Mol Cell Biol, 2011. **12**(4): p. 246-58.
409. Quinn, J.J. and H.Y. Chang, *Unique features of long non-coding RNA biogenesis and function.* Nat Rev Genet, 2016. **17**(1): p. 47-62.
410. Ponting, C.P., P.L. Oliver, and W. Reik, *Evolution and functions of long noncoding RNAs.* Cell, 2009. **136**(4): p. 629-41.
411. Mercer, T.R., M.E. Dinger, and J.S. Mattick, *Long non-coding RNAs: insights into functions.* Nat Rev Genet, 2009. **10**(3): p. 155-9.
412. Khandewal, D., N.V. Ballal, and M.V. Saraswathi, *Comparative evaluation of accuracy of 2 electronic Apex locators with conventional radiography: an ex vivo study.* J Endod, 2015. **41**(2): p. 201-4.
413. Keniry, A., et al., *The H19 lincRNA is a developmental reservoir of miR-675 that suppresses growth and Igf1r.* Nat Cell Biol, 2012. **14**(7): p. 659-65.
414. Wutz, A., *Gene silencing in X-chromosome inactivation: advances in understanding facultative heterochromatin formation.* Nat Rev Genet, 2011. **12**(8): p. 542-53.
415. Thebault, P., et al., *Transcription regulation by the noncoding RNA SRG1 requires Spt2-dependent chromatin deposition in the wake of RNA polymerase II.* Mol Cell Biol, 2011. **31**(6): p. 1288-300.
416. Feng, J., et al., *The Evf-2 noncoding RNA is transcribed from the Dlx-5/6 ultraconserved region and functions as a Dlx-2 transcriptional coactivator.* Genes Dev, 2006. **20**(11): p. 1470-84.
417. Wang, K.C., et al., *A long noncoding RNA maintains active chromatin to coordinate homeotic gene expression.* Nature, 2011. **472**(7341): p. 120-4.
418. Biomarkers Definitions Working, G., *Biomarkers and surrogate endpoints: preferred definitions and conceptual framework.* Clin Pharmacol Ther, 2001. **69**(3): p. 89-95.
419. Ng, E.K., et al., *Differential expression of microRNAs in plasma of patients with colorectal cancer: a potential marker for colorectal cancer screening.* Gut, 2009. **58**(10): p. 1375-81.
420. Stuopelyte, K., et al., *The utility of urine-circulating miRNAs for detection of prostate cancer.* Br J Cancer, 2016. **115**(6): p. 707-15.
421. Calin, G.A., et al., *MicroRNA profiling reveals distinct signatures in B cell chronic lymphocytic leukemias.* Proc Natl Acad Sci U S A, 2004. **101**(32): p. 11755-60.
422. Ciafre, S.A., et al., *Extensive modulation of a set of microRNAs in primary glioblastoma.* Biochem Biophys Res Commun, 2005. **334**(4): p. 1351-8.
423. Yanaihara, N., et al., *Unique microRNA molecular profiles in lung cancer diagnosis and prognosis.* Cancer Cell, 2006. **9**(3): p. 189-98.
424. Cheng, J., et al., *piRNA, the new non-coding RNA, is aberrantly expressed in human cancer cells.* Clin Chim Acta, 2011. **412**(17-18): p. 1621-5.
425. Cui, L., et al., *Detection of circulating tumor cells in peripheral blood from patients with gastric cancer using piRNAs as markers.* Clin Biochem, 2011. **44**(13): p. 1050-7.
426. Laxman, B., et al., *A first-generation multiplex biomarker analysis of urine for the early detection of prostate cancer.* Cancer Res, 2008. **68**(3): p. 645-9.
427. Bullock, M.D., et al., *Stratifying risk of recurrence in stage II colorectal cancer using deregulated stromal and epithelial microRNAs.* Oncotarget, 2015. **6**(9): p. 7262-79.
428. Bjorner, S., et al., *Epithelial and stromal microRNA signatures of columnar cell hyperplasia linking Let-7c to precancerous and cancerous breast cancer cell proliferation.* PLoS One, 2014. **9**(8): p. e105099.
429. Muller, S., et al., *Next-generation sequencing reveals novel differentially regulated mRNAs, lncRNAs, miRNAs, sdRNAs and a piRNA in pancreatic cancer.* Mol Cancer, 2015. **14**: p. 94.
430. Chen, X., et al., *Characterization of microRNAs in serum: a novel class of biomarkers for diagnosis of cancer and other diseases.* Cell Res, 2008. **18**(10): p. 997-1006.

431. Fernandez-Mercado, M., et al., *The circulating transcriptome as a source of non-invasive cancer biomarkers: concepts and controversies of non-coding and coding RNA in body fluids.* J Cell Mol Med, 2015. **19**(10): p. 2307-23.
432. Denoix, P.F., *[Note on the possible role of the International Union against Cancer in nomenclature, classification, analytical index, bibliography and documentation].* Acta Unio Int Contra Cancrum, 1952. **8**(Special No): p. 92-6.
433. Sun, Y., et al., *Examining plasma microRNA markers for colorectal cancer at different stages.* Oncotarget, 2016. **7**(10): p. 11434-49.
434. Blenkiron, C., et al., *MicroRNA expression profiling of human breast cancer identifies new markers of tumor subtype.* Genome Biol, 2007. **8**(10): p. R214.
435. Chen, J., et al., *Low Expression LncRNA TUBA4B is a Poor Predictor of Prognosis and Regulates Cell Proliferation in Non-Small Cell Lung Cancer.* Pathol Oncol Res, 2016.
436. Haakensen, V.D., et al., *Subtype-specific micro-RNA expression signatures in breast cancer progression.* Int J Cancer, 2016. **139**(5): p. 1117-28.
437. Ji, P., et al., *MALAT-1, a novel noncoding RNA, and thymosin beta4 predict metastasis and survival in early-stage non-small cell lung cancer.* Oncogene, 2003. **22**(39): p. 8031-41.
438. Lin, J., et al., *miR-200c enhances radiosensitivity of human breast cancer cells.* J Cell Biochem, 2013. **114**(3): p. 606-15.
439. Gasparini, P., et al., *Protective role of miR-155 in breast cancer through RAD51 targeting impairs homologous recombination after irradiation.* Proc Natl Acad Sci U S A, 2014. **111**(12): p. 4536-41.
440. Gee, H.E., et al., *MicroRNA-Related DNA Repair/Cell-Cycle Genes Independently Associated With Relapse After Radiation Therapy for Early Breast Cancer.* Int J Radiat Oncol Biol Phys, 2015. **93**(5): p. 1104-14.
441. Liu, G., Y.I. Li, and X. Gao, *Overexpression of microRNA-133b sensitizes non-small cell lung cancer cells to irradiation through the inhibition of glycolysis.* Oncol Lett, 2016. **11**(4): p. 2903-2908.
442. Song, G., Y. Zhang, and L. Wang, *MicroRNA-206 targets notch3, activates apoptosis, and inhibits tumor cell migration and focus formation.* J Biol Chem, 2009. **284**(46): p. 31921-7.
443. Ranade, A.R., et al., *MicroRNA 92a-2*: a biomarker predictive for chemoresistance and prognostic for survival in patients with small cell lung cancer.* J Thorac Oncol, 2010. **5**(8): p. 1273-8.
444. Sorrentino, A., et al., *Role of microRNAs in drug-resistant ovarian cancer cells.* Gynecol Oncol, 2008. **111**(3): p. 478-86.
445. Wang, Z., et al., *MicroRNA-25 regulates chemoresistance-associated autophagy in breast cancer cells, a process modulated by the natural autophagy inducer isoliquiritigenin.* Oncotarget, 2014. **5**(16): p. 7013-26.
446. Wang, Q.E., et al., *Stem cell protein Piwil2 modulates chromatin modifications upon cisplatin treatment.* Mutat Res, 2011. **708**(1-2): p. 59-68.
447. Johnson, C.D., et al., *The let-7 microRNA represses cell proliferation pathways in human cells.* Cancer Res, 2007. **67**(16): p. 7713-22.
448. Cortez, M.A., et al., *PDL1 Regulation by p53 via miR-34.* J Natl Cancer Inst, 2016. **108**(1).
449. Li, L., et al., *MiR-34a inhibits proliferation and migration of breast cancer through down-regulation of Bcl-2 and SIRT1.* Clin Exp Med, 2013. **13**(2): p. 109-17.
450. Kato, M., et al., *The mir-34 microRNA is required for the DNA damage response in vivo in C. elegans and in vitro in human breast cancer cells.* Oncogene, 2009. **28**(25): p. 2419-24.
451. Sun, L., et al., *LncRNA DQ786243 contributes to proliferation and metastasis of colorectal cancer both in vitro and in vivo.* Biosci Rep, 2016. **36**(3).
452. Bronisz, A., et al., *Reprogramming of the tumour microenvironment by stromal PTEN-regulated miR-320.* Nat Cell Biol, 2012. **14**(2): p. 159-67.
453. Kelnar, K., et al., *Quantification of therapeutic miRNA mimics in whole blood from nonhuman primates.* Anal Chem, 2014. **86**(3): p. 1534-42.
454. Assumpcao, C.B., et al., *The role of piRNA and its potential clinical implications in cancer.* Epigenomics, 2015. **7**(6): p. 975-84.

455. Li, C., et al., *PIWIL1 destabilizes microtubule by suppressing phosphorylation at Ser16 and RLIM-mediated degradation of Stathmin1.* Oncotarget, 2015. **6**(29): p. 27794-804.
456. Kalluri, R. and R.A. Weinberg, *The basics of epithelial-mesenchymal transition.* J Clin Invest, 2009. **119**(6): p. 1420-8.
457. Batlle, E., et al., *The transcription factor snail is a repressor of E-cadherin gene expression in epithelial tumour cells.* Nat Cell Biol, 2000. **2**(2): p. 84-9.
458. Gregory, P.A., et al., *The miR-200 family and miR-205 regulate epithelial to mesenchymal transition by targeting ZEB1 and SIP1.* Nat Cell Biol, 2008. **10**(5): p. 593-601.
459. Wang, J., et al., *Overexpression of long non-coding RNA LOC400891 promotes tumor progression and poor prognosis in prostate cancer.* Tumour Biol, 2016. **37**(7): p. 9603-13.
460. Beg, M., et al., *4LBA A phase 1 study of first-in-class microRNA-34 mimic, MRX34, in patients with hepatocellular carcinoma or advanced cancer with liver metastasis.* European Journal of Cancer, 2014. **50**: p. 196.
461. Quinn, A.M., et al., *Diagnostic Mutation Profiling and Validation of Non-Small-Cell Lung Cancer Small Biopsy Samples using a High Throughput Platform.* J Thorac Oncol, 2015. **10**(5): p. 784-92.
462. Dannull, J., et al., *Melanoma immunotherapy using mature DCs expressing the constitutive proteasome.* J Clin Invest, 2013. **123**(7): p. 3135-45.
463. Schultheis, B., et al., *First-in-human phase I study of the liposomal RNA interference therapeutic Atu027 in patients with advanced solid tumors.* J Clin Oncol, 2014. **32**(36): p. 4141-8.
464. Golan, T., et al., *RNAi therapy targeting KRAS in combination with chemotherapy for locally advanced pancreatic cancer patients.* Oncotarget, 2015. **6**(27): p. 24560-70.
465. Salomon, C., et al., *Exosomal signaling during hypoxia mediates microvascular endothelial cell migration and vasculogenesis.* PLoS One, 2013. **8**(7): p. e68451.
466. Wei, G., et al., *Dendritic cells derived exosomes migration to spleen and induction of inflammation are regulated by CCR7.* Sci Rep, 2017. **7**: p. 42996.
467. Hosseini-Beheshti, E., et al., *Exosomes confer pro-survival signals to alter the phenotype of prostate cells in their surrounding environment.* Oncotarget, 2016. **7**(12): p. 14639-58.
468. Liang, X., et al., *Exosomes secreted by mesenchymal stem cells promote endothelial cell angiogenesis by transferring miR-125a.* J Cell Sci, 2016. **129**(11): p. 2182-9.
469. Zhang, Z., et al., *Pretreatment of Cardiac Stem Cells With Exosomes Derived From Mesenchymal Stem Cells Enhances Myocardial Repair.* J Am Heart Assoc, 2016. **5**(1).
470. Probert, C., et al., *Communication of prostate cancer cells with bone cells via extracellular vesicle RNA; a potential mechanism of metastasis.* Oncogene, 2018.
471. Prosser, H.M., et al., *A resource of vectors and ES cells for targeted deletion of microRNAs in mice.* Nat Biotechnol, 2011. **29**(9): p. 840-5.
472. Sayan, A.E., et al., *SIP1 protein protects cells from DNA damage-induced apoptosis and has independent prognostic value in bladder cancer.* Proc Natl Acad Sci U S A, 2009. **106**(35): p. 14884-9.
473. Sayan, A.E., et al., *Fra-1 controls motility of bladder cancer cells via transcriptional upregulation of the receptor tyrosine kinase AXL.* Oncogene, 2012. **31**(12): p. 1493-503.
474. Cellura, D., et al., *miR-19-Mediated Inhibition of Transglutaminase-2 Leads to Enhanced Invasion and Metastasis in Colorectal Cancer.* Mol Cancer Res, 2015. **13**(7): p. 1095-105.
475. Ling, H., et al., *The clinical and biological significance of MIR-224 expression in colorectal cancer metastasis.* Gut, 2016. **65**(6): p. 977-89.
476. Zhang, L., et al., *miR-153 supports colorectal cancer progression via pleiotropic effects that enhance invasion and chemotherapeutic resistance.* Cancer Res, 2013. **73**(21): p. 6435-47.
477. ACPGBI, *Guidelines for the management of colorectal cancer*. 3rd ed. 2007, London: ACPGBI. 117.
478. Scott, N., et al., *Total mesorectal excision and local recurrence: a study of tumour spread in the mesorectum distal to rectal cancer.* Br J Surg, 1995. **82**(8): p. 1031-3.

479. Hida, J., et al., *Lymph node metastases detected in the mesorectum distal to carcinoma of the rectum by the clearing method: justification of total mesorectal excision.* J Am Coll Surg, 1997. **184**(6): p. 584-8.
480. Reynolds, J.V., et al., *Pathological evidence in support of total mesorectal excision in the management of rectal cancer.* Br J Surg, 1996. **83**(8): p. 1112-5.
481. Bhome, R., et al., *Exosomal microRNAs derived from colorectal cancer-associated fibroblasts: role in driving cancer progression.* Aging (Albany NY), 2017. **9**(12): p. 2666-2694.
482. Bhome, R., et al., *The Colorectal Cancer Microenvironment: Strategies for Studying the Role of Cancer-Associated Fibroblasts.* Methods Mol Biol, 2018. **1765**: p. 87-98.
483. Schetter, A.J., H. Okayama, and C.C. Harris, *The role of microRNAs in colorectal cancer.* Cancer J, 2012. **18**(3): p. 244-52.
484. Occhipinti, G., et al., *The choice of endogenous controls in exosomal microRNA assessments from biofluids.* Tumour Biol, 2016. **37**(9): p. 11657-11665.
485. D'Haene, B., et al., *miRNA expression profiling: from reference genes to global mean normalization.* Methods Mol Biol, 2012. **822**: p. 261-72.
486. Mathivanan, S. and R.J. Simpson, *ExoCarta: A compendium of exosomal proteins and RNA.* Proteomics, 2009. **9**(21): p. 4997-5000.
487. Bleazard, T., J.A. Lamb, and S. Griffiths-Jones, *Bias in microRNA functional enrichment analysis.* Bioinformatics, 2015. **31**(10): p. 1592-8.
488. Alhasan, A.H., et al., *Circulating microRNA signature for the diagnosis of very high-risk prostate cancer.* Proc Natl Acad Sci U S A, 2016. **113**(38): p. 10655-60.
489. Fan, Y., et al., *miRNet - dissecting miRNA-target interactions and functional associations through network-based visual analysis.* Nucleic Acids Res, 2016. **44**(W1): p. W135-41.
490. Thannickal, V.J., et al., *Myofibroblast differentiation by transforming growth factor-beta1 is dependent on cell adhesion and integrin signaling via focal adhesion kinase.* J Biol Chem, 2003. **278**(14): p. 12384-9.
491. Yang, S., et al., *Participation of miR-200 in pulmonary fibrosis.* Am J Pathol, 2012. **180**(2): p. 484-93.
492. Takahashi, Y., et al., *Visualization and in vivo tracking of the exosomes of murine melanoma B16-BL6 cells in mice after intravenous injection.* J Biotechnol, 2013. **165**(2): p. 77-84.
493. Lai, C.P., et al., *Visualization and tracking of tumour extracellular vesicle delivery and RNA translation using multiplexed reporters.* Nat Commun, 2015. **6**: p. 7029.
494. Raposo, G. and W. Stoorvogel, *Extracellular vesicles: exosomes, microvesicles, and friends.* J Cell Biol, 2013. **200**(4): p. 373-83.
495. Eldh, M., et al., *Importance of RNA isolation methods for analysis of exosomal RNA: evaluation of different methods.* Mol Immunol, 2012. **50**(4): p. 278-86.
496. Koh, H., et al., *Inhibition of Akt and its anti-apoptotic activities by tumor necrosis factor-induced protein kinase C-related kinase 2 (PRK2) cleavage.* J Biol Chem, 2000. **275**(44): p. 34451-8.
497. de Gramont, A., et al., *Leucovorin and fluorouracil with or without oxaliplatin as first-line treatment in advanced colorectal cancer.* J Clin Oncol, 2000. **18**(16): p. 2938-47.
498. Graham, M.A., et al., *Clinical pharmacokinetics of oxaliplatin: a critical review.* Clin Cancer Res, 2000. **6**(4): p. 1205-18.
499. Chambard, J.C., et al., *ERK implication in cell cycle regulation.* Biochim Biophys Acta, 2007. **1773**(8): p. 1299-310.
500. Rahmouni, S., et al., *Loss of the VHR dual-specific phosphatase causes cell-cycle arrest and senescence.* Nat Cell Biol, 2006. **8**(5): p. 524-31.
501. Hanahan, D. and R.A. Weinberg, *Hallmarks of cancer: the next generation.* Cell, 2011. **144**(5): p. 646-74.
502. Pietras, K. and A. Ostman, *Hallmarks of cancer: interactions with the tumor stroma.* Exp Cell Res, 2010. **316**(8): p. 1324-31.
503. Calon, A., et al., *Stromal gene expression defines poor-prognosis subtypes in colorectal cancer.* Nat Genet, 2015. **47**(4): p. 320-9.

504. Bullock, M.D., et al., *Pleiotropic actions of miR-21 highlight the critical role of deregulated stromal microRNAs during colorectal cancer progression.* Cell Death Dis, 2013. **4**: p. e684.
505. Volinia, S., et al., *A microRNA expression signature of human solid tumors defines cancer gene targets.* Proc Natl Acad Sci U S A, 2006. **103**(7): p. 2257-61.
506. Asangani, I.A., et al., *MicroRNA-21 (miR-21) post-transcriptionally downregulates tumor suppressor Pdcd4 and stimulates invasion, intravasation and metastasis in colorectal cancer.* Oncogene, 2008. **27**(15): p. 2128-36.
507. Toiyama, Y., et al., *Serum miR-21 as a diagnostic and prognostic biomarker in colorectal cancer.* J Natl Cancer Inst, 2013. **105**(12): p. 849-59.
508. Kanaan, Z., et al., *Plasma miR-21: a potential diagnostic marker of colorectal cancer.* Ann Surg, 2012. **256**(3): p. 544-51.
509. Garin-Chesa, P., et al., *Immunohistochemical analysis of the A4 and AO10 (gp110) cell-surface antigens of human astrocytoma.* Am J Pathol, 1990. **136**(4): p. 797-807.
510. Casey, T.M., et al., *Cancer associated fibroblasts stimulated by transforming growth factor beta1 (TGF-beta 1) increase invasion rate of tumor cells: a population study.* Breast Cancer Res Treat, 2008. **110**(1): p. 39-49.
511. Salaria, S.N., et al., *Palladin is overexpressed in the non-neoplastic stroma of infiltrating ductal adenocarcinomas of the pancreas, but is only rarely overexpressed in neoplastic cells.* Cancer Biol Ther, 2007. **6**(3): p. 324-8.
512. Liu, Y., et al., *Separation, cultivation and biological characteristics of oral carcinoma-associated fibroblasts.* Oral Dis, 2006. **12**(4): p. 375-80.
513. Calvo, F., et al., *Cdc42EP3/BORG2 and Septin Network Enables Mechano-transduction and the Emergence of Cancer-Associated Fibroblasts.* Cell Rep, 2015. **13**(12): p. 2699-714.
514. Frankel, L.B., et al., *Programmed cell death 4 (PDCD4) is an important functional target of the microRNA miR-21 in breast cancer cells.* J Biol Chem, 2008. **283**(2): p. 1026-33.
515. Ayala, G., et al., *Reactive stroma as a predictor of biochemical-free recurrence in prostate cancer.* Clin Cancer Res, 2003. **9**(13): p. 4792-801.
516. Tsujino, T., et al., *Stromal myofibroblasts predict disease recurrence for colorectal cancer.* Clin Cancer Res, 2007. **13**(7): p. 2082-90.
517. Marsh, D., et al., *Stromal features are predictive of disease mortality in oral cancer patients.* J Pathol, 2011. **223**(4): p. 470-81.
518. Sinn, M., et al., *alpha-Smooth muscle actin expression and desmoplastic stromal reaction in pancreatic cancer: results from the CONKO-001 study.* Br J Cancer, 2014. **111**(10): p. 1917-23.
519. Liu, L., et al., *Stromal Myofibroblasts Are Associated with Poor Prognosis in Solid Cancers: A Meta-Analysis of Published Studies.* PLoS One, 2016. **11**(7): p. e0159947.
520. Orimo, A., et al., *Cancer-associated myofibroblasts possess various factors to promote endometrial tumor progression.* Clin Cancer Res, 2001. **7**(10): p. 3097-105.
521. Otranto, M., et al., *The role of the myofibroblast in tumor stroma remodeling.* Cell Adh Migr, 2012. **6**(3): p. 203-19.
522. Lu, P., et al., *Extracellular matrix degradation and remodeling in development and disease.* Cold Spring Harb Perspect Biol, 2011. **3**(12).
523. Gaggioli, C., et al., *Fibroblast-led collective invasion of carcinoma cells with differing roles for RhoGTPases in leading and following cells.* Nat Cell Biol, 2007. **9**(12): p. 1392-400.
524. Ireland, L., et al., *Chemoresistance in Pancreatic Cancer Is Driven by Stroma-Derived Insulin-Like Growth Factors.* Cancer Res, 2016. **76**(23): p. 6851-6863.
525. Muerkoster, S.S., et al., *Role of myofibroblasts in innate chemoresistance of pancreatic carcinoma--epigenetic downregulation of caspases.* Int J Cancer, 2008. **123**(8): p. 1751-60.
526. Kawashiri, S., et al., *Significance of stromal desmoplasia and myofibroblast appearance at the invasive front in squamous cell carcinoma of the oral cavity.* Head Neck, 2009. **31**(10): p. 1346-53.
527. Takatsuna, M., et al., *Myofibroblast distribution is associated with invasive growth types of colorectal cancer.* Oncol Rep, 2016. **36**(6): p. 3154-3160.

528. Ahmed, D., et al., *Epigenetic and genetic features of 24 colon cancer cell lines.* Oncogenesis, 2013. **2**: p. e71.
529. Hewitt, R.E., et al., *Validation of a model of colon cancer progression.* J Pathol, 2000. **192**(4): p. 446-54.
530. Rosenfeldt, H. and F. Grinnell, *Fibroblast quiescence and the disruption of ERK signaling in mechanically unloaded collagen matrices.* J Biol Chem, 2000. **275**(5): p. 3088-92.
531. Serrano, M., et al., *Oncogenic ras provokes premature cell senescence associated with accumulation of p53 and p16INK4a.* Cell, 1997. **88**(5): p. 593-602.
532. Nho, R.S., et al., *Role of integrin-linked kinase in regulating phosphorylation of Akt and fibroblast survival in type I collagen matrices through a beta1 integrin viability signaling pathway.* J Biol Chem, 2005. **280**(28): p. 26630-9.
533. Ruebel, K., et al., *MicroRNA expression in ileal carcinoid tumors: downregulation of microRNA-133a with tumor progression.* Mod Pathol, 2010. **23**(3): p. 367-75.
534. Evans, R.A., et al., *TGF-beta1-mediated fibroblast-myofibroblast terminal differentiation-the role of Smad proteins.* Exp Cell Res, 2003. **282**(2): p. 90-100.
535. Midgley, A.C., et al., *Transforming growth factor-beta1 (TGF-beta1)-stimulated fibroblast to myofibroblast differentiation is mediated by hyaluronan (HA)-facilitated epidermal growth factor receptor (EGFR) and CD44 co-localization in lipid rafts.* J Biol Chem, 2013. **288**(21): p. 14824-38.
536. Jester, J.V., et al., *Induction of alpha-smooth muscle actin expression and myofibroblast transformation in cultured corneal keratocytes.* Cornea, 1996. **15**(5): p. 505-16.
537. Galie, P.A., M.V. Westfall, and J.P. Stegemann, *Reduced serum content and increased matrix stiffness promote the cardiac myofibroblast transition in 3D collagen matrices.* Cardiovasc Pathol, 2011. **20**(6): p. 325-33.
538. Shirakihara, T., M. Saitoh, and K. Miyazono, *Differential regulation of epithelial and mesenchymal markers by deltaEF1 proteins in epithelial mesenchymal transition induced by TGF-beta.* Mol Biol Cell, 2007. **18**(9): p. 3533-44.
539. Nishimura, G., et al., *DeltaEF1 mediates TGF-beta signaling in vascular smooth muscle cell differentiation.* Dev Cell, 2006. **11**(1): p. 93-104.
540. Lu, T.X., A. Munitz, and M.E. Rothenberg, *MicroRNA-21 is up-regulated in allergic airway inflammation and regulates IL-12p35 expression.* J Immunol, 2009. **182**(8): p. 4994-5002.
541. Denzler, R., et al., *Impact of MicroRNA Levels, Target-Site Complementarity, and Cooperativity on Competing Endogenous RNA-Regulated Gene Expression.* Mol Cell, 2016. **64**(3): p. 565-579.
542. Thomson, D.W. and M.E. Dinger, *Endogenous microRNA sponges: evidence and controversy.* Nat Rev Genet, 2016. **17**(5): p. 272-83.
543. Lianoglou, S., et al., *Ubiquitously transcribed genes use alternative polyadenylation to achieve tissue-specific expression.* Genes Dev, 2013. **27**(21): p. 2380-96.
544. Mendt, M., et al., *Generation and testing of clinical-grade exosomes for pancreatic cancer.* JCI Insight, 2018. **3**(8).
545. Iorio, M.V. and C.M. Croce, *MicroRNA dysregulation in cancer: diagnostics, monitoring and therapeutics. A comprehensive review.* EMBO Mol Med, 2012. **4**(3): p. 143-59.
546. Locker, G.Y., et al., *ASCO 2006 update of recommendations for the use of tumor markers in gastrointestinal cancer.* J Clin Oncol, 2006. **24**(33): p. 5313-27.
547. Nishida, N., et al., *Microarray analysis of colorectal cancer stromal tissue reveals upregulation of two oncogenic miRNA clusters.* Clin Cancer Res, 2012. **18**(11): p. 3054-70.
548. Nedaeinia, R., et al., *Circulating exosomes and exosomal microRNAs as biomarkers in gastrointestinal cancer.* Cancer Gene Ther, 2017. **24**(2): p. 48-56.
549. Webb, S., *The cancer bloodhounds.* Nat Biotechnol, 2016. **34**(11): p. 1090-1094.
550. Qiu, S., et al., *Interactions of miR-323/miR-326/miR-329 and miR-130a/miR-155/miR-210 as prognostic indicators for clinical outcome of glioblastoma patients.* J Transl Med, 2013. **11**: p. 10.
551. Xiao, B., et al., *MiRNA-329 targeting E2F1 inhibits cell proliferation in glioma cells.* J Transl Med, 2013. **11**: p. 172.

552. Li, Z., et al., *By downregulating TIAM1 expression, microRNA-329 suppresses gastric cancer invasion and growth.* Oncotarget, 2015. **6**(19): p. 17559-69.
553. Sun, C.C., et al., *Hsa-miR-329 exerts tumor suppressor function through down-regulation of MET in non-small cell lung cancer.* Oncotarget, 2016. **7**(16): p. 21510-26.
554. Chen, C.Z., et al., *MicroRNAs modulate hematopoietic lineage differentiation.* Science, 2004. **303**(5654): p. 83-6.
555. Pekarsky, Y., et al., *Tcl1 expression in chronic lymphocytic leukemia is regulated by miR-29 and miR-181.* Cancer Res, 2006. **66**(24): p. 11590-3.
556. Yang, C.C., et al., *miR-181 as a putative biomarker for lymph-node metastasis of oral squamous cell carcinoma.* J Oral Pathol Med, 2011. **40**(5): p. 397-404.
557. Wang, Y., et al., *Transforming growth factor-beta regulates the sphere-initiating stem cell-like feature in breast cancer through miRNA-181 and ATM.* Oncogene, 2011. **30**(12): p. 1470-80.
558. Ji, J., et al., *Identification of microRNA-181 by genome-wide screening as a critical player in EpCAM-positive hepatic cancer stem cells.* Hepatology, 2009. **50**(2): p. 472-80.
559. Kim, S., et al., *MicroRNA miR-199a* regulates the MET proto-oncogene and the downstream extracellular signal-regulated kinase 2 (ERK2).* J Biol Chem, 2008. **283**(26): p. 18158-66.
560. Fornari, F., et al., *MiR-199a-3p regulates mTOR and c-Met to influence the doxorubicin sensitivity of human hepatocarcinoma cells.* Cancer Res, 2010. **70**(12): p. 5184-93.
561. Hou, J., et al., *Identification of miRNomes in human liver and hepatocellular carcinoma reveals miR-199a/b-3p as therapeutic target for hepatocellular carcinoma.* Cancer Cell, 2011. **19**(2): p. 232-43.
562. Mudduluru, G., et al., *Regulation of Axl receptor tyrosine kinase expression by miR-34a and miR-199a/b in solid cancer.* Oncogene, 2011. **30**(25): p. 2888-99.
563. Tian, R., et al., *miR-199a-3p negatively regulates the progression of osteosarcoma through targeting AXL.* Am J Cancer Res, 2014. **4**(6): p. 738-50.
564. Seok, J.K., et al., *MicroRNA-382 induced by HIF-1alpha is an angiogenic miR targeting the tumor suppressor phosphatase and tensin homolog.* Nucleic Acids Res, 2014. **42**(12): p. 8062-72.
565. Kriegel, A.J., et al., *MicroRNA-target pairs in human renal epithelial cells treated with transforming growth factor beta 1: a novel role of miR-382.* Nucleic Acids Res, 2010. **38**(22): p. 8338-47.
566. Xu, M., et al., *miR-382 inhibits tumor growth and enhance chemosensitivity in osteosarcoma.* Oncotarget, 2014. **5**(19): p. 9472-83.
567. Xu, M., et al., *miR-382 inhibits osteosarcoma metastasis and relapse by targeting Y box-binding protein 1.* Mol Ther, 2015. **23**(1): p. 89-98.
568. Song, B., et al., *Molecular mechanism of chemoresistance by miR-215 in osteosarcoma and colon cancer cells.* Mol Cancer, 2010. **9**: p. 96.
569. Boni, V., et al., *miR-192/miR-215 influence 5-fluorouracil resistance through cell cycle-mediated mechanisms complementary to its post-transcriptional thymidilate synthase regulation.* Mol Cancer Ther, 2010. **9**(8): p. 2265-75.
570. Georges, S.A., et al., *Coordinated regulation of cell cycle transcripts by p53-Inducible microRNAs, miR-192 and miR-215.* Cancer Res, 2008. **68**(24): p. 10105-12.
571. Meng, F., et al., *MicroRNA-21 regulates expression of the PTEN tumor suppressor gene in human hepatocellular cancer.* Gastroenterology, 2007. **133**(2): p. 647-58.
572. Zhang, J.G., et al., *MicroRNA-21 (miR-21) represses tumor suppressor PTEN and promotes growth and invasion in non-small cell lung cancer (NSCLC).* Clin Chim Acta, 2010. **411**(11-12): p. 846-52.
573. Ma, X., et al., *Loss of the miR-21 allele elevates the expression of its target genes and reduces tumorigenesis.* Proc Natl Acad Sci U S A, 2011. **108**(25): p. 10144-9.
574. Lu, Z., et al., *MicroRNA-21 promotes cell transformation by targeting the programmed cell death 4 gene.* Oncogene, 2008. **27**(31): p. 4373-9.

575. Gaur, A.B., et al., *Downregulation of Pdcd4 by mir-21 facilitates glioblastoma proliferation in vivo.* Neuro Oncol, 2011. **13**(6): p. 580-90.
576. Kang, W.K., et al., *Stromal expression of miR-21 in T3-4a colorectal cancer is an independent predictor of early tumor relapse.* BMC Gastroenterol, 2015. **15**: p. 2.
577. Au Yeung, C.L., et al., *Exosomal transfer of stroma-derived miR21 confers paclitaxel resistance in ovarian cancer cells through targeting APAF1.* Nat Commun, 2016. **7**: p. 11150.
578. Tseng, W., X. Leong, and E. Engleman, *Orthotopic mouse model of colorectal cancer.* J Vis Exp, 2007(10): p. 484.
579. McIntyre, R.E., et al., *Mouse models of colorectal cancer as preclinical models.* Bioessays, 2015. **37**(8): p. 909-20.
580. Brognard, J., et al., *PHLPP and a second isoform, PHLPP2, differentially attenuate the amplitude of Akt signaling by regulating distinct Akt isoforms.* Mol Cell, 2007. **25**(6): p. 917-31.
581. Shook, D. and R. Keller, *Mechanisms, mechanics and function of epithelial-mesenchymal transitions in early development.* Mech Dev, 2003. **120**(11): p. 1351-83.
582. Nieto, M.A. and A. Cano, *The epithelial-mesenchymal transition under control: global programs to regulate epithelial plasticity.* Semin Cancer Biol, 2012. **22**(5-6): p. 361-8.
583. Puisieux, A., T. Brabletz, and J. Caramel, *Oncogenic roles of EMT-inducing transcription factors.* Nat Cell Biol, 2014. **16**(6): p. 488-94.
584. Baulida, J., *Epithelial-to-mesenchymal transition transcription factors in cancer-associated fibroblasts.* Mol Oncol, 2017. **11**(7): p. 847-859.
585. Franci, C., et al., *Expression of Snail protein in tumor-stroma interface.* Oncogene, 2006. **25**(37): p. 5134-44.
586. Stanisavljevic, J., et al., *Snail1-expressing fibroblasts in the tumor microenvironment display mechanical properties that support metastasis.* Cancer Res, 2015. **75**(2): p. 284-95.
587. Alba-Castellon, L., et al., *Snail1-Dependent Activation of Cancer-Associated Fibroblast Controls Epithelial Tumor Cell Invasion and Metastasis.* Cancer Res, 2016. **76**(21): p. 6205-6217.
588. Sung, C.O., et al., *Twist1 is up-regulated in gastric cancer-associated fibroblasts with poor clinical outcomes.* Am J Pathol, 2011. **179**(4): p. 1827-38.
589. Lee, K.W., et al., *Twist1 is a key regulator of cancer-associated fibroblasts.* Cancer Res, 2015. **75**(1): p. 73-85.
590. Bronsert, P., et al., *Prognostic significance of Zinc finger E-box binding homeobox 1 (ZEB1) expression in cancer cells and cancer-associated fibroblasts in pancreatic head cancer.* Surgery, 2014. **156**(1): p. 97-108.
591. Chang, Y.C., et al., *Arecoline-induced myofibroblast transdifferentiation from human buccal mucosal fibroblasts is mediated by ZEB1.* J Cell Mol Med, 2014. **18**(4): p. 698-708.
592. Bracken, C.P., et al., *A double-negative feedback loop between ZEB1-SIP1 and the microRNA-200 family regulates epithelial-mesenchymal transition.* Cancer Res, 2008. **68**(19): p. 7846-54.
593. Park, S.M., et al., *The miR-200 family determines the epithelial phenotype of cancer cells by targeting the E-cadherin repressors ZEB1 and ZEB2.* Genes Dev, 2008. **22**(7): p. 894-907.
594. Tang, X., et al., *Stromal miR-200s contribute to breast cancer cell invasion through CAF activation and ECM remodeling.* Cell Death Differ, 2016. **23**(1): p. 132-45.
595. Yao, L., et al., *Paracrine signalling during ZEB1-mediated epithelial-mesenchymal transition augments local myofibroblast differentiation in lung fibrosis.* Cell Death Differ, 2018.
596. Kowal, J., et al., *Proteomic comparison defines novel markers to characterize heterogeneous populations of extracellular vesicle subtypes.* Proc Natl Acad Sci U S A, 2016. **113**(8): p. E968-77.
597. Van Deun, J., et al., *The impact of disparate isolation methods for extracellular vesicles on downstream RNA profiling.* J Extracell Vesicles, 2014. **3**.
598. Baranyai, T., et al., *Isolation of Exosomes from Blood Plasma: Qualitative and Quantitative Comparison of Ultracentrifugation and Size Exclusion Chromatography Methods.* PLoS One, 2015. **10**(12): p. e0145686.

599. Tauro, B.J., et al., *Comparison of ultracentrifugation, density gradient separation, and immunoaffinity capture methods for isolating human colon cancer cell line LIM1863-derived exosomes.* Methods, 2012. **56**(2): p. 293-304.
600. Cantin, R., et al., *Discrimination between exosomes and HIV-1: purification of both vesicles from cell-free supernatants.* J Immunol Methods, 2008. **338**(1-2): p. 21-30.
601. Arroyo, J.D., et al., *Argonaute2 complexes carry a population of circulating microRNAs independent of vesicles in human plasma.* Proc Natl Acad Sci U S A, 2011. **108**(12): p. 5003-8.
602. Ford, T., J. Graham, and D. Rickwood, *Iodixanol: a nonionic iso-osmotic centrifugation medium for the formation of self-generated gradients.* Anal Biochem, 1994. **220**(2): p. 360-6.
603. Taylor, D.D. and S. Shah, *Methods of isolating extracellular vesicles impact down-stream analyses of their cargoes.* Methods, 2015. **87**: p. 3-10.
604. Watson, D.C., et al., *Efficient production and enhanced tumor delivery of engineered extracellular vesicles.* Biomaterials, 2016. **105**: p. 195-205.
605. Rider, M.A., S.N. Hurwitz, and D.G. Meckes, Jr., *ExtraPEG: A Polyethylene Glycol-Based Method for Enrichment of Extracellular Vesicles.* Sci Rep, 2016. **6**: p. 23978.
606. Li, P., et al., *Progress in Exosome Isolation Techniques.* Theranostics, 2017. **7**(3): p. 789-804.
607. Ding, M., et al., *Comparison of commercial exosome isolation kits for circulating exosomal microRNA profiling.* Anal Bioanal Chem, 2018. **410**(16): p. 3805-3814.
608. Rekker, K., et al., *Comparison of serum exosome isolation methods for microRNA profiling.* Clin Biochem, 2014. **47**(1-2): p. 135-8.
609. Tang, Y.T., et al., *Comparison of isolation methods of exosomes and exosomal RNA from cell culture medium and serum.* Int J Mol Med, 2017. **40**(3): p. 834-844.
610. Chiba, M., M. Kimura, and S. Asari, *Exosomes secreted from human colorectal cancer cell lines contain mRNAs, microRNAs and natural antisense RNAs, that can transfer into the human hepatoma HepG2 and lung cancer A549 cell lines.* Oncol Rep, 2012. **28**(5): p. 1551-8.
611. Benz, F., et al., *U6 is unsuitable for normalization of serum miRNA levels in patients with sepsis or liver fibrosis.* Exp Mol Med, 2013. **45**: p. e42.
612. Mestdagh, P., et al., *A novel and universal method for microRNA RT-qPCR data normalization.* Genome Biol, 2009. **10**(6): p. R64.
613. van der Pol, E., et al., *Single vs. swarm detection of microparticles and exosomes by flow cytometry.* J Thromb Haemost, 2012. **10**(5): p. 919-30.
614. van der Pol, E., et al., *Innovation in detection of microparticles and exosomes.* J Thromb Haemost, 2013. **11 Suppl 1**: p. 36-45.
615. Cvjetkovic, A., J. Lotvall, and C. Lasser, *The influence of rotor type and centrifugation time on the yield and purity of extracellular vesicles.* J Extracell Vesicles, 2014. **3**.
616. Soo, C.Y., et al., *Nanoparticle tracking analysis monitors microvesicle and exosome secretion from immune cells.* Immunology, 2012. **136**(2): p. 192-7.
617. Logozzi, M., et al., *High levels of exosomes expressing CD63 and caveolin-1 in plasma of melanoma patients.* PLoS One, 2009. **4**(4): p. e5219.
618. Maas, S.L., J. De Vrij, and M.L. Broekman, *Quantification and size-profiling of extracellular vesicles using tunable resistive pulse sensing.* J Vis Exp, 2014(92): p. e51623.
619. Zhu, L., et al., *Label-free quantitative detection of tumor-derived exosomes through surface plasmon resonance imaging.* Anal Chem, 2014. **86**(17): p. 8857-64.
620. Lu, T., et al., *The Non-Specific Binding of Fluorescent-Labeled MiRNAs on Cell Surface by Hydrophobic Interaction.* PLoS One, 2016. **11**(3): p. e0149751.
621. Vuckovic, S., et al., *The cationic small molecule GW4869 is cytotoxic to high phosphatidylserine-expressing myeloma cells.* Br J Haematol, 2017. **177**(3): p. 423-440.
622. Unal, B., et al., *Inhibition of neutral sphingomyelinase decreases elevated levels of nitrative and oxidative stress markers in liver ischemia-reperfusion injury.* Redox Rep, 2017. **22**(4): p. 147-159.

623. Edge, S.B. and C.C. Compton, *The American Joint Committee on Cancer: the 7th edition of the AJCC cancer staging manual and the future of TNM.* Ann Surg Oncol, 2010. **17**(6): p. 1471-4.